

Group 9 and 10 Transition Metal *N*-Heterocyclic Carbene Complexes in Catalysis

Kirsty June Hawkes B. Sc. (Hons)



Submitted in fulfilment of the requirements for the degree of
Doctor of Philosophy

School of Chemistry
Cardiff University
Cardiff, Wales
United Kingdom
March 2006

UMI Number: U584815

All rights reserved

INFORMATION TO ALL USERS

The quality of this reproduction is dependent upon the quality of the copy submitted.

In the unlikely event that the author did not send a complete manuscript and there are missing pages, these will be noted. Also, if material had to be removed, a note will indicate the deletion.



UMI U584815

Published by ProQuest LLC 2013. Copyright in the Dissertation held by the Author.
Microform Edition © ProQuest LLC.

All rights reserved. This work is protected against
unauthorized copying under Title 17, United States Code.



ProQuest LLC
789 East Eisenhower Parkway
P.O. Box 1346
Ann Arbor, MI 48106-1346

Abstract

This thesis describes the theoretical and experimental study of group 9 and 10 transition metal N-heterocyclic carbene complexes in catalytic reactions.

In order to overcome decomposition reactions discovered in the use of carbene complexes for carbon monoxide/ethylene copolymerisation, chelating thiazolium salts were prepared for the synthesis of corresponding palladium complexes. Complex formation proved difficult and experimental attempts to overcome possible side reactions caused by reactant-metal interactions were unsuccessful. Theoretical studies indicated a sulfur-palladium interaction may be contributing to alternative products, with the use of the bulky ^tBu coordination at the thiazolium 5 position likely to block this interaction enough to allow C2 carbene formation.

Theoretical calculations for the oxidative addition of azolium salts to a model Wilkinson's catalyst ($\text{RhCl}(\text{PH}_3)_3$) is described. According to free energy calculations, a six ligand associative route with a concerted three-centred transition structure may be competitive to a route in which phosphine predissociation occurs. Exchange of the phosphine molecule on the metal centre with trimethylphosphine had a significant effect in lowering the barrier to oxidative addition and decreasing the endothermicity of the reaction, while explicit and bulk solvation was found to have a moderate effect on the overall reaction.

Extension of the oxidative addition of azolium salts to rhodium carbene complexes have been examined, in which a range of ligands is described from the pi-acidic carbon monoxide ligand to multiple carbene ligands. Increasing basicity decreases activation barriers while increasing the exothermicity of the overall reaction for C-H activation, however the complex most successful at C-H activation was not considered hospitable enough for related C-C activation of 2-methylazolium salts. Switching to iridium indicated a large benefit in C-H activation. Unfortunately, C-C activation remained unfavourable for iridium due to a high barrier to reaction.

A mechanism for the experimentally successful C-C coupling of azolium salts to alkenes by nickel complexes is studied, indicating an oxidative addition, alkene insertion and reductive elimination cycle seems likely. Experimentally, the switching of catalytically active phosphine ligands to the related carbenes causes the reaction to be halted. Theoretical calculations imply minor changes to reaction conditions may

significantly affect the outcome of catalytic reactions by stabilisation of important reaction intermediates. Further studies of the alternative C4 activation of the azolium salts and use of related azoles show C4 activation and coupling may be possible, while the unactivated azoles are unlikely to be coupled using the same mechanism. The related C-C coupling of azoles with alkenes by rhodium complexes has been successfully employed in experimental conditions, with Bergman's group examining a mechanism in which a rhodium carbene complex is formed as part of the catalytic cycle. Comparisons of this mechanism to the oxidative addition, ethylene insertion and reductive elimination reaction implied for nickel are reported. Both five and six membered ring products are found experimentally, and mechanistic studies using both Bergman's recommended route and ours indicate the activation barriers for the six membered ring are lower than the corresponding five membered ring, despite the five membered ring being the thermodynamically favoured product. Other reaction factors including alkene isomerisation, the addition of adjacent methyl groups on the alkene chain and alternative alkene coordination to the metal have no impact on the favoured product. While there is no obvious indication as to which mechanism is preferred for azole coupling, addition of an acid catalyst strongly favours our mechanism.

Acknowledgements

I would like to thank my supervisors, Professor Kingsley Cavell and Associate Professor Brian Yates. Their support, guidance, and encouragement often over two continents on opposite sides of the world, has been very much appreciated.

I gratefully acknowledge the School of Chemistry, University of Wales, for financial support, and the Australian and Tasmanian Partnerships for Advanced Computing (APAC and TPAC) for liberal grants of computing time at excellent facilities.

A significant amount of this work was carried out at the University of Tasmania (Hobart, Australia). In particular, thank you to Brian for providing me with office space, and general support, both academically and personally. Thanks also to the School of Chemistry, in particular Professor Allan Canty, Ann Parkin, Dr Michael Gardiner, Dr Vicki-Anne Tollhurst, and Dr Jason Smith; all of whom provided a friendly work environment and made me feel a part of the university.

Many people at Cardiff University deserve thanks and I gratefully acknowledge the technical and personal support of all staff. In particular Professor Cameron Jones and Dr Peter Edwards for sharing their laboratory and office space during trying renovations.

Thank you to all the other postgraduate students at Cardiff University and the University of Tasmania. There are too many to name, but the knowledge, fun and help I have received over the years has been invaluable.

Thanks to the team at Dytech Solutions, who provided me with the flexibility I needed to finish and a fantastic working environment.

Thank you so much to my family and friends. Mum and Dad, you are an endless source of love and support (and dinners when I need it most), and to Leah and Gavin - I couldn't ask for more supportive and fun siblings.

There are four other people who have made this thesis possible and have gone well beyond the ordinary in their support. To Al and Dave – you're inspirations in both chemistry and friendship. To Andrew, who could easily have walked away, but instead held my hand when I needed it most. And finally to Nathan, your understanding, compassion and support have been incredible and have made reaching the end possible. Thank you.

Abbreviations

cod	1,5-cyclooctadiene
Cy	cyclohexyl
dba	dibenzylideneacetone
DCM	dichloromethane
Dipp	2,6-diisopropylphenyl
dmiy	1,3-dimethylimidazol-2-ylidene
DMSO	dimethylsulfoxide
dppe	1,3-bis(diphenylphosphino)ethane
dmpe	1,3-bis(dimethylphosphino)ethane
IMes	1,3-bis(2,4,6-trimethylphenyl)imidazol-2-ylidene
Me	methyl
MeCN	acetonitrile
Mes	mesityl, 2,4,6-trimethylphenyl
NBO	natural bond order
NHC	N-heterocyclic carbene
NMR	nuclear magnetic resonance
OAc	acetate anion
Ph	phenyl
R	alkyl or aryl group
^t Bu	<i>tertiary</i> -butyl
THF	tetrahydrofuran
TON	turn over number
X	halogen

Table of Contents

1	REVIEW OF THE CURRENT LITERATURE	1
1.1	Introduction	1
1.2	The history of carbenes	2
1.2.1	Stable singlet carbenes	3
1.2.1.1	Carbene properties and stability	4
1.2.2	Carbene complexes	7
1.2.2.1	Transition metal <i>N</i> -heterocyclic carbene complex synthesis	8
1.2.3	Carbene complexes as catalysts	12
1.2.3.1	The success of NHC carbene catalysts	13
1.2.3.2	Limitations of NHC complexes in catalysis	14
1.3	Aims and thesis overview	16
1.4	References	18
2	THIAZOLE BASED PALLADIUM CARBENE COMPLEXES	27
2.1	Introduction	27
2.2	Computational details	30
2.3	Results and discussion	31
2.3.1	Theoretical considerations – the effect of sulfur and bridging ligands on palladium carbene complexes	31
2.3.2	Chelating thiazolylidene ligands - xylene linked biscarbene complexes	32
2.3.3	Chelating thiazolylidene ligands – carbene/pyridine linked complexes	34
2.3.3.1	Bridging 3-(pyridin-2-ylmethyl)thiazolylidene ligands	34
2.3.3.2	Bulk in position 5 – will it help with palladium thiazole based carbene complexes?	37
2.4	Conclusions	48
2.5	Experimental	50
2.5.1	Salt precursors	50
2.5.2	Thiazolium salts	51
2.5.3	Palladium complexes	54
2.6	References	56

3	OXIDATIVE ADDITION OF AZOLIUM SALTS TO A MODEL WILKINSON'S CATALYST	59
3.1	Introduction	59
3.2	Computational details	61
3.3	Results and discussion	62
3.3.1	Stereoisomers	62
3.3.2	Pathway studies – dissociative vs associative	65
3.3.2.1	Dissociative route	66
3.3.2.2	Associative or dissociative route?	68
3.3.3	Phosphine ligand effects	70
3.3.4	Solvent effects	73
3.3.4.1	Explicit addition of a THF molecule	73
3.3.4.2	Bulk solvent effects	76
3.3.5	The effect of different azolium salts	78
3.3.5.1	Imidazolidium salts	78
3.3.5.2	Thiazolium salts	81
3.4	Conclusions	86
3.5	References	87
4	RHODIUM AND IRIIDIUM OXIDATIVE ADDITION REACTIONS	92
4.1	Introduction	92
4.2	Computational details	95
4.3	Results and discussion	96
4.3.1	Ligand effects – C-H activation	96
4.3.1.1	Rh(dmiy)(CO) ₂ Cl	96
4.3.1.2	Rh(dmiy)(CO)(PMe ₃)Cl	99
4.3.1.3	Rh(PH ₃) ₂ (dmiy)Cl	102
4.3.1.4	Rh(PH ₃)(dmiy) ₂ Cl	105
4.3.1.5	Chelation - Rh(PH ₃)(mbiy)Cl	108
4.3.1.6	Overall rhodium C-H activation summary	110

4.3.2	C-C activation with Rh(dmiy) ₂ (PH ₃)Cl	114
4.3.2.1	Steric influences of C-C activation	115
4.3.2.2	Electronic effects of C-C activation	116
4.3.2.3	Overall C-C activation with Rh(dmiy) ₂ (PH ₃)Cl	117
4.3.3	Oxidative addition with iridium	118
4.3.3.1	Ir(PMe ₃) ₃ Cl – C-H activation	118
4.3.3.2	Ir(PMe ₃) ₃ Cl – C-C activation	121
4.4	Conclusion	124
4.5	References	126
5	NICKEL CATALYSTS FOR AZOLIUM C-C COUPLING REACTIONS	130
5.1	Introduction	130
5.2	Computational details	132
5.3	Results and discussion	133
5.3.1	Individual step considerations	133
5.3.1.1	Starting materials	133
5.3.1.2	Oxidative addition	134
5.3.1.3	Coordination of ethylene	138
5.3.1.4	Ethylene insertion	142
5.3.1.5	Reductive elimination	146
5.3.2	Overall cycle	150
5.3.2.1	Ni(dmiy) ₂	150
5.3.2.2	Ni(PMe ₃)(dmiy)	152
5.3.2.3	Ni(PMe ₃) ₂	155
5.3.2.4	Ni(PPh ₃) ₂	158
5.3.2.5	Ni(P ^t Bu ₃) ₂	162
5.3.3	Cycle comparison	164
5.3.4	Catalysis at the azolium 5-carbon	166
5.3.5	Catalysis for N-methylimidazole	169
5.4	Conclusions	173
5.5	References	175

6	RHODIUM CATALYSTS FOR C-C COUPLING REACTIONS	178
6.1	Introduction	178
6.2	Computational details	181
6.3	Results and discussion	182
6.3.1	Imidazole catalysis	182
6.3.1.1	Completion of the Bergman cycle	182
6.3.1.2	The Cavell/McGuinness mechanism	188
6.3.1.3	Comparison of the Bergman and Cavell/McGuinness mechanisms	197
6.3.2	Imidazole catalysis - alternative products	201
6.3.2.1	Alkene binding direction	202
6.3.2.2	The influence of substrate geminal methyls	211
6.3.2.3	Conclusions for product isomer preference	218
6.3.3	Acid catalysed coupling	219
6.3.3.1	Acid catalysed Cavell/McGuinness mechanism	220
6.3.3.2	Acid catalysed Bergman mechanism	223
6.3.3.3	Overall acid catalysis effects	226
6.4	Conclusions	229
6.5	References	231

1 Review of the Current Literature

1.1 Introduction

A catalyst is described as “a substance that increases the rate of a reaction but is not itself consumed”¹. Used both in nature and in the laboratory, they have become very important in today’s industry for the production of many types of organic compounds that would otherwise not be available on an industrial scale due to slow, unselective, or expensive non-catalysed reactions. It was estimated that in 1994, catalysts contributed one-sixth the value of all manufactured goods in industrialised countries, and that 13 of the top 20 synthetic chemicals used catalysts¹. As such, it is not surprising there has been extensive study carried out in the use of catalysts in recent years.

Homogenous catalysis, where the complexes used are in the same phase as the reactants, took a big leap forward when Otto Roelen used a catalyst for the oxo synthesis in 1938². While it was originally thought homogenous catalysis would not take off due to problems with separation of the catalysts from reaction products, many benefits in their use were recognised and research in the area persisted.

In general, homogenous catalysts display high activity and high product selectivity under mild conditions and are much more stable towards poisoning than are heterogeneous catalysts³. In addition, one of the most important advantages of homogenous catalysis is the ability to investigate the mechanism for reactions much more readily than for heterogeneous methods⁴. Combined with a capacity for controlling steric and electronic properties of the catalysts themselves, this makes designing and refining homogenous catalysts for customised products possible; a huge advantage over the previously used heterogeneous catalysts.

For many important catalytic reactions to date, phosphines have been the ligands of choice for the metals in catalysts. As good 2-electron sigma donors, they provide the metal centre with direct electron density with minimal backbonding. Further, substitution of the R groups attached to the phosphine give the ligand great versatility, both electronically and sterically, allowing for excellent control over important catalyst characteristics.

Despite their popularity, phosphines possess a small number of undesirable qualities that are a cause for concern in many reaction conditions. Often the phosphines employed in catalytic reactions are not environmentally friendly and in many cases, toxic. More importantly, degradation of the catalyst occurs through P-C cleavage within the phosphine and as such, an excess of phosphine is required in many reactions.

Recently, a new type of ligand has emerged as a popular replacement for phosphines. With many similar properties to the related phosphines, carbenes display further benefits to catalysis that mean they have become an exciting ligand class for the future.

1.2 The history of carbenes

Carbenes are “uncharged compounds with a divalent carbon atom and two unshared electrons”⁵ (Figure 1-1). First introduced over 100 years ago⁶, many reactions studied at various times in the past have shown an unusually stable intermediate, which was thought to be a carbene. The demonstrated stability of these carbenes challenged researchers to isolate the free carbenes⁷.

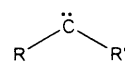


Figure 1-1
A simple carbene

In general, carbenes take on a bent shape, implying sp^2 hybridisation at the carbene carbon⁸. This leaves an unchanged p_y orbital perpendicular to the sp^2 plane, suggesting 4 possible ground state spin multiplicities: 1 triplet and 3 singlet states⁸ (Figure 1-2). In general for the three singlet states, singlet state **(b)** is more stable than **(c)**, and **(d)** can be considered an excited singlet state.

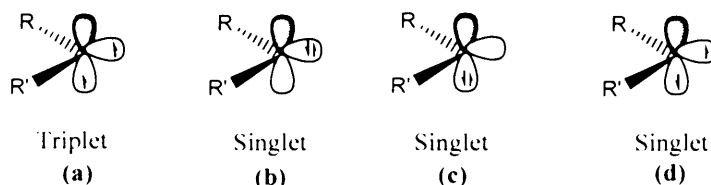


Figure 1-2 Carbene ground state spin multiplicities

The singlet/triplet gap for carbenes has been studied extensively, mainly by theoretical methods^{9, 10}. Whether a carbene takes on a singlet or triplet state depends largely on the substituents surrounding the carbene centre, with a σ - π gap of 2 eV required to give

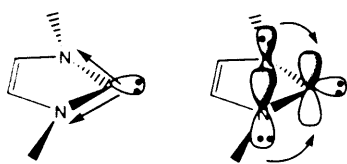


Figure 1-3 Stabilisation of the singlet carbene

a singlet carbene by interaction of the unoccupied carbene p orbital with aromatic electrons. As such, σ electron withdrawing substituents favour the singlet state as they can stabilise the carbene lone pair⁹, while π electron donors can stabilise the formally empty p π orbital^{5, 11}.¹²(Figure 1-3).

Steric bulk around the carbene centre also plays a minor role in determining the carbene ground state. The triplet state is favoured by linear molecules, and as bulkier substituents tend to repel each other, carbenes with very bulky substituents prefer the triplet state^{11, 12}.

Overall, with a large variety of both steric and electronic properties available in the substituents flanking the carbene centre, a non-linear triplet ground state has been experimentally established for the majority of carbenes⁵.

1.2.1 Stable singlet carbenes

In the 1960's, Wanzlick tried to isolate the first free nucleophilic singlet carbene using the σ electron withdrawing/ π electron donating carbene substituent hypothesis. In addition, he postulated the resonance provided by a ring structure would help stabilise the singlet carbene¹³. As such, he introduced the imidazole ring into carbene chemistry.

Unfortunately, all his attempts to isolate free carbenes based on the imidazole ring failed¹⁴ and cross coupling experiments proved the dimers he was forming were not in equilibrium with the carbenes themselves^{15, 16}. Recently, Denk et al¹⁷ and Hahn et al¹⁸ found proof to the contrary, although there is contradictory proof that Wanzlick's conclusions were valid¹⁹ with the reasons for carbene dimerisation recently becoming clearer²⁰.

Despite the disappointment at not being able to isolate free carbenes, Wanzlick did trap the carbenes he created in a mercury complex^{14, 21} (Figure 1-4).

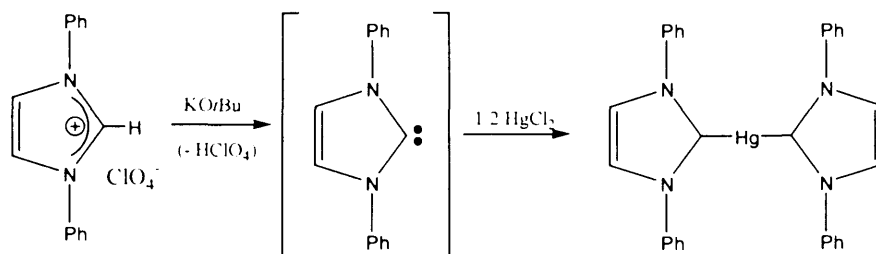


Figure 1-4 Early trapping of carbenes as a mercury complex

Thirty years later, Arduengo adopted the same ideas postulated by Wanzlick to isolate

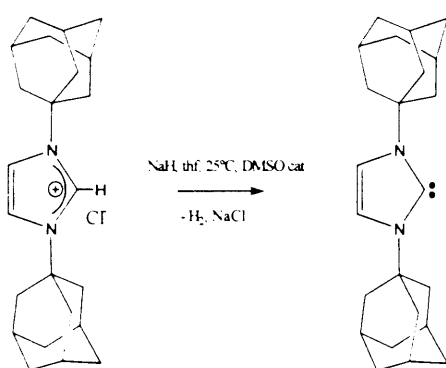


Figure 1-5 The first stable singlet carbene
(1,3-di(1-adamantyl)imidazol-2-ylidene)

the first free carbene by deprotonation of imidazolium salts using sodium hydride and catalytic amounts of the DMSO anion²² (Figure 1-5). While the NMR produced proved this was a singlet, further *ab initio* MO calculations confirmed the singlet carbene was more stable than the triplet²³.

Amazingly, this carbene showed no decomposition in d⁸-THF under a few atmospheres of carbon monoxide after several years⁷.

1.2.1.1 Carbene properties and stability

The next challenge facing singlet carbene chemistry revolved around understanding the reasons for their stability. Arduengo's free carbene contained many characteristics that could explain their unusual stability. The imidazole system provided nitrogen σ -acceptors, π -donors, and a ring system in which to delocalise the π -electron system even further. In addition, Arduengo had substituted the ring nitrogens with the very bulky adamantyl groups, providing steric protection for the carbene centre. Which of these factors, individually or in combination was most affecting the stability of the carbenes? What followed was an in depth look at both the kinetic and thermodynamic possibilities for stability²⁴⁻³³.

It is now well accepted that the main reason for the stability of *N*-heterocyclic carbenes is due to the σ -electron withdrawing and π -donation ability of the heteroatoms adjacent to the carbene carbon. Planar molecules with potential π -delocalisation (eg NCN) stabilise the carbene carbon with respect to methylene by about 70 kcal mol⁻¹²⁶. Further, when the C₄ and C₅ carbons are joined to form a saturated ring, up to 6 kcal mol⁻¹ of additional stability may be observed. Inclusion of a double bond in the backbone of the ring (C₄=C₅) creating a truly aromatic ring, may add up to 26 kcal mol⁻¹ of stability²⁶. Overall, *N*-heterocyclic carbenes that include all of these characteristics have been found to have the largest singlet/triplet gap for any divalent compound at around 85 kcal mol⁻¹³⁴.

These ideas have all been combined by various groups experimentally to isolate a considerable variety of free carbenes including saturated (**a**^{32,35}), acyclic (**b**³⁶, **c**³⁷), sterically unhindered (**d**^{38,39}), bi- (**e**⁴⁰) and tri-dentate (**f**⁴¹), functionalised (**g**⁴²), backbone substituted (**h**^{43,44}), heteroatom substituted (**i**⁴⁵, **j**⁴⁶, **k**⁴⁷, **l**⁴⁸)^{30,31,49}, and single donor carbenes (**m**⁵⁰, **n**⁵¹) (Figure 1-6).

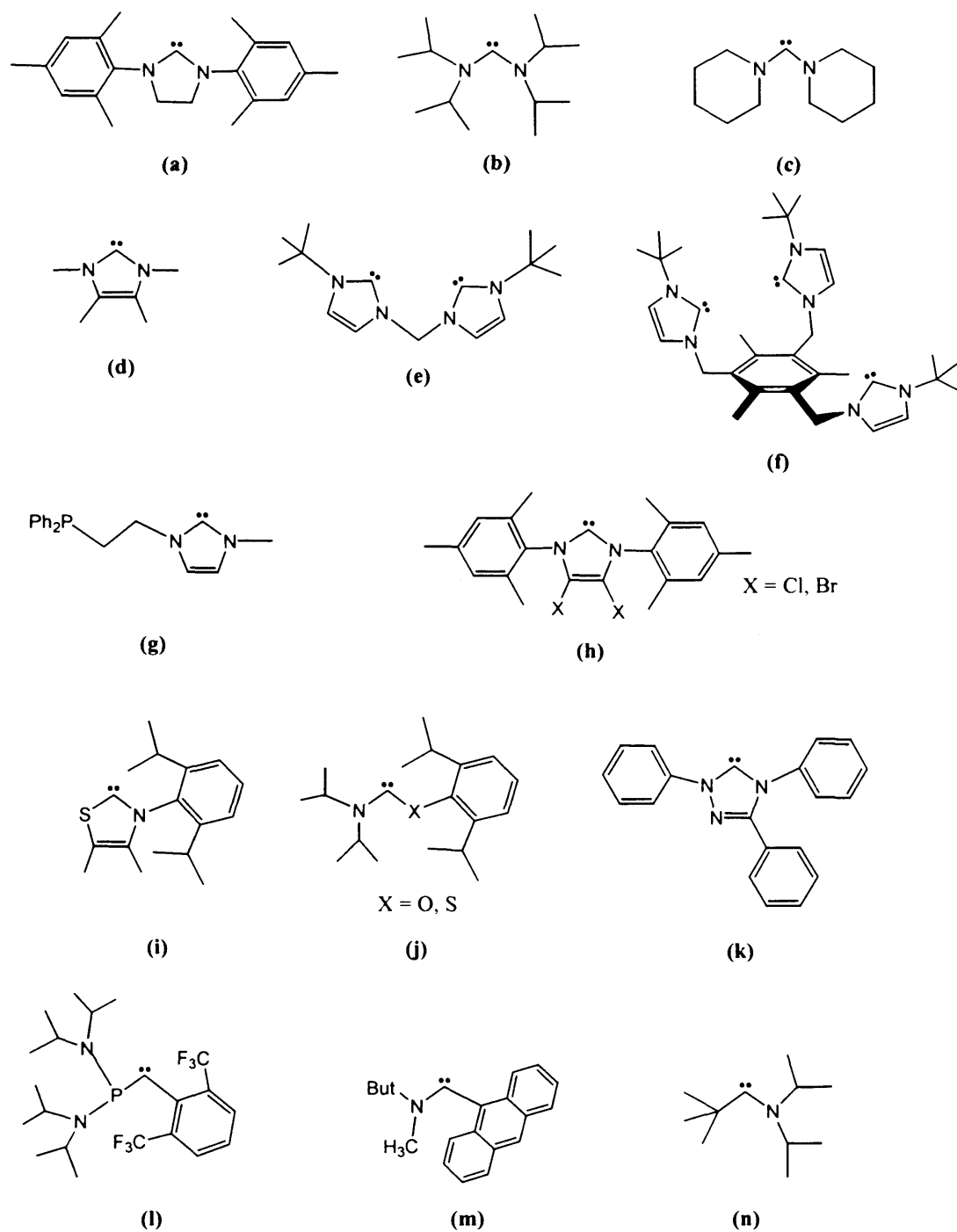
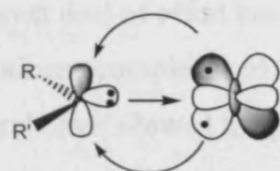


Figure 1-6 Isolated free carbenes

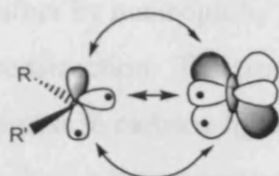
1.2.2 Carbene complexes

Fischer first introduced carbenes into organometallic chemistry in 1964⁵². The



Fischer Complex

(a)



Schrock Complex

(b)

Figure 1-7 Bonding in carbene complexes

complexes he synthesised all exhibited σ -donor/ π -acceptor behaviour for the bound carbene, and exhibited metal to carbon bonds shorter than the usual single bond⁵.

With the synthesis of further carbene complexes, it became apparent there were two distinct types of complexes emerging. Fischer carbene complexes combine weakly donating singlet carbene, which accepts back bonding from low-valent metal^{4,5,8} (Figure 1-7 a). In contrast, the Schrock carbene complexes that emerged combined a covalent triplet carbene and triplet metal fragment (Figure 1-7 b). These carbenes generally contain alkyl substituents, are nucleophilic, and coordinate with high oxidation state metals.

Arduengo's success at isolating free carbenes generated renewed interest in nucleophilic carbene complexes. At first glance, N-heterocyclic carbenes such as Arduengo's may appear to yield Fischer carbene complexes upon bonding to a metal centre, but the bonding properties actually display entirely different characteristics. Due to the back donation from the adjacent heteroatoms and their strong capacity as σ -donors to metals, N-heterocyclic carbene ligands form only a single σ -bond to metals with π -back donation negligible^{5,8} and therefore these complexes exhibit very different reaction chemistry to either Fischer- or Schrock-type complexes.

With renewed interest in the field of carbene and carbene coordination chemistry, many new carbene complexes were synthesised. Carbenes are now known to coordinate to a wide variety of metals, from main group to rare earth metals⁵³⁻⁵⁷.

Further, electron rich transition metals have been used to synthesise a variety of interesting and catalytically active carbene complexes^{58,57,59-65,66}. It is these transition metal complexes suitable for catalysis that form the basis of this study.

1.2.2.1 Transition metal *N*-heterocyclic carbene complex synthesis

As the vast majority of complexes suitable for catalysis involve transition metals, a great deal of effort has been expended refining simple methods for synthesising carbene complexes of the transition metals. A number of routes have been developed, and have allowed the preparation of complexes bearing carbene ligands with a large variety of electronic and steric properties⁶⁷.

In a significant number of cases, the azolium salt of the carbene is initially synthesised either by nucleophilic substitution of the related azole, or by a multi-component construction. The straightforward synthesis of a range of imidazolium salts provides access to carbene ligands with a variety of electronic and steric properties, ideal for tailoring the properties of the resulting complex as catalysts.

1.2.2.1.1 *In-situ deprotonation of azolium salts*

A popular and straightforward route to many carbene complexes has been the *in-situ* deprotonation of azolium salts. These methods involve the use of a base to directly deprotonate the azolium salt in the presence of a metal acceptor and do not require the free carbene to be isolated, with three main methods commonly used: basic metallate anions, basic metal ligands and external bases.

The use of basic metallate anions has the advantage that the metal used to deprotonate the azolium salt becomes the ligand acceptor. While this limits the final oxidation state of the metal, a variety of complexes have been created successfully by this method⁶⁸⁻⁷⁰ (Figure 1-8).

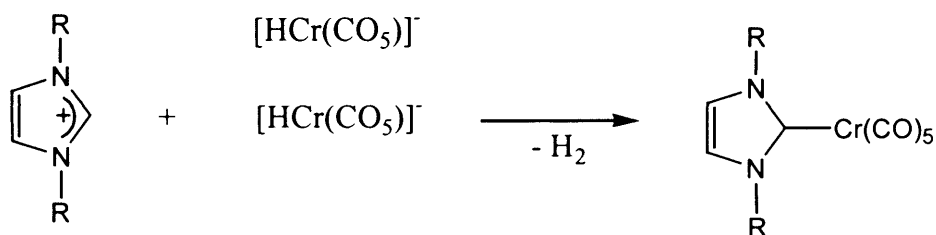


Figure 1-8 Carbene complexes through basic metallate anion deprotonation

The use of basic metal salts is another popular method for creating carbene complexes, generally through metals with acetate^{59, 71-75}, alkoxo^{59, 76} or oxide^{77, 78} ligands. Despite being a relatively simple method, the imidazolium counterion is generally incorporated into the nascent carbene complex unless non-coordinating anions are used. Good yields generally require the use of a solvent, such as THF or DMSO, however solvent-free reactions have still been successful^{59, 72} (Figure 1-9).

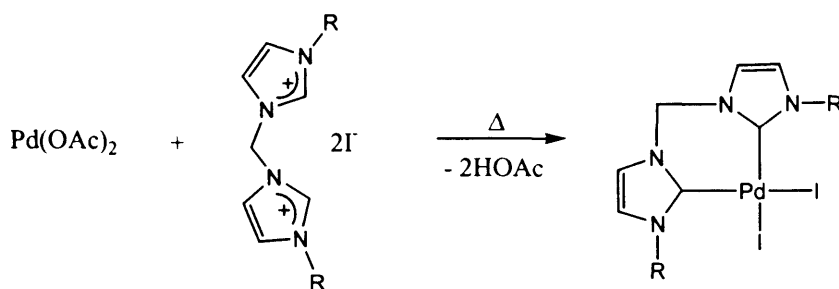


Figure 1-9 Carbene complexes through basic ligand deprotonation

The use of an external base can allow the formation of dimeric complexes not produced in other reactions. Popular external bases include potassium⁷⁹ and lithium⁸⁰ *tert*-butoxide, sodium hydride⁶⁶, butyl lithium^{81, 82}, and to a lesser extent triethylamine^{83, 84} and phosphazenes⁸⁵ (Figure 1-10).

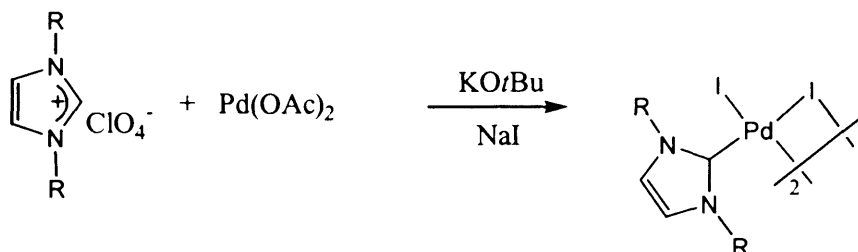


Figure 1-10 Carbene complexes through external base deprotonation

Finally, molecules of methanol and chloroform can be eliminated from the diaza-*ortho*-ester^{47, 86} and trichloromethyl-substituted⁸⁷⁻⁸⁹ relatives of imidazolium salts. Thermal elimination of the 2-substituents results in the carbene, which can then be trapped by a suitable metal precursor.

1.2.2.1.2 Complexes via free carbenes

After Arduengo first isolated 1,3-diamantylimidazol-2-ylidene, a wide variety of new carbene complexes could be synthesised readily with few requirements on the metal precursor complex. While various methods, such as thermal elimination of methanol^{47, 86} and chloroform⁸⁷⁻⁸⁹ can be utilised to generate the free carbenes, use of the strong bases sodium hydride and potassium *tert*-butoxide in THF^{22, 31}, or a mixture of THF and liquid ammonia^{42, 59} are the most popular routes (Figure 1-11).

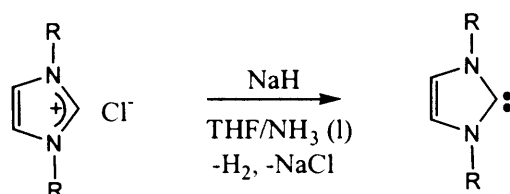


Figure 1-11 Free carbene synthesis

Once the free carbene has been formed, complexation is generally straightforward. Among the most popular methods of complex synthesis are cleavage of dimeric metal precursors with bridging ligands such as halides, or carbon monoxide^{42, 59, 90-94}, and exchange of other ligands on the metal centre such as phosphines^{40, 73, 95, 96}, carbon monoxide^{66, 80, 90, 97}, solvents^{58, 60, 63-66, 73, 98, 99}, or olefins^{61, 100-102} (Figure 1-12).

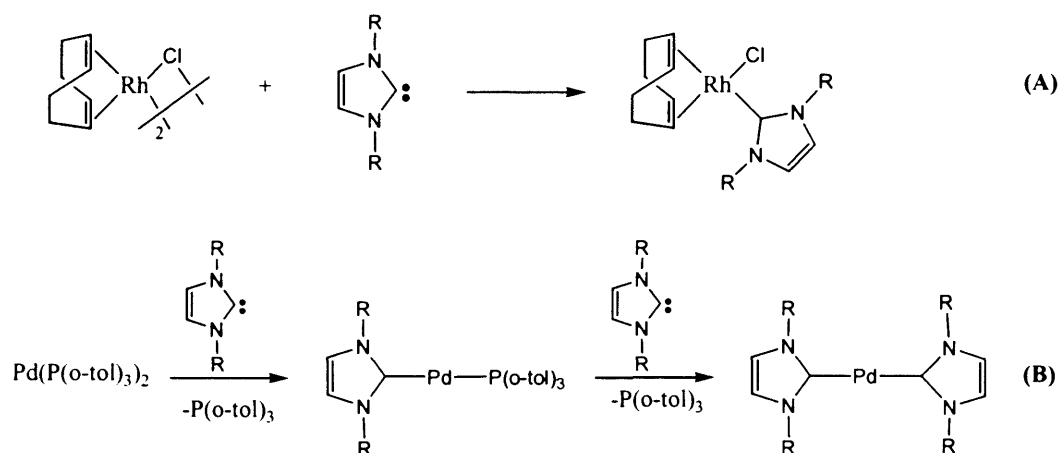


Figure 1-12 Carbene complex formation from free carbenes and dimeric cleavage (A) and phosphine exchange (B)

1.2.2.1.3 Ligand transfer reactions

Intermolecular transfer of carbene ligands from one metal to another has proved a popular method for the preparation of carbene complexes not directly accessible by other routes. This method was observed in the disproportionation of $(\text{dmiy})\text{Cr}(\text{CO})_5$, to yield $(\text{dmiy})_2\text{Cr}(\text{CO})_4$ and $\text{Cr}(\text{CO})_6$ ¹⁰³. It was then discovered chromium, molybdenum and tungsten complexes could be used for carbene transfer to a variety of metals including rhodium(I), palladium(II), platinum(II), copper(I), silver(I) and gold(I)¹⁰⁴⁻¹⁰⁶. Success has similarly been found for silver carbene complexes formed by *in-situ* deprotonation of the azolium salts with silver oxide or silver carbonate, with transfer to group 8 and 10 metals^{78, 107} (Figure 1-13).

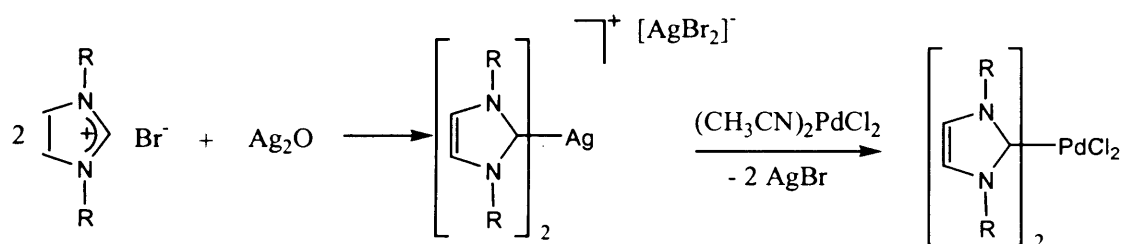


Figure 1-13 Carbene complex formation via silver transfer reactions

1.2.2.1.4 Oxidative addition reactions

Recently the acidity of the C2 substituent has been utilised in synthesising carbene complexes from C-H activation of the azolium salts by low-valent metal precursors¹⁰⁸⁻¹¹². The groups of Lappert¹¹³ and Stone *et al.* used a similar method in the 1970's for creating thiazol-2-ylidene complexes from 2-chlorothiazolium salts^{114, 115}. While generally restricted to nickel, palladium, platinum, rhodium and iridium, these are some of the more commonly used metals in catalysis and oxidative addition reactions of azolium salts may provide an easily accessible route to catalytically active carbene complexes (Figure 1-14).

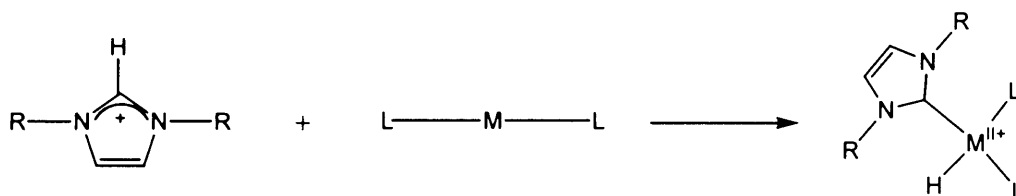


Figure 1-14 Carbene complexes from azolium oxidative addition

1.2.2.1.5 *Other methods*

Various other methods have been successfully employed for the preparation of carbene complexes. These include vapour phase synthesis for sublimable free carbenes¹¹⁶, building of the carbene onto the metal centre¹¹⁷⁻¹²⁰ and transmetallation of 2-lithioimidazoles¹²¹. Although highly successful, preparation of carbene complexes via these methods tend to be highly specific and have not been general enough to create a range of complexes for varying carbene ligands as found for other methods described above.

1.2.3 Carbene complexes as catalysts

Many of the original Fischer- and Schrock-based carbene complexes had been trialed in catalytic reactions, however they had a tendency to suffer from M-C cleavage, rendering them catalytically inactive⁵. In contrast, *N*-heterocyclic carbene ligands form exceptionally stable bonds with metals and are able to accommodate a wide range of oxidation states, making them very suitable for many catalytic cycles.

As 2-electron donors, carbene ligands are related to ethers, amines, isonitriles, and phosphines with regard to coordination chemistry⁵. In fact, the σ -donor ability of nucleophilic carbene ligands has been shown to be very similar to electron rich phosphines, and it was this that caused the realisation that the carbene complexes may be good in homogenous catalysis⁶⁶.

In fact, it was a need for polymer cross-linking catalysts that led Arduengo back to stable carbenes in the 1980's⁷. By 1994, the promise of *N*-heterocyclic carbene complexes as catalysts was steadily evolving as indicated by the publication of many patents, with the *N*-heterocyclic carbene ligands much more strongly bound to the metal centre compared to their phosphine counterparts and showing little π -backdonation from the metal centre⁵. Interestingly, these patents generally involved the use of unsaturated carbenes, as the saturated analogues tested had shown no improvement over traditional phosphine complexes^{122, 123}.

Further, as demonstrated in the previous section, a wide variety of routes are available to synthesise carbene complexes with diverse steric and electronic properties. As such, it is not surprising a substantial amount of effort has been invested into the catalytic

properties of *N*-heterocyclic carbene complexes with success found in numerous important applications.

1.2.3.1 The success of NHC carbene catalysts

Carbene complexes show a remarkable stability in many catalytic environments, and are often stable to heat, oxygen and moisture. Further, the catalysts can frequently be synthesised *in-situ* without the necessity of prior isolation. As such, the carbene complexes are now known to catalyse a wide range of organic reactions including hydrogenation of olefins¹²³⁻¹²⁵, hydroformylation¹²⁶, hydrosilylation^{42, 80, 90, 91, 123, 127-129}, olefin metathesis^{94, 95, 126, 130-133}, polymerisation of alkynes¹³⁴, cyclopropanation¹³⁵, furan synthesis¹³⁶, and atom transfer radical polymerisation of vinyl monomers¹³⁷.

Another area of importance where carbenes have found considerable success is in C-C coupling reactions, including the Suzuki, Stille and Heck reactions^{100, 138-141}. Carbenes were first used as catalysts in the Heck reaction in 1995 by Hermann and co workers^{72, 142}. The palladium carbene complexes involved were often stable beyond 300°C, and could withstand oxidative conditions that destroy their phosphine counterparts³. This unusual stability meant that chloroarenes could be successfully used in the reaction, with no byproduct-formation being observed^{3, 72, 142}.

Whilst the carbene complexes produced good TONs, the reaction seemed to have an induction period, possibly related to the reduction of Pd(II) to Pd(0) at the start of the catalytic cycle. In many cases, adding a reducing agent avoided the induction period⁷², as did starting with a Pd-methyl complex¹⁰¹. The Pd-methyl complexes produced were comparable in TONs and TOFs to the highly active palladacycles³.

Since the initial discovery of the advantages of carbene complexes in the Heck reaction, many results have been published tailoring the catalysts and investigating the probable mechanism involved^{72, 79, 100, 101, 140-146}.

1.2.3.2 Limitations of NHC complexes in catalysis

While in general carbene catalysts have performed remarkably well and show great promise as efficient and environmentally friendly catalysts, some reactions have indicated the NHC ligands may not always behave as desired and certain characteristics of the ligands should be considered when employing carbene complexes in a catalytic environment.

1.2.3.2.1 Carbene 'wrong-way' binding

Most *N*-heterocyclic carbene complexes used in catalysis contain ligands bound to the metal through the C2 carbon of the carbene. However, in a study by Crabtree *et al.* using a pyridine-linked imidazolium salt and $\text{IrH}_5(\text{PPh}_3)_2$, unusual binding was discovered with the carbenes coordinating through the ring C4¹⁴⁷ (Figure 1-15).

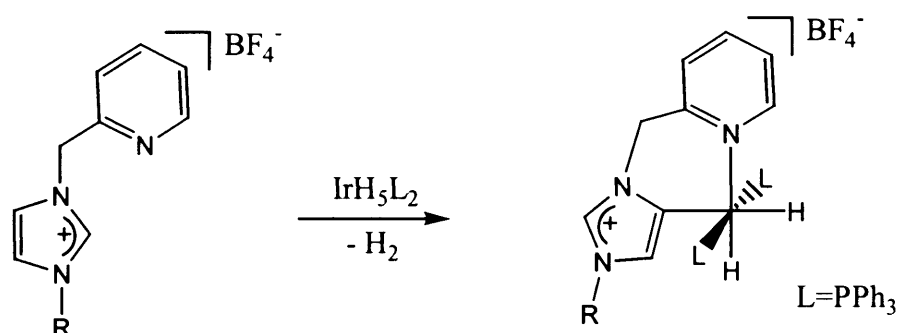


Figure 1-15 'Wrong Way' binding for iridium carbene complexes

Despite experimental and theoretical results indicating the C2 bonding is much more thermodynamically favourable¹⁴⁸, steric crowding¹⁴⁹ and the selection of imidazolium salt counter ion¹⁵⁰ can affect the binding of the carbene ligands. With many catalytic carbene complexes prepared *in-situ*, care should be taken when designing reactions as minor changes in reaction conditions can greatly affect the expected catalytic properties and hence overall reaction outcomes.

1.2.3.2.2 Catalyst decomposition

Initial success was found for the copolymerisation of CO and ethylene with application of chelating dicarbene palladium catalysts resulting in high molecular weight, strictly alternating polymers¹⁵¹. However, in a study by McGuinness *et al.*, the carbene catalyst decomposed during the reaction, giving unsatisfactory results¹⁵². Further investigation indicated decomposition was a result of reductive elimination of cis located carbene and alkyl or acyl ligands^{110, 153, 154}(Figure 1-16).

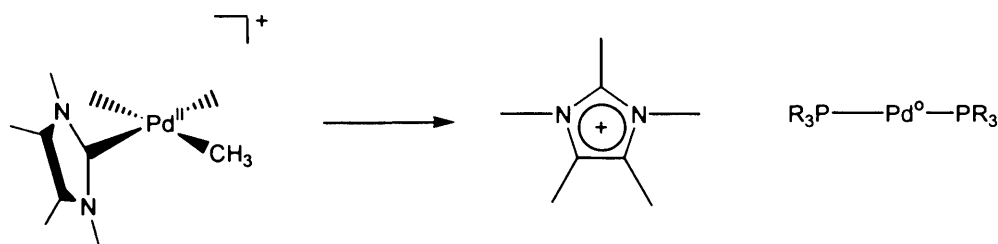


Figure 1-16 Decomposition for the carbon monoxide ethylene copolymerisation

This reaction is thought to be assisted by the twist of the carbene with respect to the square planar Pd(II) centre by approximately 60°, allowing the formally empty p orbital on the carbene centre to be directed towards the alkyl/acyl group adjacent to it on the metal centre. As the acyl/carbene intermediates are necessary intermediates in the CO/ethylene catalytic cycle, the decomposition route was quite disturbing, and there have been no further reports of successful carbene complex catalysis of this reaction.

1.3 Aims and thesis overview

Despite the recent success of many carbene-based catalysts, there remain factors adversely affecting some reactions where the cause is either unknown, or there has been no general solution. In many of these catalytic cycles, minor adjustments to environment can dramatically affect reaction outcomes. The aim of this project was to clarify selected internal and external factors affecting carbene catalysis with the intention of increasing the stability, reactivity and selectivity of some of these reactions.

In particular, focus was given to three main areas: an improved carbene catalyst for carbon monoxide/ethylene copolymerisation; factors affecting oxidative addition reactions of azolium salts to create carbene complexes; and the mechanisms involved in carbon-carbon coupling reactions between ethylene and azoles or azolium salts.

Section 1 (Chapter 2) outlines the study of novel carbene complexes designed to overcome the reductive elimination decomposition found for monodentate palladium carbene complexes for the carbon monoxide/ethylene copolymerisation. It was anticipated the different electronic and steric properties provided by chelating thiazole-based carbene ligands could overcome the factors contributing to catalyst decomposition. This chapter outlines theoretical and experimental results for thiazole-based carbene complexes and their use as catalysts.

Section 2 (Chapters 3 and 4) focuses on one of the major steps common to many catalytic systems: oxidative addition. As mentioned, reductive elimination of a carbene and an adjacent ligand can be a cause of catalyst decomposition.

Strengthening the characteristics for reversal of this reaction through oxidative addition of azolium salts may not only stabilise existing catalysts, but may lead to an easily accessible route for *in-situ* synthesis of new carbene complexes suitable for catalysis. Further, these studies have implication on the growing popularity of imidazolium ionic liquids in catalysis, with the ionic liquids not necessarily the innocent bystanders they are often assumed to be.

Chapter 3 focuses on the theoretical study of oxidative addition of 1,3-dimethylimidazolium to a system well known for these types of reactions:

Wilkinson's catalyst. The effect of phosphine ligand lability, phosphine exchange, explicit and bulk solvation, and the change of the starting azolium on product thermodynamics and reaction energetics are all examined.

As previously reported results and results from Chapter 3 indicate oxidative addition reactions are promoted by basic ligands, the study was extended to include complexes incorporating the highly basic carbene ligands in the metal reactant. As such, Chapter 4 outlines theoretical results for systematic electronic and steric exchange of carbon monoxide, phosphine and carbene ligands on the oxidative addition of 1,3-dimethylimidazolium to rhodium and iridium.

Section 3 (Chapters 5 and 6) involves theoretical mechanistic studies of carbon-carbon coupling reactions of alkenes to azoles and azolium salts. In particular, Chapter 5 centres on the nickel-based catalytic conversion of imidazolium salts to 2-alkyl imidazolium salts. Experimentally, success was found through the use of nickel phosphine complexes, with a carbene equivalent complex producing an unusually stable nickel hydride that halted further reaction. The theoretical study in this chapter presents results on an oxidative addition, alkene coordination and insertion, and reductive elimination cycle (Cavell/McGuinness mechanism) including indications as to why the carbene complex fails as a catalyst while the phosphine equivalent succeeds. Further results follow the reaction of the related azole, and the possibility of the coupling reaction occurring at position 4 or 5 of the azolium ring.

Finally, Chapter 6 examines the same mechanism studied in Chapter 5 for related azole carbon-carbon coupling reactions using a rhodium catalyst. Bergman has successfully catalysed many azoles and alkenes experimentally using a rhodium phosphine complex and in one paper proposes an unusual mechanism for the reaction involving a rhodium carbene intermediate. This chapter compares the Cavell/McGuinness mechanism to that proposed by Bergman including factors affecting the overall reaction such as phosphine lability, product thermodynamics alkene isomerisation, alkene coordination, added bulk on the alkene chain, and acid assisted catalysis.

1.4 References

- 1 D. F. Shriver, P. W. Atkins and C. H. Langford, 'Inorganic Chemistry, Second Edition', Oxford University Press, 1994.
- 2 B. Cornils, W. A. Herrmann and M. Rasch, *Angew. Chem. Int. Ed. Engl.*, 1994, **33**, 2144.
- 3 B. Cornils and W. A. Herrmann, 'Applied Homogenous Catalysis with Organometallic Compounds', VCH Verlagsgesellschaft mbH/VCH Publishers, 1996.
- 4 R. H. Crabtree, 'The Organometallic Chemistry of the Transition Metals', John Wiley & Sons, Inc, 1988.
- 5 W. A. Herrmann and C. Köcher, *Angew. Chem. Int. Ed. Engl.*, 1997, **36**, 2162.
- 6 E. Buchner and T. Curtis, *Ber. Dtsch Chem. Ges.*, 1885, 2377.
- 7 A. J. Arduengo III, *Acc. Chem. Res.*, 1999, **32**, 913.
- 8 D. Bourissou, O. Guerret, F. Gabbai and G. Bertrand, *Chem. Rev.*, 2000, **100**, 39.
- 9 K. Irkura, W. A. Goddard and J. L. Beauchamp, *J. Am. Chem. Soc.*, 1992, **114**, 48.
- 10 B. C. Gilbert, D. Griller and A. S. Nazran, *J. Org. Chem.*, 1985, **50**, 4738.
- 11 R. Hoffmann, G. D. Zeiss and G. W. Van Dine, *J. Am. Chem. Soc.*, 1968, **90**, 1485.
- 12 N. C. Baird and K. F. Taylor, *J. Am. Chem. Soc.*, 1978, **100**, 1333.
- 13 H. W. Wanzlick, *Angew. Chem. Int. Ed. Engl.*, 1962, **1**, 75.
- 14 H. J. Schönher and H. W. Wanzlick, *Chem. Ber.*, 1970, **103**, 1037.
- 15 H. E. Winberg, *Angew. Chem. Int. Ed. Engl.*, 1968, **7**, 766.
- 16 H. E. Winberg, J. E. Carnahan, D. D. Coffman and M. Brown, *J. Am. Chem. Soc.*, 1965, **87**, 2055.
- 17 M. K. Denk, K. Hatano and M. Ma, *Tetrahedron Lett.*, 1999, **40**, 2057.
- 18 F. E. Hahn, L. Wittenbecher, D. Le Van and R. Fröhlich, *Angew. Chem. Int. Ed. Engl.*, 2000, **39**, 541.

- 19 Y. Liu and D. M. Lemal, *Tetrahedron Lett.*, 2000, **41**, 5999.
- 20 R. W. Alder, M. E. Blake, L. Chaker, J. N. Harvey, F. Paolini and J. Schütz, *Angew. Chem. Int. Ed.*, 2004, **43**, 5896.
- 21 H. W. Wanzlick and H. J. Schönher, *Liebigs Ann. Chem.*, 1970, **731**, 136.
- 22 A. J. Arduengo III, R. L. Harlow and M. Kline, *J. Am. Chem. Soc.*, 1991, **113**, 361.
- 23 N. Kuhn, H. Boehmen and G. Henkel, *Z. Naturforsch B*, 1994, **49**, 1473.
- 24 C. Heinemann and W. Thiel, *Chem. Phys. Lett.*, 1994, **217**, 11.
- 25 D. A. Dixon and A. J. Arduengo III, *J. Phys. Chem.*, 1991, **95**, 4180.
- 26 C. Heinemann, T. Müller, Y. Apeloig and H. Schwarz, *J. Am. Chem. Soc.*, 1996, **118**, 2023.
- 27 C. Boehme and G. Frenking, *J. Am. Chem. Soc.*, 1996, **118**, 2039.
- 28 H. Kellmar, *Tetrahedron Lett.*, 1970, **38**, 3337.
- 29 J. Cioslowski, *Int. J. Quantum Chem.*, 1993, **27**, 309.
- 30 A. J. Arduengo III, H. V. R. Davis, D. A. Dixon, R. L. Harlow, W. T. Klooster and T. F. Koetzle, *J. Am. Chem. Soc.*, 1994, **116**, 6812.
- 31 A. J. Arduengo III, H. V. R. Davis, R. L. Harlow and M. Kline, *J. Am. Chem. Soc.*, 1992, **114**, 5530.
- 32 M. K. Denk, A. Thadani, K. Hatano and A. Lough, *Angew. Chem. Int. Ed. Engl.*, 1997, **36**, 2607.
- 33 A. R. Katritzky, M. Karelson and N. Malhotra, *Heterocycles*, 1991, **32**, 127.
- 34 D. A. Dixon, K. D. Dobbs, A. J. Arduengo III and G. Bertrand, *J. Am. Chem. Soc.*, 1991, **113**, 8782.
- 35 A. J. Arduengo III, J. Goerlich and W. J. Marshall, *J. Am. Chem. Soc.*, 1995, **117**, 11027.
- 36 R. W. Alder, P. R. Allen, M. Murray and A. G. Orpen, *Angew. Chem. Int. Ed. Engl.*, 1996, **35**, 1121.
- 37 R. W. Alder and M. E. Blake, *Chem. Commun.*, 1997, 1513.
- 38 N. Kuhn and T. Kratz, *Synthesis*, 1993,

- 39 A. J. Arduengo III, H. Bock, H. Chen, M. K. Denk, D. A. Dixon, J. C. Green, W. A. Herrmann, N. L. Jones, M. I. Wagner and R. West, *J. Am. Chem. Soc.*, 1994, **116**, 6641.
- 40 R. E. Douthwaite, D. Haussinger, M. L. H. Green, P. J. Silcock, P. T. Gomes, A. M. Martins and A. A. Danopolous, *Organometallics*, 1999, **18**, 4584.
- 41 H. V. R. Dias and W. Jin, *Tetrahedron Letters*, 1994, **35**, 1365.
- 42 W. A. Herrmann, C. Köcher, L. J. Gooßen and G. R. J. Artus, *Chem. Eur. J.*, 1996, **2**, 1627.
- 43 A. J. Arduengo III, F. Davidson, H. V. R. Dias, J. R. Goerlich, D. Khasnis, W. J. Marshall and T. K. Prakasha, *J. Am. Chem. Soc.*, 1997, **119**, 12742.
- 44 M. L. Cole, C. Jones and P. C. Junk, *New J. Chem.*, 2002, **262**, 1296.
- 45 A. J. Arduengo III, J. Goerlich and W. J. Marshall, *Liebigs Ann.*, 1997, 365.
- 46 R. W. Alder, C. P. Butts and A. G. Orpen, *J. Am. Chem. Soc.*, 1998, **120**, 11526.
- 47 D. Enders, K. Breuer, G. Raabe, J. Runsink, J. H. Teles, J. P. Melder, K. Ebel and S. Brode, *Angew. Chem. Int. Ed. Engl.*, 1995, **34**, 1021.
- 48 C. Buron, H. Gornitzka, V. D. Romanenko and G. Bertrand, *Science*, 2000, **288**, 834.
- 49 M. Regitz, *Angew. Chem. Int. Ed. Engl.*, 1996, **35**, 725.
- 50 X. Cattoen, H. Gornitzka, D. Bourissou and G. Bertrand, *J. Am. Chem. Soc.*, 2004, **126**, 1342.
- 51 V. Lavallo, J. Mafhouz, Y. Canac, B. Donnadiou, W. W. Schoeller and G. Bertrand, *J. Am. Chem. Soc.*, 2004, **126**, 8670.
- 52 E. O. Fischer and A. Maasböl, *Angew. Chem. Int. Ed. Engl.*, 1964, 580.
- 53 A. J. Arduengo III, H. V. R. Davis and J. C. Calabrese, *Inorg. Chem.*, 1993, **32**, 1541.
- 54 A. J. Arduengo III, H. V. R. Davis, F. Davidson and R. L. Harlow, *J. Organometallic Chem.*, 1993, **462**, 13.
- 55 A. J. Arduengo III, H. V. R. Davis, J. C. Calabrese and F. Davidson, *J. Am. Chem. Soc.*, 1992, **113**, 9724.

- 56 N. Kuhn, G. Henkel, T. Kratz, J. Kreutzberg, R. Boese and A. H. Maulitz, *Chem. Ber.*, 1993, **126**, 2041.
- 57 N. Kuhn, T. Kratz, D. Bläise and L. Boese, *Chem. Ber.*, 1995, **128**, 245.
- 58 W. A. Herrmann, K. Öfele, M. Elison, F. E. Kühn and P. W. Roesky, *J. Organometallic Chem.*, 1994, **480**, C7.
- 59 W. A. Herrmann, M. Elison, J. Fischer, C. Köcher and G. R. J. Artus, *Chem. Eur. J.*, 1996, **2**, 772.
- 60 A. J. Arduengo III, M. Tamm, S. J. McLain, J. C. Calabrese, F. Davidson and W. J. Marshall, *J. Am. Chem. Soc.*, 1994, **116**, 7927.
- 61 A. J. Arduengo III, S. F. Gamper, J. C. Calabrese and F. Davidson, *J. Am. Chem. Soc.*, 1994, **116**, 4391.
- 62 K. Öfele, W. A. Herrmann, D. Milhalious, M. Elison, E. Herdtreck, T. Priermeier and P. Kiprof, *J. Organometallic Chem.*, 1995, **494**, 1.
- 63 A. J. Arduengo III, H. V. R. Davis, J. C. Calabrese and F. Davidson, *Organometallics*, 1993, **12**, 3405.
- 64 H. Schumann, M. Glanz, J. Winterfield, H. Hemling, N. Kuhn and T. Kratz, *Chem. Ber.*, 1994, **127**, 2369.
- 65 H. Schumann, M. Glanz, J. Winterfield, H. Hemling, N. Kuhn and T. Kratz, *Angew. Chem. Int. Ed. Engl.*, 1994, **33**, 1733.
- 66 K. Öfele, W. A. Herrmann, D. Milhalious, M. Elison, E. Herdtreck, W. Scherer and J. Mink, *J. Organomet. Chem.*, 1993, **459**, 177.
- 67 T. Weskamp, V. P. W. Böhm and W. A. Herrmann, *J. Organometallic Chem.*, 2000, **600**, 12.
- 68 K. Öfele, E. Roos and M. Herberhold, *Z. Naturforsch B*, 1976, **31**, 1070.
- 69 K. Öfele and C. G. Kreiter, *Chem. Ber.*, 1972, **105**, 529.
- 70 K. Öfele, *Angew. Chem.*, 1969, **81**, 936.
- 71 H. W. Wanzlick and H. J. Schönher, *Angew. Chem.*, 1968, **80**, 154.
- 72 W. A. Herrmann, J. Fischer, M. Elison, C. Köcher and G. R. J. Artus, *Angew. Chem. Int. Ed. Engl.*, 1995, **34**, 2371.

- 73 W. A. Herrmann, G. Gerstberger and M. Spiegler, *Organometallics*, 1997, **16**, 2209.
- 74 W. A. Herrmann, H. Schwarz, M. G. Gardiner and M. Spiegler, *J. Organomet. Chem.*, 1999, **575**, 80.
- 75 W. A. Herrmann, H. Schwarz and M. G. Gardiner, *Organometallics*, 1999, **18**, 4082.
- 76 C. Köcher and W. A. Herrmann, *J. Organomet. Chem.*, 1997, **532**, 261.
- 77 B. Bildstein, M. Malaun, H. Kopacka, K. Wurst, M. Mitterböck, K. H. Ongania, G. Opromolla and P. Zanello, *Organometallics*, 1999, **18**, 4325.
- 78 H. M. J. Wang and I. J. B. Lin, *Organometallics*, 1998, **17**, 972.
- 79 D. Enders, H. Gielen, G. Raabe, J. Runsink and J. H. Teles, *Chem. Ber.*, 1996, 1483.
- 80 W. A. Herrmann, L. J. Gooßen and M. Spiegler, *J. Organomet. Chem.*, 1997, **547**, 357.
- 81 W. P. Fehlhammer, T. Bliss, U. Kernbach and I. Brüdgam, *J. Organomet. Chem.*, 1995, **490**, 149.
- 82 U. Kernbach, M. Ramm, P. Luger and W. P. Fehlhammer, *Angew. Chem. Int. Ed. Engl.*, 1996, **35**, 310.
- 83 D. Enders, H. Gielen, G. Raabe, J. Runsink and J. H. Teles, *Chem. Ber.*, 1997, **130**, 1253.
- 84 D. Enders, H. Gielen, J. Runsink, K. Breuer, S. Brode and K. Boehn, *Eur. J. Inorg. Chem.*, 1998, 913.
- 85 J. H. Davis Jr., C. M. Lake and M. A. Bernard, *Inorg. Chem.*, 1998, **37**, 5412.
- 86 J. H. Teles, J. P. Melder, K. Ebel, R. Schneider, E. Gehrler, W. Harder, S. Brode, D. Enders, K. Breuer and G. Raabe, *Helv. Chim. Acta*, 1996, **79**, 61.
- 87 H. W. Wanzlick and H. J. Schönher, *Justus Liebigs Ann. Chem.*, 1970, **731**, 176.
- 88 D. M. Lemal and K. I. Kawano, *J. Am. Chem. Soc.*, 1962, **84**, 1761.
- 89 H. W. Wanzlick, F. Esser and H. J. Kleiner, *Chem. Ber.*, 1963, **96**, 1208.

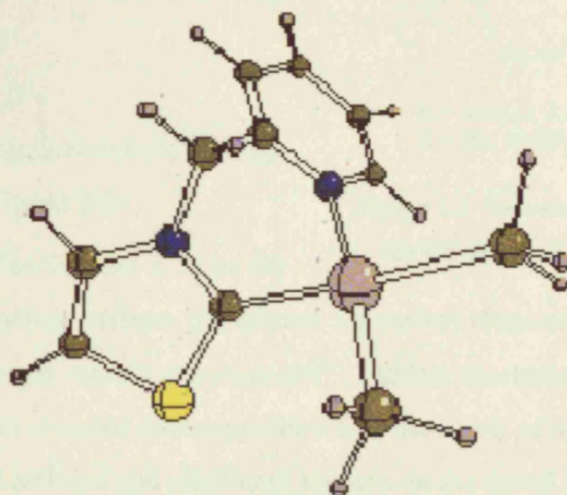
- 90 W. A. Herrmann, L. J. Gooßen, C. Köcher and G. R. J. Artus, *Angew. Chem. Int. Ed. Engl.*, 1996, **35**, 2805.
- 91 W. A. Herrmann, L. J. Gooßen, G. R. J. Artus and C. Köcher, *Organometallics*, 1997, **16**, 2472.
- 92 M. Prinz, M. Grosche, E. Herdtweck and W. A. Herrmann, *Organometallics*, 2000, **19**, 1692.
- 93 L. Jafarpour, J. Huang, E. D. Stevens and S. P. Nolan, *Organometallics*, 1999, **18**, 3760.
- 94 J. Huang, E. D. Stevens, S. P. Nolan and L. J. Petersen, *J. Am. Chem. Soc.*, 1999, **121**, 2674.
- 95 T. Weskamp, W. C. Schattenmann, M. Spiegler and W. A. Herrmann, *Angew. Chem. Int. Ed. Engl.*, 1998, **37**, 2490.
- 96 V. P. W. Böhm, C. W. K. Gstöttmayr, T. Weskamp and W. A. Herrmann, *J. Organomet. Chem.*, 2000, **595**, 186.
- 97 N. Kuhn, T. Kratz, R. Boese and D. Bläser, *J. Organomet. Chem.*, 1994, **470**, C8.
- 98 W. A. Herrmann, F. C. Munck, G. R. J. Artus, O. Runte and R. Anwänder, *Organometallics*, 1997, **16**, 2490.
- 99 B. Bildstein, M. Malaun, H. Kopacka, K. H. Ongania and K. Wurst, *J. Organomet. Chem.*, 1999, **572**, 177.
- 100 D. S. McGuinness, K. J. Cavell, B. W. Skelton and A. H. White, *Organometallics*, 1999, **18**, 1596.
- 101 D. S. McGuinness, M. J. Green, K. J. Cavell, B. W. Skelton and A. H. White, *J. Organometallic Chem.*, 1998, **565**, 165.
- 102 C. D. Abernethy, J. A. C. Clyburne, A. H. Cowley and R. A. Jones, *J. Am. Chem. Soc.*, 1999, **121**, 2329.
- 103 K. Öfele and M. Herberhold, *Angew. Chem. Int. Ed. Engl.*, 1970, **9**, 739.
- 104 C. G. Kreiter, K. Öfele and G. W. Wieser, *Chem. Ber.*, 1976, **109**, 1749.
- 105 S. T. Liu, T. Y. Hsoeh, G. H. Lee and S.-M. Peng, *Organometallics*, 1998, **17**, 993.

- 106 R. Z. Ku, J. C. Huang, J. Y. Cho, F. M. Kiang, K. R. Reddy, Y. C. Chen, K. J. Lee, G. H. Lee, S. M. Peng and S. T. Liu, *Organometallics*, 1999, **18**, 2145.
- 107 H. M. J. Wang, C. Y. L. Chen and U. B. Lin, *Organometallics*, 1999, **18**, 1216.
- 108 N. D. Clement, K. J. Cavell, C. Jones and C. J. Elsvier, *Angew. Chem. Int. Ed.*, 2004, **43**, 1277.
- 109 S. Gründemann, M. Albrecht, A. Kovacevic, J. W. Faller and R. H. Crabtree, *J. Chem. Soc. Dalton Trans.*, 2002, 2163.
- 110 D. S. McGuinness, K. J. Cavell and B. F. Yates, *Chem. Comm.*, 2001, **4**, 355.
- 111 A. Fürstner, G. Seidel, D. Kremzow and C. W. Lehmann, *Organometallics*, 2003, **22**, 907.
- 112 M. S. Viciu, G. Grasa and S. P. Nolan, *Organometallics*, 2001, **20**, 3607.
- 113 M. F. Lappert and A. J. Oliver, *J. Chem. Soc. Chem. Comm.*, 1972, 274.
- 114 P. J. Fraser, W. R. Roper and F. G. A. Stone, *J. Chem. Soc. Dalton Trans.*, 1974, 102.
- 115 P. J. Fraser, W. R. Roper and F. G. A. Stone, *J. Chem. Soc. Dalton Trans.*, 1974, 760.
- 116 P. L. Arnold, F. G. N. Cloke, T. Geldbach and P. B. Hitchcock, *Organometallics*, 1999, **18**, 3228.
- 117 I. Ugi and K. Offermann, 'Isonitrile Chemistry', Academic Press, 1971.
- 118 D. Rieger, S. D. Lotz, U. Kembach, S. Schröder, C. André and W. P. Fehlhammer, *Inorg. Chim. Acta*, 1994, **222**, 275.
- 119 W. P. Fehlhammer, K. Bartel, A. Vökl and D. Achatz, *Z. Naturforsch B*, 1982, **37**, 1044.
- 120 B. Weinberger, F. Degel and W. P. Fehlhammer, *Chem. Ber.*, 1985, **118**, 51.
- 121 F. Bonati, A. Burini, B. R. Pietroni and B. Bovio, *J. Organomet. Chem.*, 1989, **375**, 147.
- 122 J. E. Hill and T. A. Nilo, *J. Organometallic Chem.*, 1977, **137**, 293.
- 123 M. F. Lappert, 'Transition Metal Chemistry', Verlag Chemie, 1981.
- 124 A. W. Coleman, University of Sussex, 1980

- 125 A. M. Trzeciak and J. J. Ziolkowski, 'Abstracts of Papers XX Colloquy on Organometallic Chemistry, Germany-Poland', Halle-Wittenberg, 1996.
- 126 C. Köcher, Technische Universität München, 1997
- 127 T. E. Hill and T. A. Nile, *J. Organometallic Chem.*, 1977, **137**, 293.
- 128 M. F. Lappert and R. K. Maskell, *J. Organometallic Chem.*, 1984, **264**, 217.
- 129 L. J. Gooßen, Technische Universität München, 1997
- 130 T. Weskamp, F. J. Kohl, W. Hieringer, G. D. and W. A. Herrmann, *Angew. Chem. Int. Ed. Engl.*, 1999, **38**, 2416.
- 131 T. Weskamp, F. J. Kohl and W. A. Herrmann, *J. Organometallic Chem.*, 1999, **582**, 362.
- 132 L. Ackermann, A. Fürstner, T. Weskamp, F. J. Kohl and W. A. Herrmann, *Tetrahedron Lett.*, 1999, **40**, 4787.
- 133 M. Scholl, T. M. Trnka, J. P. Morgan and R. H. Grubbs, *Tetrahedron Letters*, 1999, **40**, 2247.
- 134 R. Z. Ku, D. Y. Chen, G. H. Lee, S. M. Peng and S. T. Liu, *Angew. Chem. Int. Ed. Engl.*, 1997, **36**, 2631.
- 135 B. Cetinkaya, I. Özdemir and P. H. Dixneuf, *J. Organometallic Chem.*, 1997, **534**, 153.
- 136 B. Cetinkaya, L. Özdemir, C. Bruneau and P. H. Dixneuf, *J. Mol. Catal. A*, 1997, **118**, L1.
- 137 F. Simal, L. Delaude, D. Jan, A. Demonceau and A. F. Noels, *Polym. Prepr.*, 1999, **40**, 336.
- 138 T. Weskamp, V. P. W. Böhm and W. A. Herrmann, *J. Organometallic Chem.*, 1999, 348.
- 139 C. Zhang and M. L. Trudell, *Tetrahedron Lett.*, 2000, **41**, 595.
- 140 A. M. Magill, D. S. McGuinness, K. J. Cavell, G. J. P. Britovsek, V. C. Gibson, A. J. P. White, D. J. Williams, A. H. White and B. W. Skelton, *J. Organometallic Chem.*, 2001, **617**, 546.
- 141 D. S. McGuinness and K. J. Cavell, *Organometallics*, 2000, **19**, 741.

- 142 W. A. Herrmann, R. C. P. and M. Spiegler, *J. Organometallic Chem.*, 1998, **557**, 93.
- 143 M. G. Gardiner, V. P. W. Bohm, J. Schwarz, W. Hieringer and W. A. Herrmann, *Chem. Eur. J.*,
- 144 M. J. Green, K. J. Cavell, B. W. Skelton and A. H. White, *J. Organometallic Chem.*, 1998, **554**, 175.
- 145 K. Albert, P. Gisdakis and N. Rösch, *Organometallics*, 1998, **17**, 1608.
- 146 D. Enders, H. Gielen, G. Raabe, J. Runsink and J. H. Teles, *Chem. Ber.*, 1996, **129**, 1383.
- 147 S. Gründemann, A. Kovacevic, M. Albrecht, J. W. Faller and R. H. Crabtree, *Chem. Commun.*, 2001, 2274.
- 148 G. Sini, O. Eisenstein and R. H. Crabtree, *Inorg. Chem.*, 2002, **41**, 602.
- 149 S. Gründemann, A. Kovacevic, M. Albrecht, J. W. Faller and R. H. Crabtree, *J. Am. Chem. Soc.*, 2002, **124**, 10473.
- 150 A. Kovacevic, S. Gründemann, J. R. Miecznikowski, E. Clot, O. Eisenstein and R. H. Crabtree, *Chem. Commun.*, 2002, 2580.
- 151 M. G. Gardiner, W. A. Herrmann, C. P. Reisinger, J. Schwarz and M. Spiegler, *J. Organometallic Chem.*, 1999, **572**, 239.
- 152 D. S. McGuinness, University of Tasmania, 2001
- 153 D. S. McGuinness and K. J. Cavell, *Organometallics*, 2000, **19**, 4918.
- 154 D. S. McGuinness, N. Saendig, B. F. Yates and K. J. Cavell, *J. Am. Chem. Soc.*, 2001, **123**, 4029.

Section 1



Catalysis Using Thiazole-Based Palladium Carbene Complexes

2 Thiazole Based Palladium Carbene Complexes

2.1 Introduction

Palladium carbene complexes have been used successfully in a variety of catalytic reactions, resulting in good turn over numbers in many cases. In particular, the copolymerisation of CO and ethylene has found success and resulted in high molecular weight, strictly alternating polymers when [$\{1,1'$ -di(methyl)-3,3'-methylenediimidazolin-2,2'-diylidene}palladium(II)-bis(acetonitrile)][BF_4]₂ and [$\{1,1'$ -di(mesityl)-3,3'-methylenediimidazolin-2,2'-diylidene}palladium(II)-bis(acetonitrile)][PF_6]₂ were used as catalysts¹ (Figure 2-1).

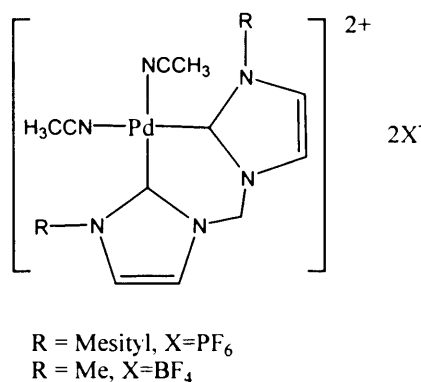


Figure 2-1 Successful carbene catalyst for CO/ethylene copolymerisation

However, in a study by McGuinness et al on the use of non-chelating palladium carbene complexes for carbon monoxide/ethylene copolymerisation, the catalyst rapidly decomposed²⁻⁴. Further theoretical and experimental investigation revealed decomposition was the result of reductive elimination of cis located carbene and alkyl/acyl ligands on the metal centre⁴⁻⁶ (Figure 2-2).

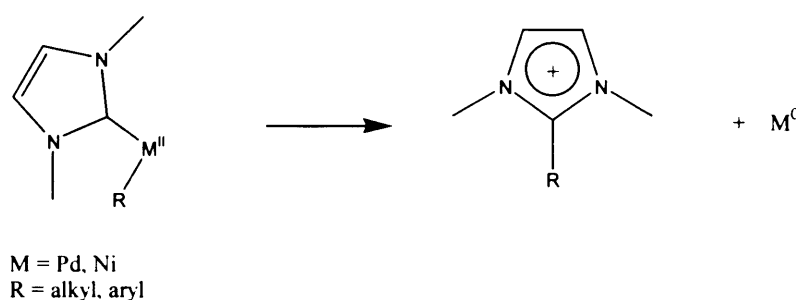


Figure 2-2 Catalyst decomposition discovered for CO/ethylene copolymerisation

Traditionally, carbene ligands used in catalysis have been based on the easily accessible and versatile imidazole ring. Due to the strong back donation of electron density from the p orbitals of the ring nitrogens to the carbene p orbital, little or no back donation from the metal centre has been found for NN carbene complexes^{7, 8}.

This effectively creates a single 2 electron σ -bond from the metal centre to the ligand, allowing the ligand to rotate freely about the ligand to metal axis.

The decomposition reaction discovered for the carbon monoxide/ethylene copolymerisation is thought to be partially assisted by ability of the carbene to twist

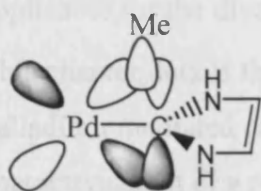


Figure 2-3 Orbital interactions causing catalysis decomposition

with respect to the square planar Pd(II) centre. With an equilibrium dihedral angle of approximately 70° , the formally empty p orbital on the carbene centre may be directed towards the adjacent alkyl or acyl group on the metal centre, facilitating interaction and consequent reductive elimination of the azolium salt (Figure 2-3).

Further, as the complex containing the acyl and carbene ligands are necessary intermediates in the carbon monoxide/ethylene catalytic cycle, the decomposition route is quite disturbing.

With previous success of carbene complexes reported, we decided to extend our investigations to attempt to create more stable group 10 metal carbene catalysts for carbon monoxide/ethylene copolymerisation. Our aim was to produce more rigid carbene catalysts using a combination of carbene heteroatom substitution and ligand chelation.

Subtle electronic benefits were anticipated with replacement of the traditional imidazole ring with the related thiazole. The larger sulfur group found in thiazoles is expected to have a less efficient orbital overlap with the carbene p orbital, resulting in only a partially filled π -orbital on the carbene centre. With the decrease in π -donation from the single nitrogen to the carbene centre, it was hoped an enhancement of the metal to ligand back donation may be found in compensation, inducing more of a double bond character in the carbene-metal bond. This in turn may inhibit the prominent twist of the ligand.

Additional stability benefits were expected with the inclusion of properly designed bidentate carbene ligands. With the addition of a chelating arm, if reductive elimination of the carbene and acyl groups did occur, chelation would hold the resultant azolium salt in the reacting sphere of the catalyst, promoting recoordination via oxidative addition and continuation of the catalytic cycle. Further, reduction in the twisting flexibility of the carbene was envisaged with chelation creating a more rigid complex in which the carbene ring is drawn back into the plane of the metal, in turn

disallowing the carbene/acyl interaction. Importantly, the thiazolylidene ligand has a distinct advantage over the corresponding imidazolylidene with respect to the amount of space required for the planar ligand. Steric disadvantages brought about by interaction of the *N*-substituent in the imidazolylidene and other metal ligands are not applicable for the divalent sulfur.

This chapter details the results for the study of chelating thiazole-based ligands in palladium mediated catalysis. Included are details on the synthesis and characterisation of a range of chelating thiazole based ligand precursors and palladium complexes, and theoretical studies of the benefits and disadvantages of thiazole based carbene complexes in catalytic environments.

2.2 Computational details

Geometry optimisations and harmonic vibrational frequencies for chelating pyridine thiazole complexes were calculated at the B3LYP⁹⁻¹¹ level of theory with the LANL2DZ basis set on palladium, which incorporates the Hay and Wadt¹² small core relativistic effective core potential and double zeta valence basis set, and 6-31g(d) on all other atoms. Zero point vibrational energy corrections were obtained using unscaled frequencies. All energies quoted in this paper refer to the final ΔH_{298} .

All other geometry optimisations and harmonic vibrational frequencies were calculated at the B3LYP⁹⁻¹¹ level of theory with the LANL2DZ basis set, which incorporates the Hay and Wadt¹² small core relativistic effective core potential and double zeta valence basis set on palladium, phosphorus and sulfur, with the Dunning and Huzinaga¹³ double zeta basis set on all other atoms. Zero point vibrational energy corrections were obtained using unscaled frequencies. All transition structures contained exactly one imaginary frequency and were characterised by following the corresponding normal mode towards the products and reactants.

All calculations were performed with the Gaussian 98¹⁴ set of programs.

2.3 Results and discussion

2.3.1 Theoretical considerations – the effect of sulfur and bridging ligands on palladium carbene complexes

One of the primary aims of this section of research was to engineer thiazole-based carbene ligands to establish if this would reduce the carbene twist in palladium complexes and in turn, produce more stable palladium carbene complexes for catalysis.

The use of thiazole-based carbene or chelating ligands are not unique to palladium complexes. Palladium bisbenzothiazolylidene complexes have been prepared¹⁵ and used to successfully catalyse aryl halide carbonylation¹⁶ and the Heck reaction¹⁷ (Figure 2-4). Similarly, many examples of chelating carbene palladium complexes exist¹⁸⁻²⁵ including pyridine functionalised complexes²⁶⁻²⁸. However, there have been no reports of the combination of chelating thiazole carbene complexes.

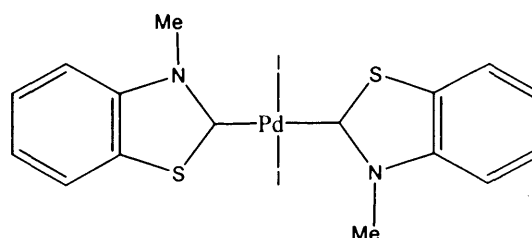


Figure 2-4 Benzothiazole based palladium complex used in catalysis

Initially, we studied the effect of the switch to the thiazolylidene ligand and additional chelation theoretically to determine if the concept was worth pursuing experimentally.

Figure 2-5 shows the optimised geometries and relative carbene twist angles for a range of simple Pd(II) diphosphine complexes containing 1,3-dimethylimidazolylidene (**1**), 3-methylthiazolylidene (**2**), a bridging 3-(pyridin-2-ylmethyl)thiazolylidene (**3**) and 3-pyridinethiazolylidene (**4**).

1	2	3	4
73.9°	74.4°	49.8°	0.1°

Figure 2-5 P-Pd-C2-N dihedral angles for various palladium carbene complexes

Based on geometry alone the results indicate the use of thiazole based carbene ligands is not enough to prevent twisting of the carbene ligands. Despite the reduced bulk of the divalent sulfur with no protruding methyl group, the lowest energy conformer remains with the carbene ligand twisted at around 74° (Figure 2-5, structure 2).

Introduction of a bridging pyridine group has a more significant effect on the geometry of the resultant carbene complex. With the thiazolyliidene ligand connected to the pyridine via a methyl bridge, the carbene ligand dihedral angle reduces to 50° (Figure 2-5, structure 3). Further, after the methyl bridge from the picolyl group is removed, the carbene ligand and pyridine ring sit almost perfectly planar (Figure 2-5, structure 4).

These results indicated chelating thiazole-based carbene ligands could have benefits over monodentate imidazolylidenes for complex stability and were worth pursuing experimentally in the hope of producing stable, active catalysts for palladium catalytic reactions.

2.3.2 Chelating thiazolyliidene ligands - xylene linked biscarbene complexes

A popular and catalytically active variety of palladium carbene complexes has emerged with the use of linked biscarbene complexes¹⁸⁻²¹. One particular type focused on by the groups of Baker^{29, 30}, Cavell²⁰, and Tessier and Youngs³¹ used xylene linked imidazolium salts as precursors to cyclophane complexes. These cyclophane complexes were successful in catalysing Heck and Suzuki reactions and as such, we decided to examine the thiazole based alternatives.

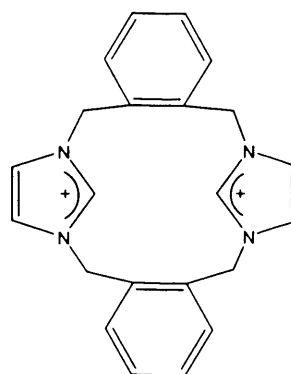


Figure 2-6 An example imidazolium linked cyclophane

As the imidazolium salts contain two nitrogen atoms, they can be linked by bridging xylene rings on both sides creating a cyclophane (Figure 2-6).

Whilst only being linked by one xylene ring, it was expected the thiazolyliidene equivalents could form interesting and useful palladium complexes, with less steric bulk and therefore different complex behaviour than their imidazolylidene counterparts.

Ortho- and *meta*-xylene thiazolium salts were synthesised by RX addition with 2 equivalents of 4-methylthiazole. Further, as carbene complexes of benzothiazole have proved successful catalysts in the past¹⁵⁻¹⁷ and the effects of different substituents on the thiazole backbone are of interest, a *m*-xylene bisbenzothiazolium salt was produced by RX addition of α,α' -dibromo-*m*-xylene with 2 equivalents of benzothiazole. Carbene complexes were then prepared by reaction of the salts with palladium acetate in DMSO (Figure 2-7).

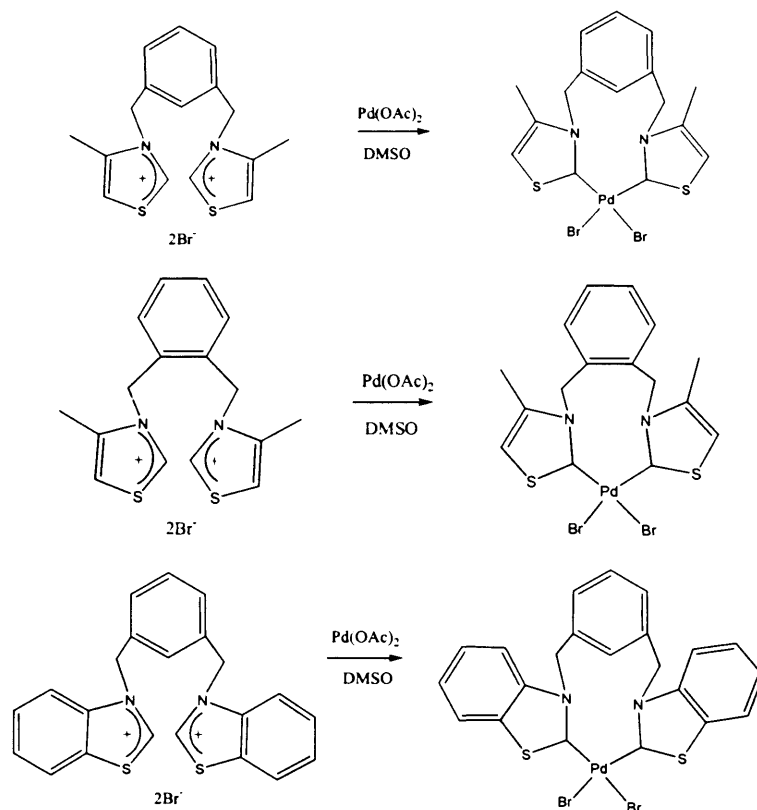


Figure 2-7 Formation of thiazole based palladium carbene complexes

Further analysis and characterisation of the resulting complexes proved difficult. The ¹H NMR of the *m*-xylene structures showed broad peaks, thought to be due to the mobility of the xylene ring or *cis/trans* isomerisation. Unfortunately, with the exception of DMSO, all complexes displayed a lack of solubility in most common solvents; a property shared with the imidazole based counterparts²⁰. Due to this lack of solubility, attempts to sharpen the peaks using low temperature NMR was not possible. Further work is required to increase the solubility through non-halide ligands before the true nature of these complexes is realised.

2.3.3 Chelating thiazolylidene ligands – carbene/pyridine linked complexes

Given that many chelating carbene complexes have been synthesised and found to be active in catalytic reactions^{1, 16-21, 30}, we decided to study the mixed donor-functionalised system containing the pyridine ring. Imidazole-based equivalent complexes have been reported^{26, 27} and found to be efficient catalysts for C-C coupling reactions²⁸ and it was anticipated this success could transfer to the thiazole based complexes.

2.3.3.1 Bridging 3-(pyridin-2-ylmethyl)thiazolylidene ligands

The first pyridine thiazolium salt attempted was that based on the methyl bridged 3-(pyridin-2-ylmethyl)thiazolium (Figure 2-8).

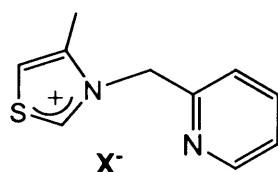


Figure 2-8 3-(pyridin-2-ylmethyl)thiazolium template

3-(pyridin-2-ylmethyl)-4-methylthiazolium chloride was produced in moderately low yields through RX addition of 2-picolyl chloride to 4-methyl thiazole. The salt was highly hygroscopic, and proved hard to separate from unreacted picolyl and thiazole.

While a variety of simple methods are known to produce carbene complexes from azolium salt precursors in high yields^{7, 8, 32, 33}, all attempts to synthesise palladium complexes from the thiazolium salt gave disappointing results (Figure 2-9).

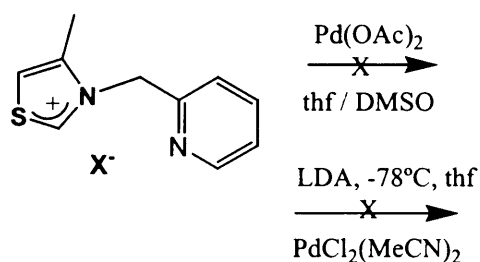


Figure 2-9 – Palladium carbene complex formation routes

The standard palladium acetate route³³ resulted in mixtures of products that were not easily separated, regardless of the solvent used. This route had proved difficult and low yielding for the imidazolium based ligands²⁸, and a more successful route has been developed involving in situ deprotonation with the soft base LDA, followed by

trapping of the resultant carbene with $\text{PdCl}_2(\text{MeCN})_2$ ²⁶. Unfortunately, this route also proved unsatisfactory for the thiazolium salt, with no carbene complex isolated.

It was envisaged the difficulty in carbene complex formation for both types of azolium salt may in part be caused by the relatively high acidity of the methylene bridge protons linking the salt with the pyridine ring. These protons are located between two electronegative nitrogens and could be removed in preference to the 2-H of the azolium salt, causing a variety of side reactions and undesired products.

To endeavour to overcome this, two new ligands were synthesised. The first contained a methyl group in place of one of the bridging hydrogens, providing both steric and electronic protection for the remaining hydrogen (Figure 2-10 a). The second ligand contained a two carbon bridge, thereby increasing the distance between the electronegative nitrogens and decreasing the direct effect on the acidity of each of the bridging hydrogens (Figure 2-10 b).

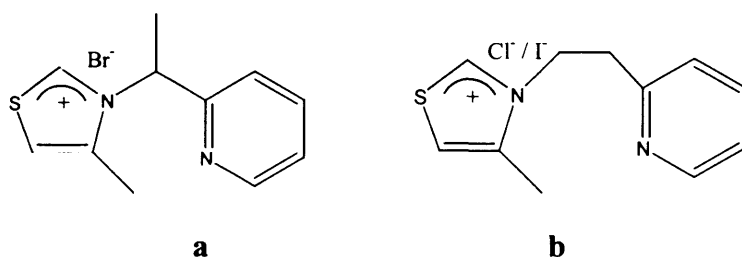


Figure 2-10 – Thiazolium salts designed to overcome the effects of highly acidic bridging hydrogens.

Both salts were prepared by RX addition of appropriate starting materials and 4-methylthiazole and once again, attempts were made to produce a palladium complex via the popular standard methods (Figure 2-11). In both cases, direct formation of carbene complexes from the palladium acetate route was attempted. Additional methods were employed for the methyl bridged salt (Figure 2-10 a) including capture of the carbene with a suitable complex precursor ($\text{PdCl}_2(\text{MeCN})_2$) after deprotonation by a base (potassium bis(trimethylsilyl)amide³⁴ and sodium hydride³⁵) and finally via transfer of a silver complex²⁸ formed with either silver oxide or silver carbonate. Again, no complexes were isolated with a mixture of unidentified complex decomposition and thiazole ring opened products formed.

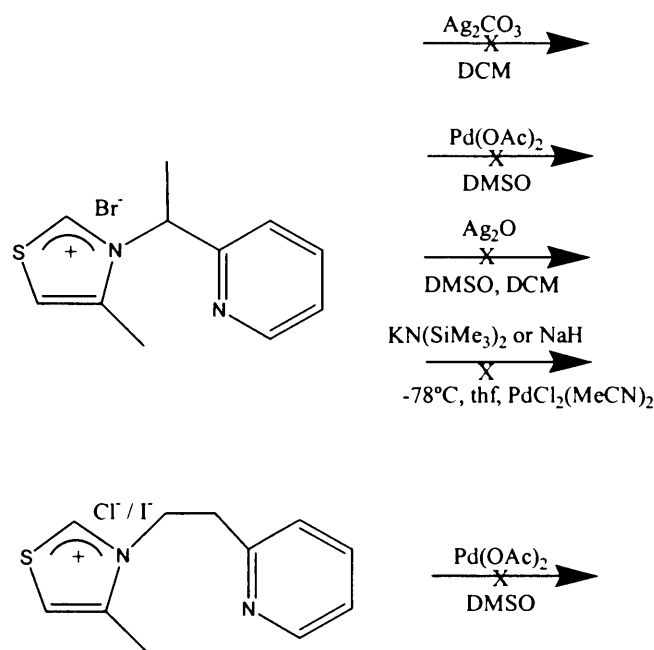


Figure 2-11 – Further attempts at bridging thiazolylidene carbene complexes

Computational studies performed by Graham on oxidative addition reactions of thiazolium, imidazolium and oxazolium salts to various metals have shown there can be a significant interaction between the sulfur atom in the thiazole ring and the metal centre³⁶. While the sulfur/metal interaction was discovered for oxidative addition reactions, in the right conditions the sulfur can behave as an independent ligand regardless of the reaction involved, and it may well be this interaction that is causing difficulties in both silver and palladium complex synthesis. Further complications may arise from ring-opening caused by this interaction for the benzothiazole system as reported previously^{37, 38}.

It is possible that this obstacle could be overcome by the use of bulky substituents in the 5 position of the thiazole ring. Any added bulk in this position could impede any sulfur/metal interaction enough to allow the carbene C2/metal centre to become the favoured interaction as desired. As such, we decided to base our studies on the oxidative addition reaction of the thiazolium salts to palladium, which initially indicated this interaction was possible (Figure 2-12).

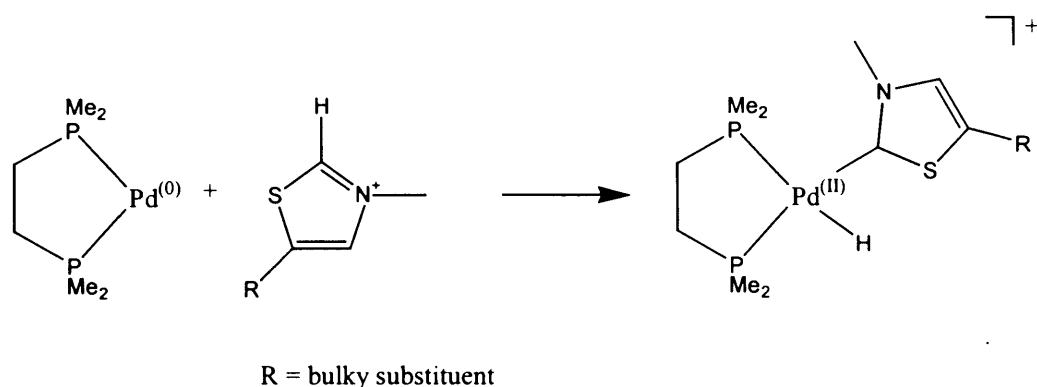


Figure 2-12 – Bulk in the thiazolium backbone to enhance carbene/metal interaction

2.3.3.2 Bulk in position 5 – will it help with palladium thiazole based carbene complexes?

As Graham demonstrated³⁶, sulfur/metal interaction could be impeding the formation of thiazole based carbene complexes. While incorporating bulk into the backbone of the thiazolium salt may aid in blocking this interaction enough for carbene formation, a literature review revealed inclusion of an unreactive bulky substituent in position 5 of the thiazolium ring may be experimentally challenging.

To initiate our studies, we synthesised a small amount of 4,5-diphenylthiazolium chloride based on the method of Karimian³⁹ by condensation of thioamide and desyl chloride. However, the reaction is very low yielding, due mainly to the instability of thioformamide intermediate. More importantly, application of a number of the standard methods as indicated above for carbene complex synthesis was unsuccessful and no palladium complexes were successfully isolated.

It is possible the two dimensional bulk of the phenyl rings does not provide enough 3 dimensional bulk to prevent the metal/sulfur interaction. Before proceeding with experimental work, we therefore decided to look theoretically at the effect of bulky substituents on the backbone of the carbene ring on the metal reaction centre.

2.3.3.2.1 2-Methyl-5-(bulk)-thiazolium salts

As Graham's study involved the study of C-C activation by palladium, we chose originally to use 2-methylthiazolium salts in our study of oxidative addition to palladium bis(dimethylphosphino)ethane so as to compare our results to those obtained previously³⁶ (Figure 2-13).

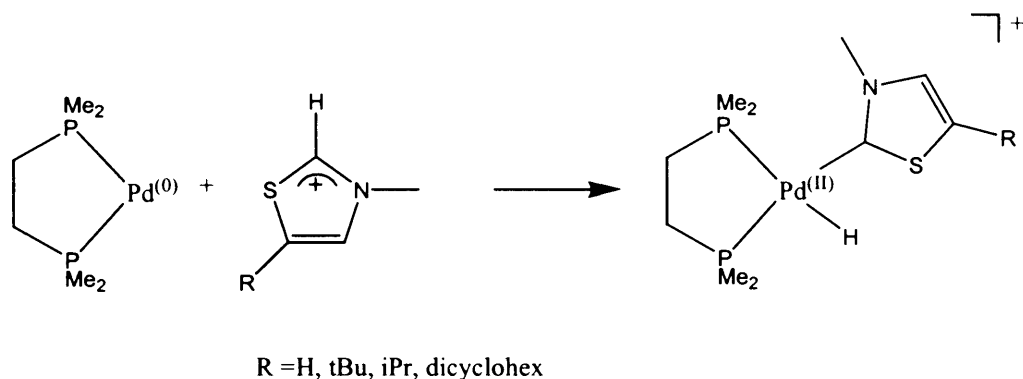


Figure 2-13 Reaction for the formation of carbene complexes with bulk on the thiazolium

Our study included the comparison of four increasingly bulky backbone substituents in the order H < *i*Pr < *t*Bu < dicyclohexylmethyl as depicted in Figure 2-14.

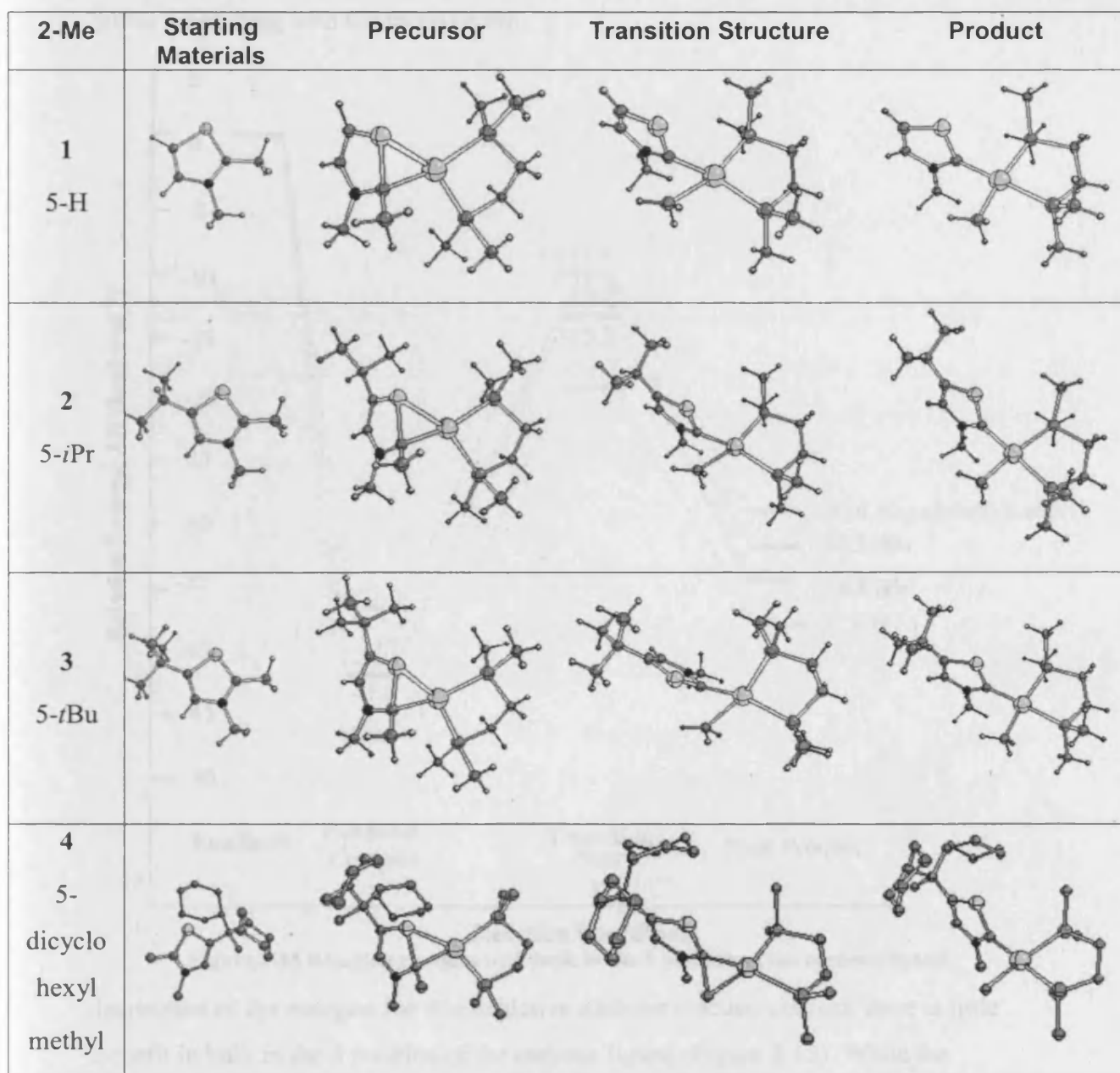


Figure 2-14 Bulk in the 5 position of the carbene ligand (structure 4 hydrogens omitted for clarity)

As can be seen in Figure 2-14, geometries at the reactive centre had very little variation, regardless of the substituent in position five of the carbene ring. Each transition structure included the three-atom centre with the 2-methyl of the thiazolium salt bending out of the salt plane before formation of the four-coordinate square-planar product. Most importantly, regardless of how ‘big’ the substituent in position 5, it does not deter the sulfur/metal interaction in the precursor complex. Even the very large dicyclohexylmethyl substituent, which appears to provide the best

protection above and below the plane in three dimensions is not enough to prevent the sulfur interacting with the metal centre.

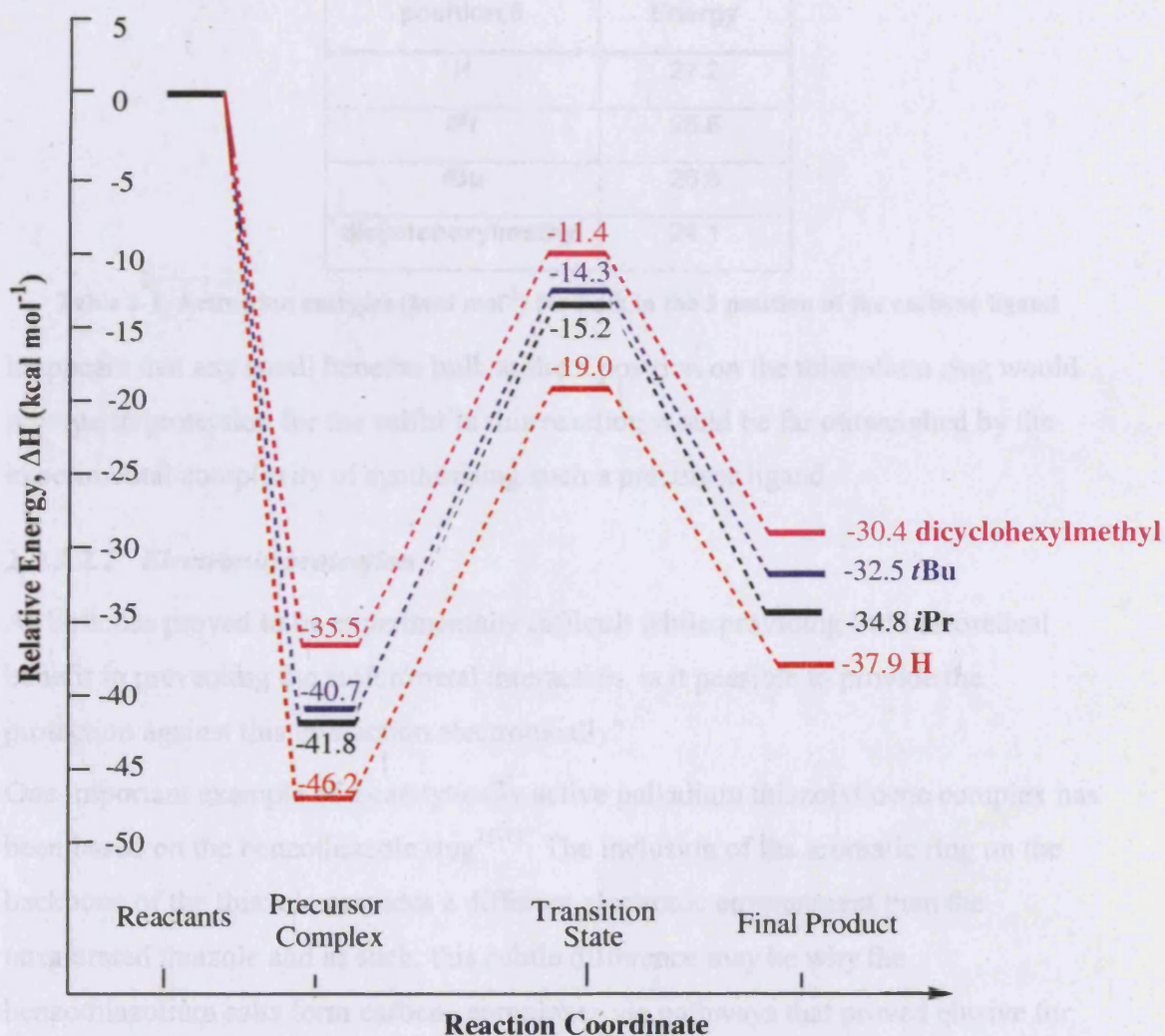


Figure 2-15 Reaction energies with bulk in the 5 position of the carbene ligand

Inspection of the energies for this oxidative addition reaction confirm there is little benefit in bulk in the 5 position of the carbene ligand (Figure 2-15). While the stability of the precursor complex with respect to the reactants does decrease when increasing the bulk from H > *i*Pr > *t*Bu > dihex, each respective point along the pathway is raised almost an equal amount. In fact, Table 2-1 reveals there is only a drop of 3.1 kcal mol⁻¹ in the activation energy from 5-H to the extremely bulky dicyclohexylmethyl substituent, with the precursor complex remaining the most thermodynamically stable structure on each pathway.

Substituent in position 5	Activation Energy
H	27.2
<i>i</i> Pr	26.6
<i>t</i> Bu	26.5
dicyclohexylmethyl	24.1

Table 2-1 Activation energies (kcal mol⁻¹) for bulk in the 5 position of the carbene ligand

It appears that any small benefits bulk at the 5 position on the thiazolium ring would provide in protection for the sulfur in this reaction would be far outweighed by the experimental complexity of synthesising such a precursor ligand.

2.3.3.2.2 *Electronic protection*

As bulk has proved to be experimentally difficult while providing little theoretical benefit in preventing the sulfur/metal interaction, is it possible to provide the protection against this interaction electronically?

One important example of a catalytically active palladium thiazolylidene complex has been based on the benzothiazole ring¹⁵⁻¹⁷. The inclusion of the aromatic ring on the backbone of the thiazole provides a different electronic environment than the unsaturated thiazole and as such, this subtle difference may be why the benzothiazolium salts form carbene complexes via pathways that proved elusive for other related thiazolium reactants.

Another form of electronic protection could be envisaged through hydrogen bonding between the sulfur atom and a nearby polarised group. Therefore, we included a study of a flexible polar group by attaching a propanol group to the thiazolium 5-position. Optimised structures for both reactions are shown in Figure 2-16.

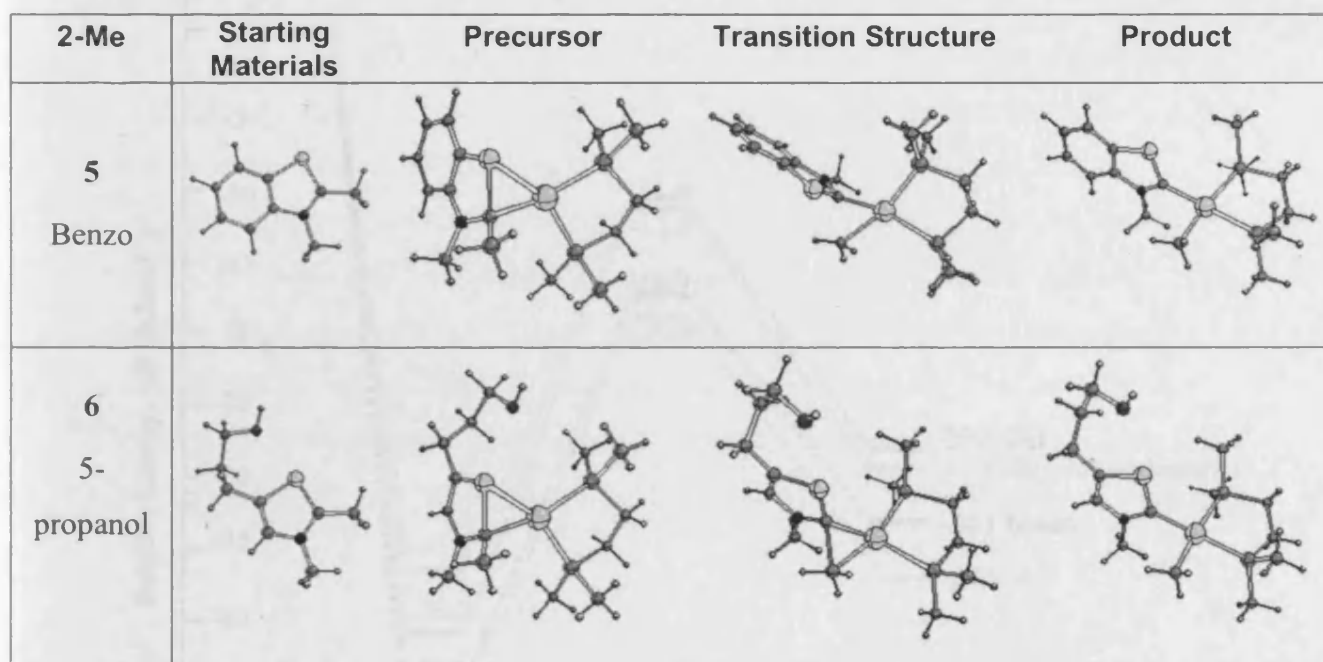


Figure 2-16 Electronic effects in the 5 position of the carbene ligand

As geometries in Figure 2-16 show, both the benzothiazolium and 5-(3-hydroxypropane)-thiazolium made no modifications to the overall barriers for the reaction, with the precursor still exhibiting strong metal/sulfur interactions.

A closer look at the 5-(3-hydroxypropane)-thiazolium reveals the result is not surprising, as no hydrogen bonding was observed in the reactant or any reaction intermediates. While the alkyl chain was long enough to allow this interaction, the low-energy conformers had the hydrogen pointing away from the sulfur, indicating no energy benefits were likely from hydrogen bonding between the alcohol and sulfur groups. Further, as no inductive electronic effects are expected due to the length of the alkyl chain, no benefit is expected from inclusion of the polarised group whatsoever.

The energies and activation energies for both the benzothiazolium and 5-(3-hydroxypropane)-thiazolium repeat the pattern previously observed with the rise in precursor instability mirrored in the transition structures and products (Figure 2-17 and Table 2-2). In fact, the small drop in activation energy observed for the 5-(3-hydroxypropyl)-thiazolium compared to the 5-H is most likely due to steric factors, with the activation energy in the same range as that observed for the 5-*i*Pr and 5-*t*Bu analogues.

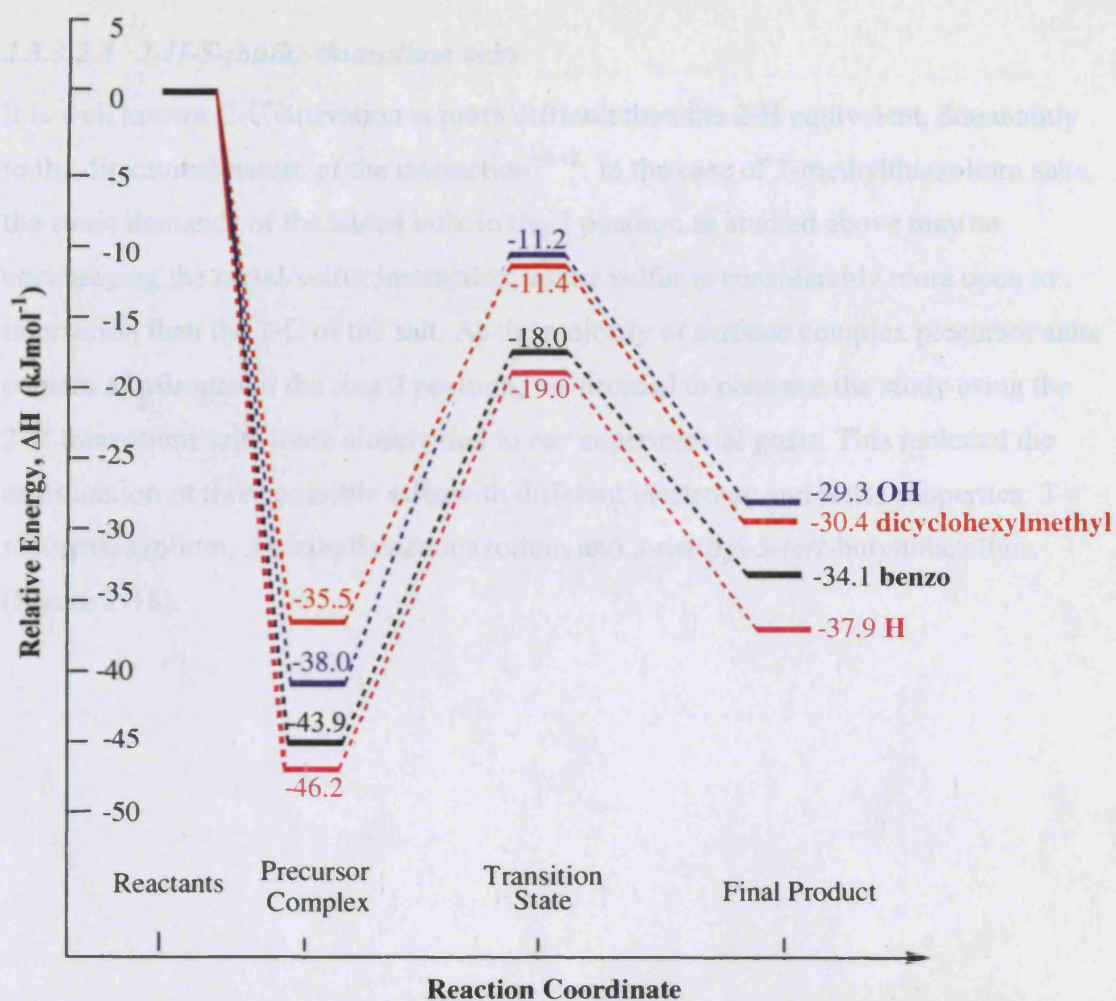


Figure 2-17 Reaction energies with electronic changes in the 5 position of the carbene ligand (kcal mol⁻¹)

Substituent in position 5	Activation Energy
H	27.2
dicyclohexylmethyl	24.1
benzo	26.0
OH	26.9

Table 2-2 Activation energies for electronic changes in the 5 position (kcal mol⁻¹)

Overall, it would appear a more drastic change in electronic structure would be required to influence the sulfur interaction without affecting the stability of the desired product.

2.3.3.2.3 2-H-5-(bulk)-thiazolium salts

It is well known C-C activation is more difficult than the 2-H equivalent, due mainly to the directional nature of the interaction⁴⁰⁻⁴². In the case of 2-methylthiazolium salts, the steric demands of the added bulk in the 2 position as studied above may be encouraging the metal/sulfur interaction, as the sulfur is considerably more open to interaction than the 2-C of the salt. As the majority of carbene complex precursor salts contain a hydrogen at the ring 2 position, we decided to continue the study using the 2-H thiazolium salts more closely tied to our experimental goals. This included the examination of three possible salts with different electronic and steric properties: 3-methylthiazolium, 3-methylbenzothiazolium and 3-methyl-5-*tert*-butylthiazolium (Figure 2-18).

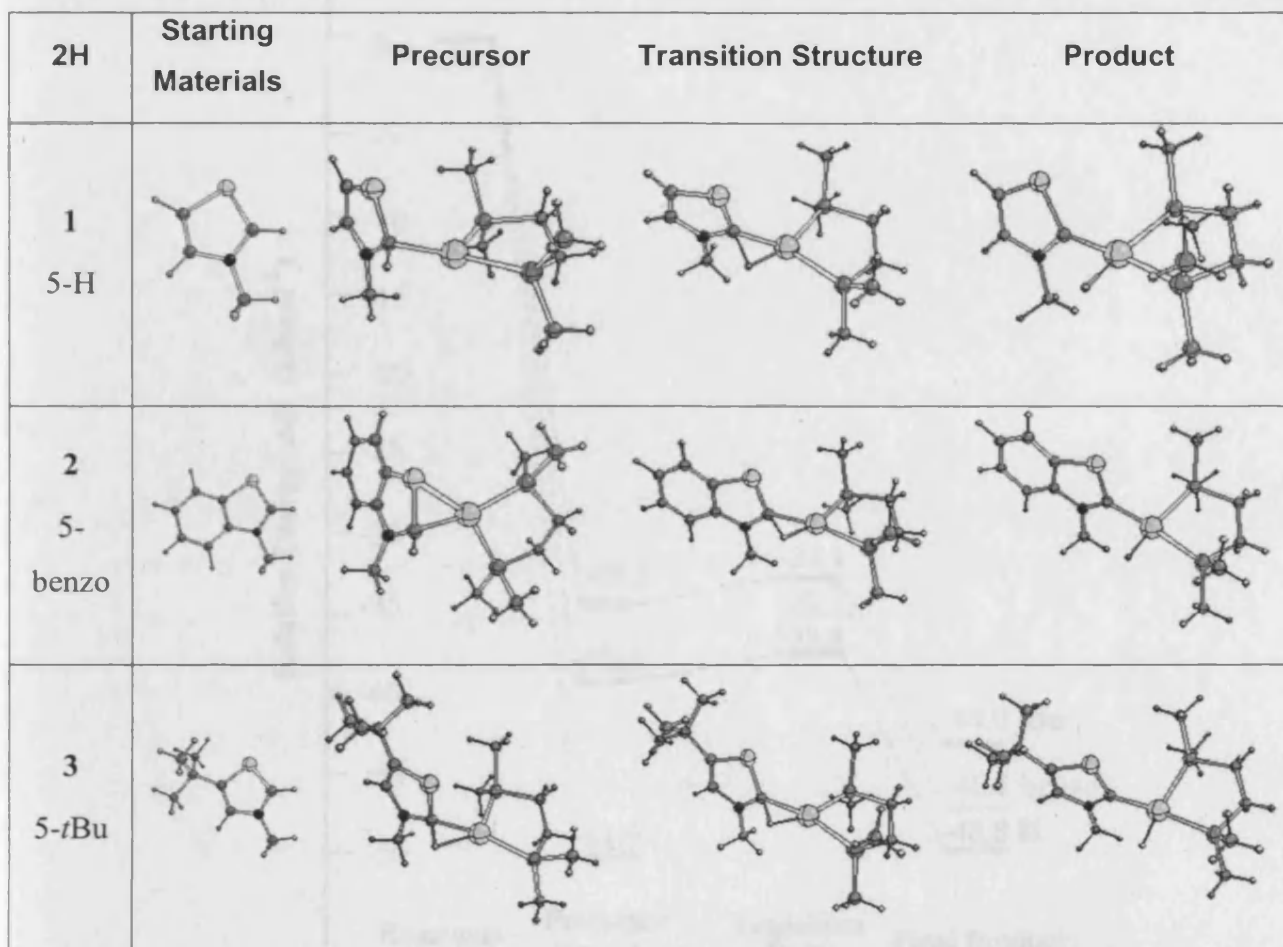


Figure 2-18 Bulk in the 5 position of the carbene ligand, 2H

As Figure 2-18 indicates, the benzothiazolium salt still displays a strong sulfur/metal interaction, with the precursor complex again the most stable in the reaction sequence. However, the oxidative addition reactions for the 5-H and 5-*t*Bu salts have precursor complexes that no longer contain a sulfur/metal interaction. Further, as shown in Figure 2-19 the products for these two reactants are the most stable species in the overall reaction sequences, which are strongly exothermic.

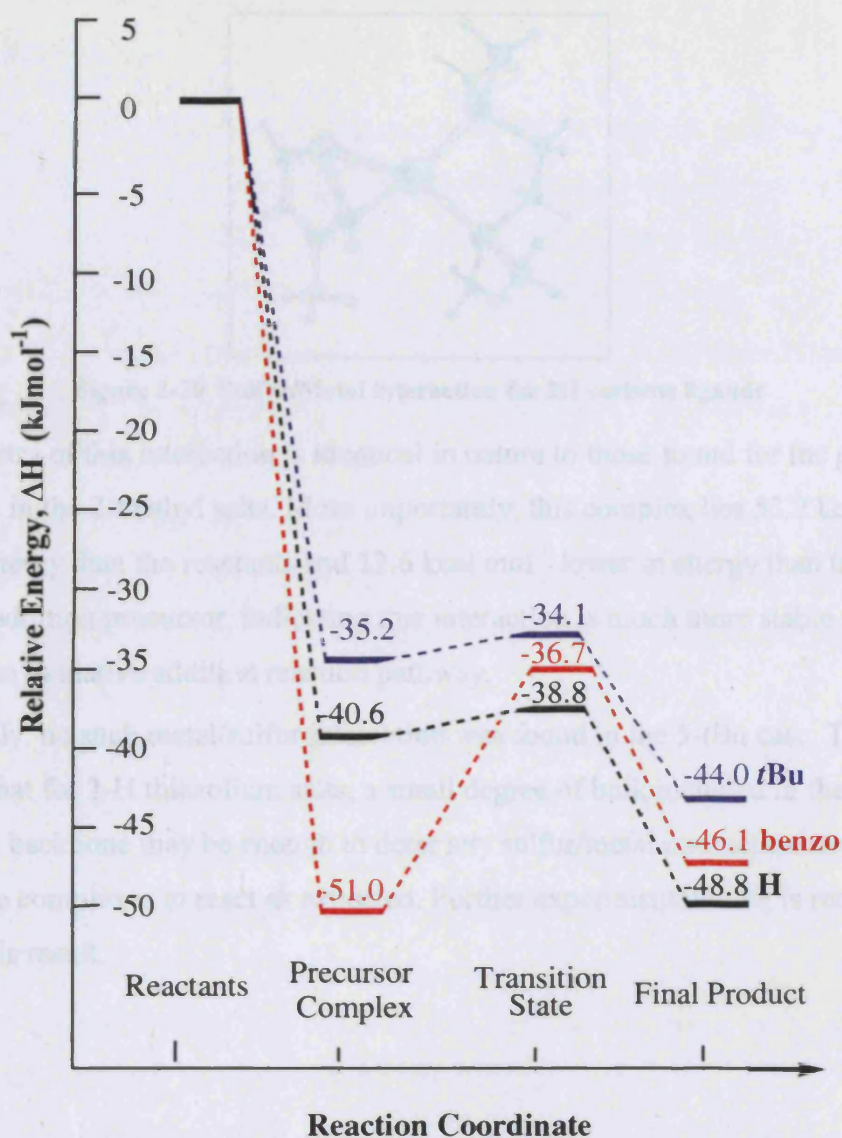


Figure 2-19 Energies for bulk in the 5 position of the carbene ligand, 2H

While the results for the 5-H and 5-*t*Bu complexes were quite promising with no sulfur interaction being present in the precursor complex, the stability of the sulfur interaction complexes in previous reactions led us to believe that there could be a corresponding sulfur interaction for the 5-H and 5-*t*Bu thiazolium salts even if it is not an intermediate in the oxidative addition reaction.

Indeed, this turned out to be the case for the 2-H thiazolium, with a sulfur interaction found as depicted in Figure 2-20.

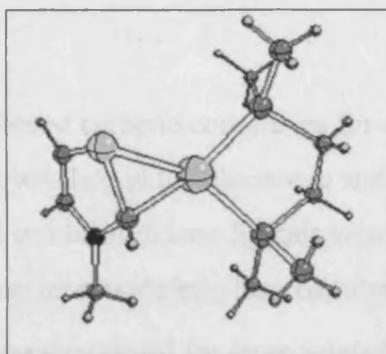


Figure 2-20 Sulfur/Metal interaction for 2H carbene ligands

The geometry of this interaction is identical in nature to those found for the precursor complexes in the 2-methyl salts. More importantly, this complex lies $53.2 \text{ kcal mol}^{-1}$ lower in energy than the reactants and $12.6 \text{ kcal mol}^{-1}$ lower in energy than the oxidative addition precursor, indicating this interaction is much more stable than any point on the oxidative addition reaction pathway.

Interestingly, no such metal/sulfur interaction was found in the 5-*t*Bu case. This result indicates that for 2-H thiazolium salts, a small degree of bulk included in the thiazolium backbone may be enough to deter any sulfur/metal interaction and allow the carbene complexes to react as expected. Further experimental work is required to confirm this result.

2.4 Conclusions

The application of thiazole-based carbene complexes for catalytic reactions has been successful in the past, and it was hoped the electronic and steric differences between chelating thiazolylidene and imidazolylidene ligands would provide stable palladium complexes suitable for carbon monoxide/ethylene copolymerisation.

While complex formation was successful for three related xylene-linked thiazolium salts, insolubility of the complexes limited their characterisation and value in catalytic reactions.

Chelation with a pyridine arm attached to the reacting thiazolium salt was another avenue explored to attempt to create stable palladium carbene catalysts. The reacting salt proved difficult to handle, with a variety of common methods for palladium complex creation ineffective.

Low yields had been discovered previously for the imidazolium equivalent reactions²⁸ and it was envisaged this could be due to the high acidity of the bridging protons, causing them to react in preference to the carbene C2 proton. As such, two slightly modified pyridine-linked thiazolium ligand precursors were synthesised to try and overcome this problem; one with an extended bridge between the thiazolium salt and the pyridine ring and another with a methyl group in place of one of the bridge protons. Again, no palladium complexes were isolated.

Previous studies have shown the sulfur from the thiazole ring could directly interact with both palladium and silver. In the case of silver, this has led to ring opening decomposition of the thiazole^{37, 38}. Studies on the inclusion of bulk in the backbone of the thiazole ring to assist in preventing unwanted interaction showed little benefit in the case of 2-methylthiazolium salts. In these cases, any interaction required for further reaction of the thiazolium C2 requires orientation that promotes the sulfur/metal interaction. Neither inductive electronic effects nor hydrogen bonding provided any further protection.

Despite being unsuccessful in blocking the sulfur/metal interaction for 2-methylthiazolium salts, bulk in the thiazolium backbone did show improvements in the 2-H salts. While sulfur/metal interaction was still found for the 5-H reactant, increasing the bulk using a 5-*t*Bu group showed promise in preventing the unwanted interaction.

Oxidative addition reactions to low valent metals have been successful in creating pyridine functionalised palladium carbene complexes⁴³. Further, 2-chloro azolium starting materials have been used to create imidazolylidene⁴⁴ and thiazolylidene⁴⁵ complexes. This method may prove successful in creating the chelating thiazolylidene complexes that have been elusive to date. Further, inclusion of bulk in the thiazolium precursor salts may provide enough protection for traditional carbene complex forming methods with these results warranting further investigation.

Overall, the thiazolylidene complexes have proved more difficult to synthesise and isolate than their imidazolylidene counterparts. Careful tuning of the thiazolium precursor salts may alleviate problems associated with standard techniques for carbene complex formation. With the different electronic and steric properties provided by the thiazolylidene ligand, these enhancements would be worth pursuing.

2.5 Experimental

2.5.1 Salt precursors

2-(α -bromoethyl)pyridine

Prepared by the method of Walker⁴⁶ with minor modifications.

To a stirred solution of N-bromosuccinimide (5.83g, 32.8mmol) and 2-ethylpyridine (3.7mL, 32.4 mmol) in anhydrous methyl acetate under argon was added a medium sized pellet of 1,1-azobis(chlorohexanecarbonitrile). The solution was covered in foil, set to reflux and a lamp shone on the flask. After 3.5 hours, the heat was turned off and the reaction left to cool slightly and the solvent removed in vacuo. The resultant orange oil and precipitate were taken up in DCM, extracted three times with 20mL water, then the organic layer was dried using MgSO₄. Removal of the DCM in vacuo left a yellow oil which deepened to red on standing. Yield: 4.37g (72%)

¹H NMR (400 MHz, CDCl₃): δ 8.57 (m, 1H, pyridyl H₆), δ 7.69 (m, 1H, pyridyl H₄), δ 7.45 (m, 1H, pyridyl H₃), δ 7.21 (m, 1H, pyridyl H₅), δ 5.12 (q, 1H, CHBrCH₃), δ 2.07(d, 3H, CHBrCH₃)

2-(2-chloroethyl)pyridine

Prepared by the method of Ohki and Noike⁴⁷.

To stirred 2-(2-hydroxyethyl)pyridine (6.26g, 50.8mmol), thionyl chloride (5mL, 68.5 mmol) was slowly added. The solution was left to stir for 15 minutes, then heated to 70°C for two hours. Excess thionyl chloride was distilled off, and the resultant solution carefully extracted with 2x10mL of 10% HCl, followed by the addition of Na₂CO₃ until the pH reached 8. Extraction with DCM (2x10mL, 1x 5mL), and removal of the solvent in vacuo produced 2-(2-chloroethyl)pyridine. Yield: 4.54g

¹H NMR (400 MHz, CDCl₃): δ 8.56 (m, 1H, pyridyl H₆), δ 7.70 (m, 1H, pyridyl H₄), δ 7.31 (m, 1H, pyridyl H₃), δ 7.23 (m, 1H, pyridyl H₅), δ 4.00 (t, 2H, CH₂CH₂Cl), δ 3.19(t, 2H, CH₂CH₂Cl)

4,5-diphenylthiazole

Prepared by the method of Karimian et al³⁹ with minor modifications:

A suspension of phosphorus pentasulfide (1.23g, 5.53 mmol) and Na₂CO₃ (0.2g, 4.44 mmol) in 20 mL dry toluene was stirred for 15 minutes. Formamide (1ml, 25.2 mmol) was very slowly syringed in, after which the yellow colour of the solution disappeared. After stirring for 10 minutes, the solution was heated to 80°C. A solution of desyl chloride (4.69g, 20.4 mmol) in dry toluene was added dropwise over an hour. After heating at 100°C for 4 days, the precipitate was removed by filtration, and the filtrate was extracted with 3x15mL 10% HCl. The aqueous phase was neutralised with Na₂CO₃ and extracted with 2x20mL ether. Removal of the solvent in vacuo gave an orange, slightly oily solid, which was recrystallised from hexane. Yield: 1.44g (30%)

2.5.2 Thiazolium salts

3-(pyridin-2-ylmethyl)-4-methylthiazolium chloride

To a solution of picolyl chloride (23.6 mmol prepared by basifying 3.87g of picolyl chloride hydrochloride) in 20mL of 1-butanol was added 4-methylthiazole (2.57g, 25.9mmol). After it was stirred and heated to 100°C overnight, the solution was allowed to cool and was dried over MgSO₄. After filtering, dry ether was added to the solution to precipitate a brown oil, which was triturated for 4 hours, filtered and washed with dry ether.

¹H NMR (400 MHz, CDCl₃): δ10.45 (s, 1H, NCHS), δ8.56 (m, 1H, pyridyl H₆), δ8.13 (s, 1H, C(CH₃)CH), δ7.98 (m, 1H, pyridyl H₄), δ7.66 (m, 1H, pyridyl H₃), δ7.47 (m, 1H, pyridyl H₅), δ6.07 (s, 2H, CH₂N), δ2.57 (s, 3H, C(CH₃)CH)

3-(pyridin-2-ylmethyl)-4-methylthiazolium iodide

This compound was prepared from 3-(pyridin-2-ylmethyl)-4-methylthiazolium chloride by heating the salt in acetone with sodium iodide. The solvent was removed *in vacuo*, and the product taken up in hot DCM and filtered. The solution was then allowed to cool and a light yellow/brown solid precipitated. This was collected by filtration and dried *in vacuo*.

¹H NMR (400 MHz, CDCl₃): δ10.32 (s, 1H, NCHS), δ8.56 (m, 1H, pyridyl H₆), δ8.13 (s, 1H, C(CH₃)CH), δ7.98 (m, 1H, pyridyl H₄), δ7.66 (m, 1H, pyridyl H₃), δ7.47 (m, 1H, pyridyl H₅), δ6.14 (s, 2H, CH₂N), δ2.77 (s, 3H, C(CH₃)CH)

3-(α-methylpicolyl)-4-methylthiazolium bromide

To a solution of 2-(α-bromoethyl)pyridine (3.37g, 18.1 mmol) in 20mL of 1-butanol was added 4-methylthiazole (2.08g, 21.0 mmol). After it was stirred and heated to 100°C overnight, the solution was allowed to cool and was dried over MgSO₄. After filtering, dry ether was added to the solution to precipitate a yellow/brown oil. The oil was dried *in vacuo*, and was subsequently washed with dry ether to produce a light brown powder. Recrystallisation from DCM or ethanol/ether produced a yellow/brown powder.

¹H NMR (400 MHz, CDCl₃): δ10.37 (s, 1H, NCHS), δ8.45 (m, 1H, pyridyl H₆), δ8.00 (s, 1H, C(CH₃)CH), δ7.87 (m, 1H, pyridyl H₄), δ7.60 (m, 1H, pyridyl H₃), δ7.36 (m, 1H, pyridyl H₅), δ6.16 (m, 1H, C(CH₃)HN), δ2.34 (s, 3H, C(CH₃)CH), δ1.88 (d, 3H, C(CH₃)HN)

3-(α-methylpicolyl)-4-methylthiazolium tetrafluoroborate

To 3-(α-methylpicolyl)-4-methylthiazolium bromide (0.51g, 1.54 mmol), silver tetrafluoroborate (0.30g, 1.54mmol), and 3Å molecular sieves under argon was added 15 mL of dry methanol. The suspension was covered with foil and left to stir overnight. The solution was then filtered through celite and the solvent concentrated *in vacuo* to 2mL. Dry ether was added to precipitate the product, which was then triturated for an hour. The solvent was decanted off and the product dried *in vacuo* to yield a yellow powder.

3-(2-ethylpyridine)-4-methylthiazolium iodide

2-(2-Chloroethyl)pyridine (4.54g, 32.1 mmol), 4-methylthiazole (3.53g, 35.6 mmol) and sodium iodide (4.04, 27.1 mmol) were added to a flask containing acetone (20mL). After refluxing for 60 hours, the solution was filtered and the acetone concentrated to 3mL in vacuo and ether added to precipitate the product.

Recrystallisation from DCM/ether produced a yellow solid.

¹H NMR (400 MHz, CDCl₃): δ10.08 (s, 1H, NCHS), δ8.60 (m, 1H, pyridyl H₆), δ8.07 (s, 1H, C(CH₃)CH), δ7.90 (m, 1H, pyridyl H₄), δ7.45 (m, 1H, pyridyl H₃), δ7.33 (m, 1H, pyridyl H₅), δ4.95 (t, 2H, CH₂CH₂N), δ3.46 (t, 2H, CH₂CH₂N), δ2.59 (s, 3H, C(CH₃)CH)

3,3'-(m-Phenylenedimethylene)-di-(4-methylthiazolium) dibromide

To a solution of α,α'-dibromo-m-xylene (2.26g, 8.56 mmol) in 20mL butanol was added 4-methylthiazole (2.18g, 22.0 mmol). The solution was heated to 100°C, and a white precipitate formed almost immediately. After heating overnight, the solution was left to cool and the precipitate was filtered off, and washed with ether. Yield: 2.24g (57%).

¹H NMR (400 MHz, CDCl₃): δ10.27 (s, 2H, NCHS), δ8.10 (s, 2H, C(CH₃)CH), δ7.52 (m, 1H, benzene H₅), δ7.35 (d, 2H, benzene H₄/H₆), δ7.25 (s, 1H, benzene H₂), δ5.83 (s, 4H, CH₂N), δ2.41 (s, 6H, C(CH₃)CH)

3,3'-(o-Phenylenedimethylene)di(4-methylthiazolium) dibromide

To a solution of α,α'-dibromo-o-xylene (2.29g, 8.68 mmol) in 20mL butanol was added 4-methylthiazole(2.00g, 20.2 mmol). The solution was heated to 100°C, and a white precipitate formed almost immediately. After heating overnight, the solution was left to cool and the precipitate was filtered off, and washed with ether. Yield: 1.72g (43%).

¹H NMR (400 MHz, CDCl₃): δ9.96 (s, 2H, NCHS), δ8.11 (s, 2H, C(CH₃)CH), δ7.43 (m, 2H, benzene H₃/H₆), δ6.90 (m, 2H, benzene H₄/H₅), δ5.94 (s, 4H, CH₂N), δ2.43 (s, 6H, C(CH₃)CH)

3,3'-(*m*-Phenylenedimethylene)dibenzothiazolium dibromide

To a solution of α,α' -dibromo-*m*-xylene (2.42g, 9.17 mmol) in 20mL acetone was added benzothiazole(2.69g, 19.9 mmol). The solution was refluxed for 42 hours. The solution was filtered of mono-substituted salt (3-(α -bromo-*m*-xylene)benzothiazolium bromide), and the solvent removed in vacuo to produce a light brown salt.

Recrystallisation from acetone/ether resulted in a pale brown product.

^1H NMR (400 MHz, CDCl_3): δ 10.93 (s, 2H, NCHS), δ 8.65 (m, 2H, benzothiazole H_2), δ 8.21 (m, 2H, benzothiazole H_5), δ 7.88- δ 7.92 (m, 4H, benzothiazole H_3/H_4), δ 7.73 (s, 1H, benzene H_2), δ 7.58- δ 7.62 (m, 3H, benzene $\text{H}_4/\text{H}_5/\text{H}_6$), δ 6.24 (s, 4H, CH_2N)

2.5.3 Palladium complexes

$\text{Pd}\{3,3'-(\textit{m}\text{-Phenylenedimethylene})\text{-di}(\text{benzothiazolin-2-ylidene})\}\text{Br}_2$

3,3'-(*m*-Phenylenedimethylene)di(4-methylthiazolium) dibromide (0.25g, 0.541mmol) and $\text{Pd}(\text{OAc})_2$ (0.11g, 0.499 mmol) were put under argon and 15mL of dry DMSO was added. The orange suspension was stirred at 60°C over night, and filtered through celite. DMSO was removed in vacuo at 40°C until approximately 2mL remained, then 30mL dry methanol was added to precipitate a very light brown product. Further washing with methanol (3x30mL), followed by thf (2x20mL) produced a yellow brown powder. Lack of solubility in most solvents prevented successful recrystallisation.

$\text{Pd}\{3,3'-(\textit{o}\text{-Phenylenedimethylene})\text{-di}(4\text{-methylthiazolin-2-ylidene})\}\text{Br}_2$

3,3'-(*o*-Phenylenedimethylene)di(4-methylthiazolium) dibromide (0.25g, 0.541mmol) and $\text{Pd}(\text{OAc})_2$ (0.11g, 0.499 mmol) were put under argon and 15mL of dry DMSO was added. The orange suspension turned very deep brown almost immediately and was stirred at 60°C over night, followed by filtering through celite. DMSO was removed in vacuo at 40°C until approximately 2mL remained, then 30mL dry methanol was added to precipitate an olive green product. Further washing with methanol (3x30mL), followed by thf (2x20mL). Lack of solubility in most solvents prevented successful recrystallisation.

Pd{3,3'-(m-Phenylenedimethylene)di(4-methylthiazolin-2-ylidene)Br₂}

3,3'-(m-Phenylenedimethylene)di(benzothiazolium) dibromide (0.25g, 0.541mmol) and Pd(OAc)₂ (0.12g, 0.535 mmol) were put under argon and 15mL of dry DMSO were added. The brown suspension was stirred at 60°C over night, and filtered through celite. DMSO was removed in vacuo at 40°C until approximately 2mL remained, then 30mL dry methanol was added to precipitate a very light brown product. Further washing with methanol (3x30mL), followed by thf (2x20mL) produced a yellow brown powder. Lack of solubility in most solvents prevented successful recrystallisation.

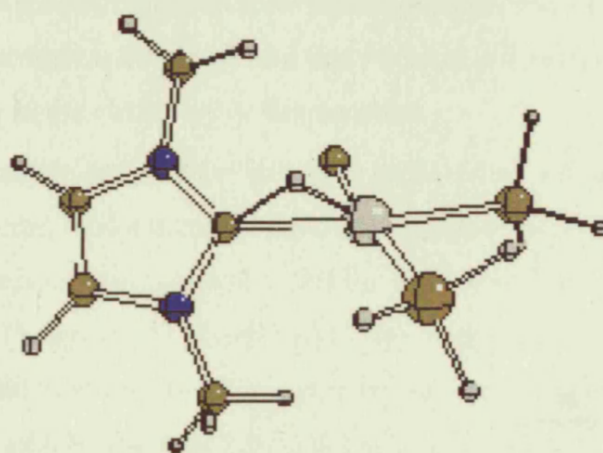
2.6 References

- 1 M. G. Gardiner, W. A. Herrmann, C. P. Reisinger, J. Schwarz and M. Spiegler, *J. Organomet. Chem.*, 1999, **572**, 239.
- 2 D. S. McGuinness, M. J. Green, K. J. Cavell, B. W. Skelton and A. H. White, *J. Organomet. Chem.*, 1998, **565**, 165.
- 3 D. S. McGuinness, K. J. Cavell, B. W. Skelton and A. H. White, *Organometallics*, 1999, **18**, 1596.
- 4 D. S. McGuinness and K. J. Cavell, *Organometallics*, 2000, **19**, 4918.
- 5 D. S. McGuinness, K. J. Cavell and B. F. Yates, *Chem. Commun.*, 2001, **4**, 355.
- 6 D. S. McGuinness, N. Saendig, B. F. Yates and K. J. Cavell, *J. Am. Chem. Soc.*, 2001, **123**, 4029.
- 7 W. A. Herrmann, *Angew. Chem. Int. Ed. Engl.*, 2002, **41**, 1290.
- 8 D. Bourissou, O. Guerret, F. Gabbai and G. Bertrand, *Chem. Rev.*, 2000, **100**, 39.
- 9 R. H. Hertwig and W. Koch, *Chem. Phys. Lett.*, 1997, **268**, 345.
- 10 P. J. Stephens, J. F. Devlin, C. F. Chabalowski and M. J. Frisch, *J. Phys. Chem.*, 1994, **98**, 11623.
- 11 A. D. Becke, *J. Chem. Phys.*, 1993, **98**, 5648.
- 12 P. J. Hay and W. R. Wadt, *J. Chem. Phys.*, 1985, **82**, 299.
- 13 T. H. Dunning and P. J. Hay, 'Modern Theoretical Chemistry', Plenum, 1976.
- 14 M. J. Frisch, G. W. Trucks, H. B. Schlegel, G. E. Scuseria, M. A. Robb, J. R. Cheeseman, V. G. Zakrzewski, J. A. Montgomery, Jr. , R. E. Stratmann, J. C. Burant, S. Dapprich, J. M. Millam, A. D. Daniels, K. N. Kudin, M. C. Strain, O. Farkas, J. Tomasi, V. Barone, M. Cossi, R. Cammi, B. Mennucci, C. Pomelli, C. Adamo, S. Clifford, J. Ochterski, G. A. Petersson, P. Y. Ayala, Q. Cui, K. Morokuma, N. Rega, P. Salvador, J. J. Dannenberg, D. K. Malick, A. D. Rabuck, K. Raghavachari, J. B. Foresman, J. Cioslowski, J. V. Ortiz, A. G. Baboul, B. B. Stefanov, G. Liu, A. Liashenko, P. Piskorz, I. Komaromi, R. Gomperts, R. L. Martin, D. J. Fox, T. Keith, M. A. Al-Laham, C. Y. Peng, A. Nanayakkara, M. Challacombe, P. M. W. Gill, B. Johnson, W. Chen, M. W.

- Wong, J. L. Andres, C. Gonzalez, M. Head-Gordon, E. S. Replogle and J. A. Pople, Gaussian 98 (Revision A.11.3), Pittsburgh PA, 2002.
- 15 V. Calò, R. Del Sole, A. Nacci, E. Schingaro and F. Scordari, *Eur. J. Org. Chem.*, 2000, 869.
- 16 V. Calò, P. Giannoccaro, A. Nacci and A. Monopoli, *J. Organometallic Chem.*, 2002, **645**, 152.
- 17 V. Calò, A. Nacci, L. Lopex and N. Mannarini, *Tetrahedron Lett.*, 2000, **41**, 8973.
- 18 W. A. Herrmann, C. P. Reisinger and M. Spiegler, *J. Organomet. Chem.*, 1998, **557**, 93.
- 19 W. A. Herrmann, M. Elison, J. Fischer and G. R. J. Artus, *Angew. Chem. Int. Ed. Engl.*, 1995, **34**, 2371.
- 20 A. M. Magill, D. S. McGuinness, K. J. Cavell, G. J. P. Britovsek, V. C. Gibson, A. J. P. White, D. J. Williams, A. H. White and B. W. Skelton, *J. Organomet. Chem.*, 2001, **617-618**, 546.
- 21 C. Zhang and M. L. Trudell, *Tetrahedron Lett.*, 2000, **41**, 595.
- 22 W. P. Fehlhammer, T. Bliss, I. Kernbach and I. Brüdgam, *J. Organomet. Chem.*, 1995, **490**, 149.
- 23 W. A. Herrmann, M. Elison, J. Fischer, C. Köcher and G. R. J. Artus, *Chem. Eur. J.*, 1996, **2**, 772.
- 24 F. E. Hahn and M. Foth, *J. Organomet. Chem.*, 1999, **585**, 241.
- 25 W. A. Herrmann, J. Schwarz, M. G. Gardiner and M. Spiegler, *J. Organomet. Chem.*, 1999, **575**, 80.
- 26 A. A. D. Tulloch, A. A. Danopoulos, R. P. Tooze, S. M. Cafferkey, S. Kleinhenz and M. B. Hursthouse, *Chem. Commun.*, 2000, 1247.
- 27 J. C. C. Chen and I. J. B. Lin, *Organometallics*, 2000, **19**, 5113.
- 28 D. S. McGuinness and K. J. Cavell, *Organometallics*, 2000, **19**, 741.
- 29 M. V. Baker, M. J. Bosnich, C. C. Williams, B. W. Skelton and A. H. White, *Aust. J. Chem.*, 1999, **52**, 823.
- 30 M. V. Baker, B. W. Skelton, A. H. White and C. C. Williams, *J. Chem. Soc. Dalton Trans.*, 2001, 111.

- 31 J. C. Garrison, R. S. Simons, J. M. Talley, C. Wesdemiotis, C. A. Tessier and W. J. Youngs, *Organometallics*, 2001, **20**, 1276.
- 32 W. A. Herrmann and C. Köcher, *Angew. Chem. Int. Ed. Engl.*, 1997, **36**, 2162.
- 33 T. Weskamp, V. P. W. Böhm and W. A. Herrmann, *J. Organomet. Chem.*, 2000, **600**, 12.
- 34 A. A. Danopoulos, S. Winston, T. Gelbrich, M. B. Hursthouse and R. P. Tooze, *Chem. Comm.*, 2002, 482.
- 35 A. J. Arduengo III, R. L. Harlow and M. Kline, *J. Am. Chem. Soc.*, 1991, **113**, 361.
- 36 D. C. Graham, Heterocyclic substitution in N-Heterocyclic carbenes, University of Tasmania, Hobart, 2003
- 37 M. Aresta and F. Ciminale, *J. Chem. Soc. Dalton Trans.*, 1981, **7**, 1520.
- 38 M. Aresta, F. Nobile, F. Ciminale and G. Bartoli, *J. Chem. Soc. Dalton Trans.*, 1976, **13**, 1203.
- 39 K. Karimian, F. Mohtarami and M. Askari, *J. Chem. Soc. Perkin Trans. II*, 1981, 1538.
- 40 J. Chatt and M. Davidson, *J. Chem. Soc.*, 1965, 843.
- 41 D. W. Evans, G. R. Baker and G. R. Newkome, *Coord. Chem. Rev.*, 1989, **93**, 155.
- 42 J. A. Martinho-Simões and J. L. Beauchamp, *Chem. Rev.*, 1990, **90**, 629.
- 43 S. Gründemann, M. Albrecht, A. Kovacevic, J. W. Faller and R. H. Crabtree, *J. Chem. Soc. Dalton Trans.*, 2002, 2163.
- 44 A. Fürstner, G. Seidel, D. Kremzow and C. W. Lehmann, *Organometallics*, 2003, **22**, 907.
- 45 P. J. Fraser, W. R. Roper and G. A. Stone, *J. Chem. Soc. Dalton Trans.*, 1974, 102.
- 46 B. H. Walker, *J. Org. Chem.*, 1960, **25**, 1047.
- 47 S. Ohki and Y. Noike, *Chem. Abstr.*, 1953, 6418i.

Section 2



Oxidative Addition Reactions of Rhodium and Iridium

3 Oxidative Addition of Azolium Salts to a Model Wilkinson's Catalyst

3.1 Introduction

Since the isolation of the first free carbene by Arduengo et al in 1991¹, there has been a resurgence in interest in the chemistry of nucleophilic carbenes and their complexes. The carbene catalysts could be used for a wide variety of reactions including C-C coupling, aryl amination, hydrosilylation and hydrogenation. Not only did the complexes in many cases return excellent turn over numbers, but the strong σ -donor nature of the ligands resulted in much more stable catalysts than the phosphine analogues². However, these studies have assumed that carbenes are innocent ligands and do not partake directly in the chemistry of the reactions.

Of importance in many catalytic cycles is the oxidative addition and reductive elimination of various species. Under certain conditions, reductive elimination of carbene ligands from palladium, platinum and nickel has been observed, resulting in catalyst decomposition^{3,4}. The groups of Cavell and Crabtree have since been successful in "reversing" this reaction, forming carbene complexes through the C-H activation of imidazolium salts by low valent metals⁴⁻⁹.

Selection of a metal to provide the right environment in which to promote oxidative addition is very important, with transition metals on the right hand side of the periodic table more conducive to oxidative addition than those on the left¹⁰. In fact, there was found to be negligible barrier for many of the group 9 and 10 metals with palladium showing almost no barrier. Conversely, however, these palladium complexes also showed the lowest barrier to reductive elimination^{11,12}.

Rhodium and iridium have long been known for their ability to perform redox reactions under mild conditions. The first example of transition metal alkane complex as an intermediate for oxidative addition and reductive elimination was in a study by Bergman involving an alkyl halide $\text{Cp}^*\text{IrPMe}_3$ complex¹³ (Figure 3-1). Similarly, the

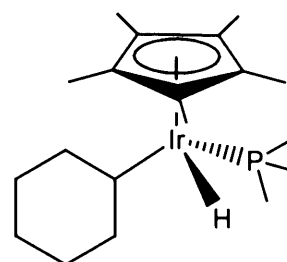


Figure 3-1 Bergman's post-oxidative addition iridium complex for oxidative addition and reductive elimination studies

first unactivated C-H insertion reactions were achieved using rhodium and iridium complexes¹⁴⁻¹⁶.

Recently, the use of rhodium and iridium as C-H and C-C activation catalysts has been of great interest for organometallic, biological and industrial processes, with several exciting results being reported¹⁷⁻³⁰. In addition, rhodium complexes have been used as catalysts for numerous hydrogenation and hydroformylation reactions using imidazolium based ionic liquids as solvents, with the catalytic cycles believed to involve many oxidative addition and reductive elimination cycles in the formation of products³¹⁻⁴².

Combining this knowledge, it seems likely that the azolium salts used as ionic liquids could become directly involved in the redox processes of rhodium based catalysts. Therefore, we thought to further extend our studies of oxidative addition/reductive elimination cycles common in catalysis to the reactions of carbene ligands themselves and related imidazolium salts with low-valent rhodium. To gain more insight into the mechanism and ease of oxidative addition of imidazolium salts to low-valent metal centres, we decided to study a catalyst system well known for this type of reaction: that of Wilkinson's Catalyst.

In this chapter we report on the reaction of a model Wilkinson's catalyst ($\text{RhCl}(\text{PH}_3)_3$) with 1,3-dimethylimidazolium by two competing pathways, and take into account the effects of changing the phosphine ligands, solvation, and the use of alternative azolium salts (Figure 3-2).

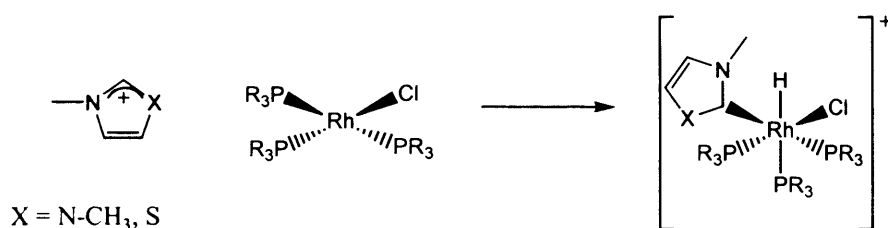


Figure 3-2 Overall oxidative addition reaction of azolium salts to $\text{Rh}(\text{PH}_3)_3\text{Cl}$

3.2 Computational details

All geometry optimisations and harmonic vibrational frequencies were calculated at the B3LYP⁴³⁻⁴⁵ level of theory with the LANL2DZ basis set, which incorporates the Hay and Wadt⁴⁶ small core relativistic effective core potential and double zeta valence basis set on rhodium, phosphorus, chlorine and sulfur, with the Dunning and Huzinaga⁴⁷ double zeta basis set on all other atoms. Zero point vibrational energy corrections were obtained using unscaled frequencies. All transition structures contained exactly one imaginary frequency and were characterised by following the corresponding normal mode towards the products and reactants. Higher level single point calculations were performed on the B3LYP/LANL2DZ optimised geometries at the B3LYP method with a LANL2augmented:6-311+G(2d,p) basis set, incorporating the LANL2 effective core potential and a large LANL2TZ+(3f) basis set on rhodium. This basis set was obtained by us in the same way as described for the Pt LANL2TZ+(3f) basis set reported previously⁴⁸. All other atoms used the 6-311+G(2d,p)⁴⁹⁻⁵¹ basis set. Energies from these single point calculations were combined with the thermodynamic corrections at the lower level of theory to obtain ΔH_{298} and ΔG_{298} numbers. All energies quoted in this chapter refer to these final ΔH_{298} or ΔG_{298} values.

Bulk solvent calculations were carried out on the B3LYP/LANL2DZ optimised structures with the polarised continuum method of Tomasi and coworkers^{52, 53} using the conductor-like polarisable continuum model⁵⁴ (CPCM) with standard tesserae area of 0.4\AA^2 and the previously discussed LANL2augmented:6-311+G(2d,p) basis set.

Radicals used to calculate bond energies were optimised using the restricted open B3LYP level of theory with the LANL2DZ basis set on rhodium and 6-31G(d) on all other atoms, with final energies using the unrestricted B3LYP method and the LANL2augmented:6-311+G(2d,p) basis set as described above. Other non-radicals were optimised and higher level energies calculated as above.

All calculations were performed with the Gaussian 98⁵⁵ set of programs.

3.3 Results and discussion

3.3.1 Stereoisomers

The oxidative addition of the C2-H bond of 1,3-dimethylimidazolium salt can result in a variety of stereoisomers. Work done previously on the $H_2/RhCl(PH_3)_3$ system by Dedieu^{56,57}, Margl³⁰ and Daniel⁵⁸ on alkane C-H activation⁵⁹ predicts that the most stable isomer for our system would be that with a chloride trans to the hydride ligand (Figure 3-3g). However, Margl and Daniel studied systems with phosphine predissociation, while Dedieu did not perform geometry optimisations, with structures based on experimental observations. As our systems involve much larger carbene ligands, we thought it prudent to consider alternate stereoisomers.

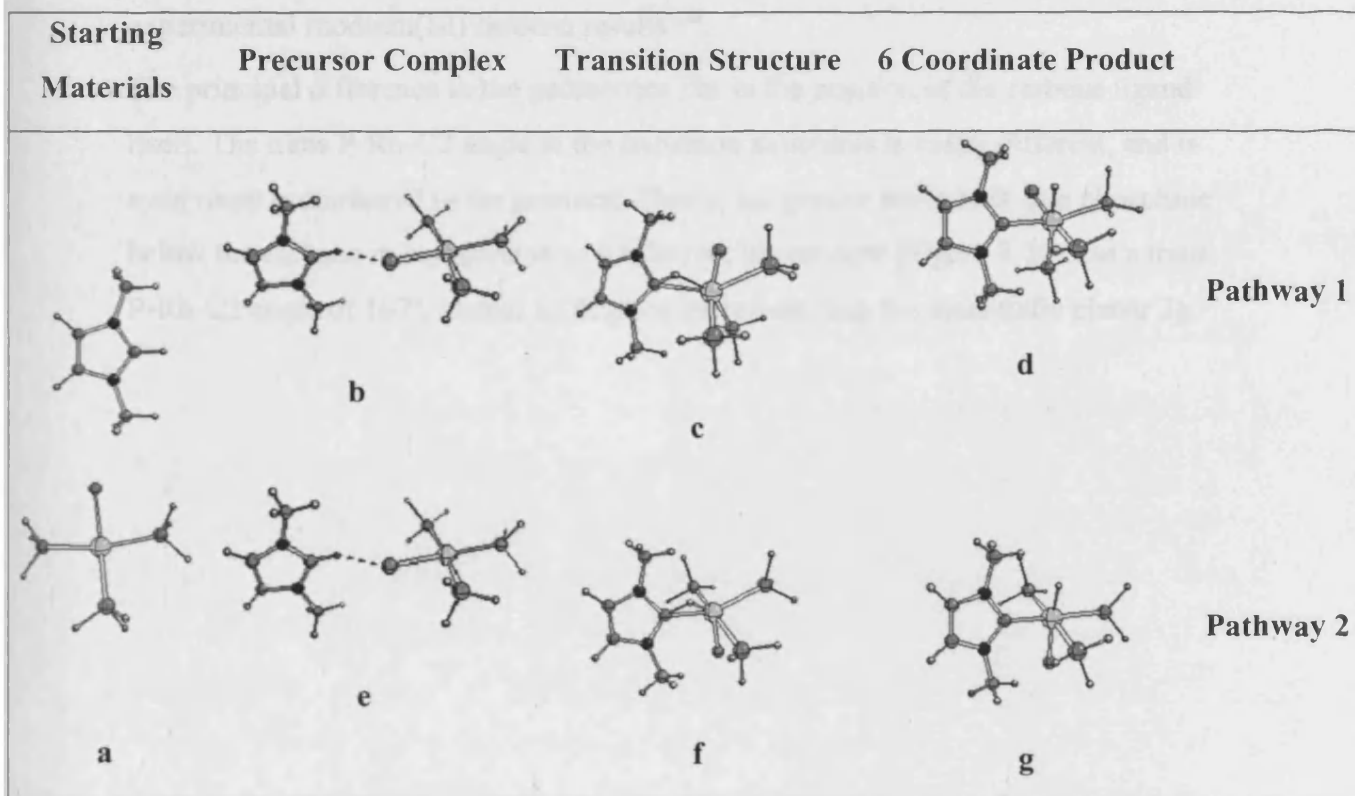


Figure 3-3 Optimised geometries of oxidative addition of 1,3-dimethylimidazolium to $Rh(PH_3)_3Cl$ with alternative direction of attack (associative routes).

Reaction pathways for the oxidative addition of 1,3-dimethylimidazolium to $RhCl(PH_3)_3$ were studied with two isomeric transition structures; one with the imidazolium salt interacting along the P-Rh-P line (Figure 3-3c), and the other along the Cl-Rh-P line (Figure 3-3f).

3.3 Results and discussion

3.3.1 Stereoisomers

The oxidative addition of the C2-H bond of 1,3-dimethylimidazolium salt can result in a variety of stereoisomers. Work done previously on the $H_2/RhCl(PH_3)_3$ system by Dedieu^{56,57}, Margl³⁰ and Daniel⁵⁸ on alkane C-H activation⁵⁹ predicts that the most stable isomer for our system would be that with a chloride trans to the hydride ligand (Figure 3-3g). However, Margl and Daniel studied systems with phosphine predissociation, while Dedieu did not perform geometry optimisations, with structures based on experimental observations. As our systems involve much larger carbene ligands, we thought it prudent to consider alternate stereoisomers.

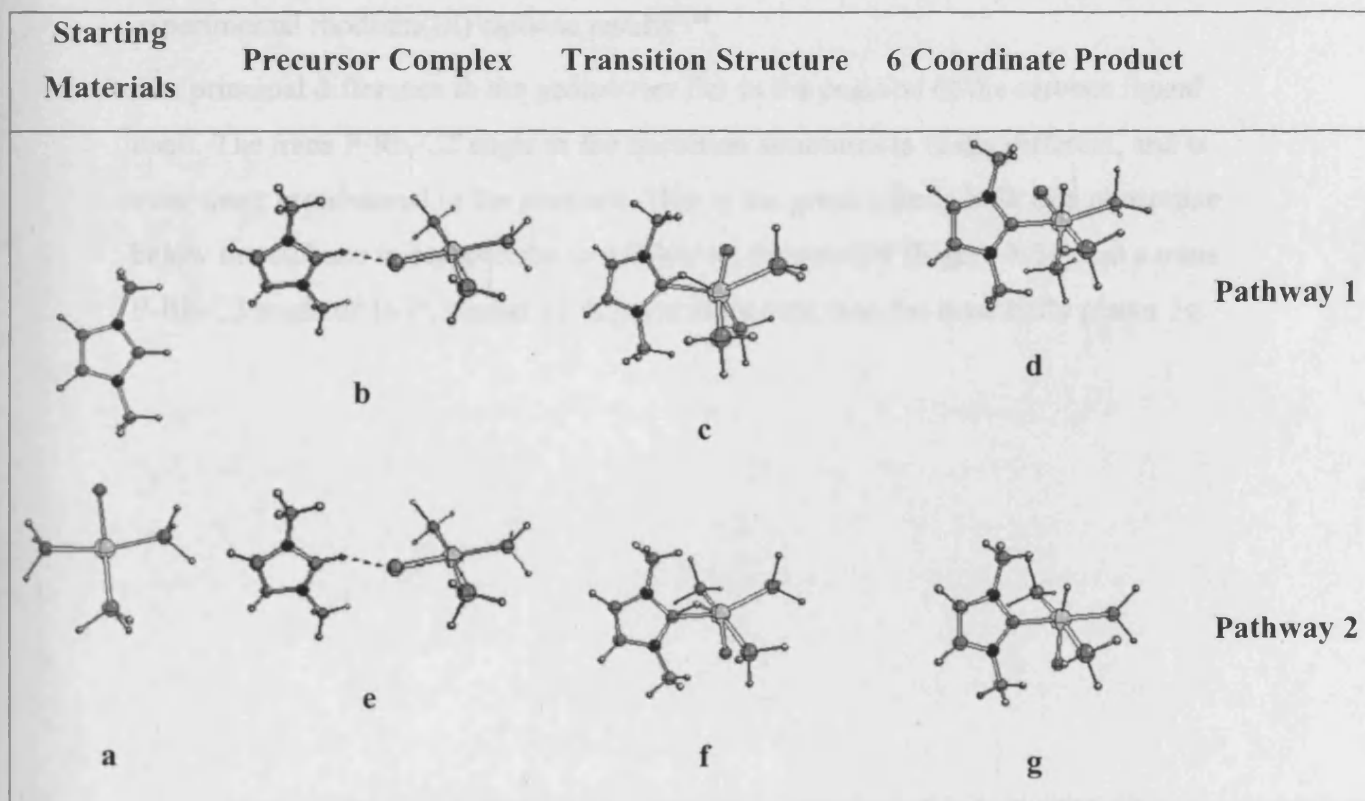


Figure 3-3 Optimised geometries of oxidative addition of 1,3-dimethylimidazolium to $Rh(PH_3)_3Cl$ with alternative direction of attack (associative routes).

Reaction pathways for the oxidative addition of 1,3-dimethylimidazolium to $RhCl(PH_3)_3$ were studied with two isomeric transition structures; one with the imidazolium salt interacting along the P-Rh-P line (Figure 3-3c), and the other along the Cl-Rh-P line (Figure 3-3f).

Each pathway originated from identical reactants and passed through the same precursor complex involving a strong hydrogen bond between the 2H on the salt and the rhodium chloride ligand (Figure 3-3b/3e), reflecting the acidity of the imidazolium hydrogen. The two transition structures show little variation in the bond lengths and angles for the carbene and hydride ligands. Although it has been shown that N-heterocyclic carbenes generally form single bonds to metal centres with consequent low barriers to rotation, the angle of the carbene ligand, with respect to the square-plane of the resultant octahedral complex probably reflects the bulk surrounding the carbene ligand itself. Similarly, the bond lengths for the respective products vary only slightly with the final C2-Rh distances of 2.06Å for 3d and 2.07Å for 3g. These distances are slightly higher, but in reasonably good agreement with experimental rhodium(III) carbene results^{7, 25}.

The principal difference in the geometries lies in the position of the carbene ligand itself. The trans P-Rh-C2 angle in the transition structures is vastly different, and is even more pronounced in the products. Due to the greater steric bulk of a phosphine below the carbene in comparison to a chloride, the product (Figure 3-3d) has a trans P-Rh-C2 angle of 167°, almost 11 degrees more bent than the essentially planar 3g.

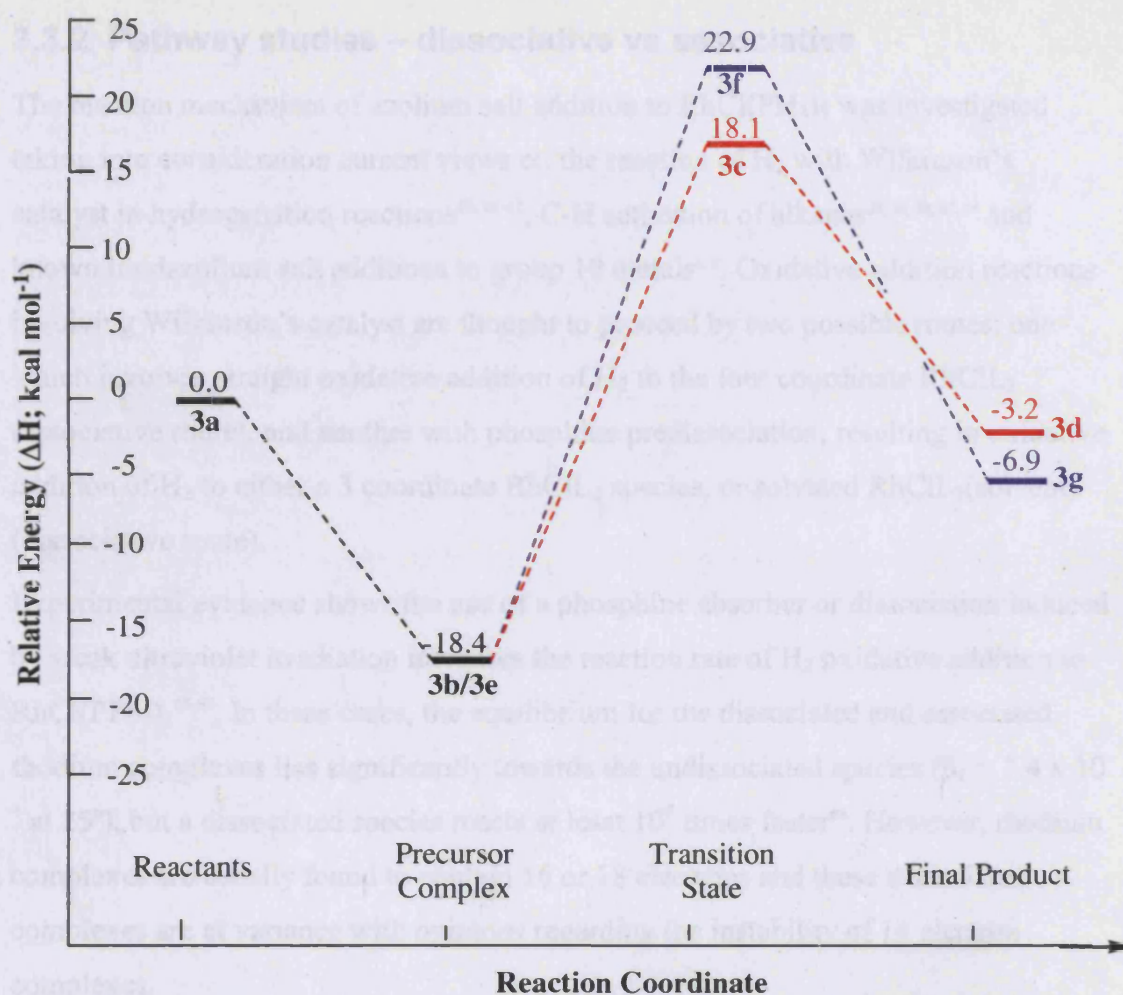


Figure 3-4 Pathway energies for oxidative addition of 1,3-dimethylimidazolium to $\text{Rh}(\text{PH}_3)_3\text{Cl}$.

The energies of each step reflect the similarity in geometries (Figure 3-4). Only 4.8 kcal mol⁻¹ separate the transition structures, and 3.7 kcal mol⁻¹ separate the products. Despite this, the reactions show opposite kinetic and thermodynamic properties. From the precursor complex, pathway 1 with the phosphine out of plane has a relatively high activation energy of 36.5 kcal mol⁻¹ and overall is exothermic by 3.2 kcal mol⁻¹. Pathway 2 with the chloride out of plane has a higher activation energy of 41.3 kcal mol⁻¹, but is exothermic by 6.9 kcal mol⁻¹. These results imply the arrangement of ligands is relatively unimportant, and either pathway or a combination thereof for the reaction seems possible in a favourable experimental environment.

For further sections, we have used the stereoisomer with the phosphine bending out of the plane, as it is supported by studies completed by other groups and more closely resembles the mechanism of the alternative dissociative route that we have also studied.

3.3.2 Pathway studies – dissociative vs associative

The reaction mechanism of azolium salt addition to $\text{RhCl}(\text{PH}_3)_3$ was investigated taking into consideration current views on the reaction of H_2 with Wilkinson's catalyst in hydrogenation reactions^{58, 60-62}, C-H activation of alkanes^{29, 30, 59, 63, 64} and known imidazolium salt additions to group 10 metals^{6, 9}. Oxidative addition reactions involving Wilkinson's catalyst are thought to proceed by two possible routes; one which involves straight oxidative addition of H_2 to the four coordinate RhClL_3 (associative route), and another with phosphine predissociation, resulting in oxidative addition of H_2 to either a 3 coordinate RhClL_2 species, or solvated $\text{RhClL}_2(\text{solvent})$ (dissociative route).

Experimental evidence shows the use of a phosphine absorber or dissociation induced by weak ultraviolet irradiation increases the reaction rate of H_2 oxidative addition to $\text{RhCl}(\text{PPh}_3)_3$ ⁶⁵⁻⁶⁷. In these cases, the equilibrium for the dissociated and associated rhodium complexes lies significantly towards the undissociated species ($\beta_1 = 1.4 \times 10^{-4}$ at 25°), but a dissociated species reacts at least 10^4 times faster⁶⁸. However, rhodium complexes are usually found to contain 16 or 18 electrons and these dissociated complexes are at variance with opinions regarding the instability of 14 electron complexes.

Therefore, when evaluating the energies for oxidative addition of an imidazolium salt to $\text{RhCl}(\text{PH}_3)_3$, we considered both possible reaction pathways (Figure 3-3, a-d; Figure 3-5, a-f). The product of each reaction was the same 6-coordinate rhodium complex, with both routes proceeding through a concerted 3-centre transition state as was shown to occur in similar reactions of azolium salts with low-valent palladium and platinum⁶. The first pathway, referred to as the associative pathway (Figure 3-3, a-d), involves straight oxidative addition to the four coordinate $\text{RhCl}(\text{PH}_3)_3$ as discussed in the previous section.

3.3.2.1 Dissociative route

It is thought that in catalytic cycles involving Wilkinson's Catalyst ($\text{Rh}(\text{PPh}_3)_3\text{Cl}$) for both C-H and C-C activation the active catalyst contains only two phosphine ligands. Although many theoretical studies focus on the use of *trans*- $\text{RhCl}(\text{PH}_3)_2$, experimental work by Brown suggests the *cis* complex may be the active one in catalytic cycles^{61, 62, 69}. We therefore looked at this reaction involving loss of phosphine, resulting in a vacant coordination site on the rhodium with phosphines in the *cis* position. The reaction can be thought of as a five step process (Figure 3-5, a-f): phosphine dissociation, an initial imidazolium/rhodium precursor complex, a transition structure, a 5-coordinate product, and finally coordination of the free phosphine to form the octahedral product.

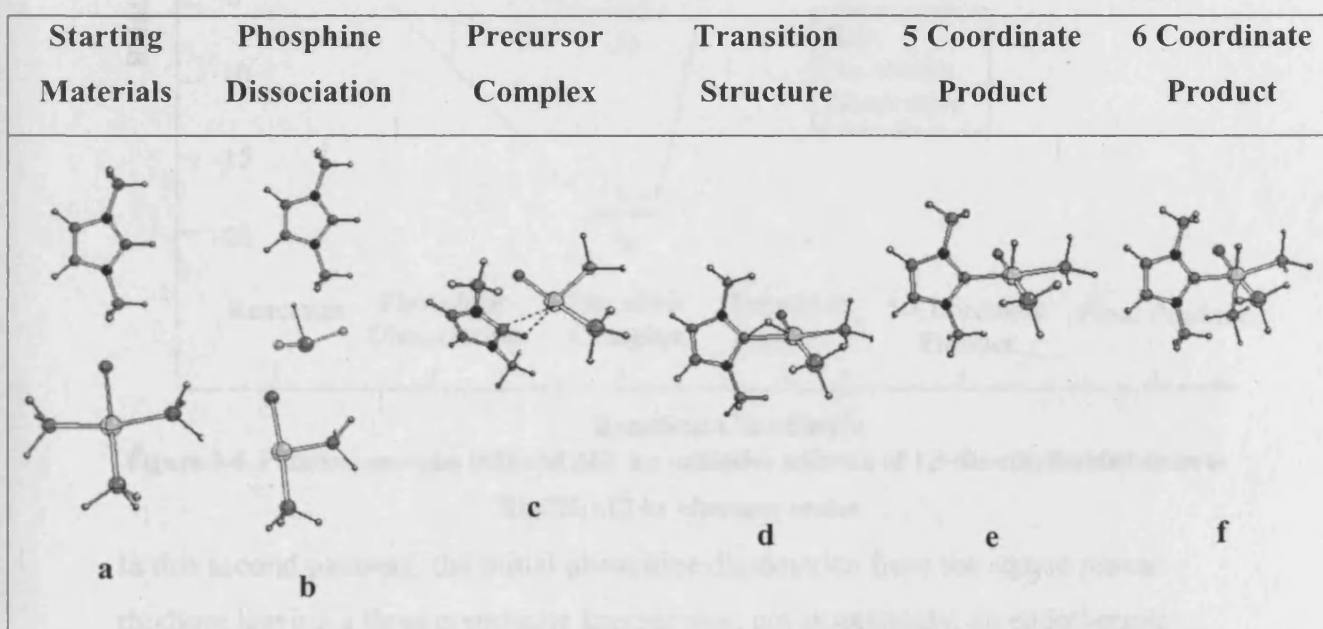


Figure 3-5 Optimised geometries of oxidative addition of 1,3-dimethylimidazolium to $\text{Rh}(\text{PH}_3)_3\text{Cl}$ with phosphine predissociation (dissociative route).

The dissociation of a phosphine ligand resulted in an almost T-shaped rhodium complex, with the ligands spreading out slightly to compensate for the vacant coordination site. The precursor complex showed a weak agostic bond as the salt approached the metal centre. This bond became even more pronounced in the transition structure. Transforming the transition structure into the product proceeded through a 5-coordinate intermediate, in which each ligand to metal bond was found to be slightly shorter than the octahedral product – a compensation to some degree for the vacant coordination site.

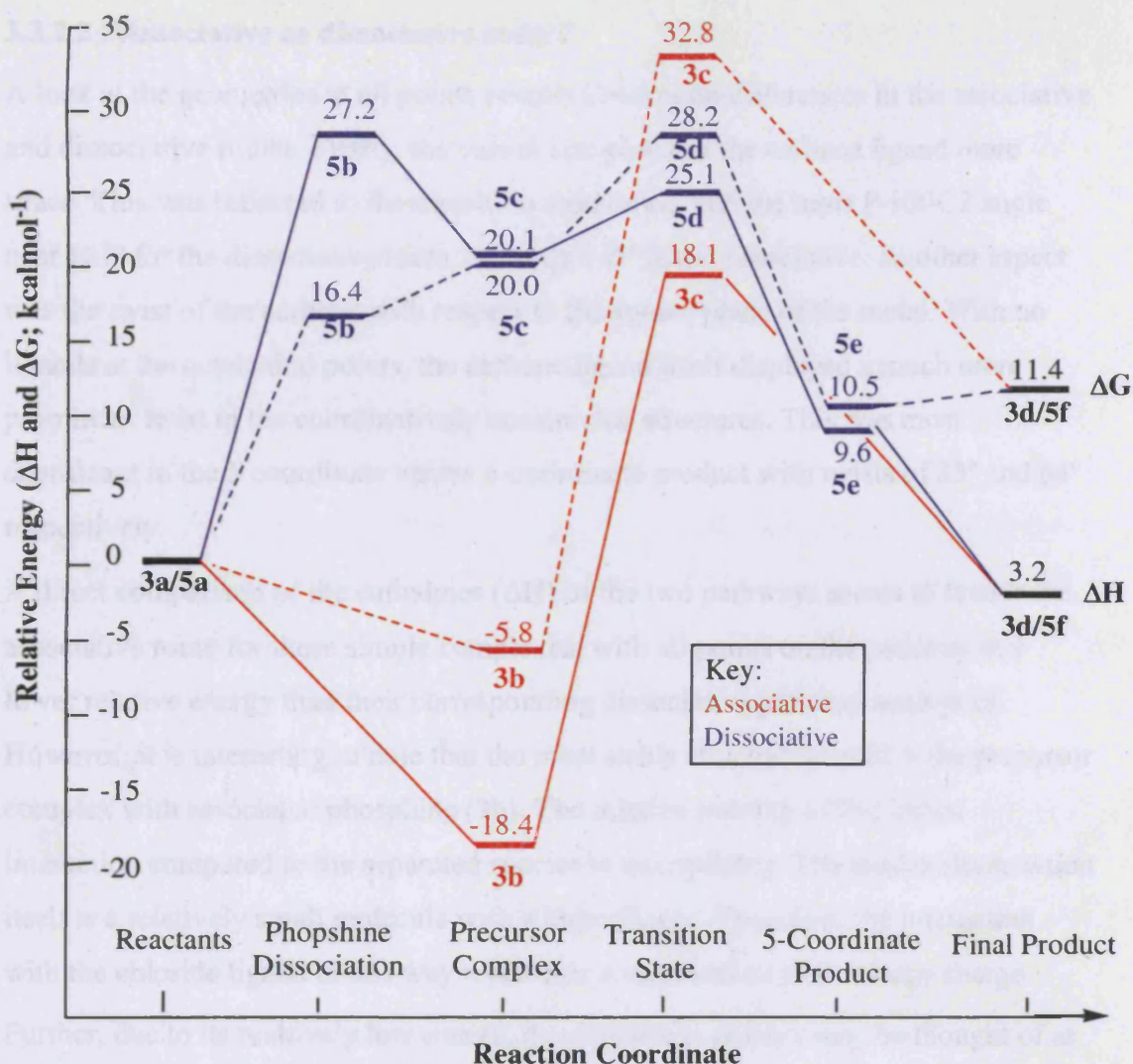


Figure 3-6 Pathway energies (ΔH and ΔG) for oxidative addition of 1,3-dimethylimidazolium to $\text{Rh}(\text{PH}_3)_3\text{Cl}$ by alternate routes

In this second pathway, the initial phosphine dissociation from the square planar rhodium leaving a three coordinate species was, not surprisingly, an endothermic process (Figure 3-6). Dissociation of a phosphine without coordination of a solvent molecule in the vacant site results in a 14 electron high energy, unstable complex. As the imidazolium salt draws near, the agostic bond stabilises the reactants somewhat in comparison to the separated species. This interaction becomes stronger in the transition structure. It seems highly unlikely that the 5-coordinate carbene hydride intermediate (Figure 3-5e), which is the initially formed product, would exist under experimental conditions, and a potential energy surface scan with a free phosphine in the vicinity of this complex proceeded towards the more thermodynamically stable 6-coordinate product with no barrier.

3.3.2.2 Associative or dissociative route?

A look at the geometries at all points revealed two main differences in the associative and dissociative routes. Firstly, the vacant site provides the carbene ligand more space. This was reflected in the transition structures, with the trans P-Rh-C2 angle near 167° for the dissociative route, but only 145° in the associative. Another aspect was the twist of the carbene with respect to the square plane of the metal. With no ligands at the octahedral points, the carbene ligand itself displayed a much more prominent twist in the coordinatively unsaturated structures. This was most significant in the 5 coordinate versus 6-coordinate product with twists of 83° and 64° respectively.

A direct comparison of the enthalpies (ΔH) of the two pathways seems to favour the associative route for these simple complexes, with all points on the pathway at a lower relative energy than their corresponding dissociative pathway analogues. However, it is interesting to note that the most stable structure overall is the precursor complex with associated phosphine (3b). The relative stability of this initial interaction compared to the separated species is unsurprising. The imidazolium cation itself is a relatively small molecule with a large charge. Therefore, the interaction with the chloride ligand in this way represents a stabilisation of this large charge. Further, due to its relatively low energy, the precursor complex may be thought of as the energetic starting point for both the associative and dissociative routes, with 3b reverting to the separated 3a before phosphine dissociation takes place in the dissociative case. The reaction barriers therefore become 36.5 kcal mol⁻¹ for the associative route (3b→3c) and a very high 45.6 kcal mol⁻¹ for the dissociative route (3b→3a→3b). However, it should be noted that there are many alternatives to consider in these types of reaction conditions. Firstly, there may be a lower energy dissociative pathway, not via 3a but instead with direct phosphine dissociation from 3b. Secondly, there are numerous alternative ways in which the stabilisation found in 3b could be achieved in a true experimental situation. It is expected both the rhodium complex and the imidazolium cation benefit from the imidazolium/chloride interaction shown. For the complex, this stabilisation could be found from solvation. In particular, if the reaction were to take place in an imidazolium ionic liquid where there is a large excess of salt, it would be expected that every point along the pathway would have the imidazolium/chloride interaction depicted in 3b. For the reacting

imidazolium cation itself, the same charge distribution could be achieved through various sources such as counter ions and solvation. As it is not possible to do calculations for all these possibilities, we chose to view the complex 3b, which was found from following the reaction pathway from the corresponding transition structure, more as a qualitative indication that there is no initial imidazolium/metal interaction as was found in the dissociative route precursor complex 3c.

From the separated starting materials, the transition structure lies $18.1 \text{ kcal mol}^{-1}$ higher in energy for the associative pathway. The dissociative pathway transition structure is slightly higher in energy again, lying $25.1 \text{ kcal mol}^{-1}$ above the reactants. Overall, however, it is the initial predissociation of a phosphine molecule to create the three-coordinate rhodium complex that gives rise to the highest energy barrier in the process and once this dissociation has taken place, the reaction proceeds smoothly to products. This result has been reflected in other theoretical studies for Wilkinson's Catalyst that assume a 3-coordinate starting material^{58, 70, 71}.

As a further consideration, while enthalpy is important for these types of reactions, it is well known that a dissociative route can often become more favourable than an associative one due to entropy effects. Therefore, it is prudent at this point to consider the energy surface with respect to the Gibbs Free Energy (Figure 3-6). As expected, examining the free energy results indicate an advantage in following a dissociative pathway. The entropy benefits of phosphine pre-dissociation drop the dissociative route energy barrier below that of the associative route. Further, the associative transition structure becomes the highest energy structure on the energy surface, with less energy required to dissociate a phosphine than to directly add the imidazolium cation. As such, it appears that the dissociative pathway could be the preferred route. However, it is important to note that despite enthalpy calculations suggesting a slightly exothermic reaction, the free energy results indicate that overall this is not a favourable reaction at 298K with the products lying $11.4 \text{ kcal mol}^{-1}$ higher in free energy than the separated reactants.

3.3.3 Phosphine ligand effects

Many oxidative addition reactions are more favourable when there is a higher electron density at the metal centre. Donation from the σ C-H orbital to empty σ -type orbitals on the metal, along with strong back donation from the metal to the σ^* C-H orbitals results in C-H activation. We therefore decided to look at the effect of substituting the model phosphine ligands with trimethylphosphine ligands, which have a higher electron donating capacity and higher steric bulk.

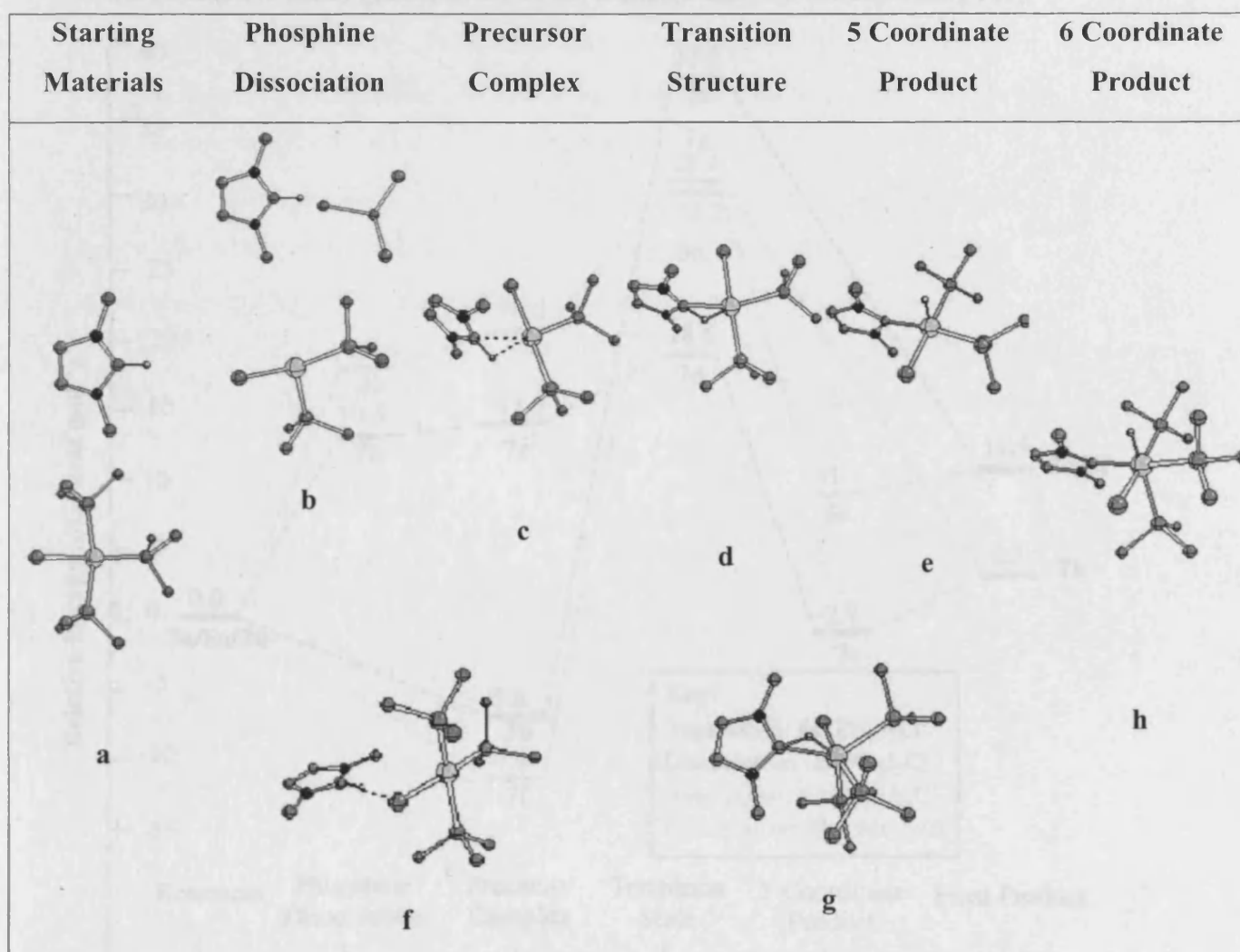


Figure 3-7 Optimised geometries of oxidative addition of 1,3-dimethylimidazolium to $\text{Rh}(\text{P}(\text{CH}_3)_3)_3\text{Cl}$ by dissociative and associative routes (non-reacting hydrogens omitted for clarity).

The change from PH_3 to the more basic and more sterically demanding PMe_3 resulted in very little change in the geometries of either reaction route (Figure 3-7, associative: 7a, 7f-h; dissociative: 7a-e, 7h). In all complexes and intermediates, the larger phosphines had longer phosphorus to metal bond distances, as expected. The most

important change in these geometries came from the direction and final position of the carbene ligand itself. With greater crowding in the square planar rhodium(I) complex caused by the PMe_3 groups, the transition structures show the imidazolium salt approaching slightly more out of the plane (7d and 7g). Similarly, in the final products the extra bulk pushes the carbene ligand slightly more perpendicular to the plane. The dissociative precursor complex also reveals the effect of the added bulk. While the interaction appears the same, the distance of the incoming imidazolium salt to the rhodium is much greater in the PMe_3 complex than the corresponding PH_3 .

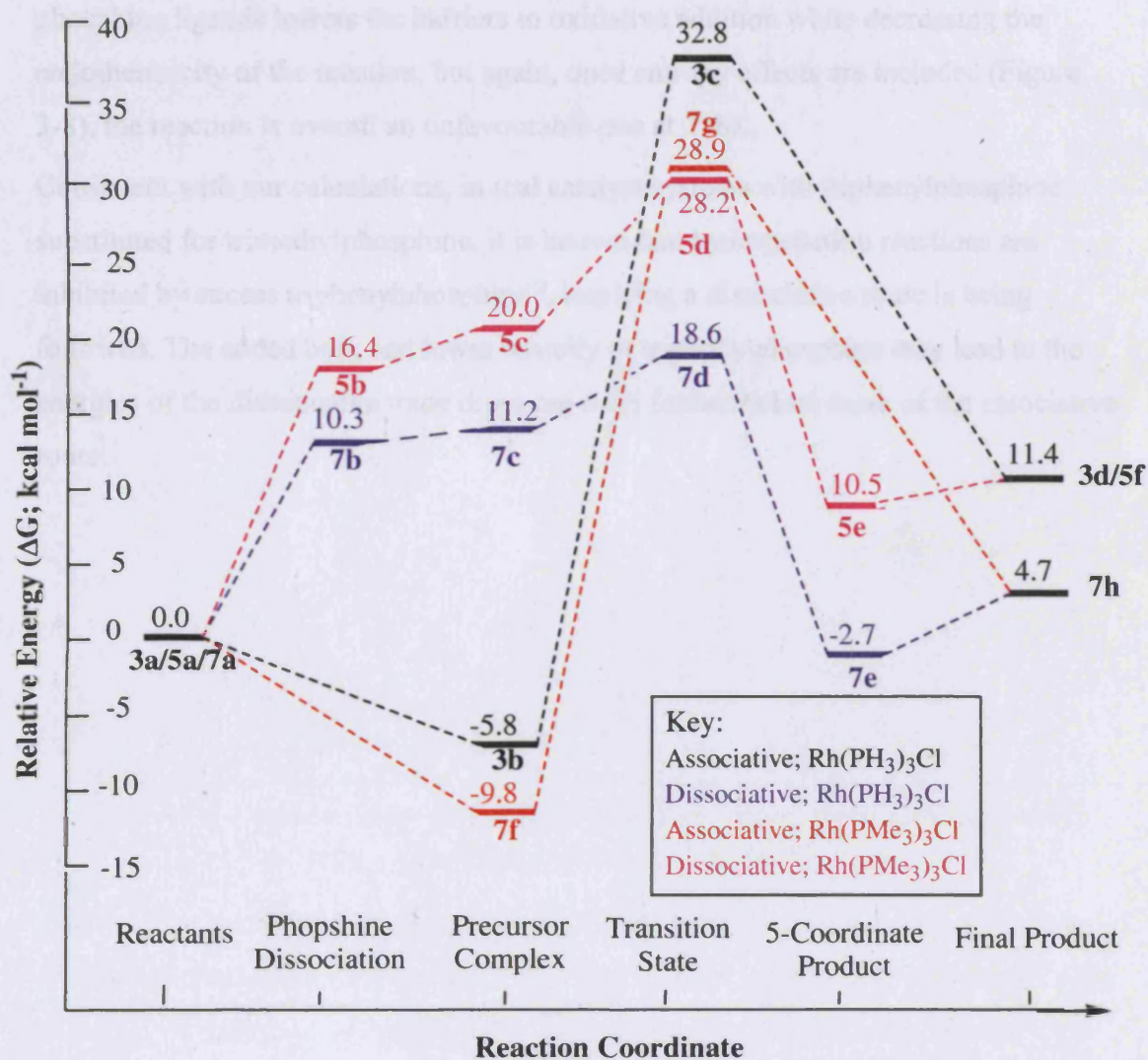


Figure 3-8 Pathway energies for oxidative addition of 1,3-dimethylimidazolium to $\text{Rh}(\text{PH}_3)_3\text{Cl}$ and $\text{Rh}(\text{P}(\text{CH}_3)_3)_3\text{Cl}$ (ΔG)

As predicted, the change to a more basic phosphine does decrease the endothermicity of the overall reaction (Figure 3-8). In fact, the switch also lowers the relative energies of all reaction points on the pathway. The precursor complex drops by 8.8 kcal mol⁻¹ for the dissociative route compared to a drop of 4.0 kcal mol⁻¹ for the associative route. Similarly, decreases of 9.6 kcal mol⁻¹ and 3.9 kcal mol⁻¹ are found respectively for the transition structures. These decreases are slightly larger at all points for the dissociative pathway, and the dissociative route is now favoured over the associative route by 10.3 kcal mol⁻¹. Overall, the increase in basicity of the phosphine ligands lowers the barriers to oxidative addition while decreasing the endothermicity of the reaction, but again, once entropy effects are included (Figure 3-8), the reaction is overall an unfavourable one at 298K.

Consistent with our calculations, in real catalyst systems with triphenylphosphine substituted for trimethylphosphine, it is known that hydrogenation reactions are inhibited by excess triphenylphosphine⁷², implying a dissociative route is being followed. The added bulk and lower basicity of triphenylphosphine may lead to the energies of the dissociative route dropping even further below those of the associative route.

3.3.4 Solvent effects

3.3.4.1 Explicit addition of a THF molecule

It is thought that in catalytic cycles involving Wilkinson's catalyst, any dissociation of a triphenylphosphine is followed by coordination of a less sterically demanding solvent molecule. In fact, in most experimental conditions it is highly likely that a solvent molecule would fill any free coordination site. Therefore, we introduced an explicit THF molecule into the reaction sequence to study the effects on energies and geometries.

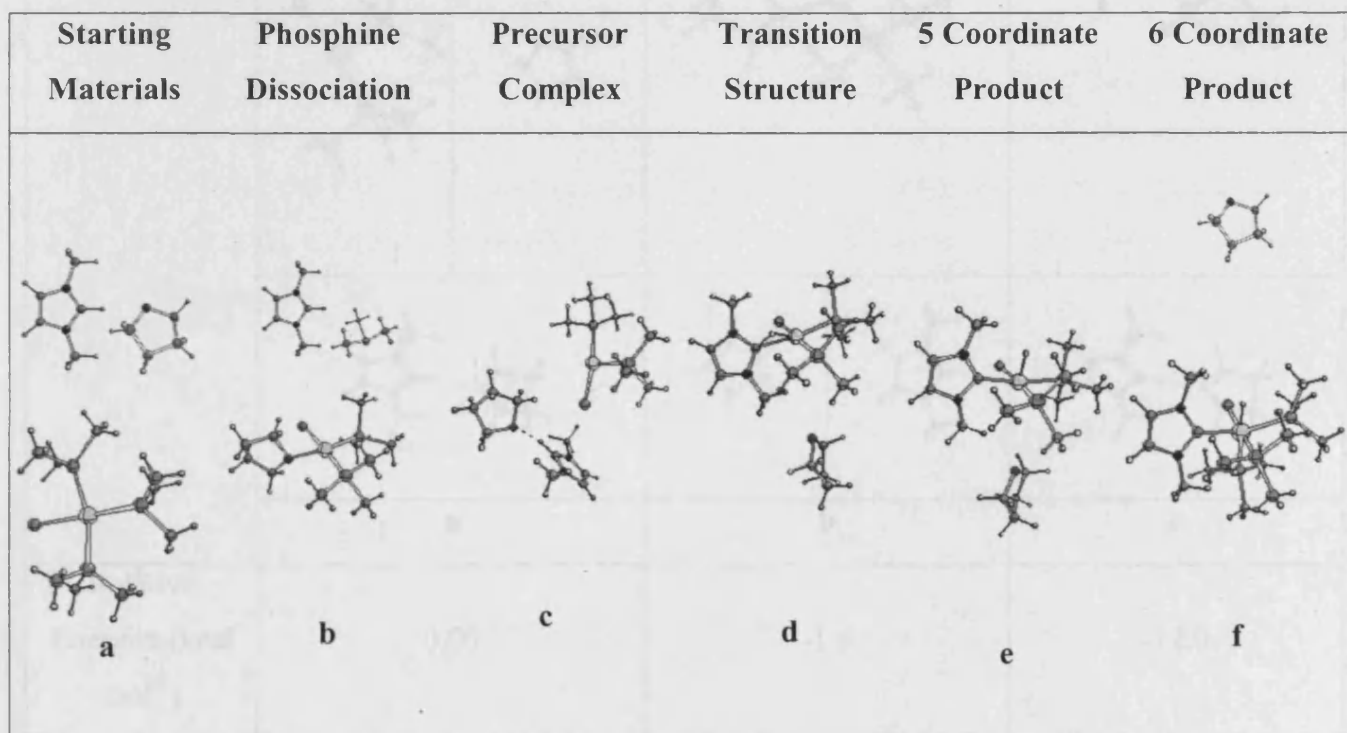


Figure 3-9 Optimised geometries of oxidative addition of 1,3-dimethylimidazolium to $\text{Rh}(\text{P}(\text{CH}_3)_3)_3\text{Cl}$ by dissociative route with THF molecule.

A look at the geometries of all points with this added THF molecule revealed some interesting information (Figure 3-9, a-f). The precursor complex exposed some of the problems in working with simplified solvation reactions. As the reaction pathway is followed from the transition structure back towards the starting materials, the imidazolium salt draws away from the rhodium and forms a hydrogen bond between the imidazolium 2-H and the oxygen on the THF (Figure 3-9c). Although this has a large stabilising effect on the salt, under experimental circumstances it would be expected that there would be another THF molecule in the vacant coordination site of the rhodium complex (Figure 3-10c). The relative energies of the three-coordinate

rhodium ($\text{Rh}(\text{PMe}_3)_2\text{Cl}$) and a THF/imidazolium interaction (Figure 3-10a) compared to the four-coordinate $\text{Rh}(\text{PMe}_3)_2(\text{THF})\text{Cl}$ and free imidazolium (Figure 3-10b) show surprisingly little difference: a mere $1.6 \text{ kcal mol}^{-1}$. In an experiment, the concentration of THF would give rise to both the stabilised THF/imidazolium and four coordinate $\text{Rh}(\text{PMe}_3)_2(\text{THF})\text{Cl}$ (Figure 3-10c) – a much more stable system ($-12.0 \text{ kcal mol}^{-1}$).[†]

	a	b	c
Relative Energies (kcal mol ⁻¹)	0.00	-1.6	-12.0

Figure 3-10 Various interactions of $\text{Rh}(\text{P}(\text{CH}_3)_3)_2$ and 1,3-dimethylimidazolium with two THF molecules.

The reaction path with the added THF molecule highlighted further interesting features. While the starting rhodium complex (Figure 3-9b) had the THF coordinated at close proximity to the metal centre (2.19 \AA), the optimisation of the transition structure resulted in a very long rhodium/THF distance of 5.22 \AA , implying the

[†] Ideally, these results suggest it would be wise to include a second, or more, THF molecules in the reaction sequence, but the increased computational time and the indirect influence of introducing this second molecule in later structures led us to continue with only one THF molecule and choose 8c to be the precursor complex as found from the reaction transition structure.

solvent molecule could at best be considered weakly bound. Further, the resulting complex had an identical geometry at the rhodium centre to that of the dissociative route without the THF. All attempts at optimising with closer rhodium/THF distances failed, indicating the long THF bond length was the lowest energy structure.

In following this transition structure to the 5-coordinate product, the THF does not fully rejoin the complex but does draw closer, resulting in a rhodium/THF distance of 4.36Å (Figure 3-9e). An almost identical product slightly higher in energy was found with a much closer rhodium/THF distance of 2.44Å in a more classical octahedral complex. While there is only a small energy difference between the two (4.5 kcal mol⁻¹) a relaxed potential energy surface scan revealed a tiny barrier, possibly due to a steric interaction between the incoming THF molecule and the rhodium phosphine ligands. Again, comparison of the geometry of these two products revealed an extra twist in the carbene ligand, with the long rhodium/THF distance allowing more room for the carbene ligand and resulting in a near 90° twist, compared to 75° in the octahedral complex.

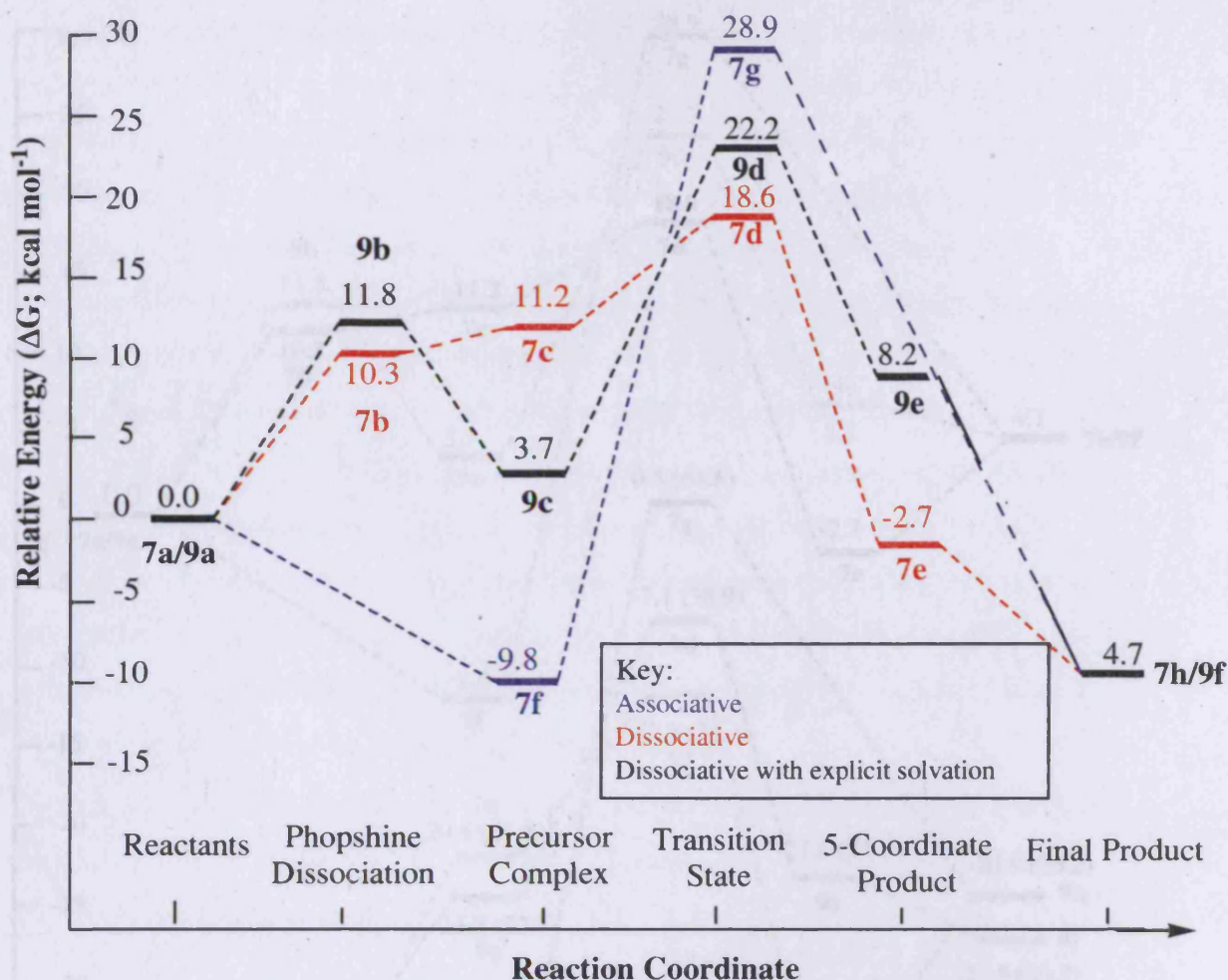


Figure 3-11 Pathway energies for oxidative addition of 1,3-dimethylimidazolium to $\text{Rh}(\text{P}(\text{CH}_3)_3)_3\text{Cl}$ and $\text{Rh}(\text{P}(\text{CH}_3)_3)_2(\text{THF})\text{Cl}$ (ΔG).

Overall, the use of an added THF molecule results in only small changes in the relative energies of the dissociative route (Figure 3-11). The most significant changes are the stabilisation of the precursor complex (Figure 3-9c) and the destabilisation of the 5-coordinate product (Figure 3-9e). A comparison of our enthalpy and free energy calculations show that the latter change is due to entropy effects.

3.3.4.2 Bulk solvent effects

The use of an added solvent molecule assisted in revealing some of the stabilising effects of solvents, so we extended this work to include energy calculations incorporating bulk solvent effects. Although a reoptimisation of the structures in solvent was not performed, recalculation of all energies including a bulk THF solvent interaction showed stabilising effects of the solvent on the charge separation within the reaction species as depicted in Figure 3-12.

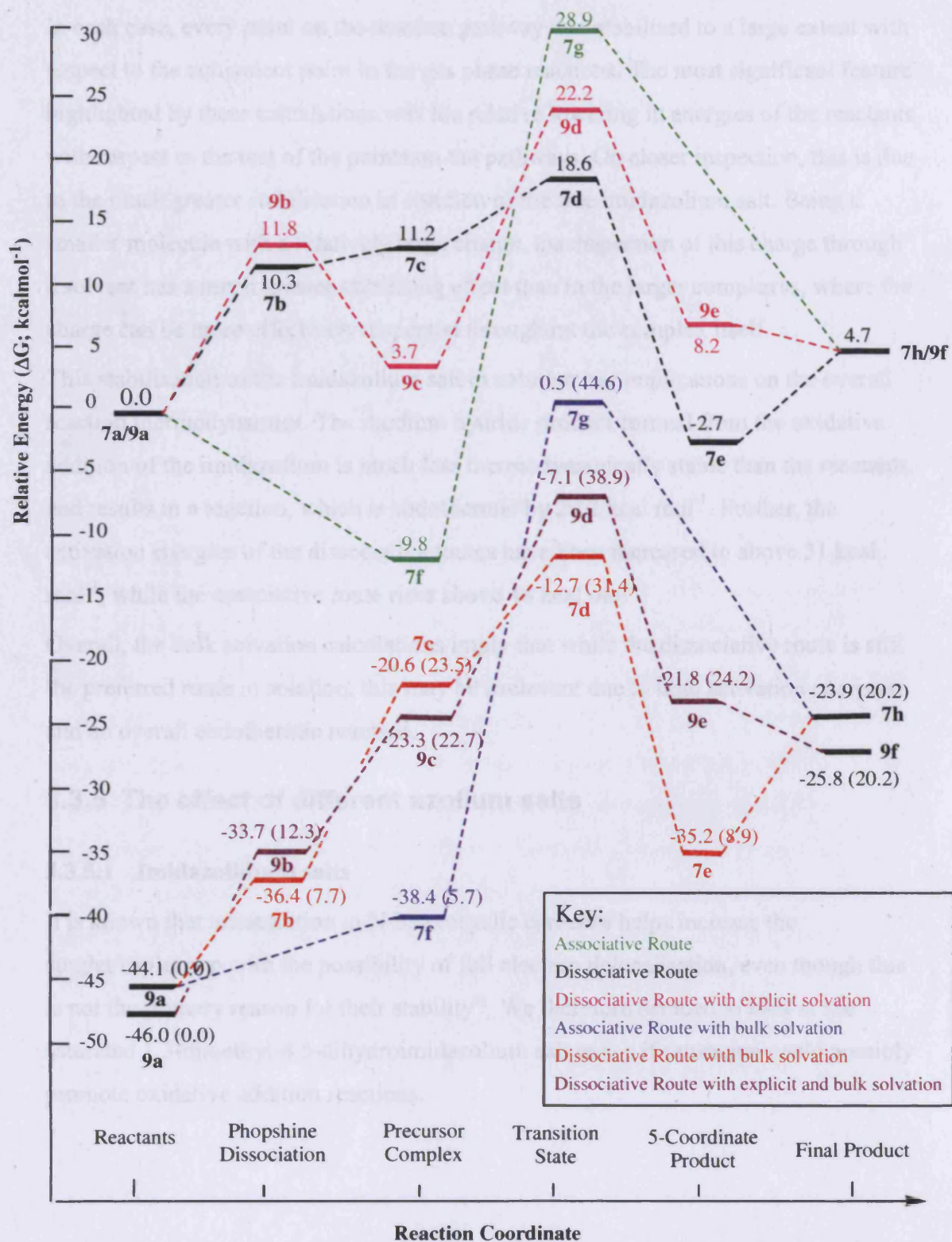


Figure 3-12 Pathway energies for oxidative addition of 1,3-dimethylimidazolium to $\text{Rh}(\text{P}(\text{CH}_3)_3)_3\text{Cl}$ and $\text{Rh}(\text{P}(\text{CH}_3)_3)_2(\text{THF})\text{Cl}$ including bulk solvent effects (ΔG).

In each case, every point on the reaction pathway was stabilised to a large extent with respect to the equivalent point in the gas phase reactions. The most significant feature highlighted by these calculations was the relative lowering in energies of the reactants with respect to the rest of the points on the pathways. On closer inspection, this is due to the much greater stabilisation in solution of the free imidazolium salt. Being a smaller molecule with a relatively large charge, the dispersion of this charge through a solvent has a much greater stabilising effect than in the larger complexes, where the charge can be more effectively dispersed throughout the complex itself.

This stabilisation of the imidazolium salt in solution has implications on the overall reaction thermodynamics. The rhodium hydride product formed from the oxidative addition of the imidazolium is much less thermodynamically stable than the reactants, and results in a reaction, which is endothermic by $20.2 \text{ kcal mol}^{-1}$. Further, the activation energies of the dissociative routes have been increased to above 31 kcal mol^{-1} , while the associative route rises above 44 kcal mol^{-1} .

Overall, the bulk solvation calculations imply that while the dissociative route is still the preferred route in solution, this may be irrelevant due to high activation energies and an overall endothermic reaction.

3.3.5 The effect of different azolium salts

3.3.5.1 Imidazolium salts

It is known that unsaturation in N-heterocyclic carbenes helps increase the singlet/triplet gap with the possibility of full electron delocalisation, even though this is not the primary reason for their stability⁷³. We therefore decided to look at the saturated 1,3-dimethyl-4,5-dihydroimidazolium salt to see if saturation could possibly promote oxidative addition reactions.

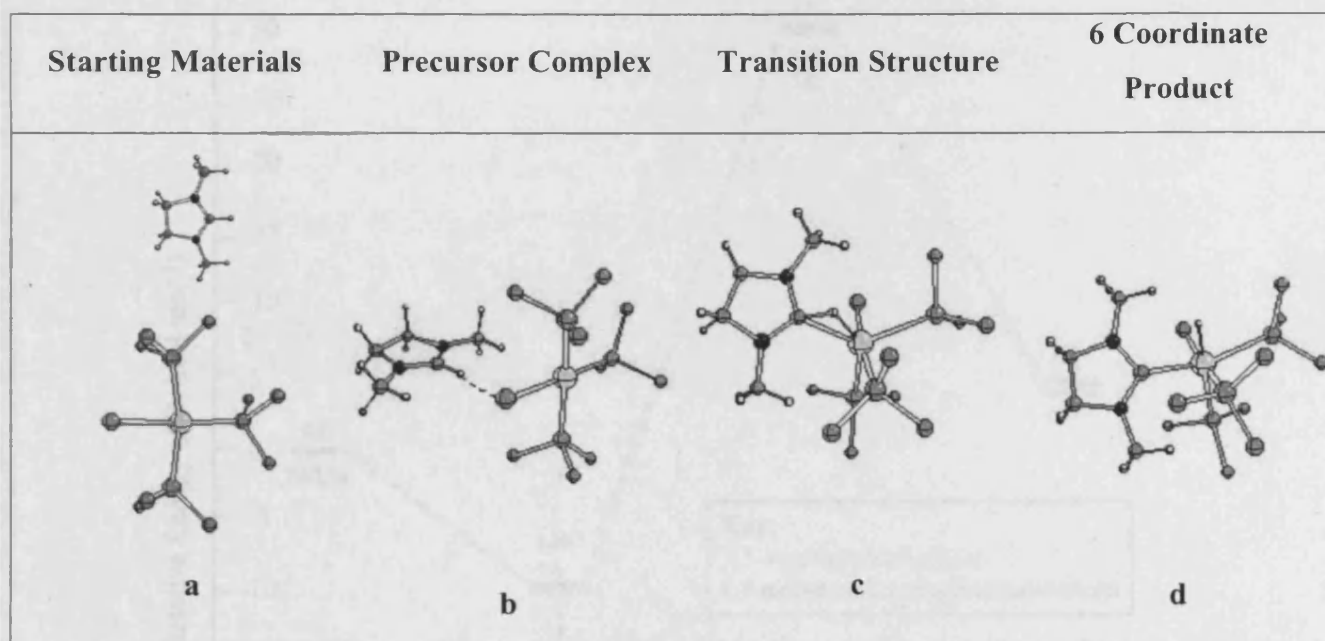


Figure 3-13 Optimised geometries of oxidative addition of 1,3-dimethyl-4,5-dihydroimidazolium to $\text{Rh}(\text{P}(\text{CH}_3)_3)_3\text{Cl}$ by associative route (phosphine hydrogens omitted for clarity).

Optimisation of all species for the saturated analogue resulted in essentially identical structures to those for the unsaturated imidazolium (Figure 3-13, a-d), with a few very minor exceptions. Firstly, due to the saturated backbone, the carbene ring itself in the transition structure (Figure 3-13c) is slightly buckled, with carbons 4 and 5 being slightly above and below the plane of the ring by about 7 degrees. The products also show the saturated carbene ligand marginally closer to the rhodium centre and the bond between the rhodium and the bottom phosphine ligand in this complex slightly longer. All other bond lengths and angles are in effect unchanged. Overall, the relative energies reflect the identical nature of the reactions, with no more than $0.3 \text{ kcal mol}^{-1}$ separating the relative energies of the saturated and unsaturated carbene complexes at any point (Figure 3-14).

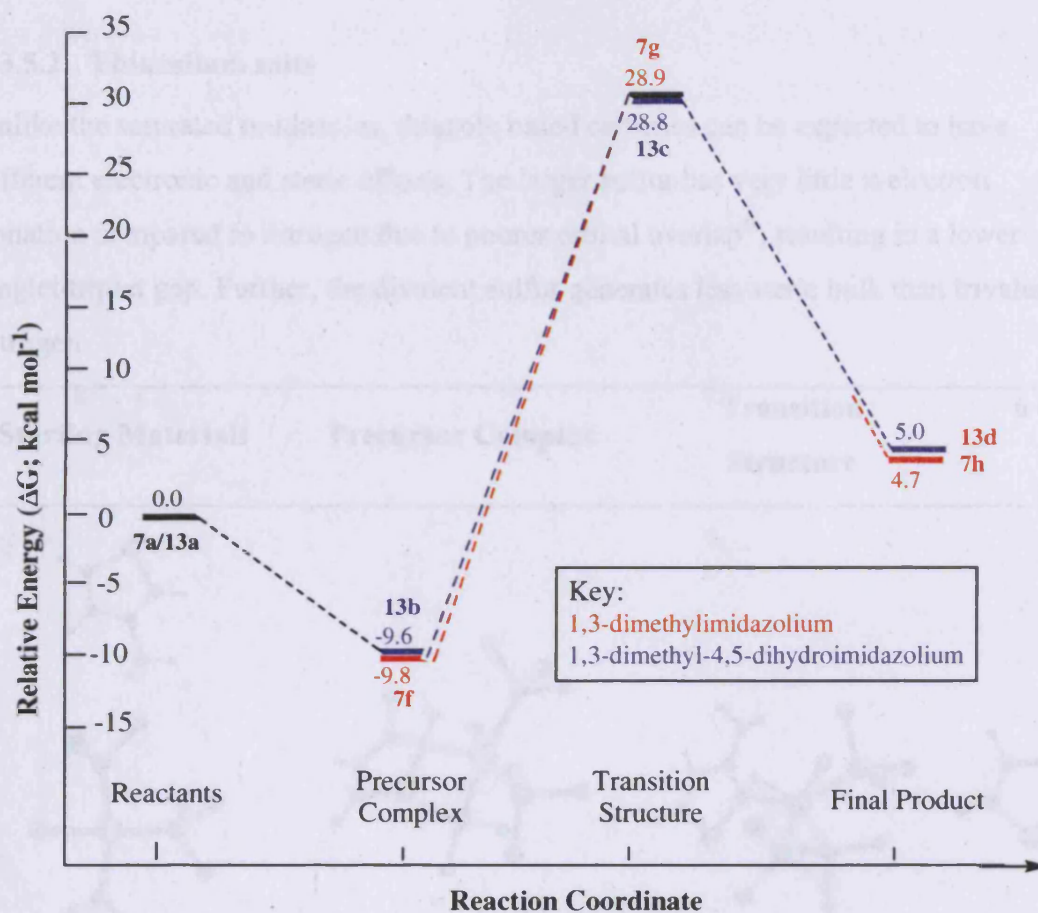


Figure 3-14 Pathway energies for oxidative addition of 1,3-dimethylimidazolium and 1,3-dimethyl-4,5-dihydroimidazolium to Rh(P(CH₃)₃)₃Cl (ΔG).

These results tend to confirm previous thoughts that the saturation of the imidazole ring has very little effect on the properties and reactivity of the carbene centre and its behaviour as a ligand. Complexes of both the saturated and unsaturated imidazole based carbene ligands have frequently proved to be similar, for example, iron carbonyl complexes of both showing similar trans CO stretching frequencies in the IR spectra⁷⁴.

3.3.5.2 Thiazolium salts

Unlike the saturated imidazoles, thiazole based carbenes can be expected to have different electronic and steric effects. The larger sulfur has very little π -electron donation compared to nitrogen due to poorer orbital overlap⁷⁵, resulting in a lower singlet/triplet gap. Further, the divalent sulfur generates less steric bulk than trivalent nitrogen.

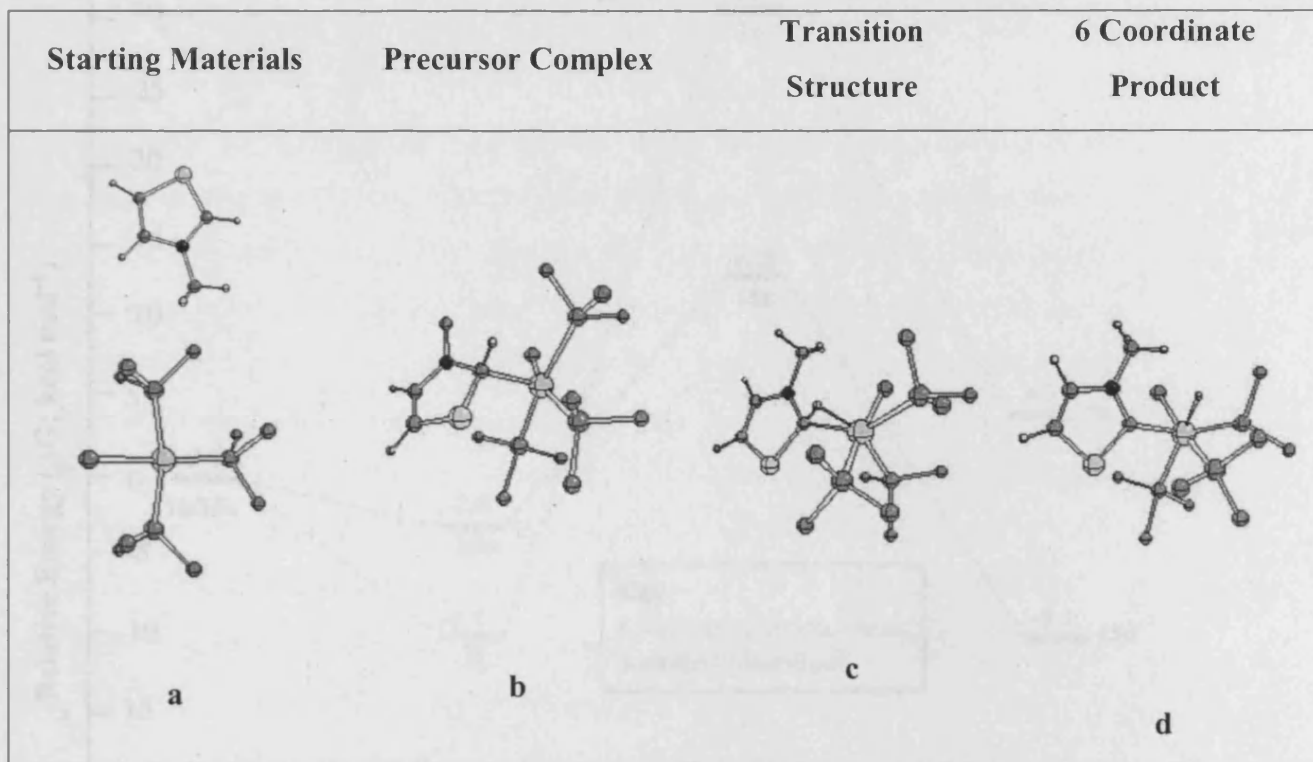


Figure 3-15 Optimised geometries of oxidative addition of 3-methylthiazolium to $\text{Rh}(\text{P}(\text{CH}_3)_3)_3\text{Cl}$ by associative route (phosphine hydrogens omitted for clarity).

Not surprisingly therefore, geometries for the thiazolium oxidative addition were different across the board (Figure 3-15, a-d). The precursor complex for the thiazolium salt showed an initial interaction between the C2 of the salt and the rhodium, with the 2-H bent out of the plane of the thiazolium ring. It was earlier shown bulk could be a factor in the choice between dissociative and associative routes and a close interaction as shown for the thiazolium salt is not as favourable for the imidazolium salts, with the methyl groups attached to two nitrogens increasing the steric bulk. The transition structure for the thiazolium is also much more advanced than that of the imidazolium: the rhodium to carbon bond is much shorter, with the carbon to hydrogen bond much longer. The extra space afforded by the divalent sulfur is also evident here. While the imidazolium ring is quite twisted with respect to the

rhodium square plane (64°), the thiazolium ring remains much closer to the plane (42°). This trend is reversed in the product, however, with the thiazolium being twisted to almost 71° compared to the imidazolium 67° . The general structures of the two products are very similar, with the thiazolium showing a slightly shorter Rh-C2 bond length.

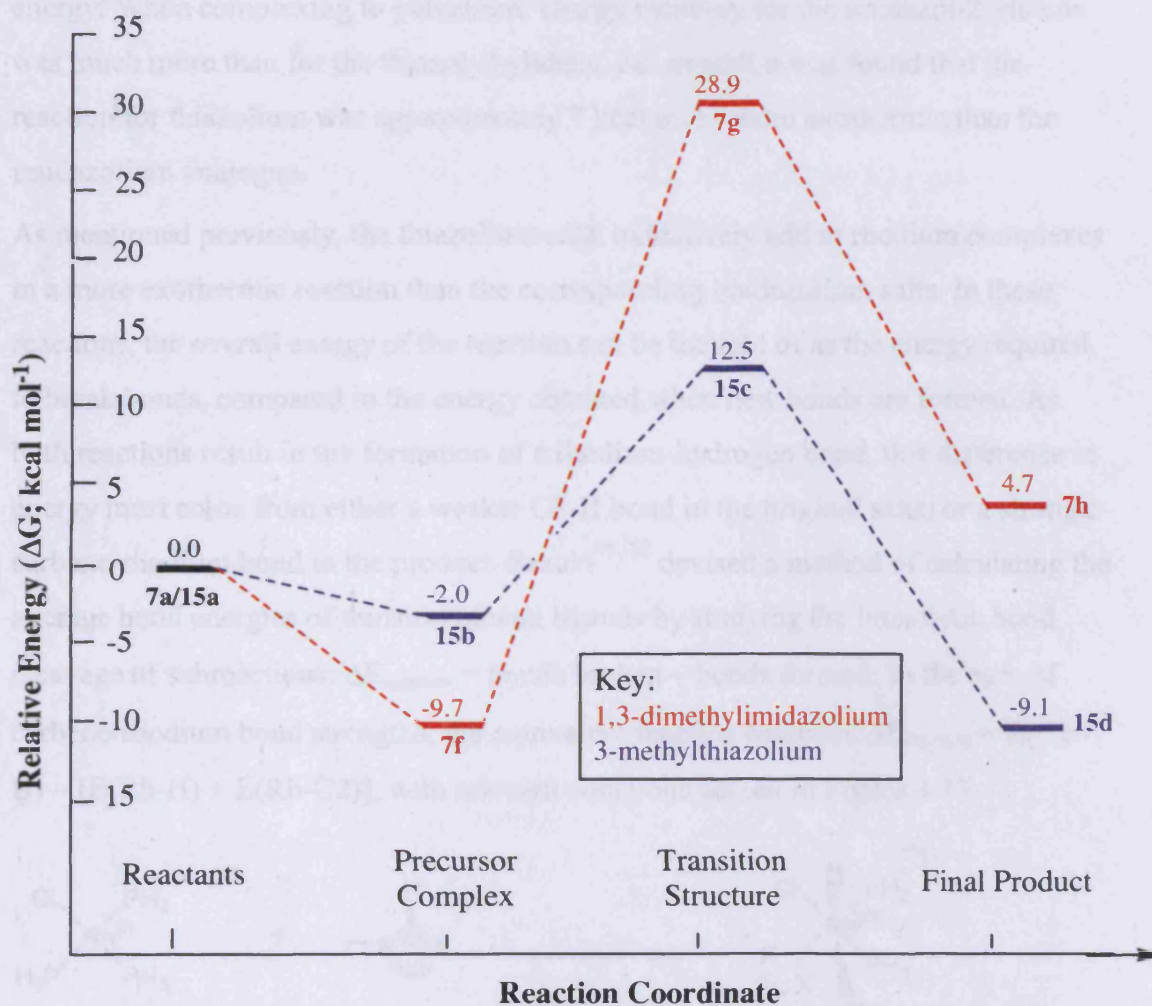


Figure 3-16 Pathway energies for oxidative addition of 1,3-dimethylimidazolium and 3-methylthiazolium to $\text{Rh}(\text{P}(\text{CH}_3)_3)_3\text{Cl}$ (ΔG).

The energies of the thiazolium pathway reveal that it is a much more thermodynamically favourable route, with the products lying $9.1 \text{ kcal mol}^{-1}$ below the reactants (Figure 3-16). Further, the activation energy is lower, with the transition structure only $12.5 \text{ kcal mol}^{-1}$ higher than the separated reactants.

3.3.5.2.1 M-Carbene bond strength

Graham has calculated the C2-H bond energy in thiazolium salts to be less than the respective bond energy in the imidazolium salts, making this bond easier to break⁷⁶. However, coordination of the formed carbene to a metal recovers much of this energy. When complexing to palladium, energy recovery for the imidazol-2-ylidene was much more than for the thiazol-2-ylidene, but overall it was found that the reaction for thiazolium was approximately 7 kcal mol⁻¹ more exothermic than the imidazolium analogue.

As mentioned previously, the thiazolium salts oxidatively add to rhodium complexes in a more exothermic reaction than the corresponding imidazolium salts. In these reactions, the overall energy of the reaction can be thought of as the energy required to break bonds, compared to the energy obtained when new bonds are formed. As both reactions result in the formation of a rhodium-hydrogen bond, this difference in energy must come from either a weaker C2-H bond in the original salts, or a stronger carbene-rhodium bond in the product. Sakaki^{77, 78} devised a method of calculating the average bond energies of transition metal ligands by studying the homolytic bond cleavage of subreactions: $\Delta E_{\text{reaction}} = \text{bonds broken} - \text{bonds formed}$. In the case of carbene-rhodium bond strengths, the equivalent reaction becomes $\Delta E_{\text{reaction}} = E(\text{C2-H}) - [E(\text{Rh-H}) + E(\text{Rh-C2})]$, with relevant equations set out in Figure 3-17.

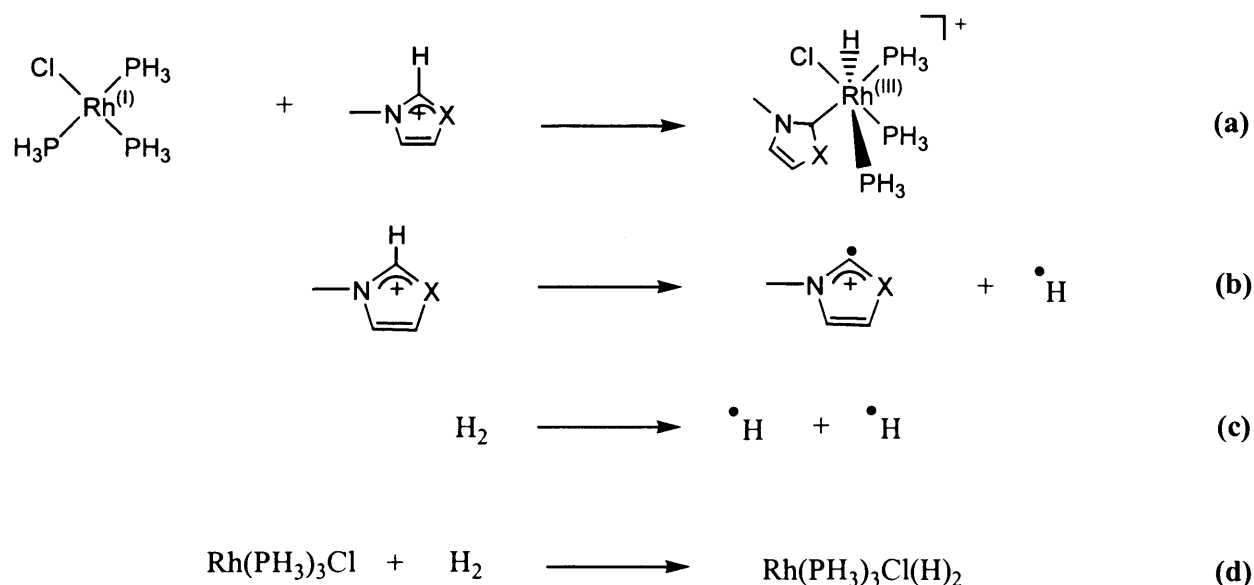


Figure 3-17 Reactions used to calculate average bond energies

Therefore, the energy of the carbene-rhodium bond can be calculated:

$$E(\text{Rh-C2}) = E(\text{C2-H}) - E(\text{Rh-H}) - \Delta E$$

Where ΔE is obtained directly from reaction (a) in Figure 3-17, the azolium C2-H bond strength ($E(\text{C2-H})$) can be calculated from reaction (b), and the Rh-H bond strength can be calculated from reactions (c) and (d). Results of all calculations are shown in Table 3-1.

Reaction	Figure 3-17 reference	C2-H bond strength [ROB3LYP/6-31g(d) // UB3LYP 6-311+G(2d,p)] (kcal/mol)
$\Delta E_{\text{imidazolium}}$	(a)	-1.6
$\Delta E_{\text{thiazolium}}$	(a)	-21.8
$E(\text{C2-H})_{\text{imidazolium}}$	(b)	152.5
$E(\text{C2-H})_{\text{thiazolium}}$	(b)	105.6
ΔE_{H2oxad}	(d)	4.7
$E(\text{H-H})$	(c)	104.5
$E(\text{Rh-H})$	$[E(\text{H-H}) - \Delta E_{\text{H2oxad}}]/2$	49.9
$E(\text{Rh-C2})_{\text{imidazolium}}$	$E(\text{C2-H}) - E(\text{Rh-H}) - \Delta E$	104.2
$E(\text{Rh-C2})_{\text{thiazolium}}$	$E(\text{C2-H}) - E(\text{Rh-H}) - \Delta E$	77.5

Table 3-1 Reaction energies used to calculate rhodium-carbene bond strength

As these results indicate, the imidazolium C2-H bond is noticeably stronger than the corresponding thiazolium bond, however much of the energy required to break the thiazolium bond is recovered in the formation of the carbene-rhodium bond in the product. Similar to the results found by Graham for palladium, the imidazole based carbene ligand forms a much stronger bond to rhodium than does the thiazol-2-ylidene, due to increased sigma donation from the carbene ligand, however the

exothermicity of the reaction is less due to the energy required to break the much stronger C2-H bond.

3.4 Conclusions

Consistent with experimental results for the oxidative addition of H₂ to Wilkinson's catalyst during the hydrogenation reactions, theoretical results for the oxidative addition of azolium salts to RhCl(PR₃)₃ show that oxidative addition could occur by either an associative or dissociative route, depending on reaction conditions.

Predissociation of a phosphine molecule does appear to be the favoured route and if it does occur the precursor complex can then be stabilised by filling the vacant coordination site with a smaller solvent molecule. Inclusion of a bulk solvent has significant effects on the overall reaction, in particular in stabilising the charge distribution for the smaller reactant molecules. With the inclusion of a bulk solvent, the products become much less thermodynamically stable, and other factors are required to increase the exothermicity of the reaction for imidazolium salts, either through the use of an alternative solvent or by using ligands with a greater electron donating capacity.

While saturation on the backbone of the carbene ligand appears to have little effect on the reaction, replacing the imidazolium salt with a thiazolium salt increases the exothermicity of the reaction while also lowering activation energies. This result appears to be influenced by both the different steric and electronic interactions of the thiazolium.

Of importance is the observation that the reductive elimination reaction, involving the carbene complex converting back to the azolium salt and rhodium(I) complex, is simply the reverse of the reactions studied. With the products being much less thermodynamically stable, and the reverse activation energies relatively lower than the forward reaction, it appears that reductive elimination could occur in rhodium carbene hydride species in solution to form the corresponding azolium salt. Electron donating auxiliary ligands, combined with the use of thiazole based carbene ligands may help produce more stable rhodium(III)-carbene complexes.

3.5 References

- 1 A. J. I. Arduengo, R. L. Harlow and M. Kline, *J. Am. Chem. Soc.*, 1991, **113**, 361.
- 2 W. A. Herrmann, *Angew. Chem., Int. Ed. Engl.*, 2002, **41**, 1290.
- 3 D. S. McGuinness and K. J. Cavell, *Organometallics*, 2000, **19**, 4918.
- 4 D. S. McGuinness, N. Saendig, B. F. Yates and K. J. Cavell, *J. Am. Chem. Soc.*, 2001, **123**, 4029.
- 5 S. Gründemann, M. Albrecht, A. Kovacevic, J. W. Faller and R. H. Crabtree, *J. Chem. Soc., Dalton Trans.*, 2002, **10**, 2163.
- 6 D. S. McGuinness, K. J. Cavell and B. F. Yates, *Chem. Commun.*, 2001, **4**, 355.
- 7 M. Albrecht, R. H. Crabtree, J. Mata and E. Peris, *Chem. Commun.*, 2002, **1**, 32.
- 8 M. A. Duin, N. D. Clement, K. J. Cavell and C. J. Elsevier, *Chem. Commun.*, 2003, **3**, 400.
- 9 D. S. McGuinness, K. J. Cavell, B. F. Yates, B. W. Skelton and A. H. White, *J. Am. Chem. Soc.*, 2001, **123**, 8317.
- 10 M. R. A. Blomberg, P. E. M. Siegbahn, E. Nagashima and J. Wennerberg, *J. Am. Chem. Soc.*, 1991, **113**, 424.
- 11 P. E. M. Siegbahn, M. R. A. Blomberg and M. Svensson, *J. Am. Chem. Soc.*, 1993, **115**, 1952.
- 12 M. R. A. Blomberg, P. E. M. Siegbahn and M. Svensson, *J. Am. Chem. Soc.*, 1992, **114**, 6095.
- 13 J. M. Buchanan, J. M. Stryker and R. G. Bergman, *J. Am. Chem. Soc.*, 1986, **108**, 1537.
- 14 A. H. Janowicz and R. G. Bergman, *J. Am. Chem. Soc.*, 1982, **104**, 352.
- 15 A. H. Janowicz and R. G. Bergman, *J. Am. Chem. Soc.*, 1983, **105**, 3929.
- 16 W. D. Jones and F. J. Feher, *J. Am. Chem. Soc.*, 1982, **104**, 4240.
- 17 M. Prinz, M. Grosche, E. Herdtweck and W. A. Herrmann, *Organometallics*, 2000, **19**, 1692.

- 18 M. Mühlhofer, T. Strassner and W. A. Herrmann, *Angew. Chem., Int. Ed. Engl.*, 2002, **42**, 1745.
- 19 C. Jian-Yang, T. Man Kin, D. Holmes, R. E. J. Maleczka and M. R. I. Smith, *Science*, 2002, **295**, 305.
- 20 D. Hermann, M. Gandelman, H. Rozenberg, L. J. W. Shimon and D. Milstein, *Organometallics*, 2002, **21**, 812.
- 21 A. Sundermann, O. Uzan and J. M. L. Martin, *Organometallics*, 2001, **20**, 1783.
- 22 S. K. Ritter, *Chem. Eng. News*, 2002, **80**, 26.
- 23 B. Rybtchinski, A. Vigalok, B. Yehoshoa and D. Milstein, *J. Am. Chem. Soc.*, 1996, **118**, 12406.
- 24 B. Rybtchinski, S. Oevers, M. Montag, A. Vigalok, H. Rozenberg, J. M. L. Martin and D. Milstein, *J. Am. Chem. Soc.*, 2001, **123**, 9064.
- 25 J. Huang, E. D. Stevens and S. P. Nolan, *Organometallics*, 2000, **19**, 1194.
- 26 M. E. van der Boom, L. Shyh-Yeon, B. Yehoshoa, M. Gozin and D. Milstein, *J. Am. Chem. Soc.*, 1998, **120**, 13415.
- 27 H. M. L. Davies and E. G. Antoulinakis, *J. Organomet. Chem.*, 2001, **617-618**, 47.
- 28 Z. Cao and M. B. Hall, *Organometallics*, 2000, **19**, 3338.
- 29 N. Koga and K. Morokuma, *J. Phys. Chem.*, 1990, **94**, 5454.
- 30 P. Margl, T. Ziegler and P. E. Blöchl, *J. Am. Chem. Soc.*, 1995, **117**, 12625.
- 31 F. Favre, H. Olivier-Bourbigou, D. Commereuc and L. Saussine, *Chem. Commun.*, 2001, **15**, 1360.
- 32 W. Keim, D. Vogt, H. Waffenschmidt and P. Wasserscheid, *J. Catal.*, 1999, **186**, 481.
- 33 P. A. Z. Suarez, J. E. L. Dullius, S. Einloft, R. F. De Souza and J. Dupont, *Polyhedron*, 1996, **15**, 1217.
- 34 Y. Chauvin, L. Mussmann and H. Olivier, *Angew. Chem., Int. Ed. Engl.*, 1995, **34**, 2698.
- 35 F. Liu, M. B. Abrams, T. Baker and W. Tumas, *Chem. Commun.*, 2001, **5**, 433.

- 36 C. P. Mehnert, E. J. Mozeleski and R. A. Cook, *Chem. Commun.*, 2002, **24**, 3010.
- 37 P. J. Dyson, D. J. Ellis and T. Welton, *Can. J. Chem.*, 2001, **79**, 705.
- 38 P. Wasserscheid, H. Waffenschmidt, P. Machnitzki, K. W. Kottsieper and O. Stelzer, *Chem. Commun.*, 2001, **5**, 451.
- 39 S. Guernik, A. Wolfson, M. Herskowitz, N. Greenspoon and S. Geresh, *Chem. Commun.*, 2001, **22**, 2314.
- 40 C. C. Brasse, U. Englert, A. Salzer, H. Waffenschmidt and P. Wasserscheid, *Organometallics*, 2000, **19**, 3818.
- 41 C. P. Mehnert, R. A. Cook, N. C. Dispenziere and M. Afeworki, *J. Am. Chem. Soc.*, 2002, **124**, 12932.
- 42 M. F. Sellin, P. B. Webb and D. J. Cole-Hamilton, *Chem. Commun.*, 2001, **8**, 781.
- 43 R. H. Hertwig and W. Koch, *Chem. Phys. Lett.*, 1997, **268**, 345.
- 44 P. J. Stephens, J. F. Devlin, C. F. Chabalowski and M. J. Frisch, *J. Phys. Chem.*, 1994, **98**, 11623.
- 45 A. D. Becke, *J. Chem. Phys.*, 1993, **98**, 5648.
- 46 P. J. Hay and W. R. Wadt, *J. Chem. Phys.*, 1985, **82**, 299.
- 47 T. H. Dunning and P. J. Hay, 'Modern Theoretical Chemistry', Plenum, 1976.
- 48 B. F. Yates, *J. Mol. Struct. (THEOCHEM)*, 2000, **506**, 223.
- 49 M. J. Frisch, J. A. Pople and J. S. Binkley, *J. Chem. Phys.*, 1984, **80**, 3265.
- 50 A. D. McLean and G. S. Chandler, *J. Chem. Phys.*, 1980, **72**, 5639.
- 51 R. Krishnan, J. S. Binkley, R. Seeger and J. A. Pople, *J. Chem. Phys.*, 1980, **72**, 650.
- 52 S. Miertus, E. Scrocco and J. Tomasi, *Chem. Phys.*, 1981, **55**, 117.
- 53 S. Miertus and J. Tomasi, *Chem. Phys.*, 1982, **65**, 239.
- 54 V. Barone and M. Cossi, *J. Phys. Chem.*, 1998, **102**, 1995.
- 55 M. J. Frisch, G. W. Trucks, H. B. Schlegel, G. E. Scuseria, M. A. Robb, J. R. Cheeseman, V. G. Zakrzewski, J. A. Montgomery, Jr. , R. E. Stratmann, J. C. Burant, S. Dapprich, J. M. Millam, A. D. Daniels, K. N. Kudin, M. C. Strain, O. Farkas, J. Tomasi, V. Barone, M. Cossi, R. Cammi, B. Mennucci, C.

- Pomelli, C. Adamo, S. Clifford, J. Ochterski, G. A. Petersson, P. Y. Ayala, Q. Cui, K. Morokuma, N. Rega, P. Salvador, J. J. Dannenberg, D. K. Malick, A. D. Rabuck, K. Raghavachari, J. B. Foresman, J. Cioslowski, J. V. Ortiz, A. G. Baboul, B. B. Stefanov, G. Liu, A. Liashenko, P. Piskorz, I. Komaromi, R. Gomperts, R. L. Martin, D. J. Fox, T. Keith, M. A. Al-Laham, C. Y. Peng, A. Nanayakkara, M. Challacombe, P. M. W. Gill, B. Johnson, W. Chen, M. W. Wong, J. L. Andres, C. Gonzalez, M. Head-Gordon, E. S. Replogle and J. A. Pople, Gaussian 98 (Revision A.11.3), Pittsburgh PA, 2002.
- 56 A. Dedieu and A. Strich, *Inorg. Chem.*, 1979, **18**, 2940.
- 57 A. Dedieu, *Inorg. Chem.*, 1980, **19**, 375.
- 58 C. Daniel, N. Koga, X. Y. Fu and K. Morokuma, *J. Am. Chem. Soc.*, 1988, **110**, 3773.
- 59 D. G. Musaev and K. Morokuma, *J. Organomet. Chem.*, 1995, **504**, 93.
- 60 D. F. Shriver, P. W. Atkins and C. H. Langford, 'Inorganic Chemistry', Oxford University Press, 1994.
- 61 J. M. Brown, P. L. Evans and A. R. Lucy, *J. Chem. Soc., Perkin Trans. II*, 1987, 1589.
- 62 J. M. Brown and A. R. Lucy, *Chem. Comm.*, 1984, 914.
- 63 D. G. Musaev, T. Matsubara, A. M. Mebel, N. Koga and K. Morokuma, *Pure & Appl. Chem.*, 1995, **67**, 257.
- 64 N. Koga and K. Morokuma, *J. Am. Chem. Soc.*, 1993, **115**, 6883.
- 65 L. Horner, H. Büthe and H. Siegel, *Tetrahedron Lett.*, 1968, **37**, 4023.
- 66 J. R. Peterson, D. W. Bennett and L. D. Spicer, *J. Catal.*, 1981, **71**, 223.
- 67 W. Strohmeier and E. Hitzel, *J. Organomet. Chem.*, 1975, **87**, 353.
- 68 J. Halpern and C. S. Wong, *Chem. Commun.*, 1973, **17**, 629.
- 69 H. Heinrich, R. Giernoth, J. Bargon and J. M. Brown, *Chem. Comm.*, 2001, 1296.
- 70 T. Matsubara, N. Koga, Y. Ding, D. G. Musaev and K. Morokuma, *Organometallics*, 1997, **16**, 1065.
- 71 N. Koga, C. Daniel, J. Han, X. Y. Fu and K. Morokuma, *J. Am. Chem. Soc.*, 1987, **109**, 3455.

- 72 D. E. Bergbreiter and M. S. Bursten, *J. Macromol. Sci. Chem.*, 1981, **A16**, 369.
- 73 W. A. Herrmann and C. Köcher, *Angew. Chem., Int. Ed. Engl.*, 1997, **36**, 2162.
- 74 W. A. Herrmann, P. W. Roesky, M. Elison, G. R. J. Artus and K. Öfele, *Organometallics*, 1995, **14**, 1085.
- 75 J. Kapp, C. Schade, A. M. El-Nahasa and P. v. R. Schleyer, *Angew. Chem., Int. Ed. Engl.*, 1996, **35**, 2236.
- 76 D. Graham, Ph.D. Thesis, University of Tasmania, Hobart, 2003
- 77 S. Sakaki, S. Kai and M. Sugimoto, *Organometallics*, 1999, **19**, 4825.
- 78 S. Sakaki, B. Biswas and M. Sugimoto, *Organometallics*, 1998, **17**, 1278.

4 Rhodium and Iridium Oxidative Addition Reactions

4.1 Introduction

The previous chapter indicated carbene ligands may be involved in oxidative addition and reductive elimination reactions from catalytically active rhodium complexes. The replacement of C-H bonds with C-X is important in numerous academic and industrial processes. However, the methods currently used to perform these conversions often require high temperatures and can be unselective, especially for abundant, but generally inert, alkanes. Due to the importance of these conversions, much experimental and theoretical study has been devoted to understanding what conditions affect the transition metal oxidative addition and reductive elimination reactions involved.

As would be expected in reactions involving metal complexes, the ligand set used on the metal can have a significant influence on the chemistry of oxidative addition, both electronically and sterically. Electronic structure requirements for a low barrier to oxidative addition involve the metal reactant being in a low-lying triplet state¹. Further, oxidative addition in general becomes more favourable as the system becomes more negatively charged². Therefore, more basic ligands with minimal back-bonding tend to enhance the oxidative addition ability of a metal.

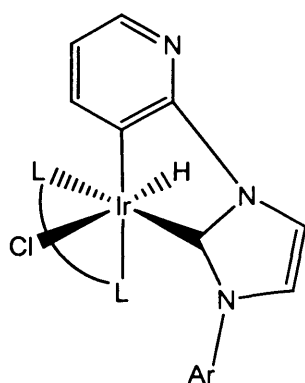


Figure 4-1 Example intramolecular C-H activation product¹¹

Sterically, the metal centre needs to be accessible to allow the reactant to interact with the metal centre. Thus, low-valent metal complexes may require heat or light for predissociation of a ligand to form a coordinatively unsaturated complex capable of oxidative addition³⁻⁶. For the same reason, oxidative addition reactions have been slowed by excess ligand, as this shifts the equilibrium towards the undissociated species⁷. Further, a bulky ligand set can often lead to undesired intramolecular cyclometallation reactions, which renders the metal centre inactive to further reaction⁸⁻¹⁰ (Figure 4-1).

As was shown in the previous chapter, a model of Wilkinson's catalyst, $\text{RhCl}(\text{PR}_3)_3$ could potentially be used to create rhodium(III) carbene complexes via C-H activation of azolium salts. Phosphines have frequently been used as ligands to create complexes capable of oxidative addition reactions, with the range of electronic and steric effects provided making it possible to tailor the environment at the metal centre so oxidative addition can occur with a low barrier and with maximum product stability.

Despite this, the exact combination of electronic and steric factors provided by the ligands is often not as obvious as may seem. Often the R groups in PR_3 ligands point away from the metal centre, resulting in only minor steric interactions at the reacting metal centre, and significant alteration of R groups directly affects the basicity of the phosphine ligands. Further, phosphine complexes have been known to degrade via P-C cleavage within the ligand itself. Traditionally, this has resulted in the requirement of excess phosphines in reaction mixtures to compensate for any ligand loss due to degradation; a condition that may suppress oxidative addition reactions.

As shown in the previous chapter, the oxidative addition of azolium salts to rhodium(I) species could be possible under the right experimental conditions. Further, a change from the PH_3 to the more basic PMe_3 ligand increased electron density on the metal centre and in turn increased the exothermicity and decreased the activation energy for the overall oxidative addition reaction. Carbenes have been shown to be more basic¹¹ and as versatile as phosphines, with substitution at the nitrogen and 4,5 positions of the carbene ring relatively easily achieved, consequently providing an alternative means of controlling both steric and electronic factors on the metal centre.

There are already many reactions known to yield carbene complexes by oxidative addition¹²⁻¹⁷.

Further, many carbene complexes have proven to be excellent catalysts in reactions with known oxidative addition/reductive elimination cycles¹⁸⁻²¹

(Figure 4-2). As such, we thought to extend our previous work on oxidative addition reactions by Wilkinson's catalyst ($\text{Rh}(\text{PR}_3)_3\text{Cl}$) by replacing the

phosphines used in the rhodium complex with carbene ligands themselves, to see if this could further promote the activation of the C2-H bond in azolium salts. This chapter presents the results of systematically altering this ligand set, ranging from the

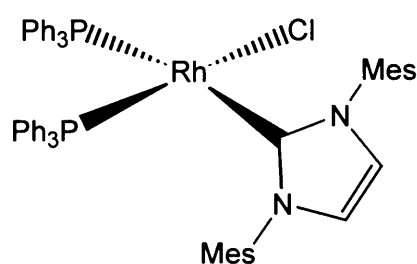


Figure 4-2 Example carbene complex for hydroformylation catalysis²³

π -acidic carbon monoxide, to the high σ -electron donation capacity of the carbene ligands themselves. In addition to C-H and C-C activation of the azolium salts, the effect of exchange of the central rhodium atom for the larger iridium is studied.

4.2 Computational details

All geometry optimisations and harmonic vibrational frequencies were calculated at the B3LYP²²⁻²⁴ level of theory with the LANL2DZ basis set, which incorporates the Hay and Wadt²² small core relativistic effective core potential and double zeta valence basis set on rhodium, phosphorus, chlorine and sulfur, with the Dunning and Huzinaga²⁵ double zeta basis set on all other atoms. Zero point vibrational energy corrections were obtained using unscaled frequencies. All transition structures contained exactly one imaginary frequency and were characterised by following the corresponding normal mode towards the products and reactants. NBO and Mulliken populations were calculated at this level of theory.

Higher level single point calculations were performed on the B3LYP/LANL2DZ optimised geometries at the B3LYP level with a LANL2augmented:6-311+G(2d,p) basis set, incorporating the LANL2 effective core potential and a large LANL2TZ+(3f) basis set on rhodium. This basis set was obtained by us in the same way as described for the Pt LANL2TZ+(3f) basis set reported previously²⁶. All other atoms used the 6-311+G(2d,p)²⁷⁻²⁹ basis set. Energies from these single point calculations were combined with the thermodynamic corrections at the lower level of theory to obtain ΔH_{298} and ΔG_{298} numbers. All energies quoted refer to these final ΔH_{298} or ΔG_{298} values.

All calculations were performed with the Gaussian 98³⁰ set of programs.



4.3 Results and discussion

4.3.1 Ligand effects – C-H activation

4.3.1.1 Rh(dmiy)(CO)₂Cl

It has been demonstrated experimentally that, in the solid state, the carbonyl ligands of Rh(dmiy)(CO)₂Cl occupy mutually *cis* positions³¹⁻³⁴. Geometry optimisations of both the *cis* and *trans* forms reflected experimental conditions with the *cis* form 9 kcal mol⁻¹ more stable than the *trans* form at the optimisation level of theory (Figure 4-3).

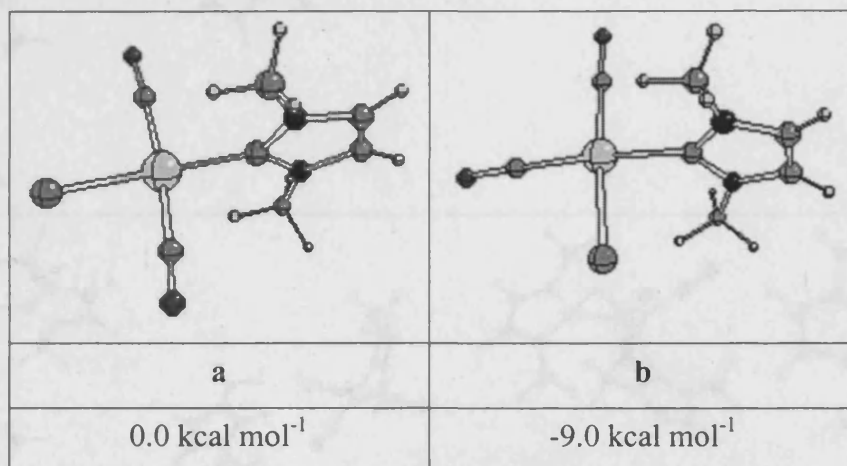


Figure 4-3 Isomers of Rh(dmiy)(CO)₂Cl

For the oxidative addition of 1,3-dimethylimidazolium to Rh(dmiy)(CO)₂Cl, two transition structures were considered; one with the incoming imidazolium pushing a CO ligand below the rhodium plane and the other with the larger carbene ligand being displaced. Not surprisingly, geometries for each pathway were very similar, with the C2-Rh and C2-H distances in the transition structures almost identical at 2.20Å (C2-Rh) and 1.44Å (C2-H) for Figure 4-4 1c and 2.18Å (C2-Rh) and 1.46Å (C2-H) for Figure 4-4 2c.

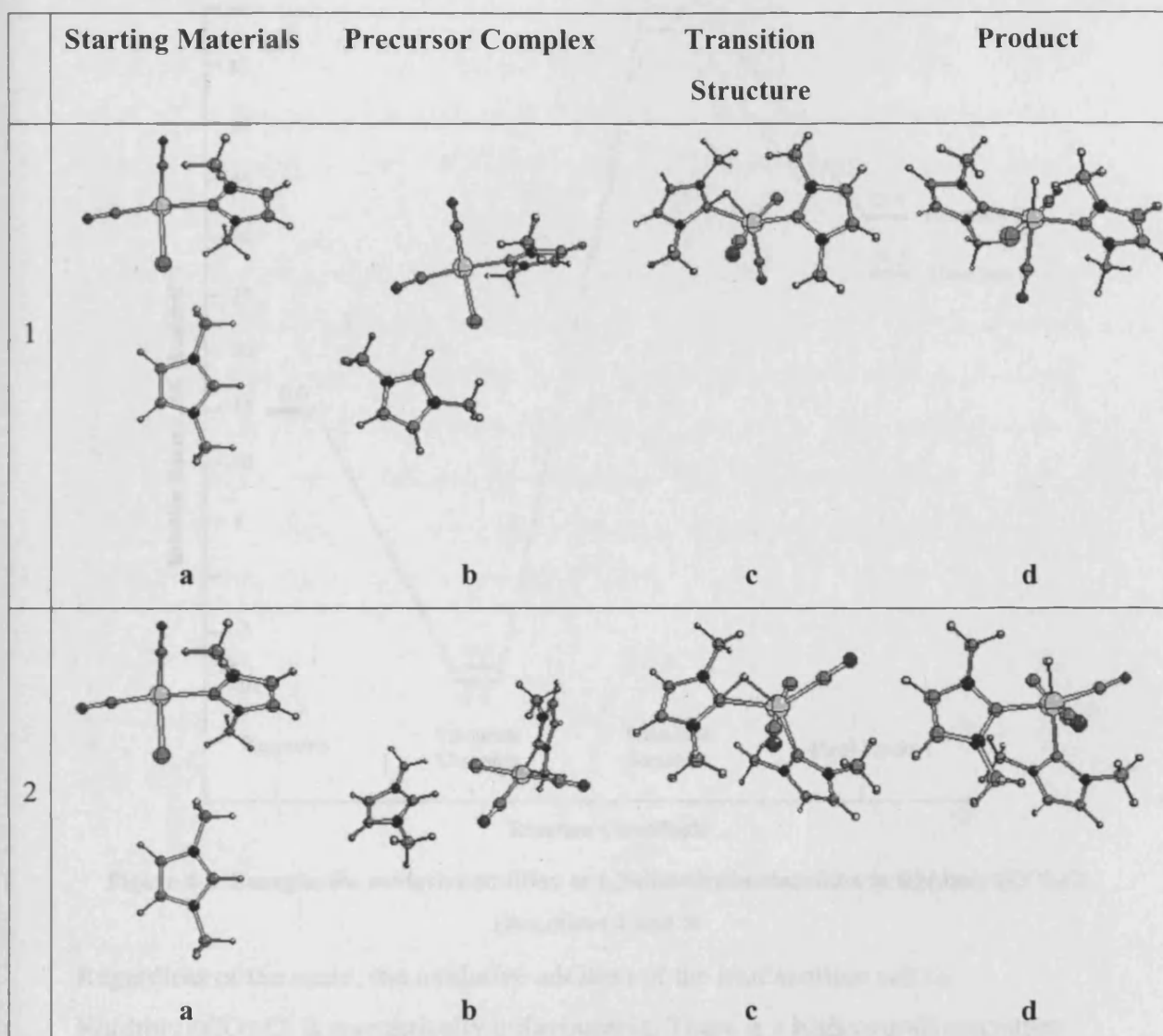


Figure 4-4 Oxidative Addition of 1,3-dimethylimidazolium to $\text{Rh}(\text{dmiy})(\text{CO})_2\text{Cl}$.

(1) Displacement of a carbonyl ligand; (2) Displacement of a dmiy ligand (Reactions 1 and 2)

Despite the similar geometries, the activation energy and overall thermodynamics marginally favour Reaction 1 with the carbene ligands located in the *trans* positions (Figure 4-5). This is most likely due to steric factors, as the carbene ligands are far bulkier than any of the remaining ligands and a *trans* arrangement affords the greatest relief of steric congestion in all reaction structures. The effect of this additional bulk in the carbene ligand is reflected in the transition structure, with the smaller CO and chloride ligands allowing the carbene more room in which to react without steric interference.

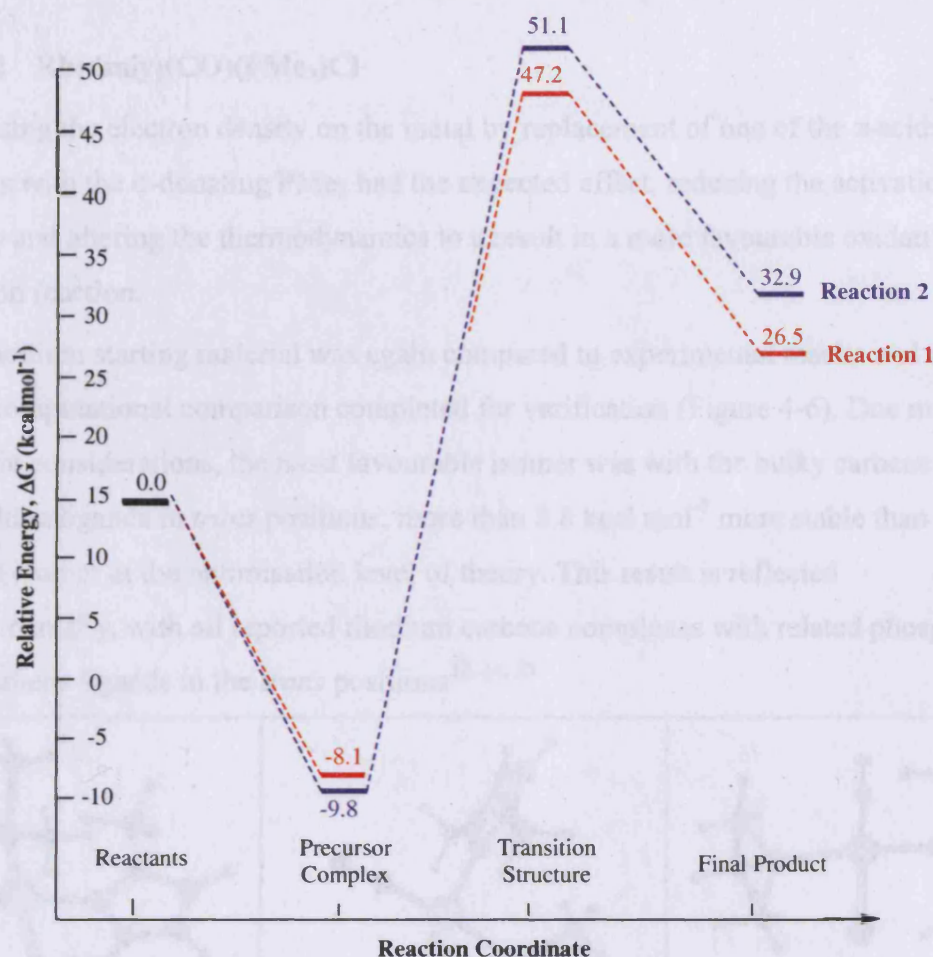


Figure 4-5 Energies for oxidative addition of 1,3-dimethylimidazolium to $\text{Rh}(\text{dmip})(\text{CO})_2\text{Cl}$ (Reactions 1 and 2)

Regardless of the route, the oxidative addition of the imidazolium salt to $\text{Rh}(\text{dmip})(\text{CO})_2\text{Cl}$ is energetically unfavourable. There is a high overall activation energy barrier of $55.3 \text{ kcal mol}^{-1}$ to overcome, and the reaction is endothermic by $26.5 \text{ kcal mol}^{-1}$ at best.

4.3.1.2 Rh(dmly)(CO)(PMe₃)Cl

Increasing the electron density on the metal by replacement of one of the π -acidic CO ligands with the σ -donating PMe₃ had the expected effect, reducing the activation energy and altering the thermodynamics to a result in a more favourable oxidative addition reaction.

The rhodium starting material was again compared to experimental results and a low level computational comparison completed for verification (Figure 4-6). Due mainly to steric considerations, the most favourable isomer was with the bulky carbene and phosphine ligands in *trans* positions; more than 8.8 kcal mol⁻¹ more stable than the closest isomer at the optimisation level of theory. This result is reflected experimentally, with all reported rhodium carbene complexes with related phosphine and carbene ligands in the *trans* positions^{32, 34, 35}.

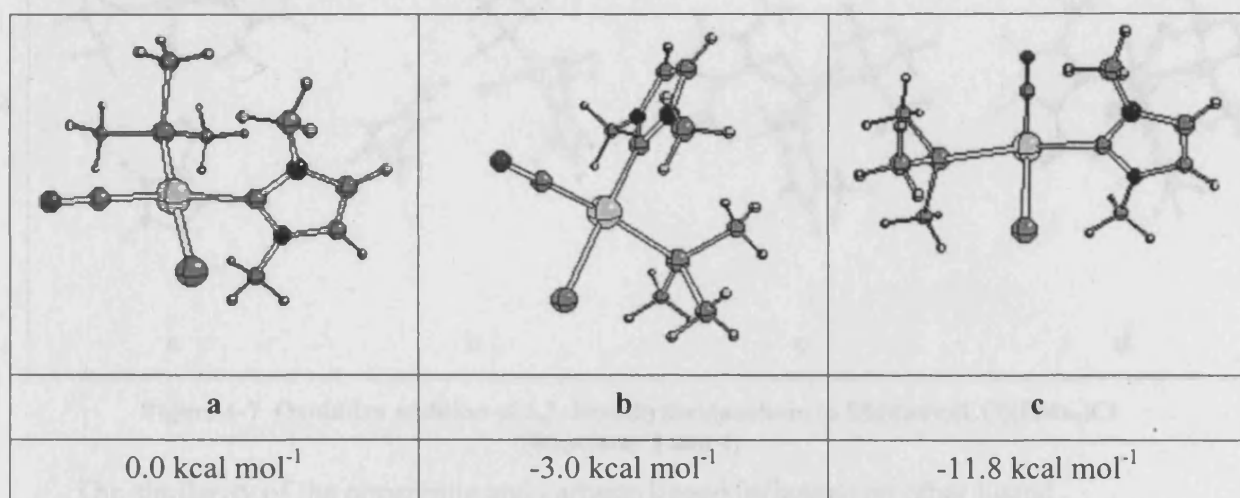


Figure 4-6 Isomers of Rh(dmly)(CO)(PMe₃)Cl

Previous results by Diggle suggest the high influence of CO ligands makes the hydride *trans* to either the carbene or phosphine a more stable product¹⁹. While the previous section indicated a CO ligand would be located *trans* to the hydride in the Rh(dmly)(CO)₂Cl oxidative addition reaction, this result is expected to be mainly influenced by steric interactions. As the larger ligands cannot be separated in the Rh(dmly)(CO)(PMe₃)Cl system, the results by Diggle were used as a template for this reaction. Hence, two transition structures were considered with the carbene and phosphine ligands *trans* to the final hydride ligand (Figure 4-7).

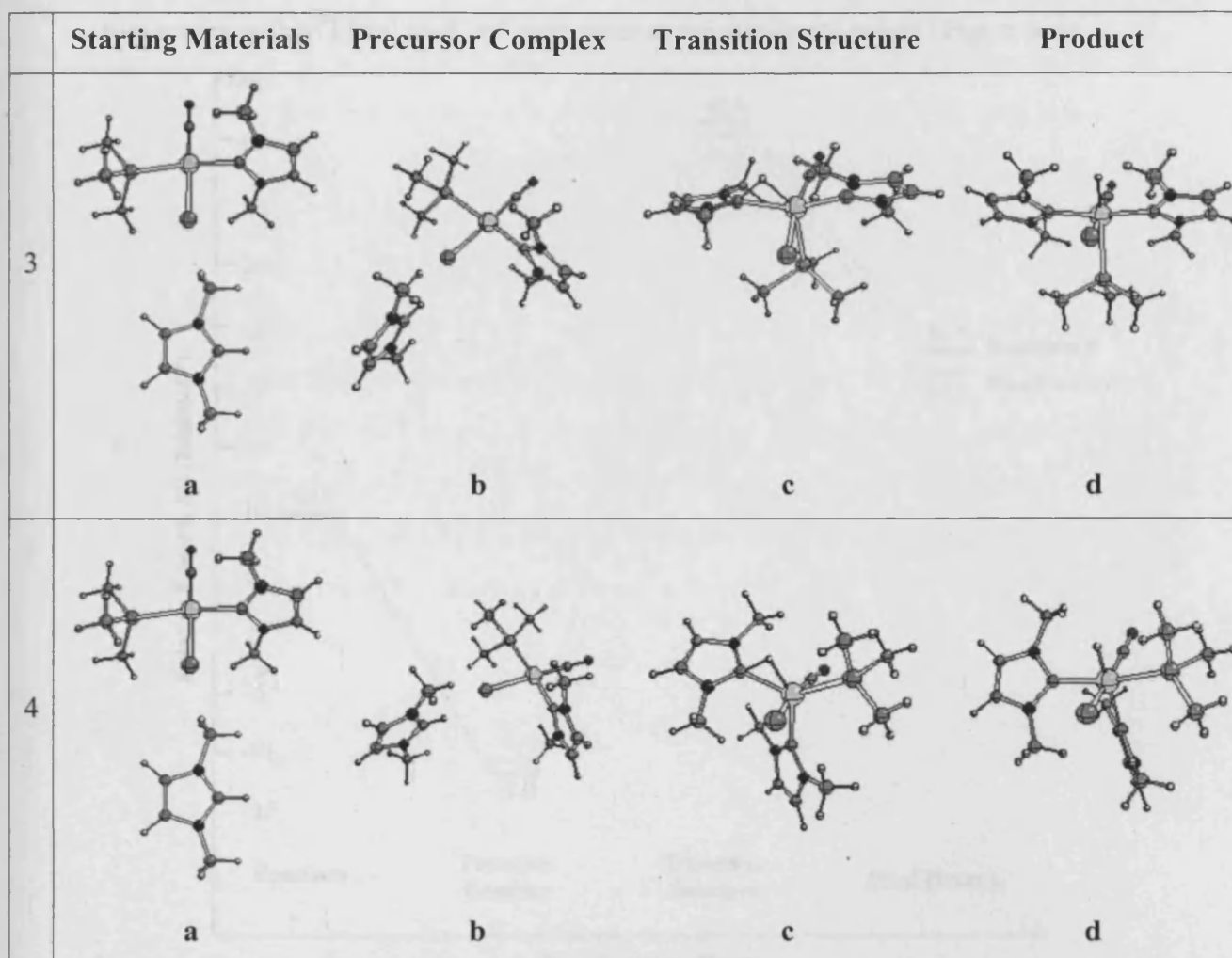


Figure 4-7 Oxidative addition of 1,3-dimethylimidazolium to $\text{Rh}(\text{dmiy})(\text{CO})(\text{PMe}_3)\text{Cl}$ (Reactions 3 and 4)

The similarity of the phosphine and carbene ligand influence on other ligand geometries is reflected in the transition structures, with the position and distance of the new carbene and hydride ligands comparable in each case.

The resemblance of the two classes of ligands is again mirrored energetically with the two routes within 2 kcal mol⁻¹ of each other at the stationary points (Figure 4-8).

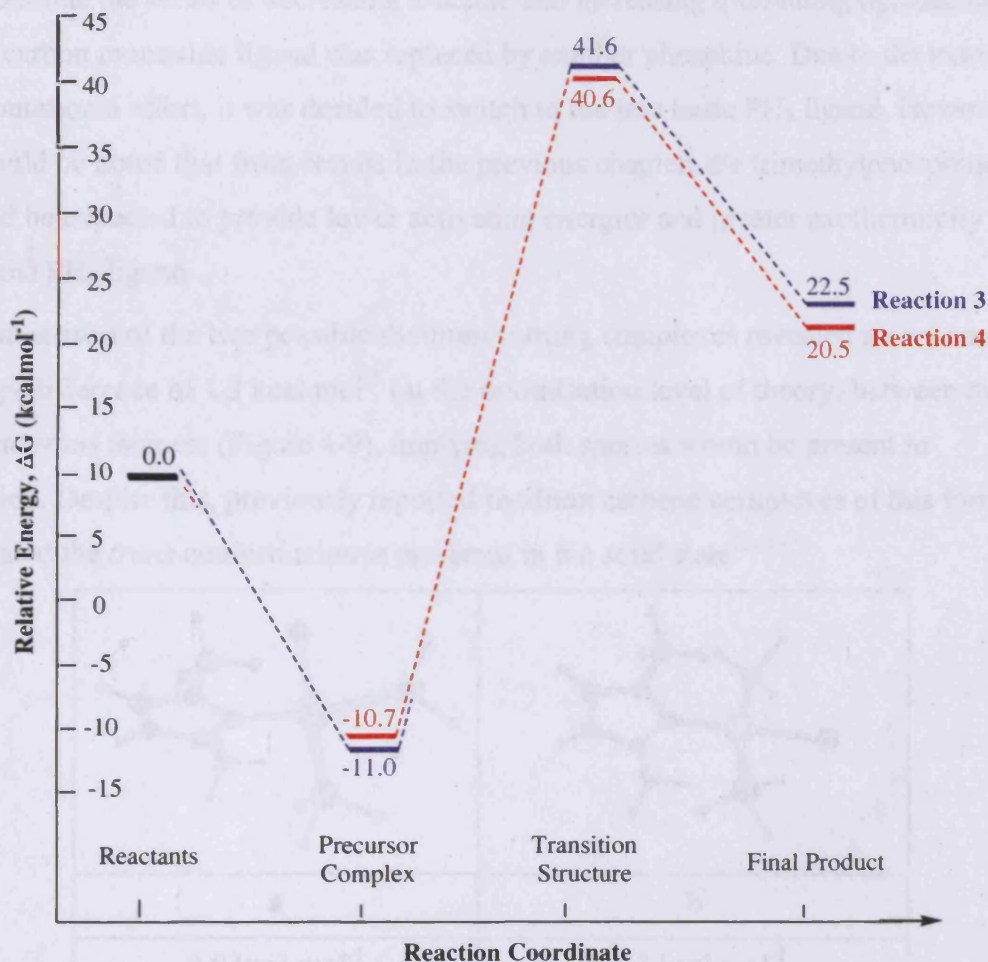


Figure 4-8 Energies for oxidative addition of 1,3-dimethylimidazolium to Rh(dmuy)(CO)(PMe₃)Cl (Reactions 3 and 4)

Despite lowering the barrier of activation and decreasing the endothermicity of the oxidative addition reaction compared to the di-carbonyl complex, the reaction is still unfavourable. The precursor complexes are by far the most stable species on the reaction pathway, with the barrier from these complexes to the transition structures over 50 kcal mol⁻¹ and overall the reaction is still slightly endothermic. In addition, a much lower barrier of 20 kcal mol⁻¹ exists for the reverse reaction in which the carbene and hydride ligands reductively eliminate to reform the salt and rhodium(I) species. This suggests that even if the oxidative addition reaction did take place, the reductive elimination of the salt would almost certainly revert any product back to the reactants.

4.3.1.3 Rh(PH₃)₂(dmiv)Cl

To continue the series of decreasing π -acidic and increasing σ -donating ligands, the final carbon monoxide ligand was replaced by another phosphine. Due to the extra computational effort, it was decided to switch to the less basic PH₃ ligand. However, it should be noted that from results in the previous chapter, the trimethylphosphine would be expected to provide lower activation energies and greater exothermicity than the PH₃ ligand.

A comparison of the two possible rhodium starting complexes revealed a very small energy difference of 1.3 kcal mol⁻¹ (at the optimisation level of theory) between the *cis* and *trans* isomers (Figure 4-9), implying both species would be present in solution. Despite this, previously reported rhodium carbene complexes of this form indicated the *trans* conformation is preferred in the solid state^{32, 36}.

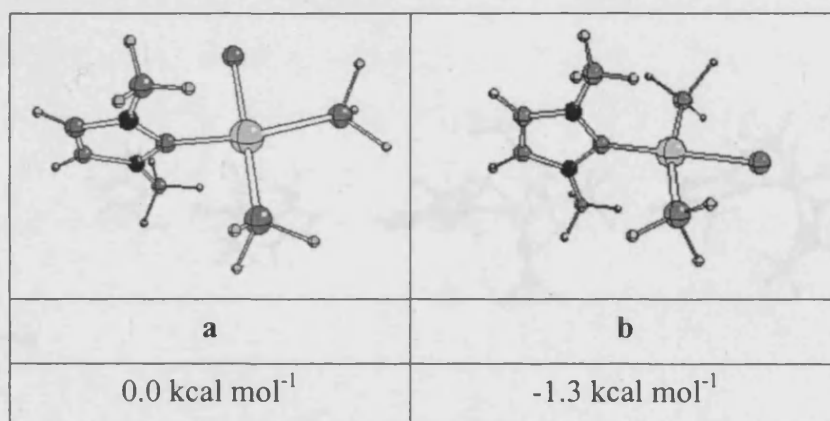
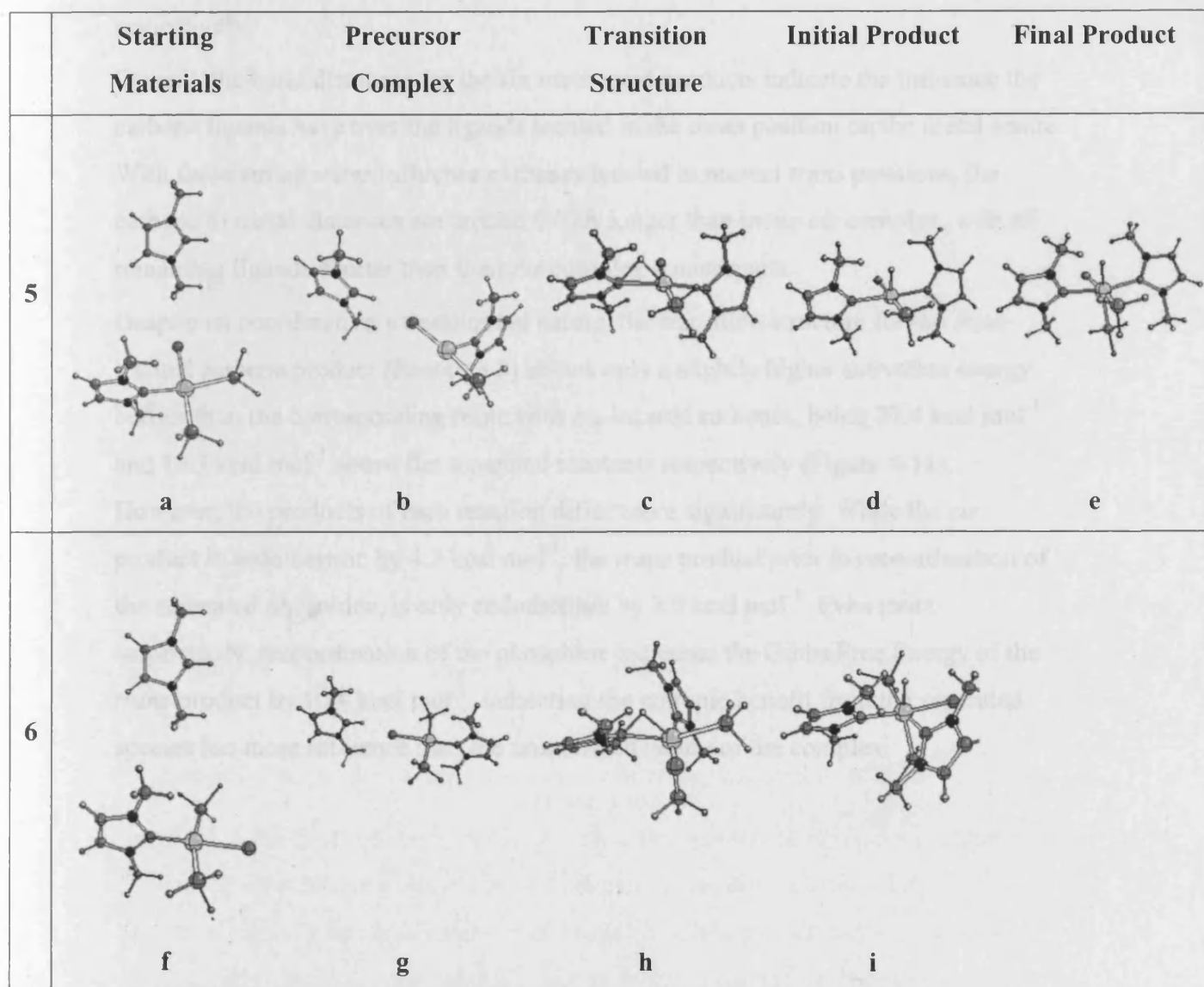


Figure 4-9 Isomers of Rh(dmiv)(PH₃)₂Cl

Preceding sections indicated a slight preference in both reaction activation and thermodynamics for phosphines over carbenes *trans* to the hydride ligand, with a further favouring for steric separation of bulky ligands. In addition, phosphines are known to be labile in many transition metal reactions and as such, two transition structures were considered, both involving one of the phosphine ligands being displaced below the ligand plane. Depending on the conformation of the starting material, this gave rise to the possibility of *trans* or *cis* located carbene ligands in the final product (Figure 4-10 a-e and Figure 4-10 f-i respectively).

Figure 4-10 Oxidative Addition of 1,3-dimethylimidazolium to $\text{Rh}(\text{dmi})\text{(PH}_3)_2\text{Cl}$

(Reactions 5 and 6)

Interestingly, while neither reaction displayed an initial salt to metal interaction, the slight variation in positioning of the phosphines contributed to vastly different reaction structures for the remainder of the reaction.

While the *cis* positioned carbenes had a transition structure very similar to those found previously, the *trans* carbene structure expelled the lower phosphine ligand from the complex altogether in a similar fashion to the dissociative route found in the preceding chapter. This transition structure for the five coordinate structure displayed little difference in bond lengths for the remaining ligands, however the overall structure is more advanced towards the products with the salt displaying longer C2-H

distance by 0.162 Å and shorter C2-Rh and H-Rh distances by 0.045 Å and 0.100 Å respectively.

Overall, the bond distances for the six membered products indicate the influence the carbene ligands have over the ligands located in the *trans* position on the metal centre. With these strong *trans* influence carbenes located in mutual *trans* positions, the carbene to metal distances are around 0.07 Å longer than in the *cis* complex, with all remaining ligands shorter than their *cis* complex counterparts.

Despite its coordinatively unsaturated nature, the transition structure for the *trans*-located carbene product (Reaction 5) shows only a slightly higher activation energy barrier than the corresponding route with *cis*-located carbenes, being 27.4 kcal mol⁻¹ and 19.3 kcal mol⁻¹ above the separated reactants respectively (Figure 4-11).

However, the products of each reaction differ more significantly. While the *cis* product is endothermic by 4.3 kcal mol⁻¹, the *trans* product prior to recoordination of the separated phosphine, is only endothermic by 2.0 kcal mol⁻¹. Even more surprisingly, recoordination of the phosphine increases the Gibbs Free Energy of the *trans* product by 10.4 kcal mol⁻¹, indicating the entropic benefit from the separated species has more influence than the unsaturated nature of the complex.

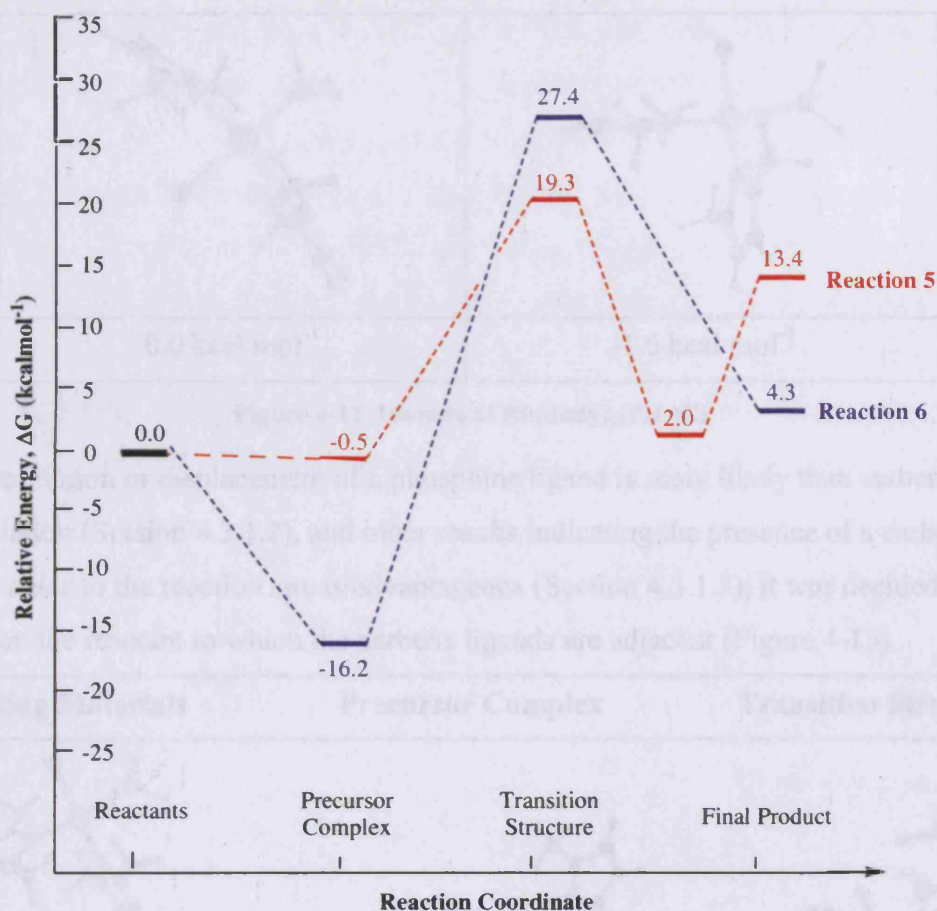


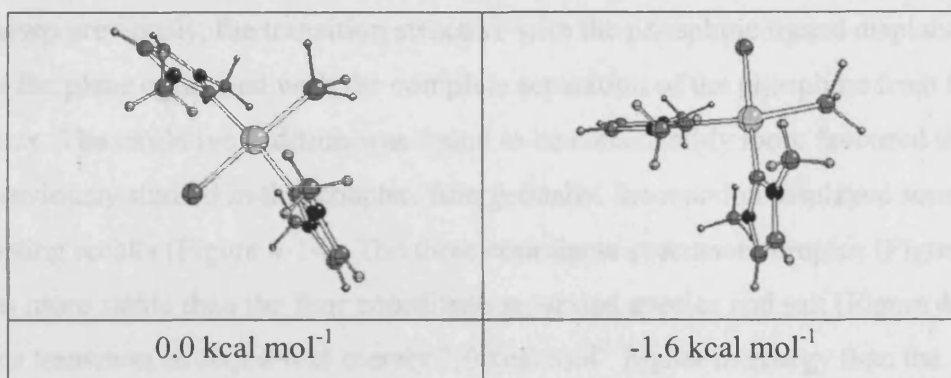
Figure 4-11 Energies for oxidative addition of 1,3-dimethylimidazolium to $\text{Rh}(\text{dmiy})(\text{PH}_3)_2\text{Cl}$ (Reactions 5 and 6)

Once again, the most stable complex overall appears to be the precursor complex with interaction between the imidazolium cation and the rhodium chloride ligand.

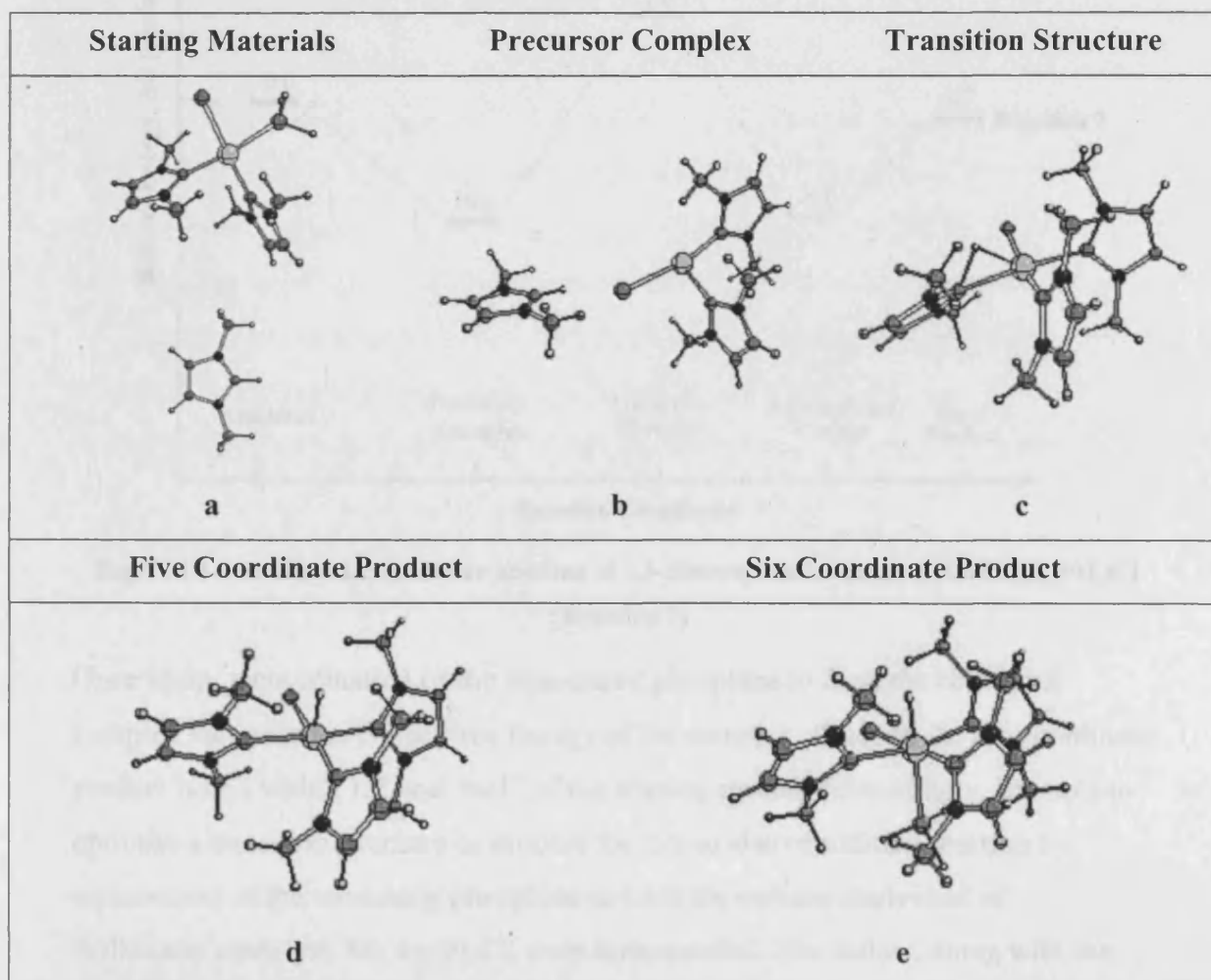
However, unlike previous systems, the reaction barriers are relatively low and the rhodium(III) products almost equal in energy to the separated reactants. In particular, the reaction in which the carbene ligands are *trans* in the final product (Reaction 5) is the oxidative addition reaction with the lowest activation energy so far.

4.3.1.4 $\text{Rh}(\text{PH}_3)(\text{dmiy})_2\text{Cl}$

With replacement of one of the phosphine ligands with a second carbene ligand, the starting $\text{Rh}(\text{PH}_3)(\text{dmiy})_2\text{Cl}$ complex could again display *cis/trans* isomerisation. Experimentally, similar rhodium complexes have been isolated and characterised with the carbene ligands in *trans* positions in the solid state^{33, 37}. Our calculations, however, indicated the *cis* complex is marginally more stable at the optimisation level of theory (Figure 4-12). Despite this, the calculated energy separation of the two isomers is experimentally insignificant at $1.6 \text{ kcal mol}^{-1}$, indicating isomerisation in solution would most likely be rapid.

Figure 4-12 Isomers of Rh(dmiy)₂(PH₃)Cl

As dissociation or displacement of a phosphine ligand is more likely than carbene dissociation (Section 4.3.1.2), and other results indicating the presence of a carbene ligand *trans* to the reaction site is advantageous (Section 4.3.1.3), it was decided to focus on the reactant in which the carbene ligands are adjacent (Figure 4-13).

Figure 4-13 Oxidative Addition of 1,3-dimethylimidazolium to Rh(dmiy)₂(PH₃)Cl (Reaction 7)

As shown previously, the transition structure with the phosphine ligand displaced below the plane optimised with the complete separation of the phosphine from the complex. The oxidative addition was found to be considerably more favoured than any previously studied in this chapter. Energetically, the reaction displayed some interesting results (Figure 4-14). The three coordinate precursor complex (Figure 4-13 b) was more stable than the four coordinate separated species and salt (Figure 4-13 a), and the transition structure was merely 7.0 kcal mol⁻¹ higher in energy than the starting materials. Further, the activation energy from the precursor to the transition structure is only 17.0 kcal mol⁻¹, with the five coordinate product exothermic by 9.0 kcal mol⁻¹.

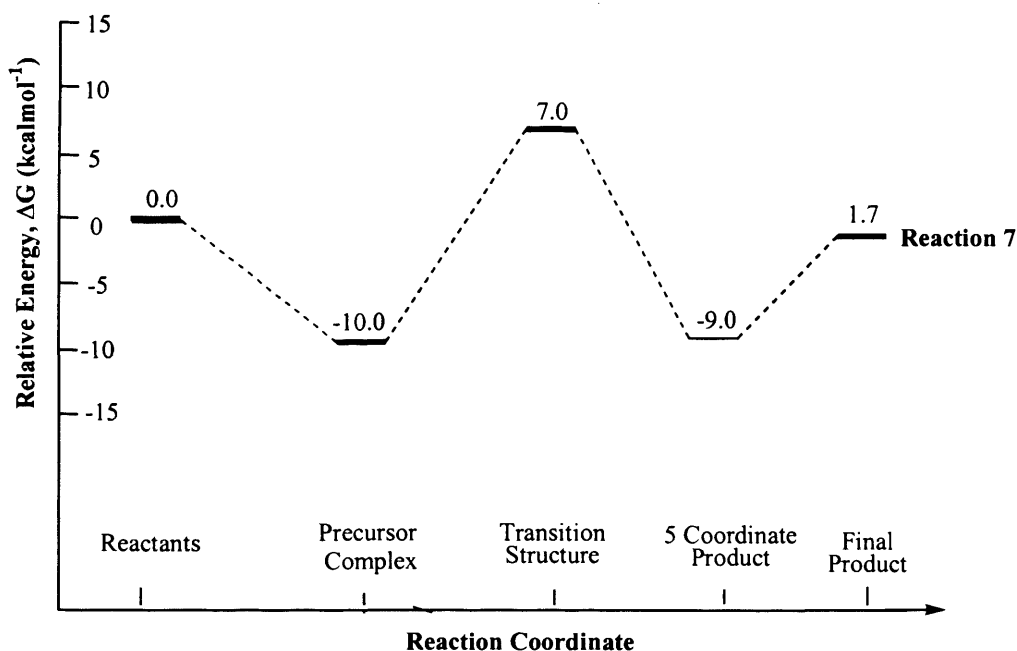


Figure 4-14 Energies for oxidative addition of 1,3-dimethylimidazolium to Rh(dmiy)₂(PH₃)Cl (Reaction 7)

Once again, recoordination of the dissociated phosphine to form the octahedral complex increases the Gibbs Free Energy of the complex, although the six-coordinate product is still within 1.7 kcal mol⁻¹ of the starting species. Interestingly, attempts to optimise a transition structure or product for this oxidative addition reaction by replacement of the remaining phosphine to form the carbene equivalent of Wilkinson's catalyst, Rh(dmiy)₃Cl, were unsuccessful. This failure, along with the results for the Rh(dmiy)₂(PH₃)Cl system indicate the extra flexibility in electronic and steric influences afforded from the labile phosphine ligands may be essential in allowing this reaction to occur at all.

Overall, the reaction using the $\text{Rh}(\text{dmly})_2(\text{PH}_3)\text{Cl}$ starting material seems much more promising in promoting the oxidative addition of imidazolium salts than any other complex considered, with the ability of the phosphine ligand to dissociate to allow steric and electronic advantages seemingly very important.

4.3.1.5 Chelation - $\text{Rh}(\text{PH}_3)(\text{mbiy})\text{Cl}$

It is known that chelating ligands such as dppe (dppe = 1,2-bis(diphenylphosphino)ethane) help promote oxidative addition reactions to zero valent palladium, platinum and nickel by creating a more sterically favourable environment^{13, 38}. In the case of group 10 metals, the $\text{M}(0)$ complexes generally prefer two ligands coordinated in a linear arrangement. Chelation of these ligands forces a bent, high energy and open structure that readily promotes oxidative addition to create four coordinate, square planar $\text{M}(\text{II})$ products.

Although oxidative addition to rhodium(I) generally forms an octahedral rhodium(III) complex in which only one new ligand joins the same plane as the majority of pre-coordinated ligands, it has been proposed that chelation of the carbene ligands in the rhodium(I) starting complex may help sterically open up the plane in which the new carbene ligand was to join, and consequently lower the barrier to oxidative addition³⁹⁻⁴¹. Therefore, we looked at an almost identical starting rhodium(I) complex to the one examined in the previous section, but with the two carbene ligands joined by a methylene bridge (mbiy - methylene bis(3-methylimidazol-2-ylidene); Figure 4-15).

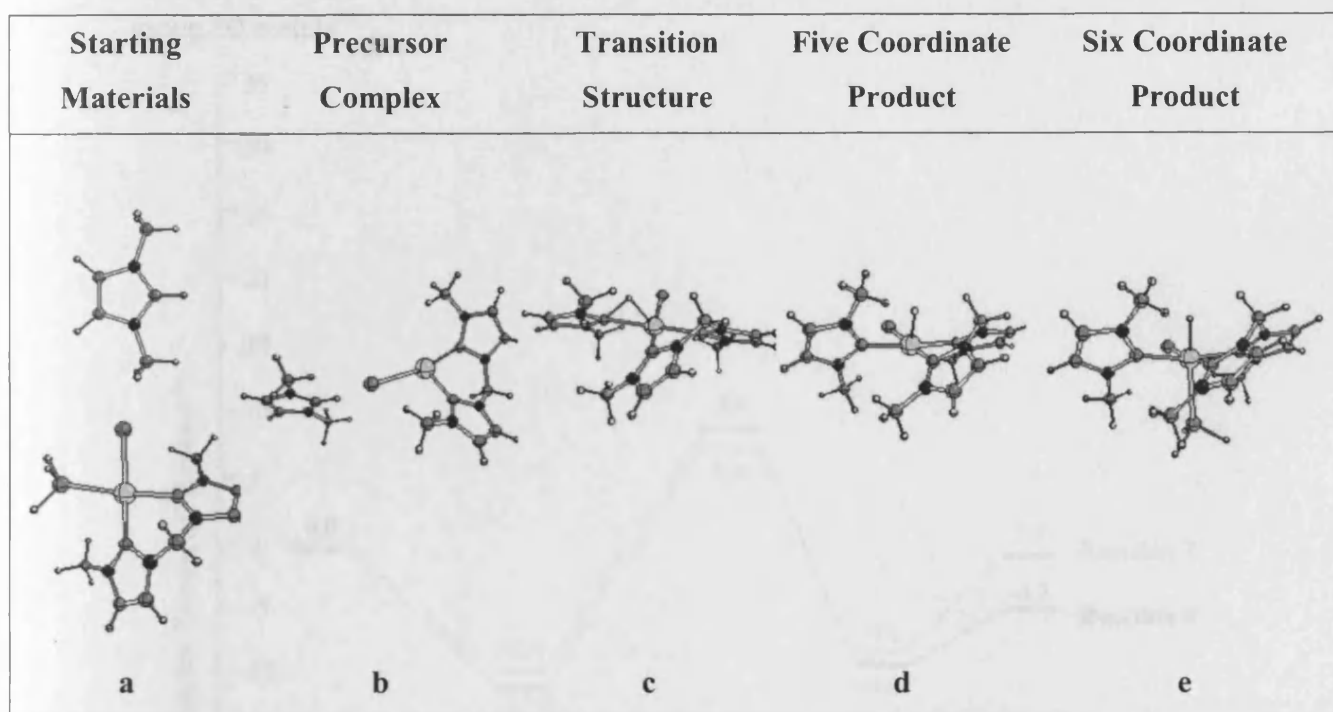


Figure 4-15 Oxidative addition of 1,3-dimethylimidazolium to Rh(mbiy)(PH₃)Cl (Reaction 8)

Despite some changes in the reaction geometries, chelation provided little benefit in the overall reaction. As found for the monodentate carbene complex, phosphine predissociation was once again observed. The angle between the carbene ligands decreased from 90.2° for the non-chelating complex down to 84.3° for the chelating complex as anticipated, however the constraining methylene bridge caused twisting of the dihedral angle of the carbene ligands from an almost perpendicular position in the non-chelating complex (58°), to a more parallel arrangement in the chelating case (140°). This flattening of the carbene rings in turn pushed the *N*-methyl of the carbene ligand into the newly created space and as a consequence, the steric advantages gained by closing the carbene-metal-carbene angle for the chelating ligand are negated by the overall increase in bulk along the metal/carbene plane.

Cancellation of steric advantages was reflected in the energetics of the reaction, with the activation energy and exothermicity for the chelating complex almost identical to that of the non-chelating analogue (Figure 4-16). Other advantages associated with chelation, such as prevention of facile phosphine dissociation in solution are not as important for carbene ligands, which have greater binding strength and are not as labile as their phosphine analogues. Therefore, it appears chelation in these rhodium

complexes does not afford the benefits in the oxidative addition reaction found for the group 10 metals⁴².

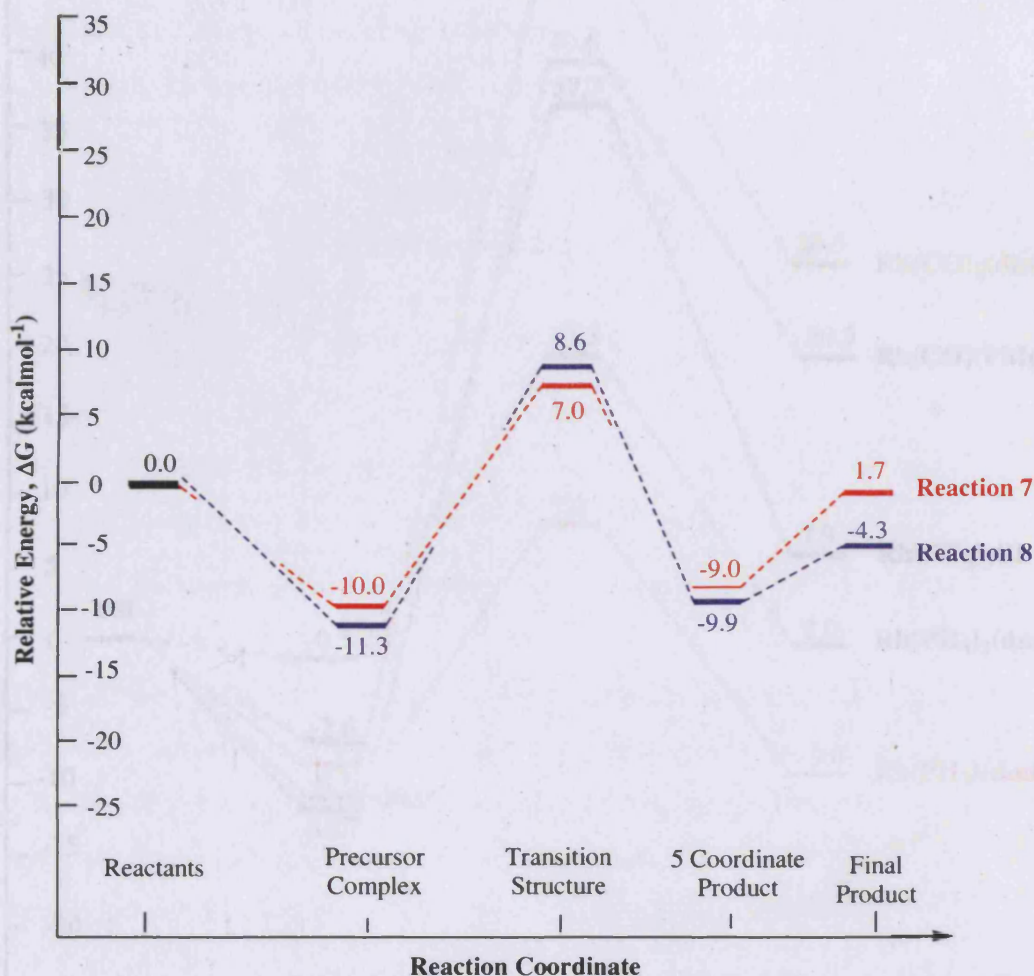


Figure 4-16 Energies for oxidative addition of 1,3-dimethylimidazolium to Rh(mbiy)(PH₃)Cl (Reactions 7 and 8)

4.3.1.6 Overall rhodium C-H activation summary

As established in the previous chapter, C-H activation of azolium salts to create rhodium carbene complexes may be possible with the use of a Rh(PR₃)₃Cl starting complex. Exchange of these phosphine ligands with at least one carbene ligand and a combination of phosphines and carbon monoxide indicated the increasing basicity of ligands promotes oxidative addition, with overall results for the dominant cycles for each starting material displayed in Figure 4-17.

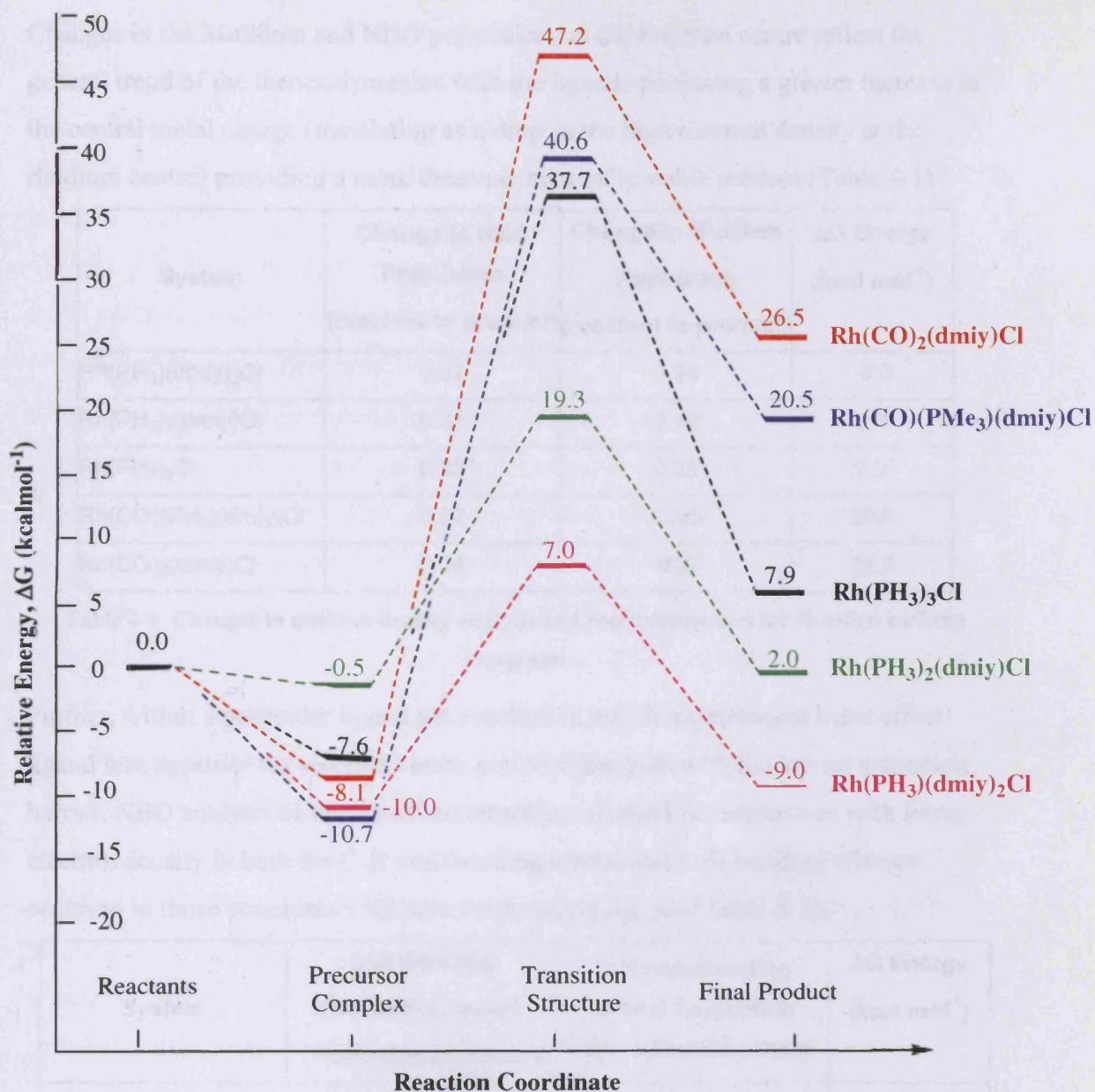
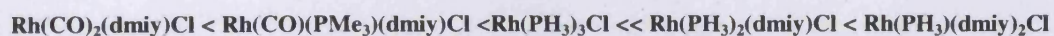


Figure 4-17 Energies for oxidative addition of 1,3-dimethylimidazolium to rhodium(I) carbene complexes

While the overall geometries remain consistent following the concerted three-centred transition structures, the energies reflect the changing electronic conditions on proceeding from the π -acidic CO ligands in $\text{Rh}(\text{CO})_2(\text{dmiy})\text{Cl}$ to the σ -donating carbenes of $\text{Rh}(\text{dmiy})_2(\text{PH}_3)\text{Cl}$. Lower activation energies and product stability followed the trend towards the more basic ligands:



Changes in the Mulliken and NBO populations at the rhodium centre reflect the general trend of the thermodynamics with the ligands producing a greater increase in the central metal charge (translating as a drop in the high electron density at the rhodium centre) providing a more thermodynamically stable product (Table 4-1).

System	Change in NBO Population (reactant to product)	Change in Mulliken Population (reactant to product)	ΔG Energy (kcal mol ⁻¹)
Rh(PH ₃)(dm ₃) ₂ Cl	0.37	0.24	-9.0
Rh(PH ₃) ₂ (dm ₃)Cl	0.31	0.10	2.0
Rh(PH ₃) ₃ Cl	0.23	0.23	7.9
Rh(CO)(PH ₃)(dm ₃)Cl	0.22	-0.05	20.5
Rh(CO) ₂ (dm ₃)Cl	0.14	-0.27	26.5

Table 4-1 Changes in electron density analysis and thermodynamics for rhodium carbene complexes

Further, within a particular ligand set, reaction in which the strongest *trans* effect ligand was opposite the reaction centre provided the path with the lowest activation barrier. NBO analysis of the transition structures showed the complexes with lower electron density in both the C-H anti-bonding orbital and C-H bonding orbitals occurred in those structures with better σ -donating ligands (Table 4-2).

System	C-H Bonding Orbital Population (Transition Structure)	C-H Anti-Bonding Orbital Population (Transition Structure)	ΔG Energy (kcal mol ⁻¹)
Rh(PH ₃)(dm ₃) ₂ Cl	1.743	0.317	-9.0
Rh(PH ₃) ₂ (dm ₃)Cl	1.752	0.322	2.0
Rh(PH ₃) ₃ Cl	1.855	0.241	7.9
Rh(CO)(PH ₃)(dm ₃)Cl	1.820	0.355	20.5
Rh(CO) ₂ (dm ₃)Cl	1.802	0.353	26.5

Table 4-2 Changes in transition structure C-H anti-bonding orbital for rhodium carbene complexes

Diggle completed a similar study of oxidative addition of H₂, CH₄ and C₂H₆ to ruthenium using a combination of carbene and phosphine ligands with Ru(CO)(carbene)_{3-n}(PH₃)_n¹⁹. His results indicated minimal change in energetics moving from the PH₃ to dmiy with slightly higher activation barriers and the products being slightly less thermodynamically favourable for the carbene complexes, especially for C-C activation. Ru-PH₃ and CO stretching frequencies did indicate the carbenes create a more electron rich metal centre, but it appeared the extra bulk of the carbenes was hindering the reaction.

While these results are interesting, replacement of the PH₃ ligand with the more basic PMe₃ did not decrease the activation barrier or produce a more favourable thermodynamic product in Diggle's study; a result contradictory to the results for the rhodium complexes examined in the previous chapter. As such, the fundamental reactions of ruthenium and rhodium oxidative addition may be different enough that slight changes to electronic and steric factors may greatly influence reaction outcomes.

Overall, results for carbene complexes containing a variety of ligand sets imply all ligands must be considered when rhodium is used for C-H activation. While carbenes possess the high basicity required for successful oxidative addition reactions, inclusion of π-acidic ligands such as carbon monoxide on the metal centre negate any benefits of the extra basicity. The combination of two carbenes and a phosphine ligand displayed the greatest promise for oxidative addition reaction, with the di-carbenes providing an electron rich metal centre and the lability of the phosphine providing easy access to a reaction site for the incoming salt. It is expected this reaction may be further enhanced through the substitution of the trihydridophosphine for the more labile triphenylphosphine, but in general, Rh(PH₃)(dmiy)Cl showed enough promise in C-H activation to encourage further study of possible C-C activation.

4.3.2 C-C activation with $\text{Rh}(\text{dmiy})_2(\text{PH}_3)\text{Cl}$

In general, alkanes are well known for being much less reactive in oxidative addition reactions than their di-hydrogen counter parts, following the order $\text{H-H} > \text{C-H} > \text{C-C}$. The reason for this trend appears to be due in part to the strength of the reacting R-R, with the strength of the M-H and M-C bonds formed in the products playing an equally important role^{9, 10, 43}.

Traditional ligands such as acetylenes and carbon monoxide have good π -accepting and σ -donating ability, generally allowing strong bonds to be formed to metals. Conversely, alkanes possess few qualities required for good ligands as they have poorly aligned orbitals that are not good donors or acceptors^{3, 44}. As such, alkyl complexes formed from oxidative addition of alkanes tend to be less stable than the starting complexes used in catalytic reactions.

Oxidative addition of C-H is generally 10 kcal mol^{-1} more difficult than H-H activation⁴⁵, with barriers to C-C activation a further $15\text{-}20 \text{ kcal mol}^{-1}$ higher in energy⁴⁶. These activation trends are thought to be caused mainly by steric factors, with the symmetry of the H-H molecule allowing easier interaction with the metal orbitals than the directional interaction required for C-H activation⁴⁶⁻⁵⁷. Going one step further, C-C activation is even more difficult with accessibility to the C-C bonding and anti-bonding orbitals far more restricted, in particular for two tetravalent sp^3 hybridised carbons⁸.

With this information in mind, the C-H activation of the sp^2 hybridised carbon in 1,3-dimethylimidazolium by $\text{Rh}(\text{PH}_3)(\text{dmiy})_2\text{Cl}$ in the previous section proved promising enough for us to study the related C-C activation of 1,2,3-trimethylimidazolium in order to create a rhodium(III) alkyl carbene complex.

4.3.2.1 Steric influences of C-C activation

The extra bulk of the 2-methyl in the imidazolium salt is immediately apparent in the steric requirements of the reaction when compared to the equivalent 2-H activation. Phosphine predissociation is required as the incoming imidazolium salt no longer approaches from the side in the transition structure, but from underneath the ligand plane (Figure 4-18); an arrangement that allows the least hindered interaction between the metal and the salt C2-alkyl group.

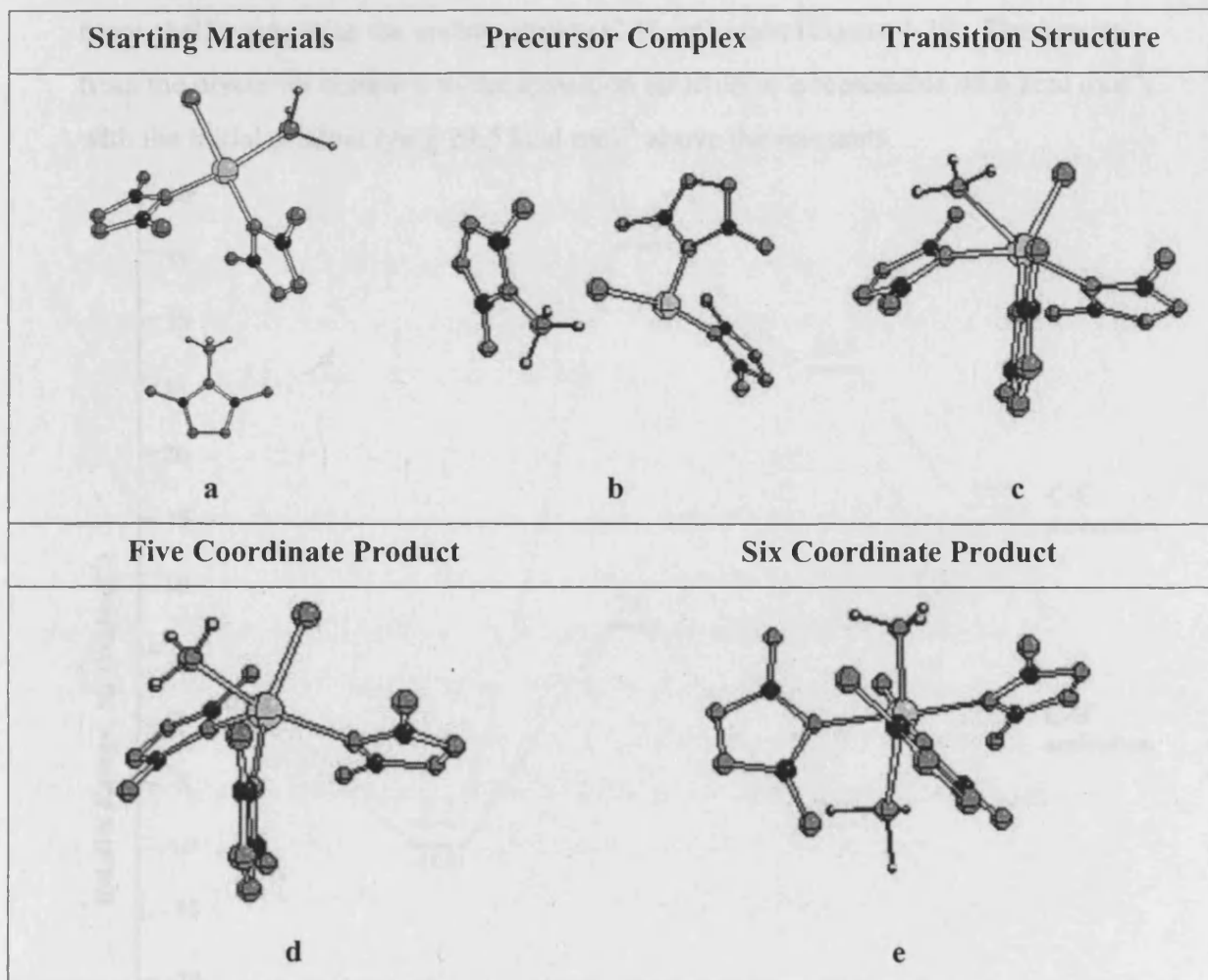


Figure 4-18 C-C activation with $\text{Rh}(\text{dmiy})_2(\text{PH}_3)\text{Cl}$
(carbene ligand hydrogens removed for clarity)

Further, C-C activation with the newly formed carbene coordinating in the same plane as the existing ligands as seen previously for the C-H activation would result in a crowded transition structure with the newly created methyl group in a region of high steric congestion, interacting with the *N*-methyl groups of the three carbene ligands. Attack of the salt from below the ligand plane allows a reduction in this congestion and results in a lower energy structure. As a result, the initial product has more of a

distorted square pyramid geometry in which the methyl ligand remains in the plane with the original carbene ligands, with the newly formed carbene below. Rearrangement of this complex into a more traditional square pyramid where the methyl group occupies the point of the pyramid results in a more classical shape and a lower energy product.

4.3.2.2 Electronic effects of C-C activation

As expected, the reaction barrier and thermodynamics of the C-C activation are much more challenging than the corresponding C-H activation (Figure 4-19). The barrier from the precursor complex to the transition structure is a reasonable $45.6 \text{ kcal mol}^{-1}$, with the initial product lying $29.5 \text{ kcal mol}^{-1}$ above the reactants.

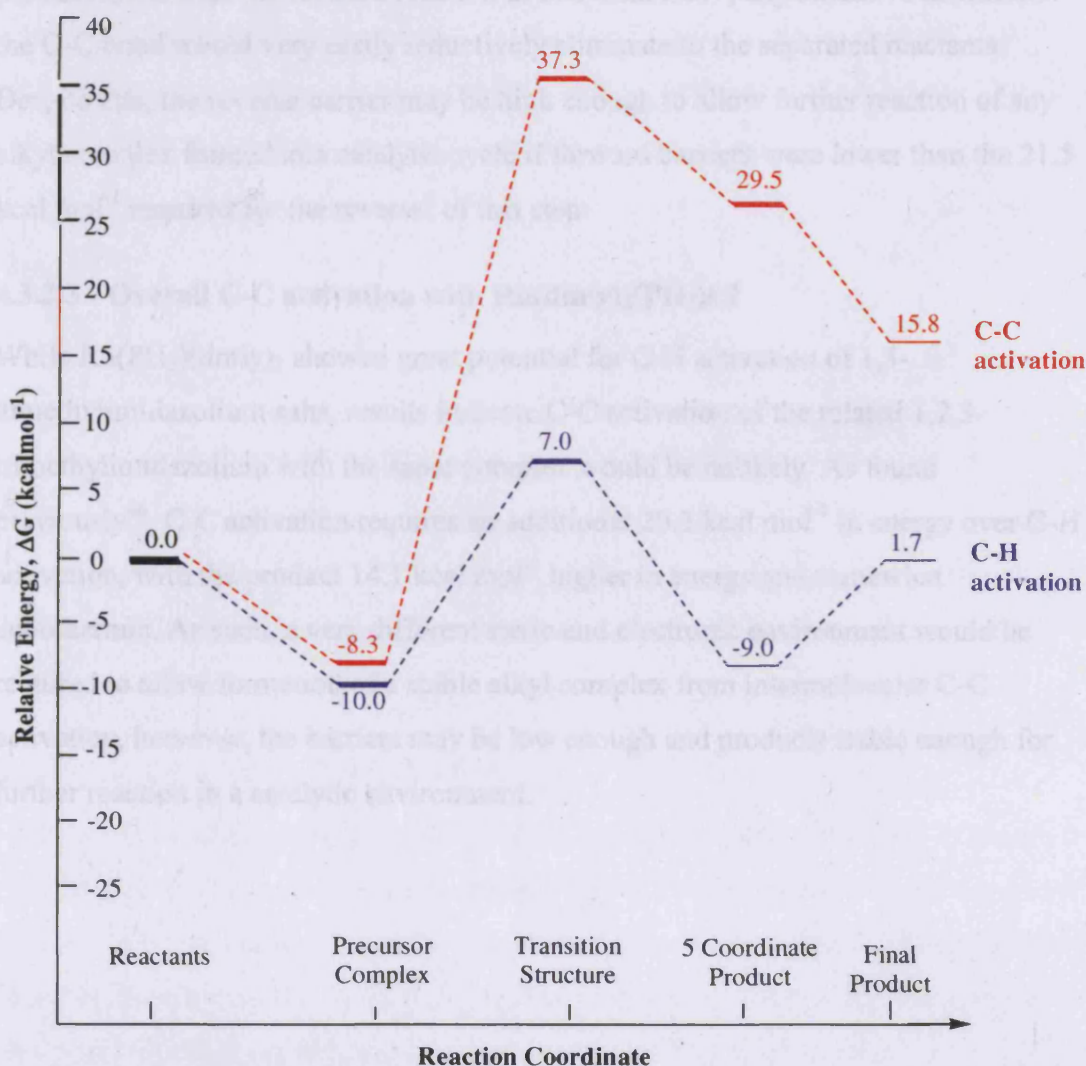


Figure 4-19 Energies for oxidative addition of 1,2,3-trimethylimidazolium to $\text{Rh}(\text{dmip})_2(\text{PH}_3)\text{Cl}$

Rearrangement of the initial product to the more traditional square pyramid results in a $13.7 \text{ kcal mol}^{-1}$ decrease in energy, however this complex still remains endothermic by $15.8 \text{ kcal mol}^{-1}$. Further, any attempt to find a transition structure that would directly result in the lower energy product rearranged to the transition structure indicated in Figure 4-18. As such, it appears this transition structure gives the greatest steric and electronic advantage to C-C activation and formation of the lower energy product would be achieved via product isomerisation, not through a lower energy transition structure.

Another important observation is the potential for the reverse reaction. With the activation energy for the reductive elimination of the methyl and a carbene from the product lower than the forward reaction at $21.5 \text{ kcal mol}^{-1}$, any oxidative addition of the C-C bond would very easily reductively eliminate to the separated reactants. Despite this, the reverse barrier may be high enough to allow further reaction of any alkyl complex formed in a catalytic cycle if forward barriers were lower than the $21.5 \text{ kcal mol}^{-1}$ required for the reversal of this step.

4.3.2.3 Overall C-C activation with $\text{Rh}(\text{dmiy})_2(\text{PH}_3)\text{Cl}$

While $\text{Rh}(\text{PH}_3)(\text{dmiy})_2$ showed great potential for C-H activation of 1,3-dimethylimidazolium salts, results indicate C-C activation of the related 1,2,3-trimethylimidazolium with the same complex would be unlikely. As found previously⁴⁶, C-C activation requires an additional $20.3 \text{ kcal mol}^{-1}$ in energy over C-H activation, with the product $14.1 \text{ kcal mol}^{-1}$ higher in energy and somewhat endothermic. As such, a very different steric and electronic environment would be required to allow formation of a stable alkyl complex from intermolecular C-C activation, however, the barriers may be low enough and products stable enough for further reaction in a catalytic environment.

4.3.3 Oxidative addition with iridium

While rhodium is used as a catalyst in many reactions with excellent selectivity towards both reactants and products, iridium is often more effective at promoting oxidative addition reactions, frequently resulting in thermodynamically stable products that are not found for the rhodium analogues⁵. For gaseous iridium ions, oxidative addition calculations show there are three reasons for the ease of these reactions: the ability of Ir⁺ to change spin easily, the strength of the Ir-H and Ir-C bonds and ability of Ir⁺ to form up to four covalent bonds⁵⁸.

Recently, there has been a growing interest in the C-H and C-C activation of phosphine-based iridium complexes⁵⁹⁻⁶⁵. While these complexes use the advantages of a phosphine pincer to promote the C-C activation by forcing the reacting alkyl group close to the metal centre, it is none-the-less exciting that the reactions proceed smoothly at room temperature⁵⁹ (Figure 4-20).

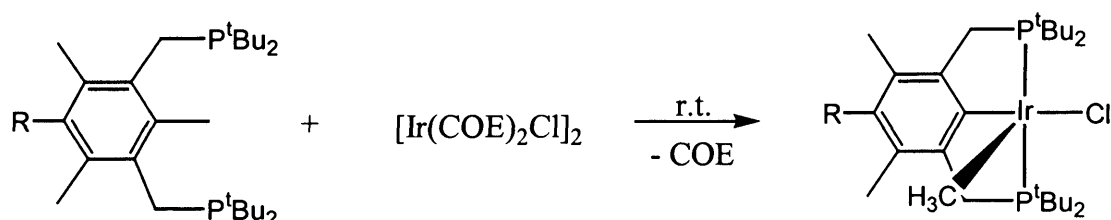


Figure 4-20 Room temperature C-C activation by iridium

Further, many iridium carbene complexes have been isolated^{33, 66-68}, including several iridium hydride complexes^{41, 69, 70}. As such, we decided to continue our studies of the C-H activation of imidazolium salts by iridium complexes, initially using a model iridium complex equivalent to Wilkinson's Catalyst.

4.3.3.1 Ir(PMe₃)₃Cl – C-H activation

Unlike the dissociation preferred for rhodium, the larger iridium is known to maintain all ligands in going from the four-coordinate square planar iridium(I) to the octahedral products of oxidative addition. This was supported in our work with an investigation of a possible dissociative route, showing that, as expected, the pre-dissociation of a phosphine ligand required considerably more energy for iridium than the corresponding rhodium complex, standing at 16.3 kcal mol⁻¹ for dissociation. Any attempt to find a transition structure ultimately resulted in direct formation of the product, and introduction of the imidazolium salt into the proximity of the three-

coordinate $\text{Ir}(\text{PMe}_3)_2\text{Cl}$ complex proceeded smoothly to the products with no apparent barrier. However, as the energy required for the initial pre-dissociation of a phosphine is considerable, we studied the reaction using the associative pathway used in the previous chapter for rhodium.

The geometry of the reaction of $\text{Ir}(\text{PMe}_3)_3\text{Cl}$ with 1,3-dimethylimidazolium proceeded in a very similar manner to that observed for rhodium. In general, the C2-M bond distances are almost identical between the rhodium and iridium carbene complexes. The most significant difference occurred in the transition structure with the iridium transition structure considerably more advanced towards the products. In this case, a much larger C2-H distance and closer M-C2 and M-H lengths are found, which is to be expected for the more favourable reaction.

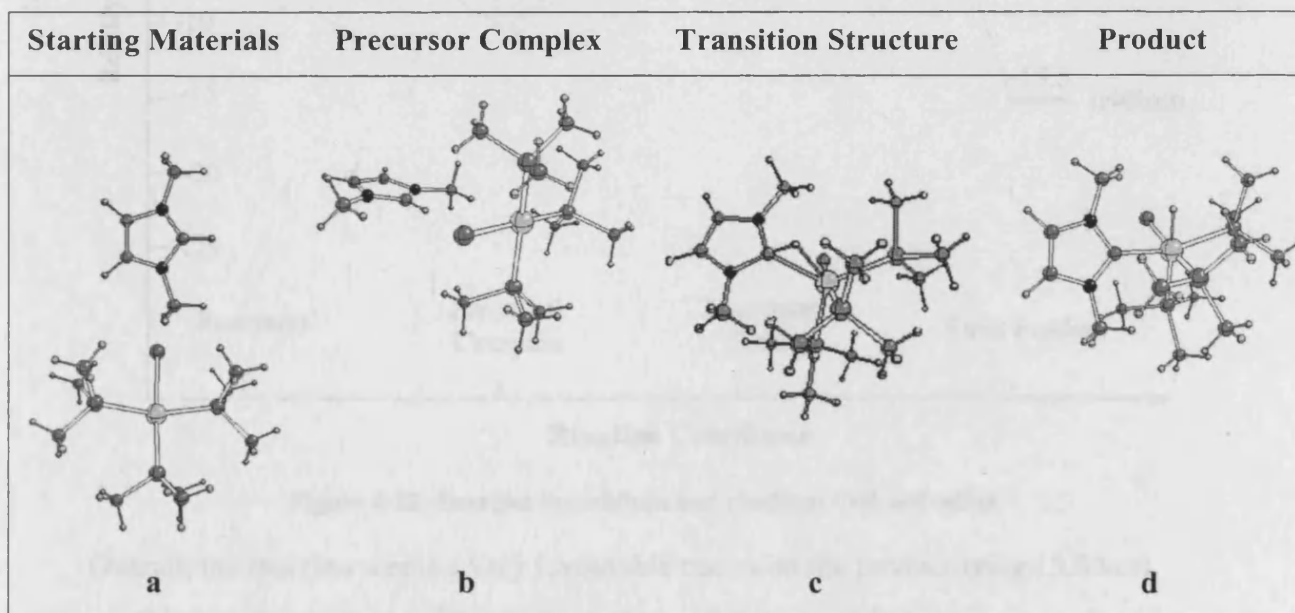


Figure 4-21 Oxidative addition of 1,3-dimethylimidazolium to $\text{Ir}(\text{PMe}_3)_3\text{Cl}$

Once again, the precursor complex in which a bond between the 2-H of the imidazolium salt and iridium chloride ligand is formed shows a very large stabilising effect for the salt (Figure 4-22). While the activation energy from the precursor to the transition structure is fairly high at $35.7 \text{ kcal mol}^{-1}$, the transition structure is still reasonably low in energy, only $26.8 \text{ kcal mol}^{-1}$ higher in energy than the separated reactants.

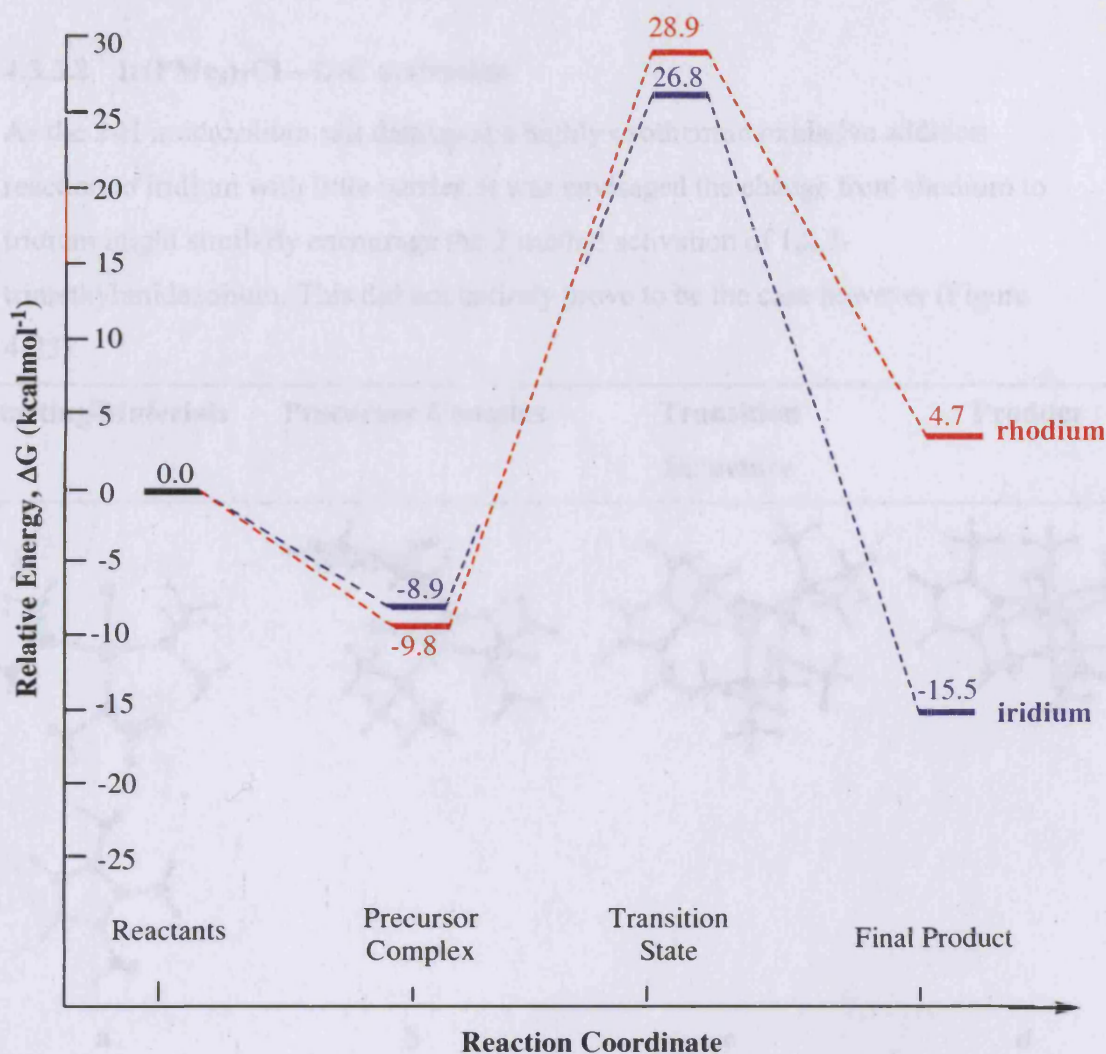


Figure 4-22 Energies for iridium and rhodium C-H activation

Overall, the reaction seems a very favourable one, with the product lying 15.5 kcal mol⁻¹ below the reactants. This high exothermicity is certainly not unexpected, with carbene complexes formed *in-situ* under reasonably mild conditions in work previously reported by Crabtree⁷¹.

4.3.3.2 $\text{Ir}(\text{PMe}_3)_3\text{Cl}$ – C-C activation

As the 2-H imidazolium salt displayed a highly exothermic oxidative addition reaction to iridium with little barrier, it was envisaged the change from rhodium to iridium might similarly encourage the 2-methyl activation of 1,2,3-trimethylimidazolium. This did not entirely prove to be the case however (Figure 4-23).

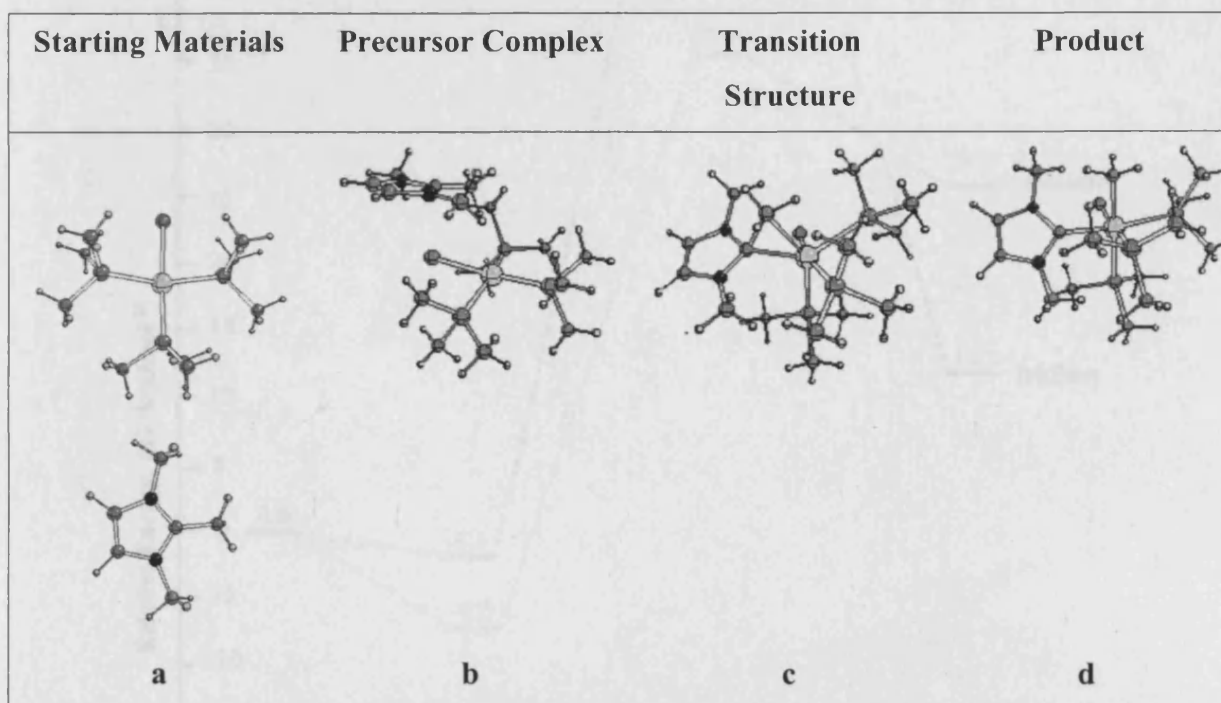


Figure 4-23 Oxidative addition of 1,2,3-trimethylimidazolium to $\text{Ir}(\text{PMe}_3)_3\text{Cl}$

With the product standing $11.3 \text{ kcal mol}^{-1}$ higher in energy than the reactants, the overall reaction is less endothermic than the rhodium counterpart; however the activation energy from the precursor complex to the transition structure was very high at $63.4 \text{ kcal mol}^{-1}$ (Figure 4-24).

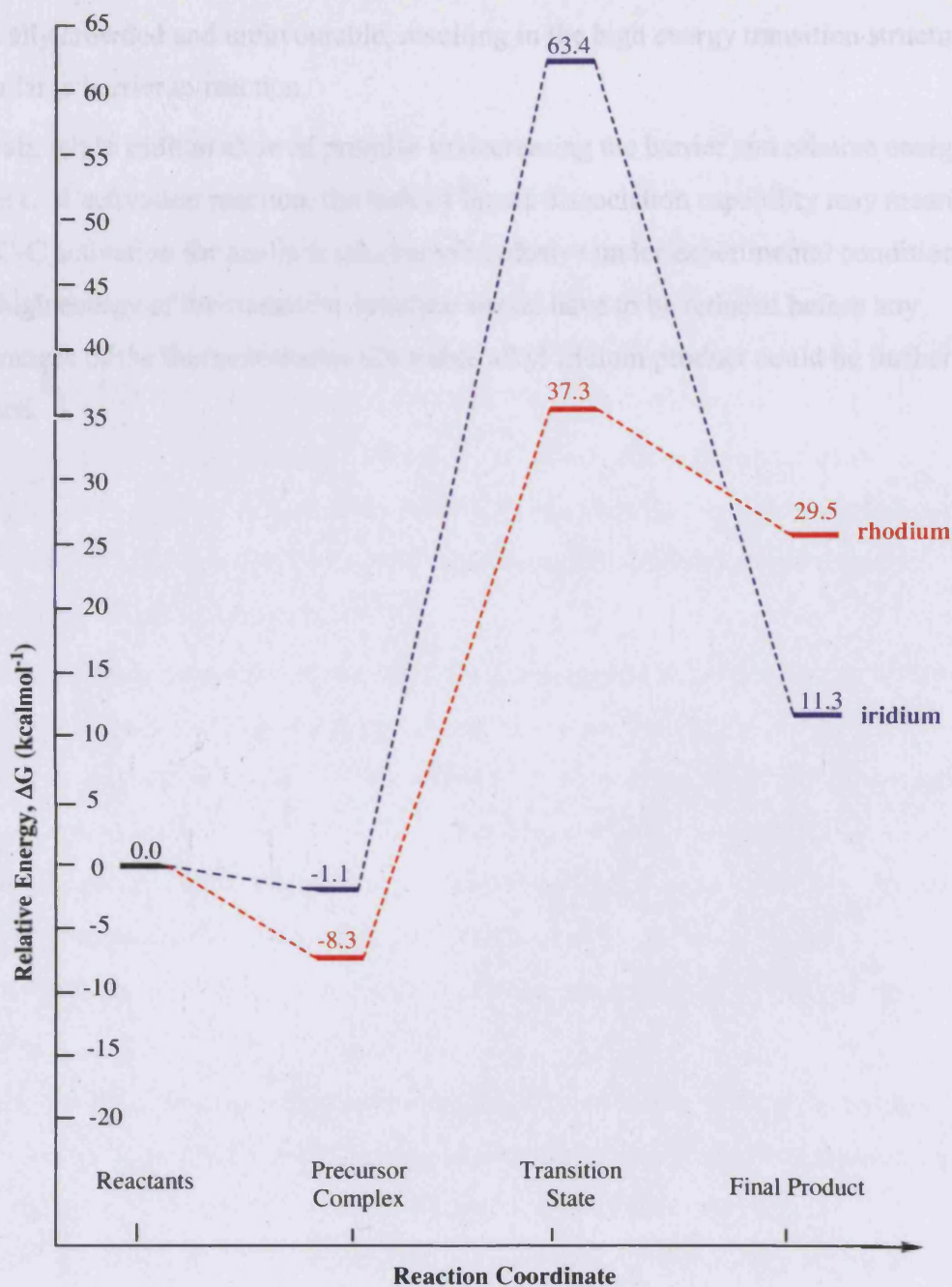


Figure 4-24 Energies for iridium and rhodium C-C activation

This exceptionally high barrier is thought to be due mainly to steric factors. The rhodium 2-methyl activation occurs with phosphine pre-dissociation and the incoming salt attacking below the plane of the rhodium(I) ligands, consequently allowing considerable space for the newly formed carbene ligand. With slightly different steric and electronic properties, iridium phosphine pre-dissociation does not occur before the oxidative addition reaction takes place and as a result, the transition structure is

sterically crowded and unfavourable, resulting in the high energy transition structure and a large barrier to reaction.

Overall, while iridium showed promise in decreasing the barrier and relative energy of the C-H activation reaction, the lack of ligand dissociation capability may mean that C-C activation for azolium salts remains elusive under experimental conditions. The high energy of the transition structure would have to be reduced before any advantages of the thermodynamically stable alkyl iridium product could be further utilised.

4.4 Conclusion

Recently carbene complexes have been utilised in numerous catalytic cycles involving oxidative addition reactions, suggesting they could be strong C-H and C-C activation complexes in a variety of conditions. Further, new carbene complexes have been synthesised through the C2 activation of azolium salts. In this chapter we combined these results to examine whether rhodium carbene complexes could be used to further activate azolium salts to produce rhodium(III) carbene complexes.

The combinations of ligands used varied from the π -acidic carbon monoxide to phosphines. In general, replacing the less basic ligands with the better sigma donors decreased the activation barriers significantly and decreased the thermodynamic instability of the reaction products.

While the carbon monoxide ligand strongly discouraged oxidative addition with high activation barriers and high energy products, use of $\text{Rh}(\text{dmly})_2(\text{PH}_3)\text{Cl}$ indicated promise as a promoter of the C-H activation with a low energy transition structure and a thermodynamically favourable product. Further, within the isomer alternatives for a particular reaction, those complexes in which the stronger *trans* effect ligands were positioned opposite the reaction site provided a smoother route for reaction thought to be caused by promoting interaction of the metal orbitals with the C2-H antibonding orbitals.

Despite the promise shown for $\text{Rh}(\text{dmly})_2(\text{PH}_3)\text{Cl}$ as a C-H activating complex, C-C activation remains elusive with the transition structure and products of the reaction 40 kcal mol^{-1} and 15 kcal mol^{-1} higher in energy than their C-H counterparts, respectively. While not unexpected, this outcome is somewhat disappointing as results are at the high end of the range generally observed for the barrier and product separation between related C-H and C-C activation reactions.

A change to the larger and more reactive iridium resulted in an increased capacity for C-H activation for 1,3-dimethylimidazolium. The reaction was highly exothermic, with little barrier to reaction. As such, it was expected C-C activation may follow suit and become a possibility under reaction conditions. While the reaction did remain exothermic, extra bulk around the metal centre combined with an inability to dissociate coordinated ligands discouraged C-C activation and increased the

activation barrier far beyond that displayed for any other system examined in this chapter.

Overall, both iridium and rhodium complexes seem capable of C-H activation of azolium salts to produce carbene complexes if basic ligands are combined with an accessible metal centre. Further work is required for C-C activation however, as electronic factors are not favourable for rhodium, while steric factors discourage the reaction for iridium.

4.5 References

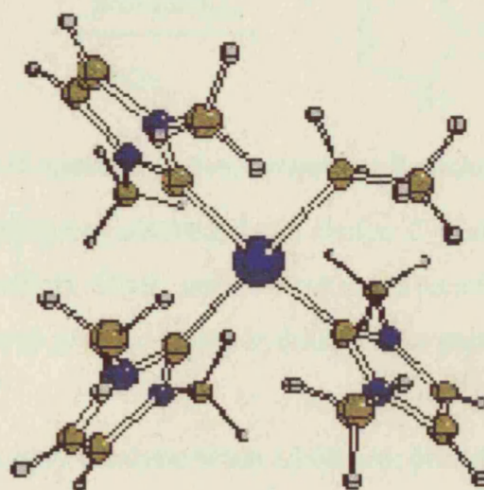
- 1 P. E. M. Siegbahn and M. Svensson, *J. Am. Chem. Soc.*, 1994, **116**, 10124.
- 2 E. N. Rodríguez-Arias, L. Rincón and F. Ruetter, *Organometallics*, 1992, **11**, 3677.
- 3 A. E. Shilov and G. B. Shul'pin, *Chem. Rev.*, 1997, **97**, 2879.
- 4 R. A. Periana and R. G. Bergman, *Organometallics*, 1984, **3**, 508.
- 5 M. J. Wax, J. M. Stryker, J. M. Buchanan, C. A. Kovac and R. G. Bergman, *J. Am. Chem. Soc.*, 1984, **106**, 1121.
- 6 R. G. Bergman, *J. Organomet. Chem.*, 1990, 273.
- 7 A. D. Ryabov, *Chem. Rev.*, 1990, **90**, 403.
- 8 R. H. Crabtree, *J. Chem. Soc., Dalton Trans.*, 2001, 2437.
- 9 J. Chatt and M. Davidson, *J. Chem. Soc.*, 1965, 843.
- 10 D. W. Evans, G. R. Baker and G. R. Newkome, *Coord. Chem. Rev.*, 1989, **93**, 155.
- 11 A. M. Magill, K. J. Cavell and B. F. Yates, *J. Am. Chem. Soc.*, 2004, **126**, 8717.
- 12 A. Fürstner, G. Seidel, D. Kremzow and C. W. Lehmann, *Organometallics*, 2003, **22**, 907.
- 13 D. S. McGuinness, K. J. Cavell and B. F. Yates, *Chem. Comm.*, 2001, **4**, 355.
- 14 S. Gründemann, M. Albrecht, A. Kovacevic, J. W. Faller and R. H. Crabtree, *J. Chem. Soc., Dalton Trans.*, 2002, 2163.
- 15 N. D. Clement, K. J. Cavell, C. Jones and C. J. Elsevier, *Angew. Chem. Int. Ed.*, 2004, **43**, 1277.
- 16 M. F. Lappert and A. J. Oliver, *J. Chem. Soc. Chem. Comm.*, 1972, 274.
- 17 M. A. Duin, N. D. Clement, K. J. Cavell and C. J. Elsevier, *Chem. Commun.*, 2003, 400.
- 18 H. C. Martin, N. H. James, J. Aitken, J. A. Gaunt, H. Adams and A. Haynes, *Organometallics*, 2003, **22**, 4451.
- 19 R. A. Diggle, S. A. Macgregor and M. K. Whittlesey, *Organometallics*, 2004, **23**, 1857.

- 20 J. Huang, E. D. Stevens and S. P. Nolan, *Organometallics*, 2000, **19**, 1194.
- 21 W. A. Herrmann, *Angew. Chem. Int. Ed.*, 2002, **41**, 1290.
- 22 P. J. Hay and W. R. Wadt, *J. Chem. Phys.*, 1985, **82**, 299.
- 23 P. J. Stephens, J. F. Devlin, C. F. Chabalowski and M. J. Frisch, *J. Phys. Chem.*, 1994, **98**, 11623.
- 24 A. D. Becke, *J. Chem. Phys.*, 1993, **98**, 5648.
- 25 T. H. Dunning and P. J. Hay, 'Modern Theoretical Chemistry', Plenum, 1976.
- 26 B. F. Yates, *J. Mol. Struct. (THEOCHEM)*, 2000, **506**, 223.
- 27 M. J. Frisch, J. A. Pople and J. S. Binkley, *J. Chem. Phys.*, 1984, **80**, 3265.
- 28 A. D. McLean and G. S. Chandler, *J. Chem. Phys.*, 1980, **72**, 5639.
- 29 R. Krishnan, J. S. Binkley, R. Seeger and J. A. Pople, *J. Chem. Phys.*, 1980, **72**, 650.
- 30 M. J. Frisch, G. W. Trucks, H. B. Schlegel, G. E. Scuseria, M. A. Robb, J. R. Cheeseman, V. G. Zakrzewski, J. A. Montgomery, Jr. , R. E. Stratmann, J. C. Burant, S. Dapprich, J. M. Millam, A. D. Daniels, K. N. Kudin, M. C. Strain, O. Farkas, J. Tomasi, V. Barone, M. Cossi, R. Cammi, B. Mennucci, C. Pomelli, C. Adamo, S. Clifford, J. Ochterski, G. A. Petersson, P. Y. Ayala, Q. Cui, K. Morokuma, N. Rega, P. Salvador, J. J. Dannenberg, D. K. Malick, A. D. Rabuck, K. Raghavachari, J. B. Foresman, J. Cioslowski, J. V. Ortiz, A. G. Baboul, B. B. Stefanov, G. Liu, A. Liashenko, P. Piskorz, I. Komaromi, R. Gomperts, R. L. Martin, D. J. Fox, T. Keith, M. A. Al-Laham, C. Y. Peng, A. Nanayakkara, M. Challacombe, P. M. W. Gill, B. Johnson, W. Chen, M. W. Wong, J. L. Andres, C. Gonzalez, M. Head-Gordon, E. S. Replogle and J. A. Pople, Gaussian 98 (Revision A.11.3), Pittsburgh PA, 2002.
- 31 K. Denk, P. Sirsch and W. A. Herrmann, *J. Organomet. Chem.*, 2002, **649**, 219.
- 32 M. J. Doyle, M. F. Lappert, P. L. Pye and P. Terreros, *J. Chem. Soc., Dalton Trans.*, 1984, 2355.
- 33 A. R. Chianese, L. Xingwei, M. C. Janzen, J. W. Faller and R. H. Crabtree, *Organometallics*, 2003, **22**, 1663.
- 34 C. Köcher and W. A. Herrmann, *J. Organomet. Chem.*, 1997, **532**, 261.

- 35 A. C. Chen, L. Ren, A. Decken and C. M. Crudden, *Organometallics*, 2000, **19**, 3459.
- 36 M. J. Doyle, M. F. Lappert, G. M. McLaughlin and J. McMeeking, *J. Chem. Soc., Dalton Trans.*, 1974, 1494.
- 37 W. A. Herrmann, J. Fischer, K. Öfele and F. R. J. Artus, *J. Organomet. Chem.*, 1997, **530**, 259.
- 38 D. S. McGuinness, N. Saendig, B. F. Yates and K. J. Cavell, *J. Am. Chem. Soc.*, 2001, **123**, 4029.
- 39 J. A. Mata, A. R. Chianese, J. R. Miecznikowski, M. Poyatos, E. Peris, J. W. Faller and R. H. Crabtree, *Organometallics*, 2004, **23**, 1253.
- 40 M. Poyatos, M. Sanaú and E. Peris, *Inorg. Chem.*, 2003, **42**, 2572.
- 41 A. A. Danopoulos, S. Winston and M. B. Hursthouse, *J. Chem. Soc., Dalton Trans.*, 2002, 3090.
- 42 D. S. McGuinness, Ph.D. Thesis, University of Tasmania, Hobart, 2001
- 43 J. A. Martinho-Simões and J. L. Beauchamp, *Chem. Rev.*, 1990, **90**, 629.
- 44 C. Hall and R. N. Perutz, *Chem. Rev.*, 1996, **96**, 3125.
- 45 J. Halpern, *Inorg. Chim. Acta.*, 1985, **100**, 41.
- 46 M. R. A. Blomberg, P. E. M. Siegbahn, E. Nagashima and J. Wennerberg, *J. Am. Chem. Soc.*, 1991, **113**, 424.
- 47 J. Y. Saillard and R. Hoffmann, *J. Am. Chem. Soc.*, 1984, **106**, 2006.
- 48 M. R. A. Blomberg, E. Brandemark and P. E. M. Siegbahn, *J. Am. Chem. Soc.*, 1983, **105**, 5557.
- 49 M. D. Su and S. Y. Chu, *J. Phys. Chem.*, 1998, **102**, 10159.
- 50 M. D. Su and S. Y. Chu, *Organometallics*, 1997, **16**, 1621.
- 51 M. D. Su and S. Y. Chu, *Inorg. Chem.*, 1998, **37**, 3400.
- 52 T. Ziegler, V. Tschinke, L. Fan and A. D. Becke, *J. Am. Chem. Soc.*, 1989, **111**, 9177.
- 53 N. Koga and K. Morokuma, *J. Phys. Chem.*, 1990, **94**, 5454.
- 54 T. R. Cundari, *J. Am. Chem. Soc.*, 1994, **116**, 340.
- 55 J. Song and M. B. Hall, *Organometallics*, 1993, **12**, 3118.
- 56 P. Margl, T. Ziegler and P. E. Blöchl, *J. Am. Chem. Soc.*, 1995, **117**, 12625.

- 57 J. Espinosa-Garcia, J. C. Corchado and D. G. Truhlar, *J. Am. Chem. Soc.*, 1997, **119**, 9891.
- 58 J. K. Perry, G. Ohanessian and W. A. I. Goddard, *Organometallics*, 1994, **13**, 1870.
- 59 B. Rybtchinski, A. Vigalok, B. Yehoshoa and D. Milstein, *J. Am. Chem. Soc.*, 1996, **118**, 12406.
- 60 M. E. van der Boom, L. Shyh-Yeon, B. Yehoshoa, M. Gozin and D. Milstein, *J. Am. Chem. Soc.*, 1998, **120**, 13415.
- 61 Z. Cao and M. B. Hall, *Organometallics*, 2000, **19**, 3338.
- 62 S. K. Ritter, *Chem. Eng. News*, 2002, **80**, 26.
- 63 D. Hermann, M. Gandelman, H. Rozenberg, L. J. W. Shimon and D. Milstein, *Organometallics*, 2002, **21**, 812.
- 64 A. Sundermann, O. Uzan and J. M. L. Martin, *Organometallics*, 2001, **20**, 1783.
- 65 B. Rybtchinski, S. Oevers, M. Montag, A. Vigalok, H. Rozenberg, J. M. L. Martin and D. Milstein, *J. Am. Chem. Soc.*, 2001, **123**, 9064.
- 66 A. C. Hillier, H. M. Lee, E. D. Stevens and S. P. Nolan, *Organometallics*, 2001, **20**, 4246.
- 67 P. J. Fraser, W. R. Roper and F. G. A. Stone, *J. Chem. Soc., Dalton Trans.*, 1974, 102.
- 68 A. T. Termaten, M. Schakel, A. W. Ehlers, M. Lutz, A. L. Spek and K. Lammertsma, *Chem. Eur. J.*, 2003, **9**, 3577.
- 69 P. J. Fraser, W. R. Roper and F. G. A. Stone, *J. Chem. Soc., Dalton Trans.*, 1974, 760.
- 70 M. Prinz, M. Grosche, E. Herdtweck and W. A. Herrmann, *Organometallics*, 2000, **19**, 1692.
- 71 A. Kovacevic, A. Gründemann, J. R. Miecznikowski, E. Clot, O. Eisenstein and R. H. Crabtree, *Chem. Commun.*, 2002, 2580.

Section 3



Catalytic Studies of Carbon-Carbon Coupling Reactions

5 Nickel Catalysts for Azolium C-C Coupling Reactions

5.1 Introduction

Recently, Bergman's group have used rhodium complexes to produce inter- and intra-molecular C-C coupled 2-alkyl azoles¹⁻⁷ (Figure 5-1). It is believed the reaction is initiated by C-H activation of the equivalent 2-H azole, with experimental results indicating a rhodium carbene complex may be involved as a reaction intermediate¹.

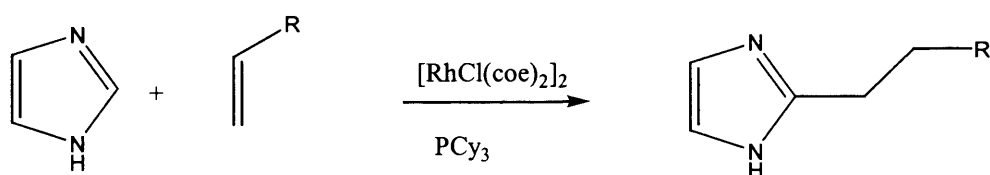


Figure 5-1 C-C coupling reaction performed by Bergman

In addition to this work, our group has succeeded in a similar C-C coupling reaction using nickel and palladium catalysts which, unlike Bergman's reaction, occurs via the activation of 2-H azolium salts to give a carbene hydride before going on to create the coupled 2-alkyl azolium salts⁸.

Interestingly, this reaction was only catalytic when a Ni(cod)₂ precursor complex was used with 2.2 equivalents of PPh₃. When the corresponding carbene catalyst Ni(dmiy)₂ was trialed, the C-C coupled product was not produced, as a stable nickel(II) hydride was formed⁹ (Figure 5-2).

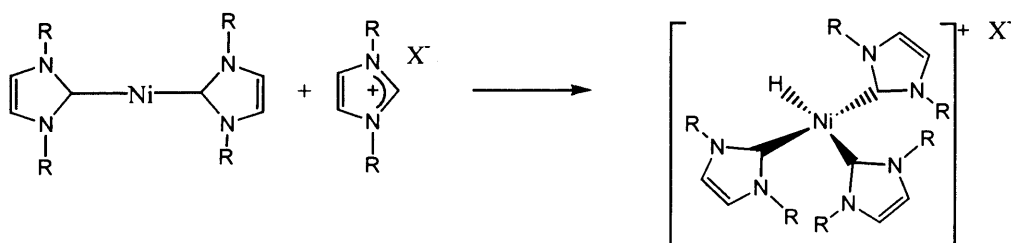


Figure 5-2 Isolated carbene nickel hydride complex

Despite the general similarities between phosphine and carbene ligands, this result again highlighted some major differences between the two classes of ligands. We believe the catalytic cycle discovered using Ni(PPh₃)₂ proceeds through a mechanism of oxidative addition of the azolium salt, replacement of a weakly bound ligand by

alkene, followed by insertion of the alkene into the metal hydride and finally, reductive elimination of the product (McGuinness/Cavell Mechanism - Figure 5-3).

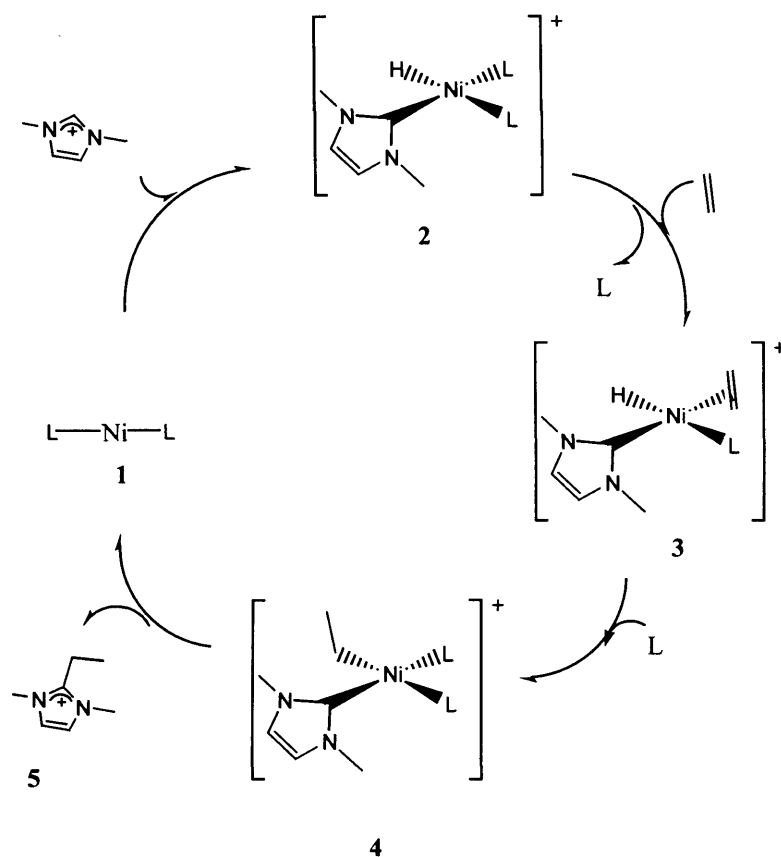


Figure 5-3 Proposed catalytic cycle (McGuinness/Cavell Mechanism)

This chapter describes the computational study of the proposed reaction mechanism for the successful coupling of ethylene and 1,3-dimethylimidazolium by a range of NiL_1L_2 systems. As revealed experimentally, changes in electronic and steric properties dramatically affect the outcome of the reaction and as such, we considered a range of ligand sets including $L_1 = L_2 = 1,3$ -dimethylimidazol-2-ylidene; $L_1 = 1,3$ -dimethylimidazol-2-ylidene, $L_2 =$ trimethylphosphine; $L_1 = L_2 =$ trimethylphosphine; $L_1 = L_2 =$ triphenylphosphine; $L_1 = L_2 =$ tri-*tert*-butylphosphine.

5.2 Computational details

Geometry optimisations and harmonic vibrational frequencies for the Ni(dmiy)₂, Ni(PMe₃)₂ and Ni(PMe₃)(dmiy) systems were calculated using the B3LYP¹⁰⁻¹² method with the LANL2DZ basis set, which incorporates the Hay and Wadt¹³ small core relativistic effective core potential and double zeta valence basis set on nickel and phosphorus with the Dunning and Huzinaga¹⁴ double zeta basis set on all other atoms. Zero point vibrational energy corrections were obtained using unscaled frequencies. All transition structures contained exactly one imaginary frequency and were characterised by following the corresponding normal mode towards the products and reactants.

Geometry optimisations and frequency calculations for Ni(P^tBu₃)₂ and Ni(PPh₃)₂ and associated cycle were calculated using the ONIOM method¹⁵⁻²¹, with the phosphine phenyl groups partitioned in the lower layer using molecular mechanics (uff²²), and all other atoms using B3LYP/LANL2DZ level of theory.

Higher level single point energy calculations were performed on all optimised geometries at the B3LYP/6-311+G(2d,p)²³⁻²⁵ level of theory. Energies from these single point calculations were combined with the thermodynamic corrections at the lower level of theory to obtain ΔG_{298} numbers. All energies quoted in this chapter refer to these final ΔG_{298} values.

All calculations were performed with the Gaussian 03²⁶ set of programs.

5.3 Results and discussion

5.3.1 Individual step considerations

The overall cycle studied consisted of four main steps: oxidative addition of the imidazolium salt to the nickel starting complex (Figure 5-3: 1 → 2), coordination and insertion of an ethylene ligand into the metal hydride bond (Figure 5-3: 2 → 3 → 4), and reductive elimination of the product (Figure 5-3: 4 → 1). The main characteristics, mechanism and effects of the different ligands on each of the individual steps are described in detail below.

5.3.1.1 Starting materials

In general, the nickel starting complexes displayed highly symmetric geometries. L_1 -Ni- L_2 angles were almost linear ranging from 178.23° for the $Ni(PMe_3)(dmiy)$ system to 179.92° for the $Ni(P^tBu_3)_2$ structure. The exception lay in the $Ni(PPh_3)_2$ complex, which displayed a slightly bent configuration, with an L_1 -Ni- L_2 angle of 167.44° .

The $Ni(dmiy)_2$ calculated geometry is in excellent agreement with known crystal structures of similar complexes^{27, 28}. Intra-carbene N-C-N angles are almost identical to experimental values (Calculated (N-Me): 102.32° ; Caddick (N- t Bu)²⁷: 102.25° ; Arduengo²⁸ (N-Mes): 102.0°), and the calculated nickel-carbene bond distance of 1.864\AA shows only minor variation from the metal-carbene distances obtained by Caddick²⁷ (N- t Bu: 1.874\AA) and Arduengo²⁸ (N-Mes: 1.829\AA). This variation can be attributed to the difference in carbene basicity with slightly longer bond distances associated with more basic ligands.

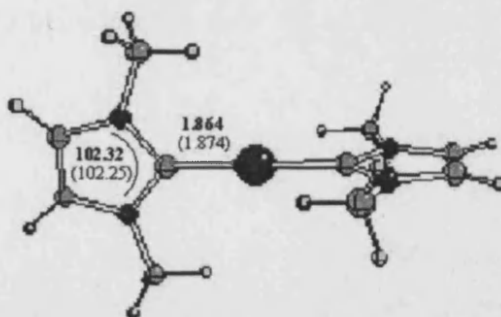


Figure 5-4 $Ni(dmiy)_2$ bond angles and distances (experimental values in brackets²⁷)

The phosphine complexes reflected the same trend for increased metal-ligand bond distance as ligand basicity increased, with the diphosphine nickel(0) complexes

ranging from 2.182Å for triphenylphosphine ligands, 2.192Å for trimethylphosphine, to 2.214Å for the more basic tri-*tert*-butylphosphine. The nickel(dmip)(PMe₃) distances highlighted the increased σ -donor strength of the carbene ligands compared to phosphines, with the nickel-carbene distance slightly shorter than was found in the dicarbene case (1.852Å), and the nickel-phosphine distance longer (2.214Å).

5.3.1.2 Oxidative addition

It has been shown previously that the oxidative addition of imidazolium salts to group 10 metals can occur readily to form M(II) hydride products^{9, 29-31} (Figure 5-5).

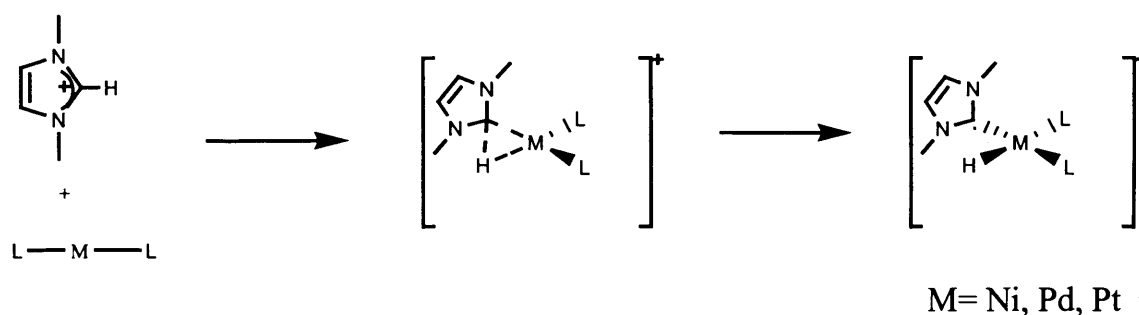


Figure 5-5 Successful experimental oxidative addition reactions

Theoretical studies have indicated this occurs initially through a weak interaction between the metal centre and the salt C2, leading to a concerted three-centred transition structure in which the C2-H bond becomes elongated as the salt draws closer to the metal^{29, 30}. The four-coordinate product has generally been formed with little or no barrier and the overall reaction is exothermic.

For the series of ligands used in this study, the geometries for the precursor complexes and transition structures were quite varied. While all species displayed some form of initial interaction, these interactions were by no means uniform (Figure 5-6).

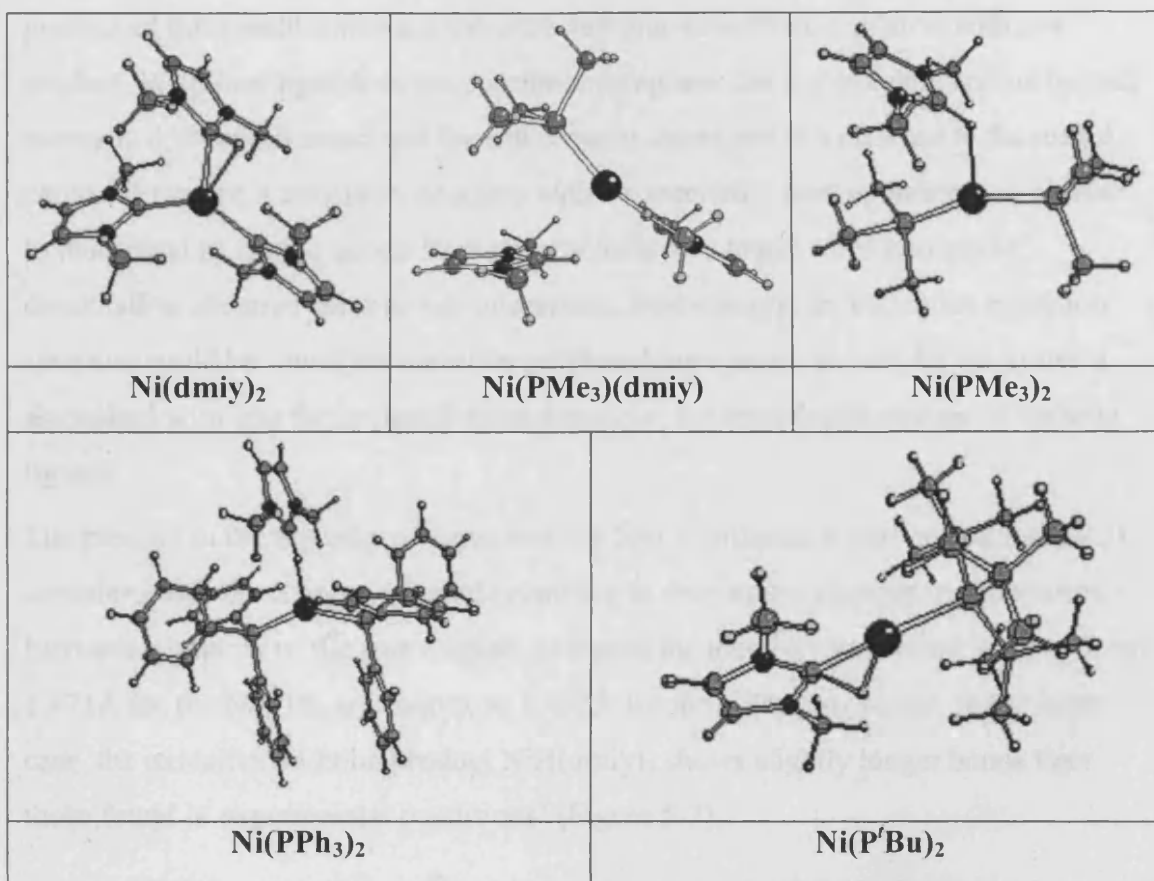


Figure 5-6 Oxidative addition transition structures

The Ni(dmiy)₂ complex begins with a C2-metal interaction which bends the 2-H of the salt out of the imidazolium plane, but does not significantly lengthen the C2-H bond distance. The oxidative addition itself proceeds as the C2 and 2-H draw closer to the metal, with the transition structure geometry only marginally altered from the precursor complex; the major differences a lengthening of the C2-H bond by 0.036 Å, and a decrease in the L₁-Ni-L₂ angle to more closely resemble the square planar geometry.

The diphosphine systems Ni(PMe₃)₂ and Ni(PPh₃)₂ were the first indication of the differences between phosphine and carbene ligands in the catalytic cycle. Both systems displayed an initial 2-H to metal interaction with the transition structures indicating the only driving force necessary for oxidative addition is a slight tilt of the incoming imidazolium to simultaneously expose the C2 and the 2-H to the metal centre.

While a similar transition structure could be found for the $\text{Ni}(\text{P}^t\text{Bu}_3)_2$ system, the product of this reaction was not the expected four-coordinate oxidative addition product. With four ligands in the coordination sphere, the *tert*-butylphosphine ligands overcrowd the small metal and the salt remains intact and at a distance to the nickel centre. However, a transition structure with a concerted 3-centred interaction similar to that found in similar group 10 metal reactions was found when phosphine dissociation occurred prior to salt interaction. Interestingly, an analogous transition structure could be found for the triphenylphosphine system, but not for the systems associated with less facile ligand dissociation i.e. the trimethylphosphine or carbene ligands.

The product in the majority of cases was the four coordinate square-planar nickel(II) complex, with the change in ligands resulting in only minor changes in geometries. Increasing basicity of the *trans* ligand increased the metal-hydride bond, ranging from 1.471 Å for the $\text{Ni}(\text{PPh}_3)_2$ complex to 1.493 Å for the $\text{Ni}(\text{dmiy})_2$ ligand. In the latter case, the oxidative addition product $\text{NiH}(\text{dmiy})_3$ shows slightly longer bonds than those found in experimental conditions⁹ (Figure 5-7).

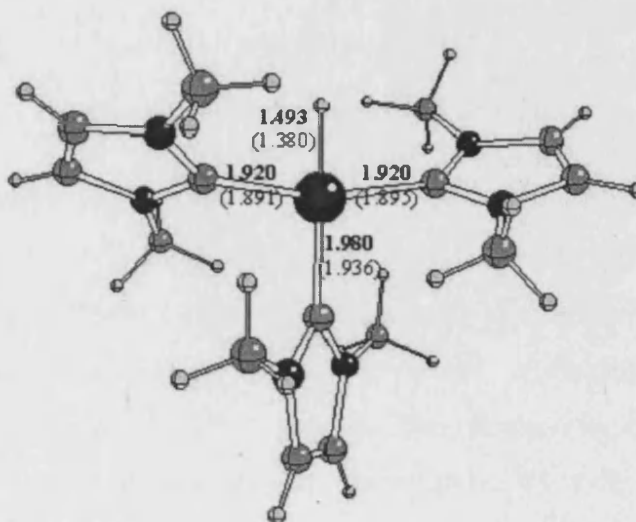


Figure 5-7 $\text{NiH}(\text{dmiy})_3$ bond distances (experimental values in brackets)

The longer distances are consistent with the slightly higher basicity of the N-Me carbene over their N-(2,6-dimethyl)phenyl analogues, increasing the *trans* effect and therefore M-L distances. In fact, this trend continues through the calculated series with both the carbene Ni-C2 and Ni-H distances decreasing as the basicity of the auxiliary ligands decreases (Table 5-1).

System	Ni-Carbene	Ni-H	Ni-L ₁	Ni-L ₂
NiH(dmiy) ₃	1.920	1.493	1.920	1.980
NiH(dmiy) ₂ (PMe ₃)	1.912	1.480	1.914	2.366
NiH(dmiy)(PMe ₃) ₂	1.902	1.481	2.355	2.299
NiH(dmiy)(PPh ₃) ₂	1.894	1.471	2.375	2.326
NiH(dmiy)(P ^t Bu ₃)*	1.881	1.433	2.336	-

Table 5-1 NiH(dmiy)L₂ bond distances (*NiH(dmiy)(P^tBu₃) three coordinate)

Despite the diversity in encounter complexes and transition structures, the ease of this initial step in the cycle is highlighted by the relative energies of the products and starting materials in all cases (Figure 5-8). Minor barriers around 3 kcal mol⁻¹ exist from precursor complex to transition structure for all nickel complexes, with each oxidative addition product lying well below its respective starting materials in Gibbs Free Energy. While this may not be surprising for the four-coordinate complexes, it is an interesting result for the coordinatively unsaturated tri-*tert*-butylphosphine complex and is an early indication of the effect of using very bulky ligands in catalytic cycles.

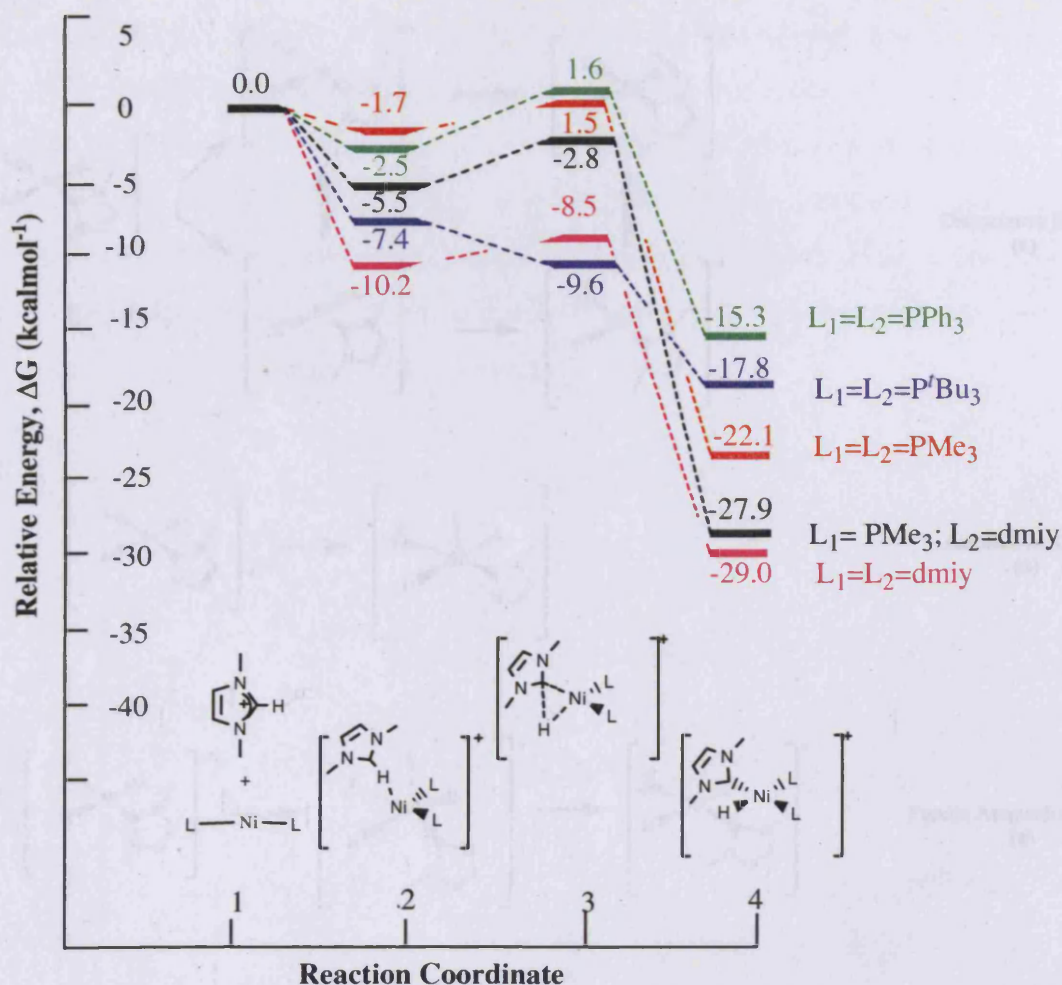


Figure 5-8 Energies for the oxidative addition step

5.3.1.3 Coordination of ethylene

For the catalytic cycle to continue after oxidative addition, the alkene must be able to coordinate to the metal centre before subsequent insertion into the metal-hydride bond. Coordination may occur by two alternative routes or a combination of the two (Figure 5-9). In a dissociative route, a previously coordinated ligand would leave the coordination sphere of the metal, creating an unsaturated three-coordinate metal centre to which an ethylene ligand can then coordinate to reform a four-coordinate nickel complex either in a *cis* or *trans* arrangement (Figure 5-9 a). Alternatively, five-coordinate nickel complexes have been identified previously³², so an associative route may be followed in which a five-coordinate NiH(dmiy)L₂(ethylene) intermediate is formed (Figure 5-9 b). Finally, a combination of these options is conceivable in which an incoming ethylene directly prompts the dissociation of another ligand (Figure 5-9 c).

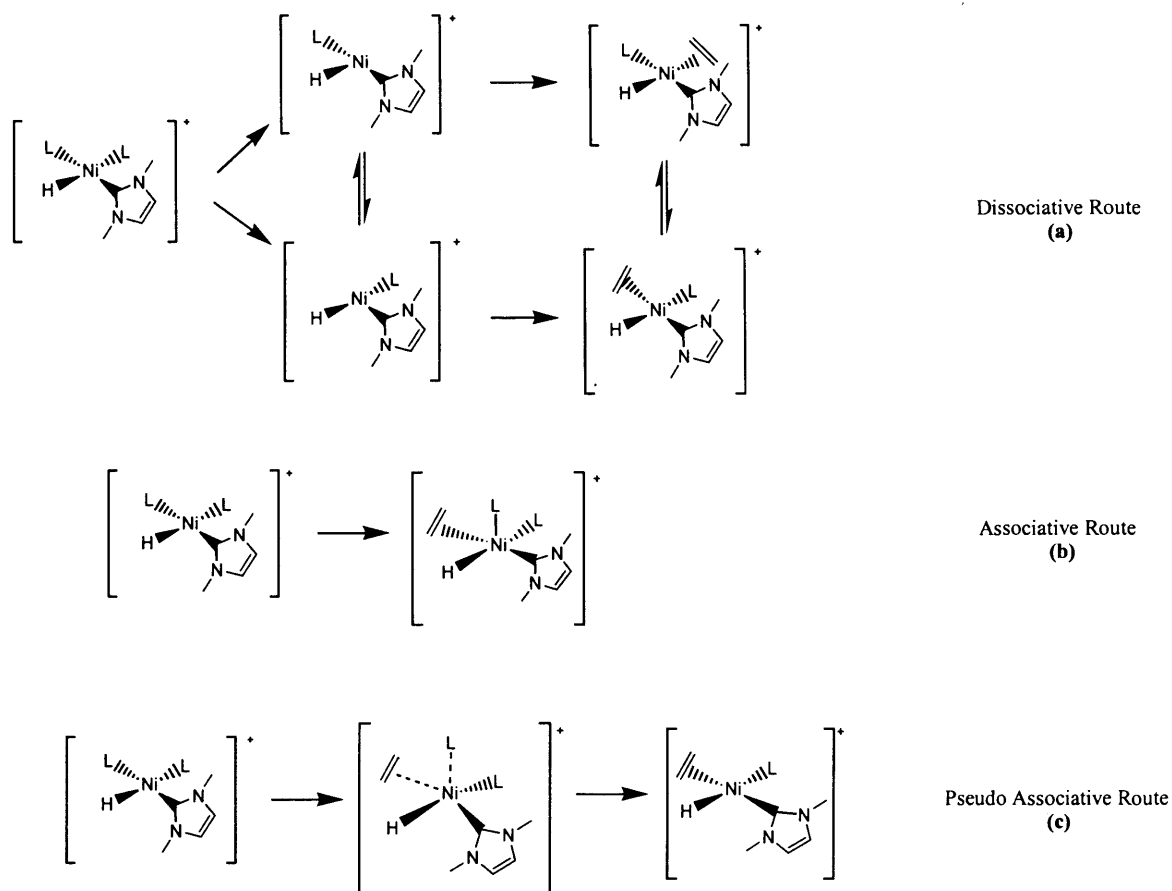


Figure 5-9 Ethylene coordination reaction mechanisms

A study of these possibilities using the $\text{Ni}(\text{PMe}_3)_2$ as the model indicated a dissociative route was most likely for this reaction step. Ethylene does not bind strongly enough to the nickel to directly displace an existing ligand in a pseudo associative route. Further, the nickel complex with 5 ligands present in the coordination sphere consistently rearranged to a four coordinate state with the ethylene ligand excluded from the metal centre, regardless of the starting geometry.

As relatively low-energy three-coordinate structures were located and similar nickel complexes with high electron donating ligands have been established in experimental conditions³³, it is likely this is the preferred route in the cycle studied.

For the dissociative route, geometry optimisations revealed the initial three-coordinate dissociated complexes optimised with a T-shaped configuration with all ligands slightly closer to the metal than their four coordinate counterparts. Phosphine dissociation appears relatively straight forward, requiring $18.0 \text{ kcal mol}^{-1}$ for ejection of the trimethylphosphine (Figure 5-10). This lowers to $15.2 \text{ kcal mol}^{-1}$ for the mixed carbene/phosphine system, indicating the extra stability of the nickel complex

associated with the stronger and more basic carbene ligand. As expected, the larger and more weakly bound triphenylphosphine reduces the dissociation barrier considerably, with dissociation only requiring $7.9 \text{ kcal mol}^{-1}$ for formation of the three-coordinate intermediate. Further, from the oxidative addition step discussed in the previous section, the triphenylphosphine and tri-*tert*-butylphosphine systems may initially proceed through a dissociated route, therefore making subsequent ethylene coordination straightforward for these systems.

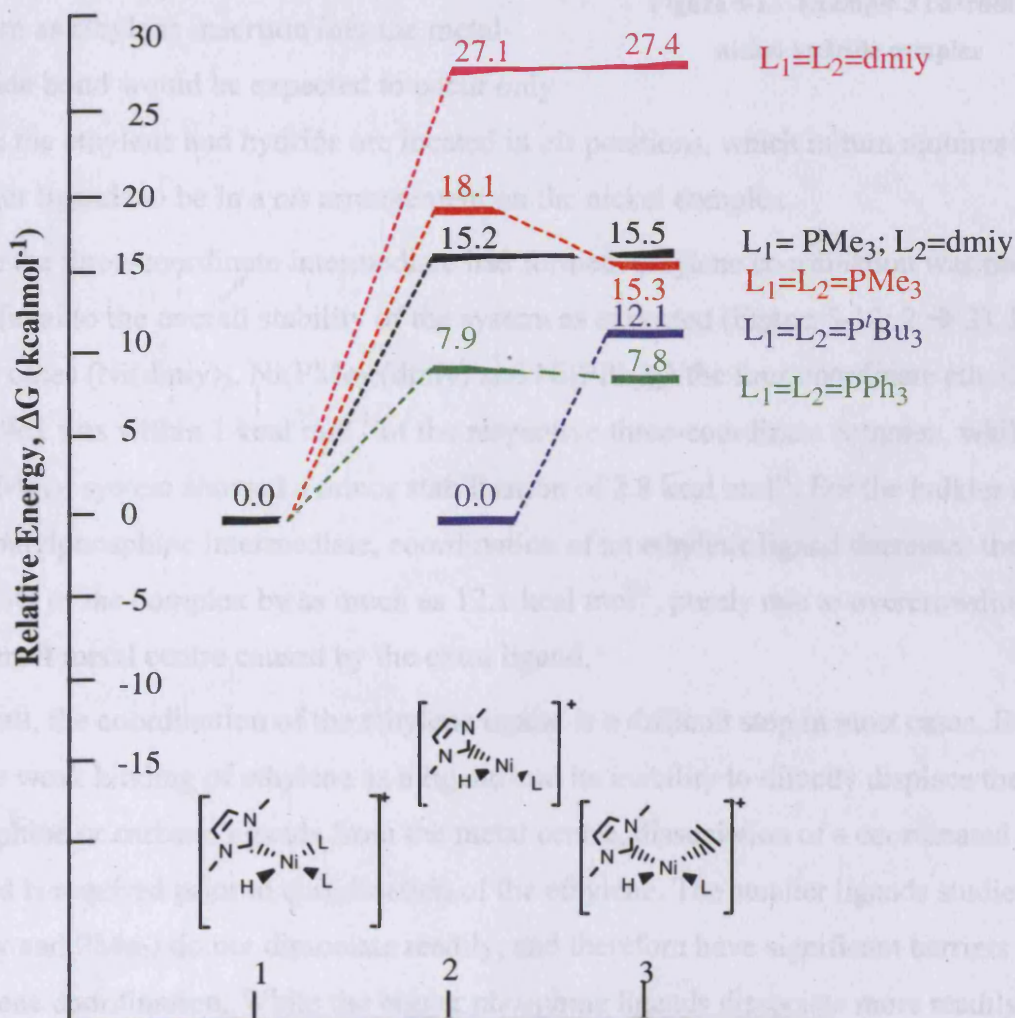


Figure 5-10 Energies for the ethylene coordination step

In contrast, dissociation of a carbene ligand for the $\text{Ni}(\text{dmiy})_2$ system appears very limited. While the imidazole-based carbenes have been isolated³⁴ and it is therefore highly probable they can exist in reaction cycles such as these, they also form very strong metal bonds. A combination of this strength and the relative instability of nickel three-coordinate complexes increases the barrier for the $\text{Ni}(\text{dmiy})_2$ system to $27.1 \text{ kcal mol}^{-1}$ for this step.

In general, only the isomers with the L_1 and L_2 ligands in the *trans* positions were stable for the three-coordinate intermediates (Figure 5-11). The sole exception was the triphenylphosphine system in which an L_1/L_2 *cis* form was found with only $2.0 \text{ kcal mol}^{-1}$ separating the *cis* and *trans* isomers. This anomaly may prove to be important in our system as ethylene insertion into the metal-hydride bond would be expected to occur only

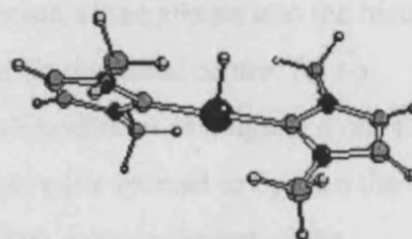


Figure 5-11 Example 3 coordinate nickel hydride complex

when the ethylene and hydride are located in *cis* positions, which in turn requires the bulkier ligands to be in a *cis* arrangement on the nickel complex.

Once the three-coordinate intermediate had formed, ethylene coordination was not as beneficial to the overall stability of the system as expected (Figure 5-10: 2 \rightarrow 3). In three cases ($\text{Ni}(\text{dmiy})_2$, $\text{Ni}(\text{PMe}_3)(\text{dmiy})$ and $\text{Ni}(\text{PPh}_3)_2$) the four-coordinate ethylene complex was within 1 kcal mol^{-1} of the respective three-coordinate complex, while the $\text{Ni}(\text{PMe}_3)_2$ system showed a minor stabilisation of $2.8 \text{ kcal mol}^{-1}$. For the bulkier *tert*-butylphosphine intermediate, coordination of an ethylene ligand decreases the stability of the complex by as much as $12.1 \text{ kcal mol}^{-1}$, purely due to overcrowding of the small metal centre caused by the extra ligand.

Overall, the coordination of the ethylene ligand is a difficult step in most cases. Due to the weak binding of ethylene as a ligand and its inability to directly displace the phosphine or carbene ligands from the metal centre, dissociation of a coordinated ligand is required prior to coordination of the ethylene. The smaller ligands studied (*dmiy* and PMe_3) do not dissociate readily, and therefore have significant barriers to ethylene coordination. While the bigger phosphine ligands dissociate more readily, the remaining bulk on the small metal increases the energy of the four-coordinate ethylene intermediate. Despite this, the triphenylphosphine system provides the smoothest path for ethylene coordination when compared to all other ligand combinations, with a balance between ease of dissociation and excessive bulk in the coordination sphere.

5.3.1.4 Ethylene insertion

Ethylene coordination may only be followed by insertion of the alkene into the metal-hydride bond if the ethylene and hydride are adjacent on the metal centre. As no stable five-coordinate nickel species was found and dissociation of a ligand *trans* to a carbene is thought to occur, the initial ethylene complex is expected to contain the ethylene and hydride ligands in *trans* positions. As such, rearrangement of the ethylene complex to the equivalent *cis* form would be required before insertion may occur.

The size of the metal ligands had the most significant impact on stability of the *cis* form of the ethylene-hydride intermediates. For the smaller ligands (dmiy and PMe_3 combinations), a *cis* arrangement of the ethylene and hydride moieties resulted in a significantly more stable complex than the corresponding *trans* form. Interestingly, these complexes displayed a very close H-ethylene bond and are reminiscent of an insertion precursor complex (Figure 5-12).

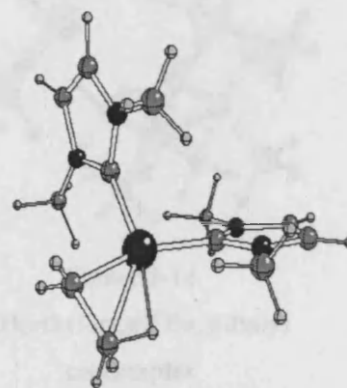


Figure 5-12 Example nickel ethylene hydride *cis* complex

A more conventional *cis* intermediate can be found

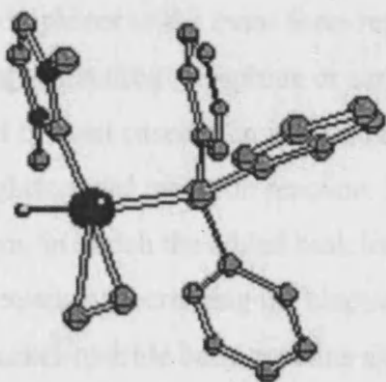


Figure 5-13 $\text{NiH}(\text{ethylene})(\text{PPh}_3)(\text{dmiy})$ *cis* complex (hydrogens removed for clarity)

for the $\text{Ni}(\text{PPh}_3)_2$ complex in which the ethylene ligand is almost perpendicular to the plane of the nickel coordination sphere (Figure 5-13). The energy of this complex reflects the phosphine ligand bulk, which can be more easily accommodated when the phosphine and carbene ligands are located *trans* to one another. With the two larger ligands in adjacent positions, the square planar arrangement becomes distorted to

partially overcome the negative influence from interaction of these ligands, however a twist of the ethylene ligand does result in a much more stable ‘insertion precursor’ type complex as found for the other systems. While it may seem contradictory that the ethylene parallel to the plane takes up less room than the perpendicular alternative, it

is the combination of ethylene and hydride that reduces steric strain with the C2-Ni-P angle opening to 103.2° compared to 97.5° for the conventional *cis* NiH(ethylene)(dmip)(PPh₃) complex.

The tri-*tert*-butylphosphine ligand exacerbates the instability of the four-coordinate ethylene complexes as found for the Ni(PPh₃)₂ system. While the *trans* located ethylene and hydride complex is reasonably stable, enforcing a *cis* complex greatly increases the energy of the intermediate as the two large ligands are positioned in such close proximity (Figure 5-14). This strain is most evident in the nickel-phosphine distance which increases from 2.482 Å for the *trans* complex to 2.943 Å in the *cis* equivalent to attempt to compensate for the overcrowding. Further, there is no stable insertion-like precursor complex as found with the complexes containing the smaller ligands. As such, it is expected any twist of the ethylene ligand will directly result in insertion of the ligand into the metal-hydride bond and formation of a three-coordinate ethyl product.

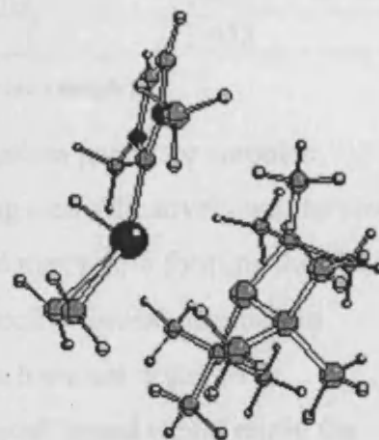


Figure 5-14
NiH(ethylene)(P'Bu₃)(dmip)
cis complex

Another important factor for migratory insertion comes from the electronic benefits of strong *trans* effect ligands opposite the hydride ligand (Table 5-2). Rearrangement of the complexes to the *trans* form results in exchange of the ethylene ligand for the stronger donating phosphine or carbene ligands opposite the coordinated hydride. The effect in most cases is an increase in the metal-hydride distance, supporting a more straightforward insertion reaction. The only exception once again is for the Ni(P'Bu₃)₂ system, in which the added bulk increases the phosphine ligand to metal bond, consequently decreasing the electronic influence of the phosphine ligand. As a result, the nickel-hydride bond remains almost constant.

System	Ni-H <i>cis</i> complex (Å)	Ni-H <i>trans</i> complex (Å)
Ni(dmiy) ₂	1.817	1.462
Ni(dmiy)(PMe ₃)	1.817	1.462
Ni(PMe ₃) ₂	2.091	1.464
Ni(PPh ₃) ₂	1.761	1.471
Ni(P ^t Bu ₃) ₂	1.450	1.453

Table 5-2 Ni-H distances for the *cis* and *trans* complexes

For the smaller ligand systems that form the pseudo insertion precursor complex, insertion is thought to either occur spontaneously leaving a coordinatively unsaturated nickel alkyl intermediate to which the dissociated ligand may rejoin forming the alkyl complex, or recoordination of the dissociated ligand directly ‘forces’ insertion to occur (Figure 5-15). Further, as double alkene insertions have not occurred in experimental conditions, it is envisaged that the dissociated ligand would rejoin the complex in preference to another alkene.

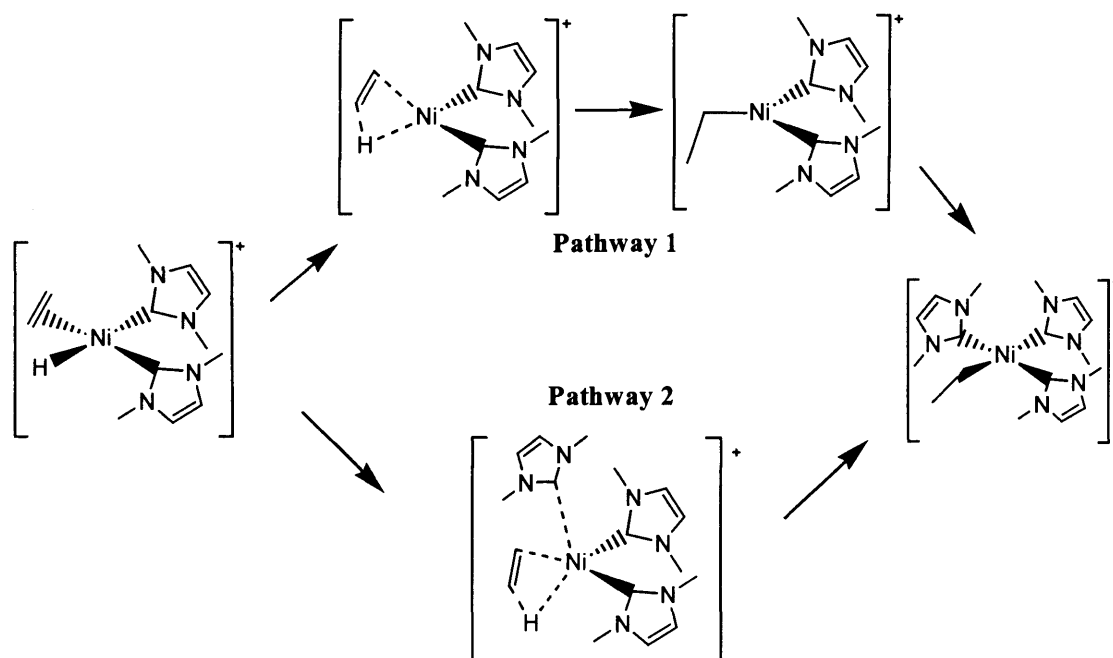


Figure 5-15 Ethylene insertion reaction

While the three-coordinate alkyl intermediate can be found in all systems, a potential energy surface scan indicated direct recoordination of the incoming ligand proceeded smoothly towards the ethyl insertion product for the smaller ligands and as such, it is expected this would be the route taken in experimental conditions. This was not the case for the large triphenylphosphine and tri-*tert*-butylphosphine systems, where the

increased size of the ligand indicated the three-coordinate complex was the favoured structure with no stable four coordinate Ni(ethyl)(P^tBu₃)₂(dmly) complex located.

Despite the smaller systems indicating direct conversion from the 'insertion precursor' complexes to the four coordinate ethyl products with assistance from ligand reassociation (Figure 5-15 pathway 2), the 3 coordinate complexes have been included in all following reaction energy diagrams so as to afford a more direct comparison for all systems studied.

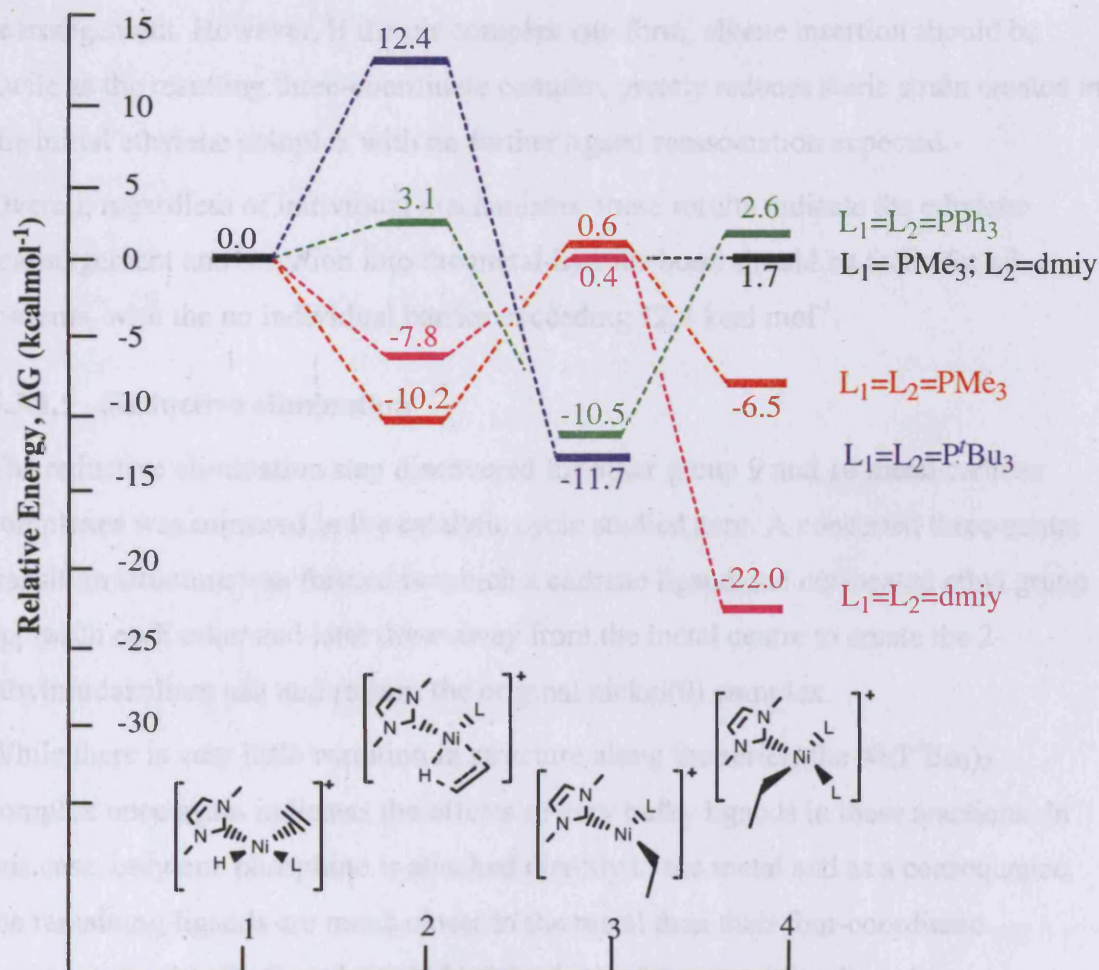


Figure 5-16 Energies for the ethylene insertion step

For the smaller ligand systems, the form of the complex in which the hydride and ethylene are adjacent provides a relatively large decrease in energy compared to the corresponding *trans* form (Figure 5-16). This decrease in energy would provide a reasonable driving force for the rearrangement with barriers to the subsequent insertion reaction relatively small. Combined with the *cis* form of the ethylene complex comparable in energy to the insertion product, the low reaction barrier results in a straightforward, yet reversible, insertion step for these systems.

The Ni(PPh₃)₂ system provides a somewhat different result. While there is little energy difference between the *cis* and *trans* forms, the added bulk in these systems gives rise to a more stable three-coordinate ethyl complex, with recoordination of the dissociated phosphine significantly increasing the energy of the four-coordinate insertion product.

The effect of extra bulk is even more prominently displayed in the tri-*tert*-butylphosphine system, with much larger barriers to alkene *trans-cis* complex rearrangement. However, if the *cis* complex can form, alkene insertion should be facile as the resulting three-coordinate complex greatly reduces steric strain created in the initial ethylene complex with no further ligand reassociation expected.

Overall, regardless of individual mechanisms, these results indicate the ethylene rearrangement and insertion into the metal-hydride bond should be facile for all systems, with the no individual barrier exceeding 12.4 kcal mol⁻¹.

5.3.1.5 Reductive elimination

The reductive elimination step discovered for other group 9 and 10 metal carbene complexes was mirrored in the catalytic cycle studied here. A concerted three-centre transition structure was formed in which a carbene ligand and *cis* located ethyl group approach each other and later draw away from the metal centre to create the 2-ethylimidazolium salt and reform the original nickel(0) complex.

While there is very little variation in structure along the series, the Ni(P^{*t*}Bu₃)₂ complex once again indicates the effects of very bulky ligands in these reactions. In this case, only one phosphine is attached directly to the metal and as a consequence, the remaining ligands are much closer to the metal than their four-coordinate counterparts, despite the relatively high basicity of the remaining ligands.

In general, the transition structures for all the nickel complexes studied are very similar, with the carbene carbon to nickel distances slightly smaller than the ethyl precursor complexes. Surprisingly, the complexes have Ni-C2 distance within 0.007 Å of each other (1.870 Å–1.877 Å) for all but the tri-*tert*-butylphosphine complex, which has a slightly shorter bond distance of 1.852 Å in compensation for the coordinatively unsaturated nature of the metal centre. The angle of the interaction between the carbene and ethyl ligands further results in a weak interaction between one of the ethyl hydrogens and the metal centre (Figure 5-17).

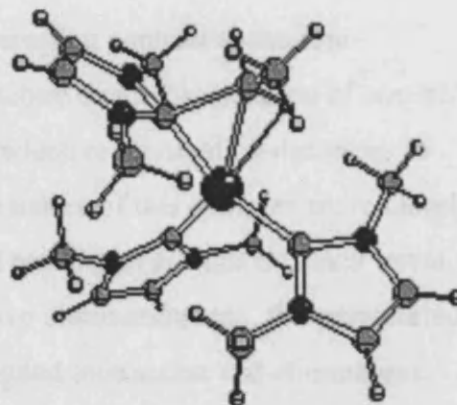


Figure 5-17 Example reductive elimination transition structure

As the transition structure moves towards the final products, the resultant imidazolium salt interacts quite closely with the nickel(0) complex through the carbene C2 and one of the ring nitrogens, breaking the planarity of the imidazolium ring. All L_1 -Ni- L_2 angles in the product more closely resemble a four-coordinate nickel complex than a two-coordinate planar complex consequently stabilising the unsaturated nickel(0) complex.

In previous studies, it has been shown that increasing the bulk or decreasing the basicity of ligands decreases the barrier to reductive elimination. While this was generally true for the ligands used in this study, it was highlighted that electronic and steric factors are equally important and cannot be viewed in isolation. The highly basic carbene ligands do not have the 3-dimensional steric influence of the phosphines and as such, the four coordinate ethyl complex that is the precursor to reductive elimination is quite stable, with the barrier for formation of the 2-ethyl salt a high 24.5 kcal mol⁻¹. Further, the reductive elimination step in the Ni(dmiy)₂ case energetically favours the nickel(II) ethyl complex over the separated product by 11.2 kcal mol⁻¹. The exchange of just one of these ligands with the less basic PMe₃ ligand lowers the barrier to 19.3 kcal mol⁻¹ and the reductive elimination from the nickel(II) alkyl complex becomes a favourable reaction by 4.6 kcal mol⁻¹. However, the double exchange to PMe₃ or PPh₃ ligands only slightly decreases the overall barrier to 17.7 kcal mol⁻¹ and 17.4 kcal mol⁻¹ respectively. The reductive elimination step remains

favourable in both cases, with the added bulk of the triphenylphosphine ligands increasing the stability of the separated nickel(0) products slightly more than for the PMe_3 ligands.

The tri-*tert*-butylphosphine ligand provides an interesting contrast to the four-coordinate counterparts. Despite the unsaturated nature due to dissociation of one tri-*tert*-butylphosphine ligand, the overall barrier to reductive elimination decreases to $14.8 \text{ kcal mol}^{-1}$. While it could be conceivable the nature of this complex more closely resembles a nickel(0) complex with the combined basicity of all ligands much lower than other complexes, which promotes the reductive elimination step, the unsaturated nature may equally be seen as a disadvantage to ligand interaction and elimination. Further investigation is required to elicit the true factors affecting this reaction.

While the separated reductive elimination products range from $\pm 9 \text{ kcal mol}^{-1}$ in energy around their respective nickel(II) ethyl complexes, reversal of this step in all cases is unlikely with continuation of the cycle by replacement of the loosely bound 2-ethylimidazolium with another 1,3-dimethylimidazolium salt providing a lower barrier to reaction than the reverse oxidative addition of the 2-ethylimidazolium (Figure 5-18).

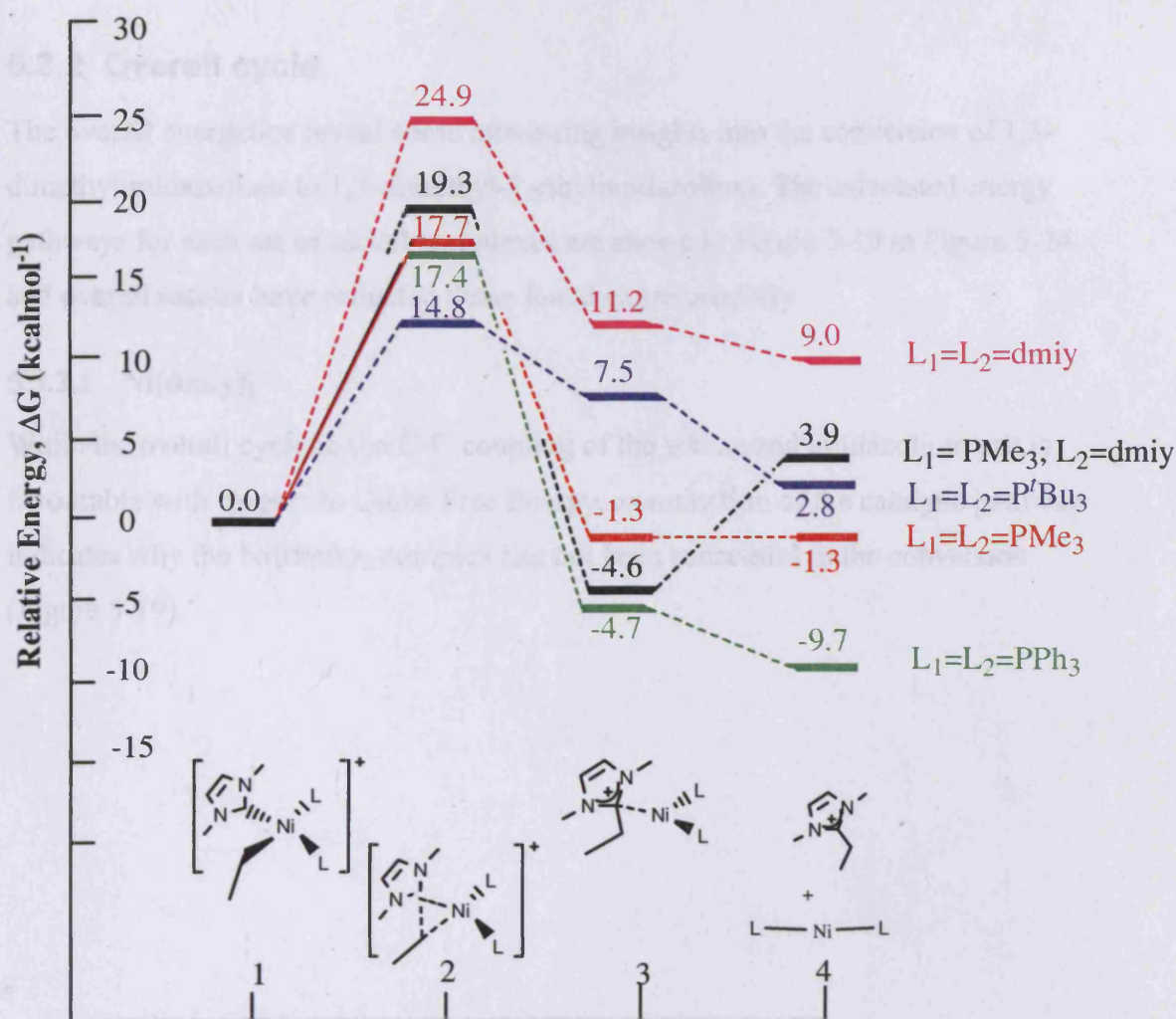


Figure 5-18 Energies for reductive elimination

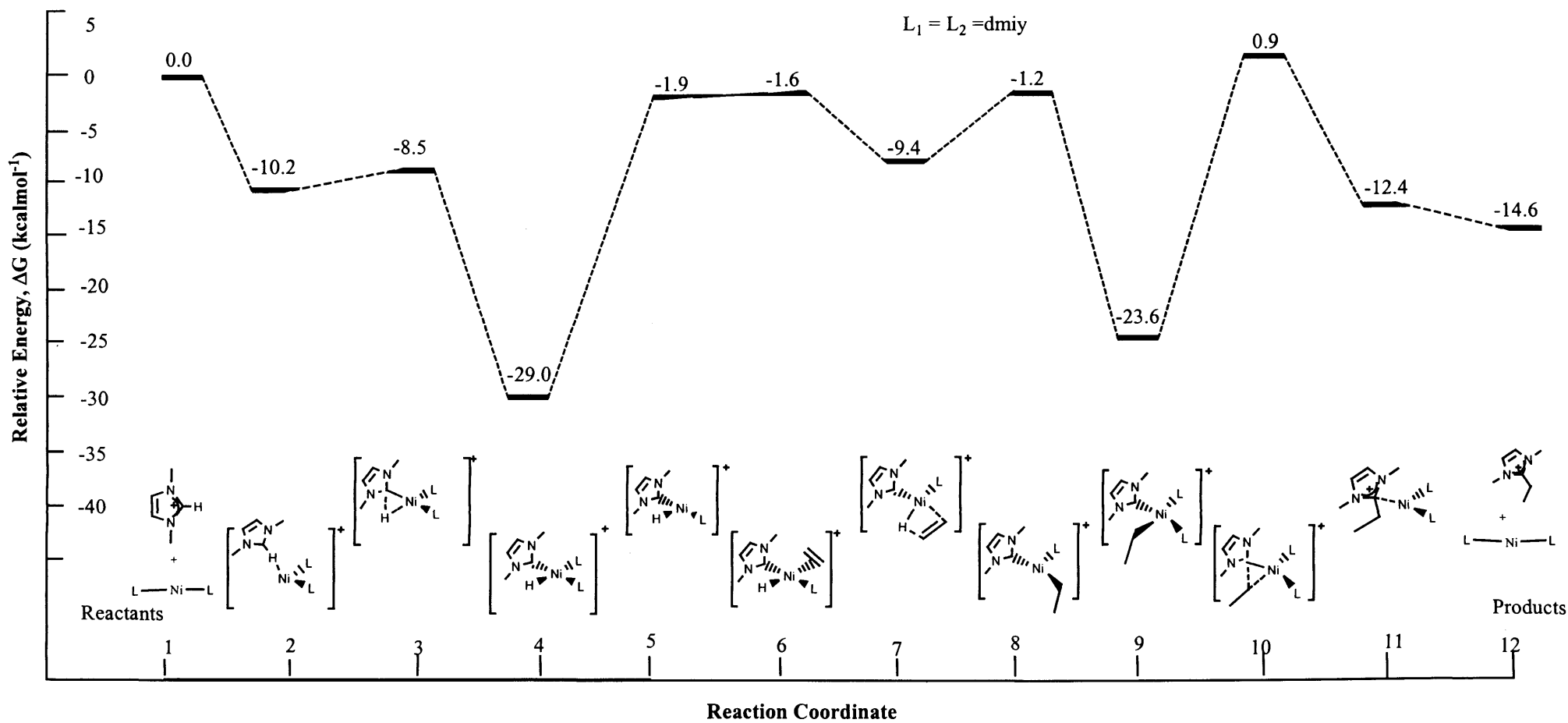
Overall, the reductive elimination step holds a reasonable barrier for all systems. Not only is the transition structure relatively high in energy, but the nickel(II) ethyl intermediates are low energy complexes in all cases, including the unsaturated tri-*tert*-butylphosphine complex. As such, the system that provides the least demanding route is the Ni(P^tBu₃)₂ system with a relatively high energy ethyl complex and a lower energy transition structure.

5.3.2 Overall cycle

The overall energetics reveal some interesting insights into the conversion of 1,3-dimethylimidazolium to 1,3-dimethyl-2-ethylimidazolium. The calculated energy pathways for each set of nickel complexes are shown in Figure 5-19 to Figure 5-24 and overall results have reflected those found experimentally.

5.3.2.1 Ni(dmiy)₂

While the overall cycle in the C-C coupling of the alkene and imidazolium salt is favourable with respect to Gibbs Free Energy, examination of the catalytic pathway indicates why the Ni(dmiy)₂ complex has not been successful in the conversion (Figure 5-19).

Figure 5-19 Overall cycle for Ni(dmip)₂

Although the initial oxidative addition step is facile, there is a significant barrier for ethylene coordination ($27.1 \text{ kcal mol}^{-1}$) caused by a combination of the unusual stability of the nickel hydride complex and the strength of the metal-carbene bond and hence reluctance of carbene ligands to dissociate. Later in the cycle, another sizeable barrier of $24.5 \text{ kcal mol}^{-1}$ exists for the reductive elimination of the final 2-alkyl product. While these barriers are significant, they are not insurmountable and as such are not what is expected to be the cause of the unsuccessful conversion to the 2-alkyl salt. Closer examination of the pathway reveals the nickel dicarbene system is ineffective in converting the original salt due to the stability of the reaction intermediates compared to that of the final products. In particular, the oxidative addition product (Figure 5-19 structure 4) is the lowest energy structure on the pathway by more than 5 kcal mol^{-1} ; a condition reflected in experimental results. Further, an overall reaction barrier for the forward reaction (lowest energy structure to highest energy structure) is $29.9 \text{ kcal mol}^{-1}$ while the activation barriers for the reverse reaction are significantly lower, indicating any product that did form could easily revert to the stable hydride.

On the whole, the calculated energy pathway for the $\text{Ni}(\text{dmiy})_2$ system indicates that the stability of the hydride intermediate and relatively high reaction barriers do not encourage catalytic conversion of the imidazolium to the 2-ethylimidazolium; a condition further supported by the isolation of the nickel(II) hydride product despite the presence of alkene reactants in experimental conditions.

5.3.2.2 $\text{Ni}(\text{PMe}_3)(\text{dmiy})$

Substitution of one carbene ligand for a trimethylphosphine results in minor changes to the catalytic cycle when compared to the dicarbene complex (Figure 5-20).

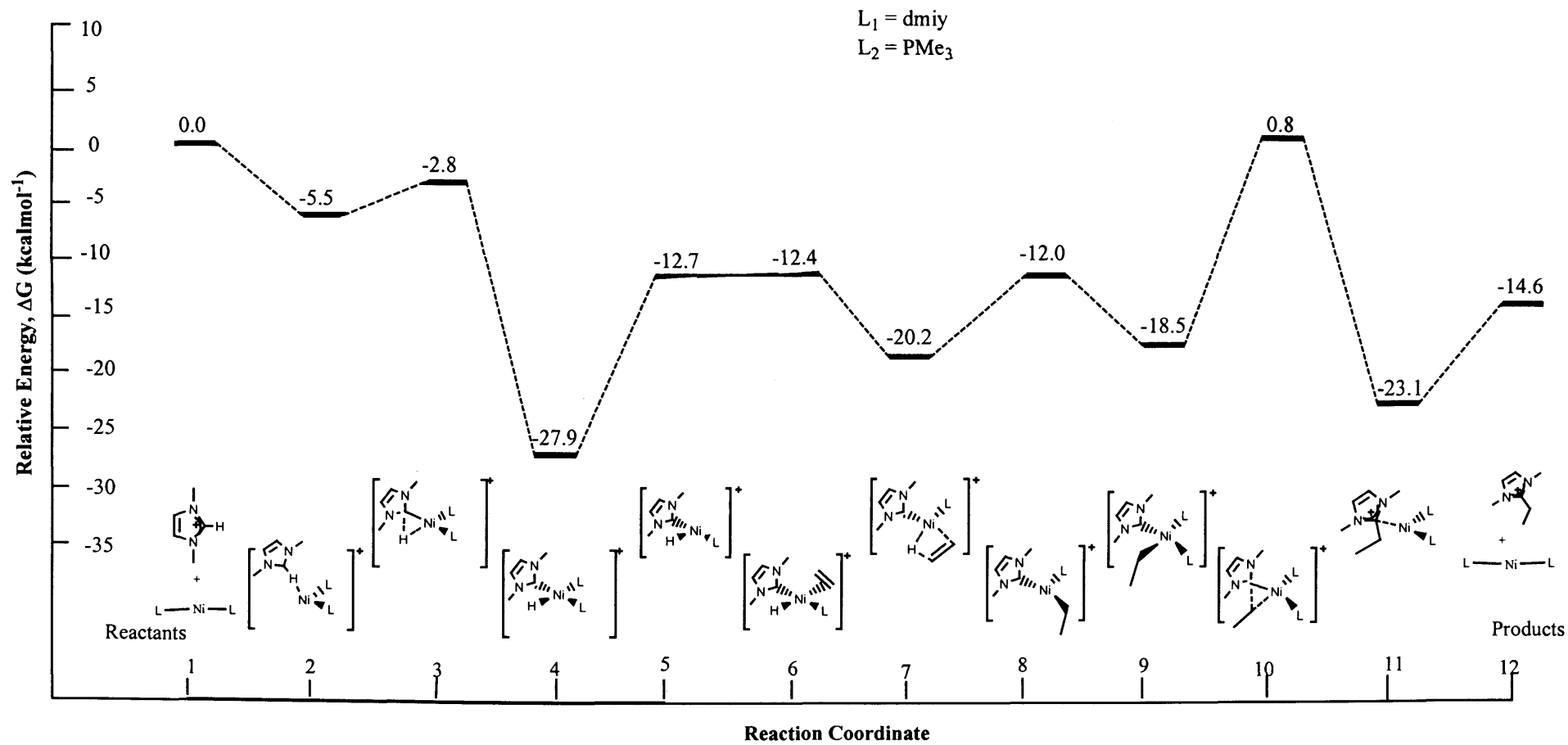


Figure 5-20 Overall cycle for $\text{Ni}(\text{PMe}_3)(\text{dmiy})$

As a dissociative route seems probable for the central steps of the cycle and phosphine dissociation is preferred by $18.7 \text{ kcal mol}^{-1}$ over carbene dissociation, four of the central structures remain identical to the $\text{Ni}(\text{dmiy})_2$ route. As such, energies for the $\text{Ni}(\text{PMe}_3)(\text{dmiy})$ route display the same general profile as those found for the $\text{Ni}(\text{dmiy})_2$ cycle, but reflect the advantage of having a more easily displaced phosphine ligand.

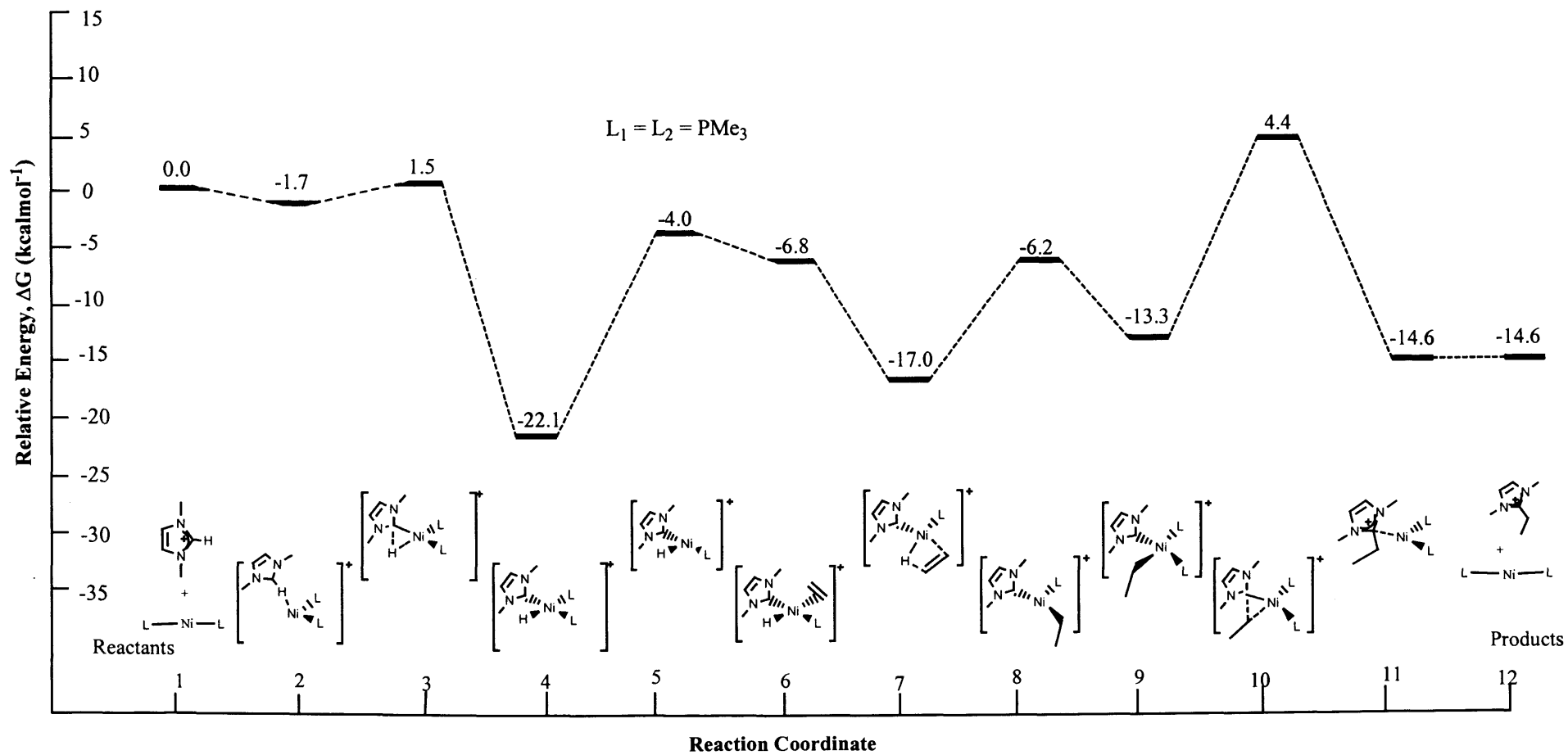
In this mixed ligand system, the nickel hydride oxidative addition product is once more the lowest energy structure on the overall cycle. Although only marginally lower in energy than the four-coordinate ethyl complex ($4.8 \text{ kcal mol}^{-1}$), the nickel hydride lies a significant $13.3 \text{ kcal mol}^{-1}$ lower in energy than the separated catalyst and 2-ethylimidazolium product and could once again be the undesired resting state of the cycle.

While the initial oxidative addition product is still the lowest energy structure on the pathway, the two major barriers for ethylene coordination and reductive elimination of the final product have been significantly reduced from $27.1 \text{ kcal mol}^{-1}$ and $24.5 \text{ kcal mol}^{-1}$ to $15.2 \text{ kcal mol}^{-1}$ and $19.3 \text{ kcal mol}^{-1}$ respectively. While the overall barrier to reaction from lowest energy structure to highest energy structure remains high at $28.7 \text{ kcal mol}^{-1}$, there are relatively low energy intermediates along the pathway that provide a smoother pathway with smaller steps to overcome the overall barrier, rather than requiring a significant amount of energy for a single step. Further, if the barriers to ethylene coordination and reductive elimination are overcome and the cycle is allowed to continue to completion, the reverse reaction for oxidative addition of the 2-ethylimidazolium product now has a higher individual barrier of $23.9 \text{ kcal mol}^{-1}$ to overcome compared to continuation of the cycle by oxidative addition of another imidazolium salt.

This reversal of reaction barriers combined with the closer relative energies of the reaction intermediates and products presents a much more favourable cycle for the C-C coupling reaction despite the overall barrier from lowest energy structure to highest remaining relatively high at $28.7 \text{ kcal mol}^{-1}$.

5.3.2.2 Ni(PMe₃)₂

Replacement of both carbene ligands with trimethylphosphine did not significantly alter the geometries or overall energy trends of the reaction (Figure 5-21).

Figure 5-21 Overall cycle for $\text{Ni}(\text{PMe}_3)_2$

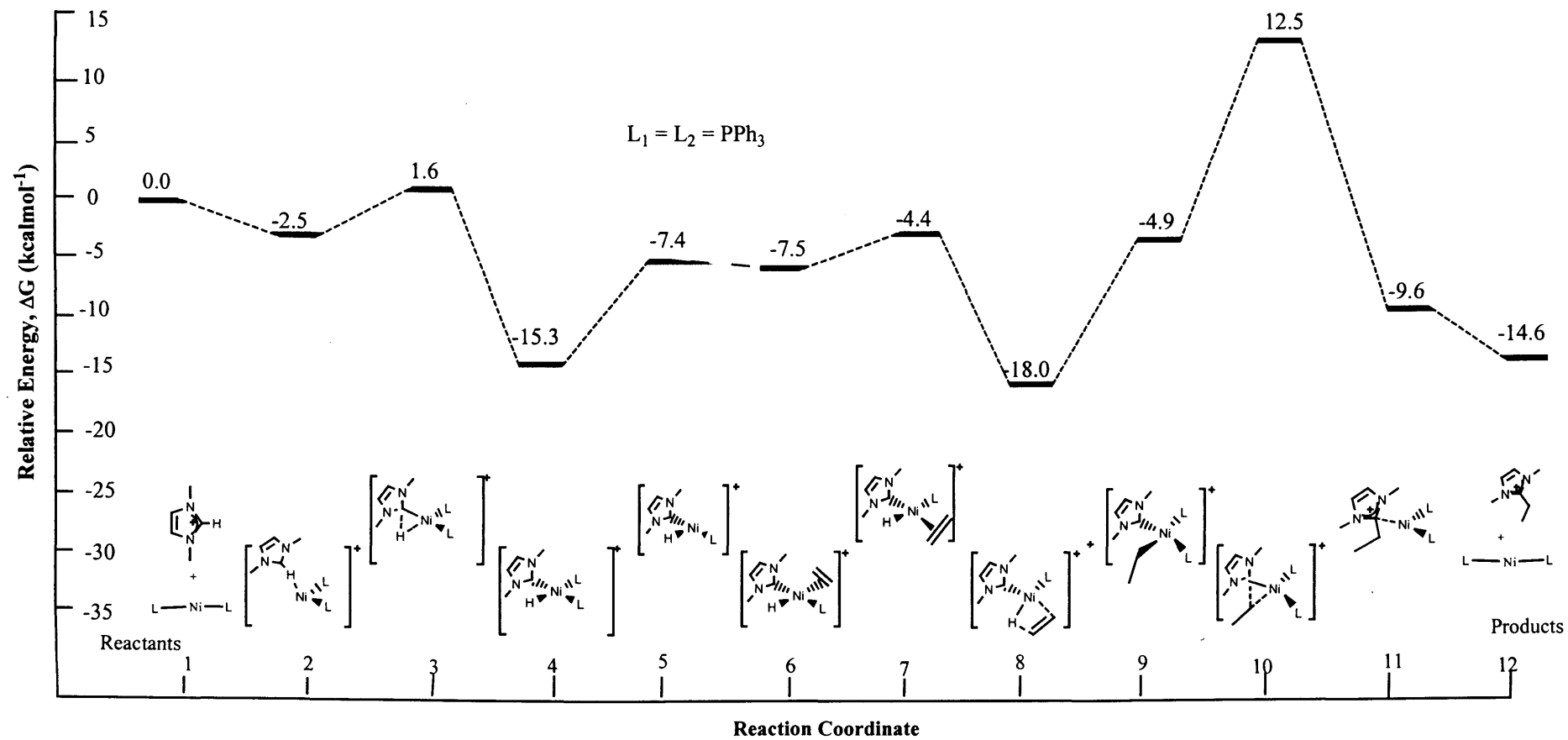
The nickel hydride complex is yet again the most stable structure on the pathway lying $7.5 \text{ kcal mol}^{-1}$ below the desired product, however the relative energy of this intermediate with respect to the rest of the cycle indicates the intermediate is considerably less stable than the $\text{NiH}(\text{dmiy})_3$ structure discussed previously. Despite the advantages of the higher energy hydride with double exchange of the carbene ligands to phosphines, the next step of the reaction indicates dissociation of the phosphine prior to ethylene coordination is marginally more challenging. With the inferior electron donating capacity of the phosphine ligand, the three coordinate intermediate created with dissociation of a ligand is a higher energy complex than the one with two highly basic carbene ligands. In fact, the relative stability of all intermediates has been raised in the double exchange, with each respective step approximately 5 kcal mol^{-1} less stable than the corresponding mixed ligand system. This instability is not enough to be restrictive on the overall reaction and can be seen as being advantageous as the final products become closer in energy to the low energy intermediates.

Overall, the barriers for reaction are marginally lower than that of the mixed carbene/phosphine system with the overall barrier down to $26.5 \text{ kcal mol}^{-1}$. More importantly, with the energy gap between the hydride and product lower, the $\text{Ni}(\text{PMe}_3)_2$ system appears to be an improved catalyst for the C-C coupling reaction over the dicarbene or mixed ligand systems.

5.3.2.3 Ni(PPh₃)₂

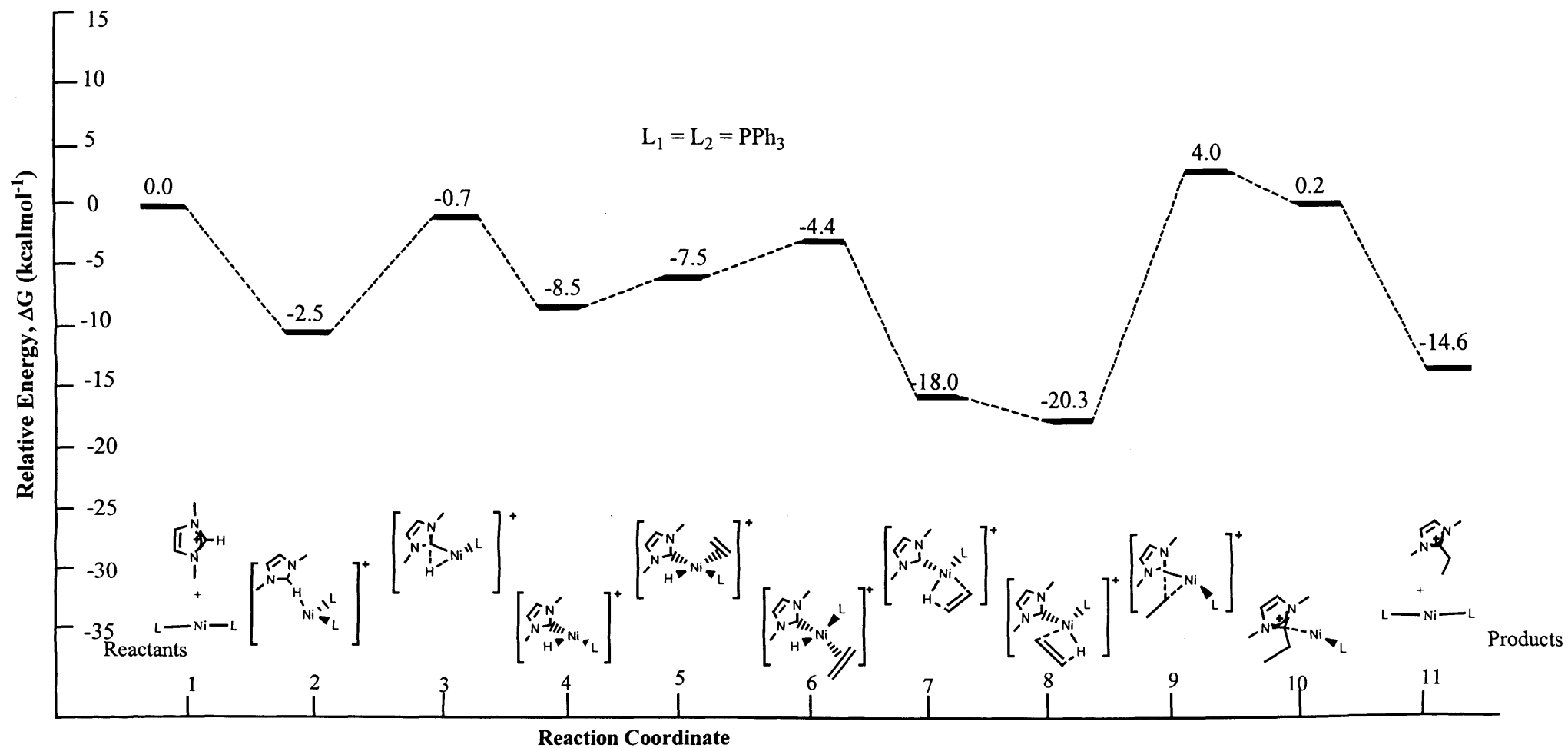
Examination of the potential energy surfaces for the reaction cycle using the Ni(dmuy)₂ complex indicated catalysis may be halted due to a combination of the stability of the nickel hydride intermediate and metal bond strength of the carbene ligand disallowing ethylene coordination. While replacement of the carbene ligands with trimethylphosphines indicated an improvement in overcoming the obstacles for catalysis, the difference in bulk and basicity between the trimethyl and triphenyl phosphines exhibited a remarkable effect in the catalytic cycle that indicates why the Ni(PPh₃)₂ system is so successful in this reaction.

Initially, we studied the triphenylphosphine cycle using the same pathway followed in previous systems, with dissociation of a ligand occurring to allow coordination of ethylene. As indicated in Figure 5-22, the Ni(PPh₃)₂ catalyst provides a reaction with a low energy pathway. Initial reaction barriers do not exceed 7.9 kcal mol⁻¹ and for the first time, the important intermediates are relatively less stable and lie within 3.4 kcal mol⁻¹ of the final product.

Figure 5-22 Overall associative cycle for $\text{Ni}(\text{PPh}_3)_2$

While this cycle in general indicated a very smooth start to the reaction, the reductive elimination step was a cause for concern. It was expected that recoordination of a ligand would occur before reductive elimination. The extra bulk around the metal has been known to promote reductive elimination, at least in part by the reductive elimination reducing steric strain around the metal. In this case, recoordination of the dissociated ligand increased the energy of the four coordinate ethyl complex by 13.1 kcal mol⁻¹ and the reductive elimination transition structure was a further 17.4 kcal mol⁻¹ higher in energy. As no other intermediates are thought to occur in between the recoordination of the ligand and reductive elimination, this resulted in an overall barrier of a high 30.5 kcal mol⁻¹ for this step alone; a higher barrier than in any other reaction studied.

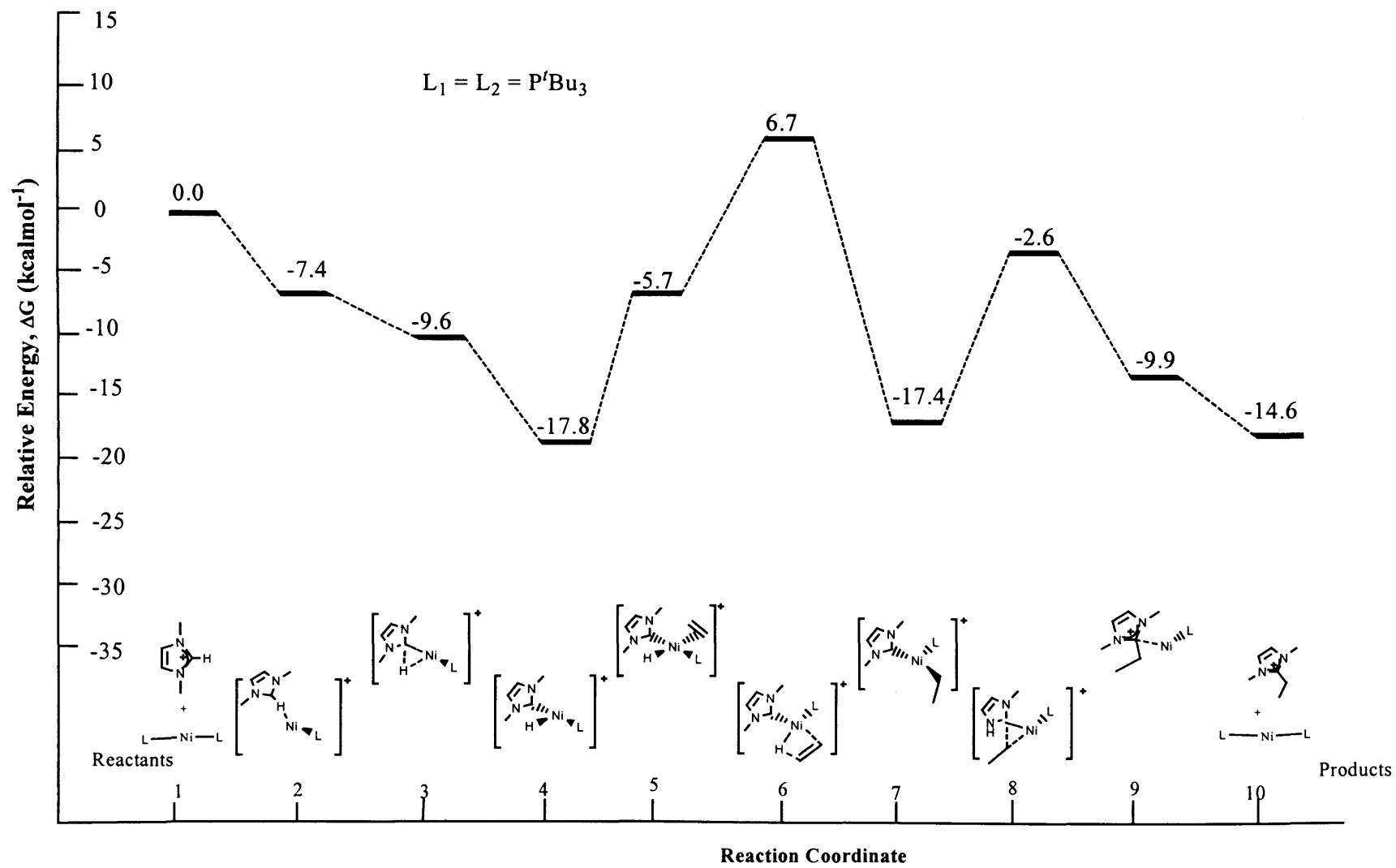
As this reaction has been catalytically active in relatively mild conditions, the high barrier found for reductive elimination was unexpected and it appeared likely another route may exist. Due to the ease of dissociation of the triphenylphosphine ligands, we looked at an overall catalytic route in which one triphenylphosphine remained dissociated for the duration of the catalytic cycle as was found for the tri-*tert*-butyl system. As indicated in Figure 5-23, a dissociative route is not only possible, but has distinct advantages over an associative one. Most importantly, despite still being the largest barrier to overcome, the energy required for reductive elimination drops to 24.3 kcal mol⁻¹, with the transition structure now only 4.0 kcal mol⁻¹ higher in Gibbs Free Energy than the separated products. All other barriers remain low with corresponding intermediates neither too stable nor unstable.

Figure 5-23 Overall dissociative cycle for $\text{Ni}(\text{PPh}_3)_2$

It must further be remembered that the ability of the phosphine to dissociate and rejoin as required creates a very flexible system. In experimental conditions, a combination of these mechanisms may well occur, in which a phosphine may be joined to an intermediate and released as a transition structure is reached. Even though it is not possible to study all combinations of these types of interactions, the results for the distinct associative and dissociative routes reveal an overall catalytic cycle in which the intermediates remain close in energy and transition structures relatively low in energy, indicating the procession of the reaction would be relatively free flowing.

5.3.2.4 Ni(P^tBu₃)₂

As the triphenylphosphine cycle shows a smooth run for the early part of the catalytic cycle with the greatest barrier to reaction being the large amount of energy required to reductively eliminate the final product, it was hoped the change to the tri-*tert*-butylphosphine ligand would reduce the energy of the final step and smooth the overall reaction. As has been shown in previous studies, increasing the bulk of the ligands on the metal centre can facilitate reductive elimination, and while the change to the bulkiest phosphine in the tri-*tert*-butylphosphine did reduce the reductive elimination barrier to 14.8 kcal mol⁻¹, it also resulted in dramatic changes to the overall reaction energetics (Figure 5-24).

Figure 5-24 Overall cycle for Ni(P^tBu₃)₂

At all points on the reaction pathway, the extra bulk from the *tert*-butyl groups causes overcrowding on the small nickel centre with all optimised structures containing only one phosphine attached to the metal centre. While this arrangement allows facile oxidative addition and reductive elimination reactions with relatively stable three-coordinate intermediates, the extra bulk adversely affects the coordination and insertion of ethylene. The limited space around the metal results in a reasonably high energy four coordinate ethylene complex. Conversion of this complex to the *cis* form required for ethylene insertion increases the barrier for the overall ethylene reaction to 24.5 kcal mol⁻¹. As such, it would be expected that the ethylene coordination could be the limiting factor when these ligands are in use and not the reductive elimination as found in all other systems. Despite this, the significant intermediates remain close in energy to the separated products, indicating the reaction may be possible and once the ethyl complex has formed, continuation of the catalytic cycle would proceed smoothly.

5.3.3 Cycle comparison

Overall, the results for all ligand combinations reflect the delicate nature of the catalytic cycle. Three ligand characteristics appear to have an impact on the success of the cycle: basicity, bulk and metal-ligand bond strength.

Ligand basicity appears to play only a minor role with the cycle marginally favouring the less basic ligands. Increasing the ligand basicity further stabilises some important low energy intermediates, in particular the initial nickel hydride and later the nickel ethyl complex. In fact, the hydride intermediate is so stable in the Ni(dmiy)₂ system catalysis halts after the initial oxidative addition step. Decreasing ligand basicity by the successive replacement of the carbenes with phosphine ligands destabilises these intermediates without excessively raising barriers to further reaction. Despite this, examination of the changes in energies from the Ni(dmiy)₂ through Ni(PMe₃)(dmiy) to Ni(PMe₃)₂ systems does indicate the basicity of ligands has only trivial consequences with respect to other characteristics in the system.

The most influential effect on catalysis for this reaction appears to come from the ligand bulk and dissociation ability. The major benefit found in the Ni(PPh₃)₂ system not applicable to any of the other systems is the ability of the phosphine to dissociate

and rejoin the metal as required. As carbenes form strong bonds to the metals with the free form of the ligand relatively unstable in comparison to other ligands, it is unsurprising the Ni(dmiy)₂ system fails as ligand dissociation is required prior to ethylene coordination. In particular, the stability of the hydride complex and inability of the carbene to readily dissociate make this step insurmountable under normal reaction conditions. While these barriers are considerably lower for the trimethylphosphine, the reaction becomes straightforward for the triphenylphosphine; a ligand well known for easy dissociation. Further, the added bulk of the triphenylphosphine ligand can sterically protect the metal centre with the electron donating capacity of the newly formed carbene ligand stabilising from an electronic viewpoint. However, increasing the bulk and basicity excessively as found in the *tert*-butylphosphine system has harmful consequences on the cycle, with the benefits in lowering the barrier of reductive elimination counteracted by the overcrowding and therefore destabilisation of four coordinate ethylene intermediates.

Changing the basicity and the bulk of the ligands has dramatic effects on the overall reaction, with basicity decreasing the energy of some major intermediates to the point that they can be isolated in experimental conditions. A balance of bulk and basicity must be found however as excessive bulk causes overcrowding of the small metal and greatly decreases the ability of the intermediates to form the required alkene and alkyl complexes. Overall, the cycles show the catalytic conversion of 1,3-dimethylimidazolium to 2-ethyl-1,3-dimethylimidazolium can be significantly influenced by minor changes in steric or electronic properties of the nickel catalyst. The Ni(PPh₃)₂ complex studied displays the most favourable reaction conditions, with all barriers relatively small and the important intermediates not excessively stable; a result reflected in experimental conditions.

5.3.4 Catalysis at the azolium 5-carbon

Catalysis using the NiL_2 system has been shown to be successful in creating 2-alkyl azolium salts. In addition, Crabtree's group reported carbene complexes from azolium metallation where the carbene was attached to iridium through the C5 carbon instead of the usual C2 bonding³⁵⁻³⁷. Our group later reported similar C5 carbene attachment to platinum via oxidative addition reactions³⁸. As such, it may be possible to create 5-alkyl complexes by using the same catalysts studied in this chapter and blocking the C2 position of the starting azolium salt.

In order to study a model of the C5 addition, we chose the trimethylphosphine catalyst as our basis for comparison. Although the triphenylphosphine is the successful catalyst in experimental conditions, it is computationally expensive and the comparison between the two systems in the previous sections gives an indication as to the trend expected for the simpler reaction.

Overall, the reaction geometries for the C5 addition are remarkably similar to those for the corresponding C2 reaction. The major difference for the two reactions is the stability of the oxidative addition precursor, with a relatively stable precursor found for the C5 addition where both salt backbone carbons form a weak bond to the nickel causing the attached hydrogens to be bent out of the plane of the imidazolium ring

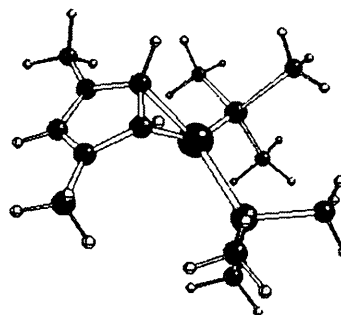


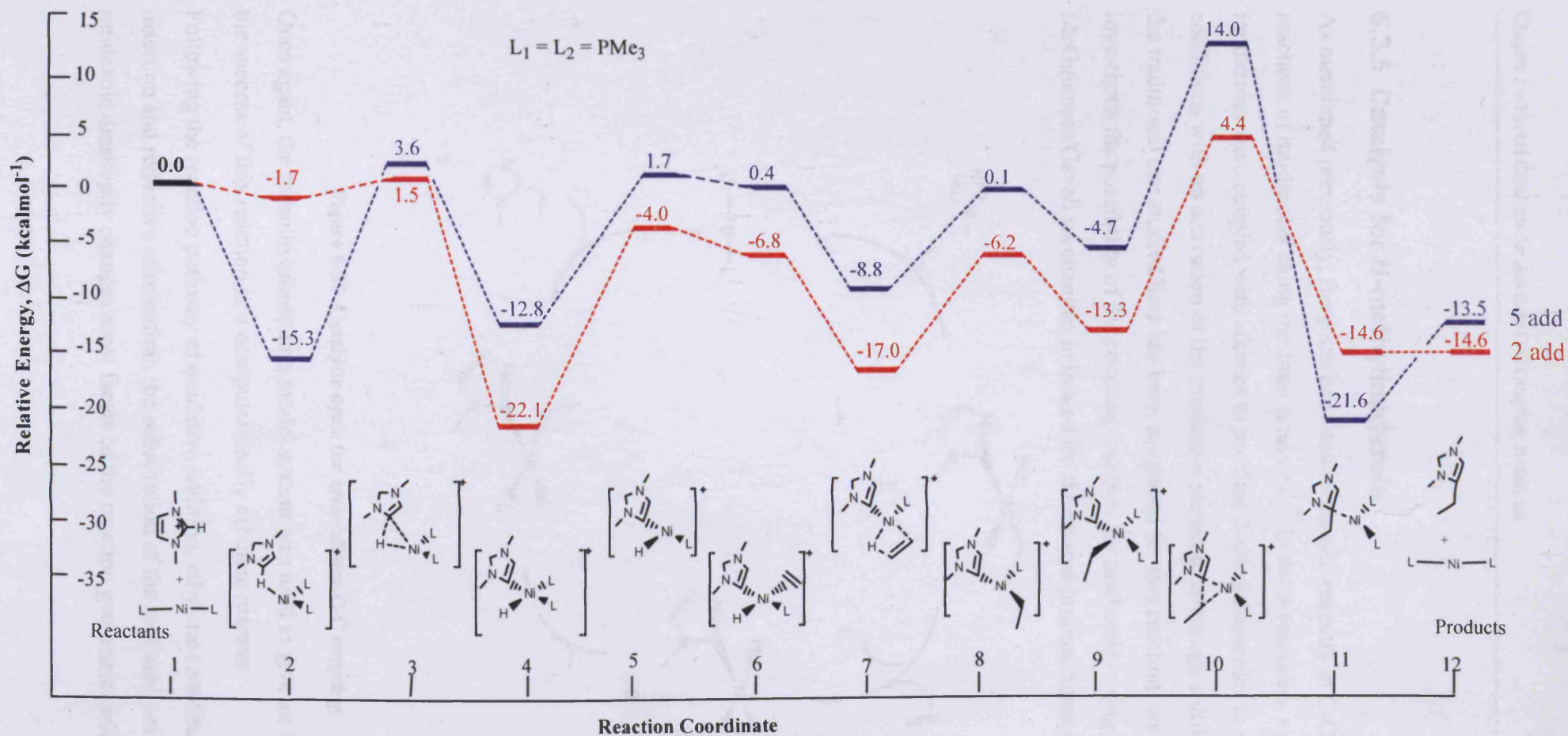
Figure 5-25 Azolium 5 addition oxidative addition precursor

(Figure 5-25). These bonds must be broken before the traditional oxidative addition transition state is reached, forming a reasonable barrier of $18.9 \text{ kcal mol}^{-1}$ not found for any of the reactions where addition occurs in the 2 position.

Energy results indicate addition at the 5 position could be possible following the same catalytic cycle proposed for the C2 addition (Figure 5-26). The overall reaction displays a very similar trend to its C2 counterpart, with barriers to ethylene coordination, insertion and reductive elimination almost identical. Despite this, all intermediates for the 5 addition are higher in energy than their 2-addition counterparts by between 5 to 10 kcal mol^{-1} . As the only differing factor in this reaction is the carbene ligand itself, this difference can be attributed to the strength of the carbene

ligand formed, with the C2 flanked by 2 nitrogens resulting in a stronger and more symmetrical ligand than the C5 equivalent.

On the whole, the C2 addition product is slightly more favourable in energy than the 5-ethylimidazolium and when this result is combined with the instability of the 5-addition intermediates, it would be assumed that addition would occur at position 2 if the option of both 2-H and 5-H addition were available in experimental conditions. However, these results do indicate that 5-addition may be possible under favourable conditions if the 2-position were blocked, for example by having a 2-alkylimidazolium starting material.

Figure 5-26 Overall cycle for azolium 5 catalysis with $\text{Ni}(\text{PMe}_3)_2$

5.3.5 Catalysis for N-methylimidazole

As mentioned previously, Bergman has been successful recently in C-C coupling reactions of imidazoles using rhodium catalysts¹⁻⁷. In these reactions, various imidazoles were coupled with alkenes to produce 2-alkylimidazoles in relatively mild conditions with no activation of the imidazole required. Although a different route to the traditional one studied here has been suggested for this reaction, we decided to investigate the possibility of the coupling reaction for imidazoles using nickel and the McGuinness/Cavell mechanism indicated for the related imidazoliums (Figure 5-27).

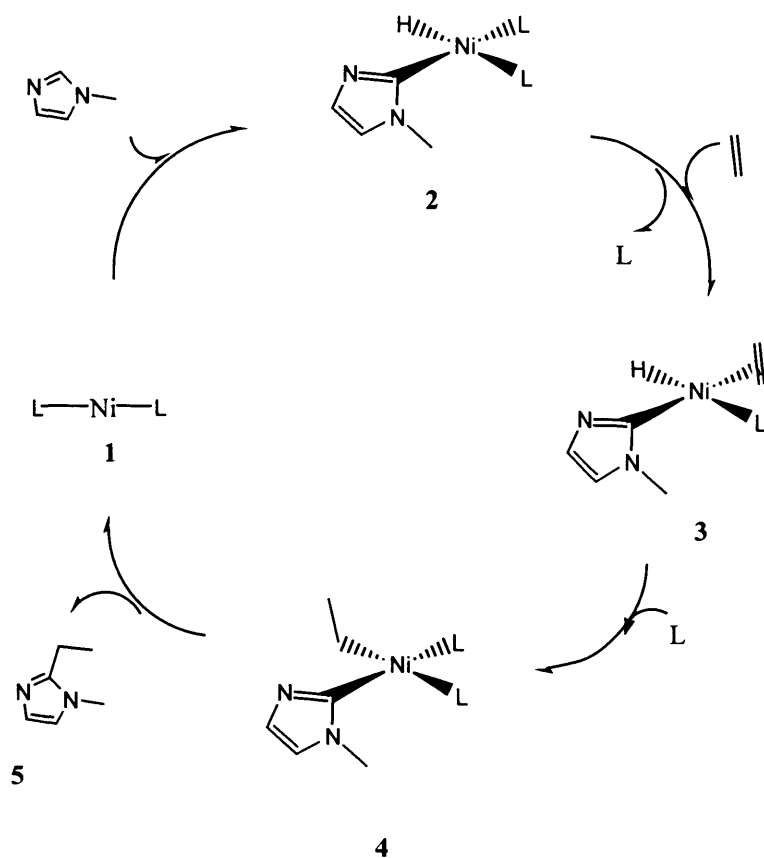


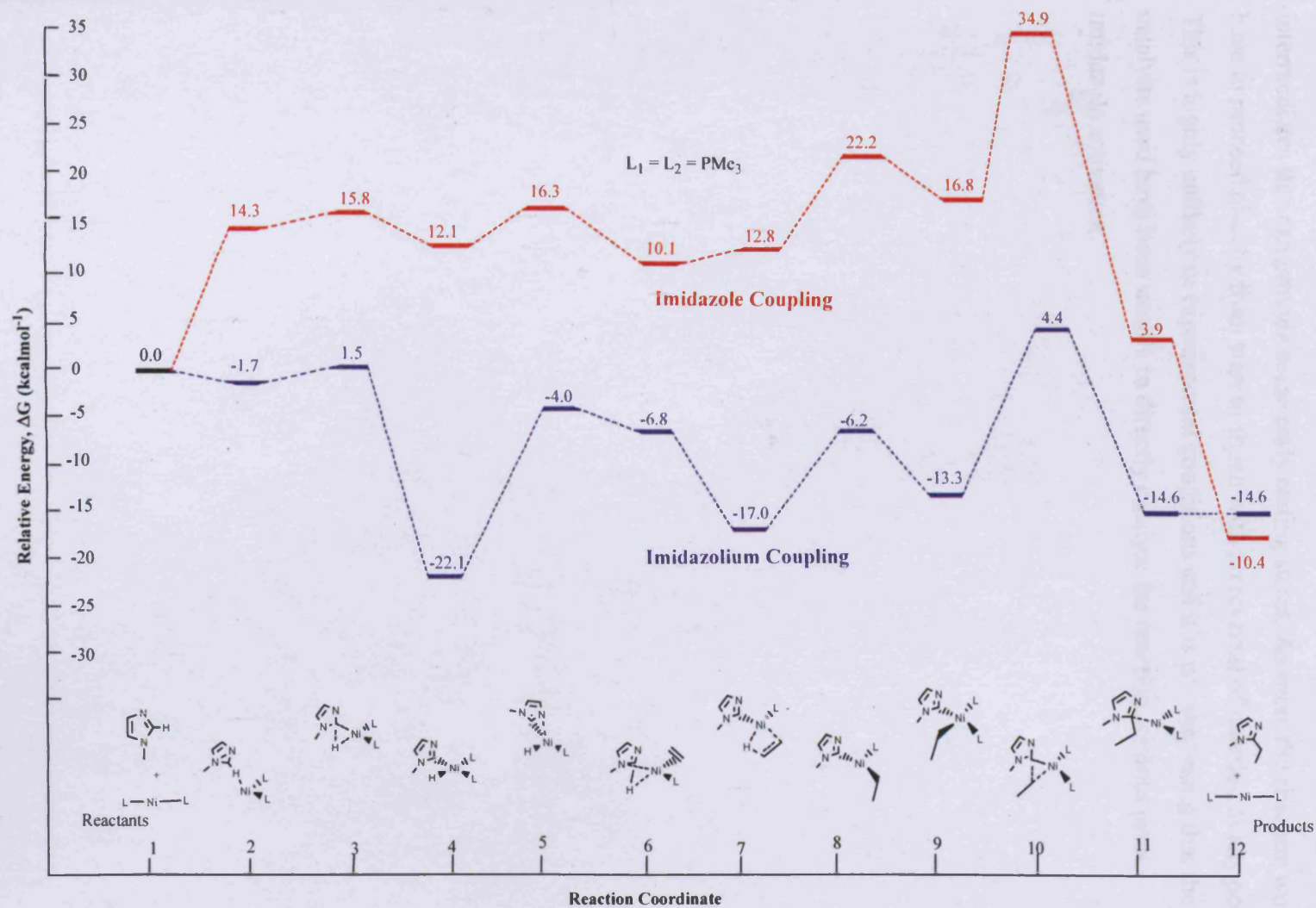
Figure 5-27 Catalytic cycle for azole/alkene C-C coupling

Once again, the trimethylphosphine model system was used to give an indication of the success of this reaction in a computationally efficient manner.

Following the reaction pathway of oxidative addition, ethylene coordination and insertion and reductive elimination, the substitution of the imidazolium salt reactant to imidazole drastically changes most facets of the reaction geometries and energies.

While the overall conversion is energetically more favourable than for the corresponding imidazolium salt (Figure 5-28), the intermediates present some interesting challenges to overcome if the reaction is to be successful.

The initial oxidative addition step is endothermic, with the barrier not insurmountable, but relatively large at $15.8 \text{ kcal mol}^{-1}$. Once the four-coordinate complex has formed, ethylene coordination, rearrangement and insertion into the metal-hydride bond does not require a large amount of extra energy, however each intermediate is still relatively unstable when compared to the starting materials. Most importantly, the reductive elimination transition state is a considerable $34.9 \text{ kcal mol}^{-1}$ above the separated starting materials.

Figure 5-28 Overall cycle for N-methylimidazole catalysis with $\text{Ni}(\text{PMe}_3)_2$

While previous cycles for the corresponding imidazolium indicated similar barriers from highest point to lowest point, the cycle in this case has no lower energy intermediates that can provide some early resting states. As such, the reaction would have to proceed directly from start to finish with no reversal of reaction at any point. This is highly unlikely in experimental conditions and it is not surprising that the catalysts used have been unable to directly catalyse the reaction without prior imidazole activation.

5.4 Conclusions

The calculated energies herein combined with experimental results indicate the mechanism for the catalytic conversion of imidazolium salts to 2-ethylimidazolium salts follows a route of oxidative addition, followed by ethylene coordination, insertion and reductive elimination of the product.

The Ni(dmiy)₂ complex does not catalyse the reaction experimentally, however, the isolation of the oxidative addition product along with the calculations here indicate the hydride complex is indeed an intermediate for the catalysis using similar phosphine ligands. Calculations reveal the hydride complex is consistently one of the more stable intermediates on all pathways, and the barriers for ethylene coordination via replacement of a strong carbene ligand, and reductive elimination are high and discourage the catalytic cycle in the dicarbene case.

In contrast, the Ni(PPh₃)₂ complex successfully catalyses the reaction in experimental conditions. Calculations indicate a reasonable barrier to product reductive elimination still exists in this case, however, the bulk and lower basicity of the triphenylphosphine ligands destabilises many of the intermediates with respect to their Ni(dmiy)₂ counterparts, allowing a smoother reaction with a relatively more stable product. As the overall barrier for reaction (lowest energy structure to highest energy structure) is almost identical for the two reactions (Ni(dmiy)₂: 29.9 kcal mol⁻¹; Ni(PPh₃)₂: 30.5 kcal mol⁻¹), it becomes clear the destabilising of important intermediates is vital for the cycle to continue.

While the other nickel complexes have not been tested experimentally for catalytic activity, they provide interesting insight into the factors affecting the overall cycle. Increasing the basicity of the ancillary ligands has the most significant effect on the oxidative addition reaction and while facile in all cases, the most basic ligands increases the relative stability of the four-coordinate nickel hydride complex. In all cases, the ethylene insertion occurs relatively easily, with the initial formation of the ethylene complex the most significant barrier. The instability of the five-coordinate ethylene complexes suggests that a dissociative route must be followed. As such, ligand dissociation must be facile, which is not the case for the strongly bound carbene ligands. Dissociation occurs much more readily for the phosphine ligands, with both bulk and basicity playing a part in the stabilisation of the dissociated complex. However, excessive bulk as found in the case of the tri-*tert*-butylphosphine

ligands adversely affects some important intermediates by overcrowding the metal centre and decreasing the stability of the four coordinate ethylene complex required before insertion can take place.

Once again, reductive elimination is enhanced by the bulk of the ligands. Although basicity brings down the relative energy of the transition states, it also lowers the relative stability of the precursor ethyl complex and leaves the barrier to reaction unchanged. The bulky ligands indicate a destabilisation of the transition structure and lowering of the barrier to reductive elimination; an important factor as results show this transition structure is the highest energy structure that must be overcome in all but the $\text{Ni}(\text{P}^t\text{Bu}_3)_2$ reaction pathway.

Overall, the results indicate the delicate nature of the catalytic cycle with ligand bulk, basicity and ligand-metal bond strength all playing a part. Despite only the $\text{Ni}(\text{PPh}_3)_2$ complex catalysing the C-C coupling reaction experimentally, substitution to other ligands has provided vital input in elucidating the mechanism and facilitating catalyst engineering.

In reactions involving azole and azolium salts have generally shown C2 activation and coupling, recent results indicate reaction at the C4 or C5 positions is possible in certain conditions. Energy calculations using the McGuinness/Cavell mechanism indicate the unhindered C2 reaction is the favourable one, with all corresponding intermediates and reaction barriers at lower relative energy. Despite this, the energy differences between the two reactions are moderate with the majority of C5 complexes lying within 10 kcal mol^{-1} of their C2 counterparts. As indicated in experimental results, blocking of the ring C2 could well lead to alternative reaction at the ring C5 position.

Further results by Bergman indicate the related azoles can be successfully coupled in similar reactions using rhodium catalysts. While the reactions in this case were successful with unactivated azole reactants, theoretical results indicate this would be unlikely for related nickel catalysts under the redox mechanism studied herein, with all intermediates much higher in energy than the azolium counterparts and the reductive elimination barrier being particularly restrictive.

5.5 References

- 1 K. L. Tan, R. G. Bergman and J. A. Ellman, *J. Am. Chem. Soc.*, 2002, **124**, 3202.
- 2 K. L. Tan, R. G. Bergman and J. A. Ellman, *J. Am. Chem. Soc.*, 2001, **123**, 2685.
- 3 K. L. Tan, S. Park, J. A. Ellman and R. G. Bergman, *J. Org. Chem.*, 2004, **69**, 7329.
- 4 K. L. Tan, A. Vasudevan, R. G. Bergman, J. A. Ellman and A. J. Souers, *Org. Lett.*, 2003, **5**, 2131.
- 5 K. L. Tan, R. G. Bergman and J. A. Ellman, *J. Am. Chem. Soc.*, 2002, **124**, 13964.
- 6 S. H. Wiedemann, R. G. Bergman and J. A. Ellman, *Org. Lett.*, 2004, **6**, 1685.
- 7 J. C. Lewis, S. H. Wiedemann, R. G. Bergman and J. A. Ellman, *Org. Lett.*, 2004, **6**, 35.
- 8 N. D. Clement and K. J. Cavell, *Angew. Chem. Int. Ed.*, 2004, **43**, 3845.
- 9 N. D. Clement, K. J. Cavell, C. Jones and C. J. Elsvier, *Angew. Chem. Int. Ed.*, 2004, **43**, 1277.
- 10 R. H. Hertwig and W. Koch, *Chem. Phys. Lett.*, 1997, **268**, 345.
- 11 P. J. Stephens, J. F. Devlin, C. F. Chabalowski and M. J. Frisch, *J. Phys. Chem.*, 1994, **98**, 11623.
- 12 A. D. Becke, *J. Chem. Phys.*, 1993, **98**, 5648.
- 13 P. J. Hay and W. R. Wadt, *J. Chem. Phys.*, 1985, **82**, 299.
- 14 T. H. Dunning and P. J. Hay, 'Modern Theoretical Chemistry', Plenum, 1976.
- 15 F. Maseras and K. Morokuma, *Int. J. Quant. Chem.*, 1995, **16**, 1170.
- 16 S. Humbel, S. Sieber and K. Morokuma, *J. Chem. Phys.*, 1996, **105**, 1959.
- 17 T. Matsubara, S. Sieber and K. Morokuma, *Int. J. Quant. Chem.*, 1996, **60**, 1101.
- 18 M. Svensson, S. Humbel, R. D. J. Froese, T. Matsubara, S. Sieber and K. Morokuma, *J. Phys. Chem.*, 1996, **100**, 19357.
- 19 M. Svensson, S. Humbel and K. Morokuma, *J. Chem. Phys.*, 1996, **105**, 3654.

- 20 S. Dapprich, I. Komaromi, K. S. Byun, K. Morokuma and M. J. Frisch, *J. Mol. Struct. (THEOCHEM)*, 1999, **462**, 1.
- 21 T. Vreven and K. Morokuma, *IBM J. Res. & Dev.*, 2001, **45**, 367.
- 22 A. K. Rappé, C. J. Casewit, K. S. Colwell, W. A. Goddard III and W. M. Skiff, *J. Am. Chem. Soc.*, 1992, **114**, 10024.
- 23 M. J. Frisch, J. A. Pople and J. S. Binkley, *J. Chem. Phys.*, 1984, **80**, 3265.
- 24 A. D. McLean and G. S. Chandler, *J. Chem. Phys.*, 1980, **72**, 5639.
- 25 R. Krishnan, J. S. Binkley, R. Seeger and J. A. Pople, *J. Chem. Phys.*, 1980, **72**, 650.
- 26 M. J. Frisch, G. W. Trucks, H. B. Schlegel, G. E. Scuseria, M. A. Robb, J. R. Cheeseman, J. A. Montgomery Jr., T. Vreven, K. N. Kudin, J. C. Burant, J. M. Millam, S. S. Iyengar, J. Tomasi, V. Barone, B. Mennucci, M. Cossi, G. Scalmani, N. Rega, G. A. Petersson, H. Nakatsuji, M. Hada, M. Ehara, K. Toyota, R. Fukuda, J. Hasegawa, M. Ishida, T. Nakajima, Y. Honda, O. Kitao, H. Nakai, M. Klene, X. Li, J. E. Knox, H. P. Hratchian, J. B. Cross, C. Adamo, J. Jaramillo, R. Gomperts, R. E. Stratmann, O. Yazyev, A. J. Austin, R. Cammi, C. Pomelli, J. W. Ochterski, P. Y. Ayala, K. Morokuma, G. A. Voth, P. Salvador, J. J. Dannenberg, V. G. Zakrzewski, S. Dapprich, A. D. Daniels, M. C. Strain, O. Farkas, D. K. Malick, A. D. Rabuck, K. Raghavachari, J. B. Foresman, J. V. Ortiz, Q. Cui, A. G. Baboul, S. Clifford, J. Cioslowski, B. B. Stefanov, G. Liu, A. Liashenko, P. Piskorz, I. Komaromi, R. L. Martin, D. J. Fox, T. Keith, M. A. Al-Laham, C. Y. Peng, A. Nanayakkara, M. Challacombe, P. M. W. Gill, B. Johnson, W. Chen, M. W. Wong, C. Gonzalez and J. A. Pople, Gaussian 03 (Revision C.02), Wallingford CT, 2004.
- 27 S. Caddick, F. G. N. Cloke, P. B. Hitchcock and A. K. d. K. Lewis, *Angew. Chem. Int. Ed.*, 2004, **43**, 5824.
- 28 A. J. Arduengo III, S. F. Gamper, J. C. Calabrese and F. Davidson, *J. Am. Chem. Soc.*, 1994, **116**, 4391.
- 29 D. S. McGuinness, K. J. Cavell, B. F. Yates, B. W. Skelton and A. H. White, *J. Am. Chem. Soc.*, 2001, **123**, 8317.

- 30 D. S. McGuinness, K. J. Cavell and B. F. Yates, *Chem. Commun.*, 2001, **4**, 355.
- 31 M. A. Duin, N. D. Clement, K. J. Cavell and C. J. Elsevier, *Chem. Commun.*, 2003, **3**, 400.
- 32 C. S. Shultz, J. M. DeSimone and M. Brookhart, *Organometallics*, 2001, **20**, 16.
- 33 R. Dorta, E. D. Stevens, C. D. Hoff and S. P. Nolan, *J. Am. Chem. Soc.*, 2003, **125**, 10490.
- 34 D. Bourissou, O. Guerret, F. Gabbai and G. Bertrand, *Chem. Rev.*, 2000, **100**, 39.
- 35 A. Kovacevic, A. Gründemann, J. R. Miecznikowski, E. Clot, O. Eisenstein and R. H. Crabtree, *Chem. Commun.*, 2002, 2580.
- 36 S. Gründemann, A. Kovacevic, M. Albrecht, J. W. Faller and R. H. Crabtree, *Chem. Commun.*, 2001, 2274.
- 37 S. Gründemann, A. Kovacevic, M. Albrecht, J. W. Faller and R. H. Crabtree, *J. Am. Chem. Soc.*, 2002, **124**, 10473.
- 38 D. Bacciu, K. J. Cavell, I. A. Fallis and L. Ooi, *Angew. Chem. Int. Ed.*, 2005, **44**, 2.

6 Rhodium Catalysts for C-C Coupling Reactions

6.1 Introduction

In 2001, Bergman *et al.* reported the intramolecular coupling of alkenes to heterocycles to create 2-functionalised azoles under mild conditions¹⁻⁵ (Figure 6-1). Their work extended to a range of different imidazoles, thiazoles and even oxazoles¹. Variations on the initial reactants were later found to be successful, including functionalisation built into the reacting alkene, electron withdrawing and donating groups in the imidazole ring itself, and intermolecular reactions in which the alkene was not a chelating arm of the reacting azole²⁻⁵.

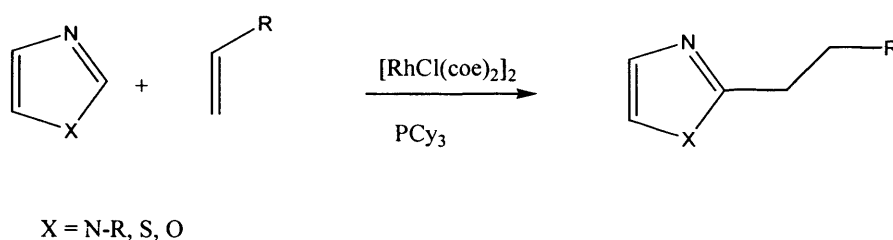


Figure 6-1 C-C coupling reaction

In general, the C-C coupling reactions were performed using a $[\text{RhCl}(\text{coe})_2]_2$ precatalyst in the presence of PCy_3 . While the reaction was catalytic at 150°C with yields frequently in the 70-80% range, addition of a weak acid was found to increase the rate of the reaction considerably³.

To try to elucidate a mechanism for the catalysis, the reaction was performed at reduced temperature with stoichiometric quantities of the rhodium precatalyst and phosphine ligand². This change in experimental conditions led to the isolation of a rhodium(I) carbene complex (Figure 6-2) which, when reintroduced into a catalytic environment, proceeded with identical results to those established previously. Monitoring of the reaction by NMR confirmed the carbene intermediate was present in significant quantities throughout the reaction sequence, indicating it is an important intermediate in the catalytic cycle.

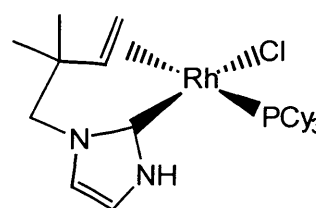


Figure 6-2 Isolated rhodium carbene intermediate

As such, Bergman *et al.* combined experimental and theoretical results to propose a mechanism for the reaction involving initial C-H activation of the azole to form the

carbene complex (Figure 6-3: **A** → **B**), followed by insertion of the alkene into the rhodium-carbene bond (Figure 6-3: **B** → **D**), proton transfer (Figure 6-3: **D** → **F**) and reductive elimination of the final product² (Figure 6-3: **F** → **A**).

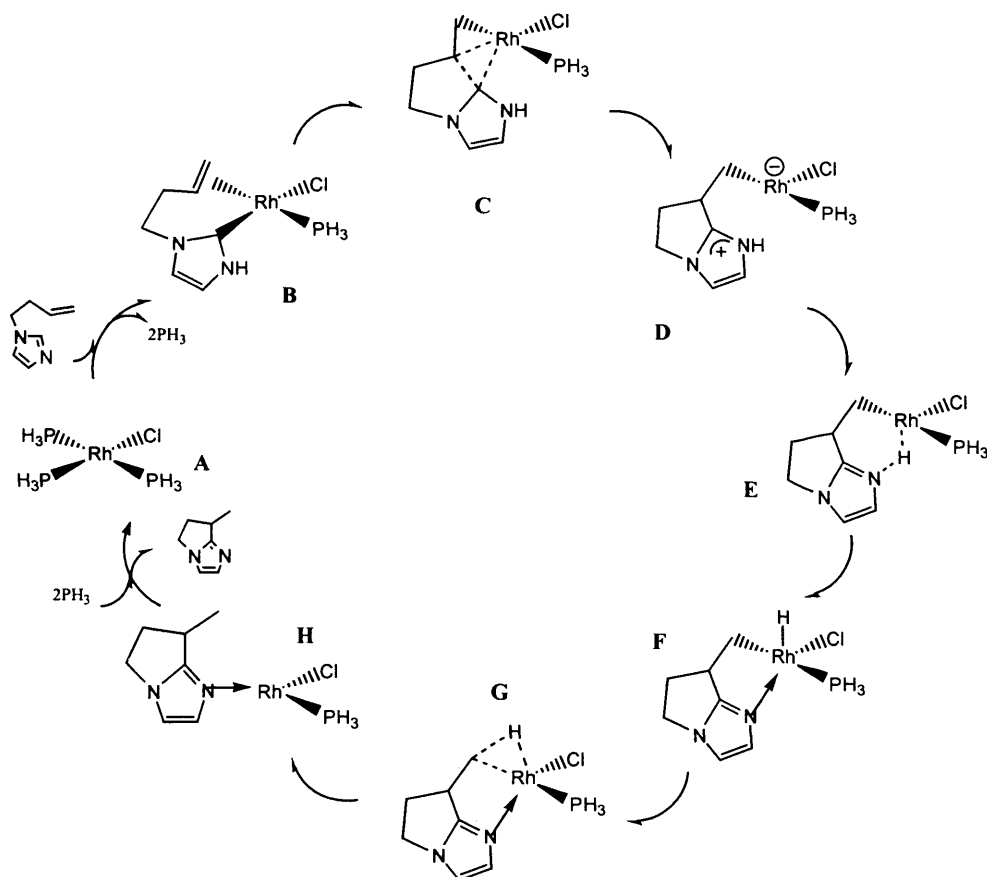


Figure 6-3 Catalytic cycle for intramolecular C-C coupling proposed by Bergman

As the carbene complex (Figure 6-3: **B**) appeared to be a resting state of the cycle, theoretical results for the proposed mechanism presented by Bergman proceeded from this complex and did not include formation of this rhodium carbene from the reactants. However, from this point, the highest barrier to reaction was associated with the alkene insertion (Figure 6-3: **B** → **D**), standing at 47 kcal mol^{-1} with subsequent steps progressively less energetically demanding.

In general, the rhodium C-C coupling reaction between azoles and alkenes performed by Bergman appeared remarkably similar to the related azolium salt/alkene coupling studied in the previous chapter using the Cavell/McGuinness mechanism for nickel catalysts⁶⁻⁸. Further, the proposed mechanism for the rhodium catalysis involved similar steps, albeit in a modified order and with additional steps. As such, it seems possible the oxidative addition, insertion and reductive elimination cycle of the Cavell/McGuinness

mechanism may be a viable alternative to the Bergman mechanism for rhodium C-C coupling reactions in certain circumstances (Figure 6-4).

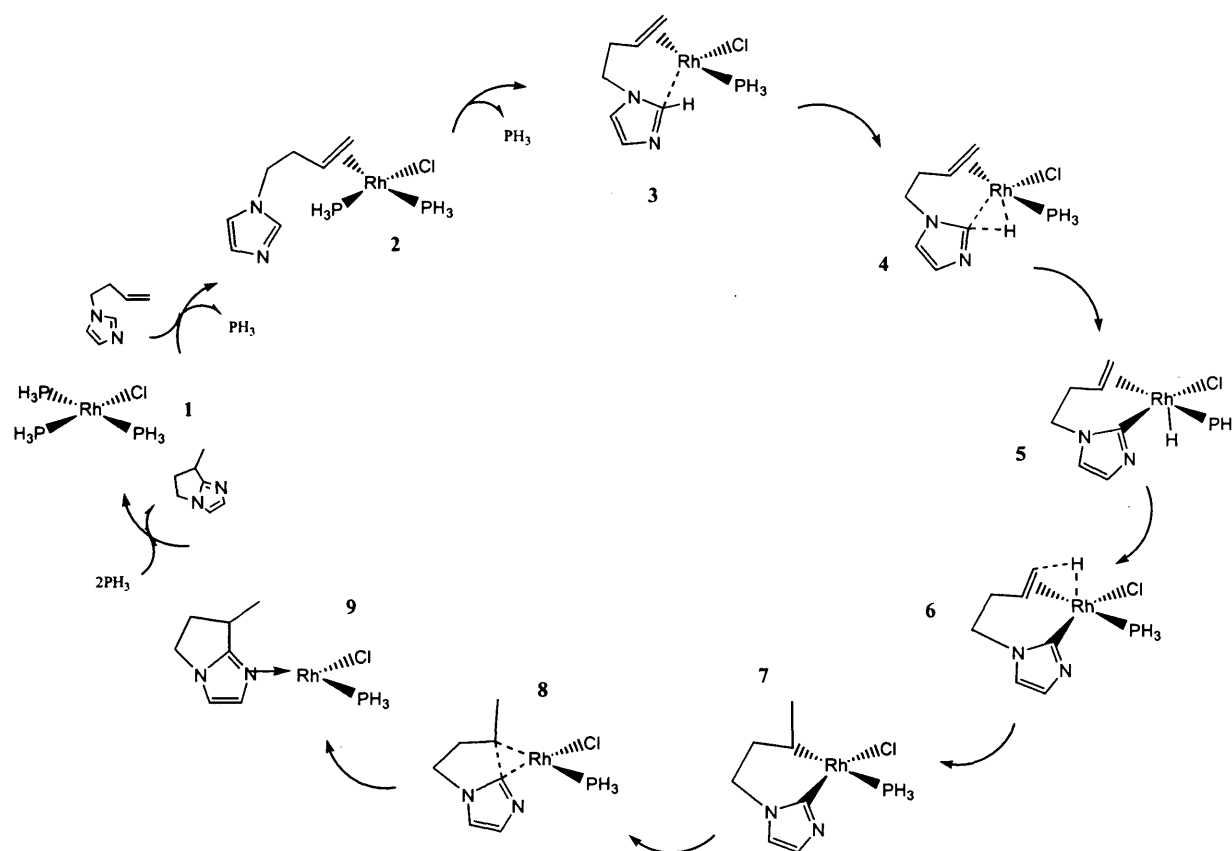


Figure 6-4 Proposed catalytic cycle for intramolecular C-C coupling of N-butylimidazole

This chapter outlines studies of the initial steps of Bergman's cycle to create the rhodium carbene complex, with a comparison of the completed Bergman cycle to the Cavell/McGuinness mechanism. Further, alternative products due to alkene isomerisation and alternative alkene coordination are examined, in addition to the introduction of an acid catalyst into the reaction environment.

6.2 Computational details

Geometry optimisations and harmonic vibrational frequencies for all systems were calculated at the B3LYP⁹⁻¹¹ level of theory with the LANL2DZ basis set, which incorporates the Hay and Wadt¹² small core relativistic effective core potential and double zeta valence basis set on rhodium, phosphorus, chlorine and sulfur with the Dunning and Huzinaga¹³ double zeta basis set on all other atoms. Zero point vibrational energy corrections were obtained using unscaled frequencies. All transition structures contained exactly one imaginary frequency and were characterised by following the corresponding normal mode towards the products and reactants.

Higher level single point calculations were performed on the optimised geometries at the B3LYP level with a LANL2augmented:6-311+G(2d,p) basis set, incorporating the LANL2 effective core potential and a large LANL2TZ+(3f) basis set on rhodium. This basis set was obtained by us in the same way as described for the Pt LANL2TZ+(3f) basis set reported previously¹⁴. All other atoms used the 6-311+G(2d,p)¹⁵⁻¹⁷ basis set. Energies from these single point calculations were combined with the thermodynamic corrections at the lower level of theory to obtain ΔG_{298} numbers. All energies quoted in this chapter refer to these final ΔG_{298} values

All calculations were performed with the Gaussian 03¹⁸ set of programs.

6.3 Results and discussion

6.3.1 Imidazole catalysis

6.3.1.1 Completion of the Bergman cycle

As mentioned in the introduction, the cycle proposed by Bergman proceeded from the rhodium carbene complex without investigation of the mechanism for the formation of this complex. He did, however, mention this complex was most likely formed through alkene coordination to the starting rhodium complex, followed by C-H activation. This section outlines computational studies on these initial steps and the subsequent completion of Bergman's catalytic cycle.

6.3.1.1.1 Alkene coordination and oxidative addition

Due to the nature of the reaction studied, it is assumed the alkene arm of the imidazole would at some phase in the cycle be directly coordinated to the rhodium centre. While it is feasible that coordination may occur either before or after oxidative addition, the triphenylphosphine ligand used in experimental conditions is labile and it is likely an unsaturated $\text{Rh}(\text{PR}_3)_2\text{Cl}$ fragment and the alkene arm of an imidazole could combine relatively easily to form an alkene complex prior to oxidative addition (Figure 6-4 1 \rightarrow 2).

In fact, displacement of a phosphine by the alkene in our model system indicated the alkene complex was only $8.5 \text{ kcal mol}^{-1}$ higher in energy than the triphosphine starting complex, with the imidazole effectively 'dangling' and having no direct interaction with the metal (Figure 6-5).

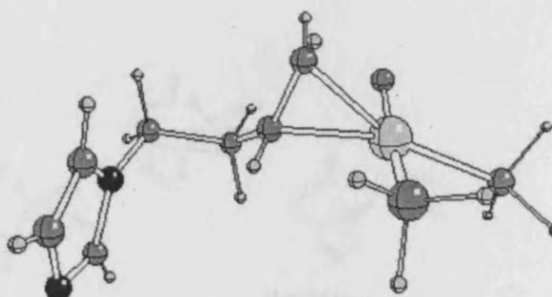


Figure 6-5 Initial rhodium alkene complex (2)

Dissociation of an additional phosphine from the initial alkene complex would allow the imidazole to interact with the metal centre and consequently permit oxidative addition (Figure 6-4 3 \rightarrow 5), promoted in part by the close proximity of the imidazole to the reacting centre facilitated by the chelation of the alkene arm. Geometry optimisations of this initial interaction show a weak bond forming between the rhodium and the C2 of the imidazole, with the hydrogen bent out of the plane of the ring (3). As found for previous oxidative addition reactions^{19, 20}, the initial C2 interaction is

followed by a three-centred transition structure (4) before formation of a five coordinate hydride complex (5).

The oxidative addition reaction for the imidazole is not an energetically favourable one (Figure 6-6).

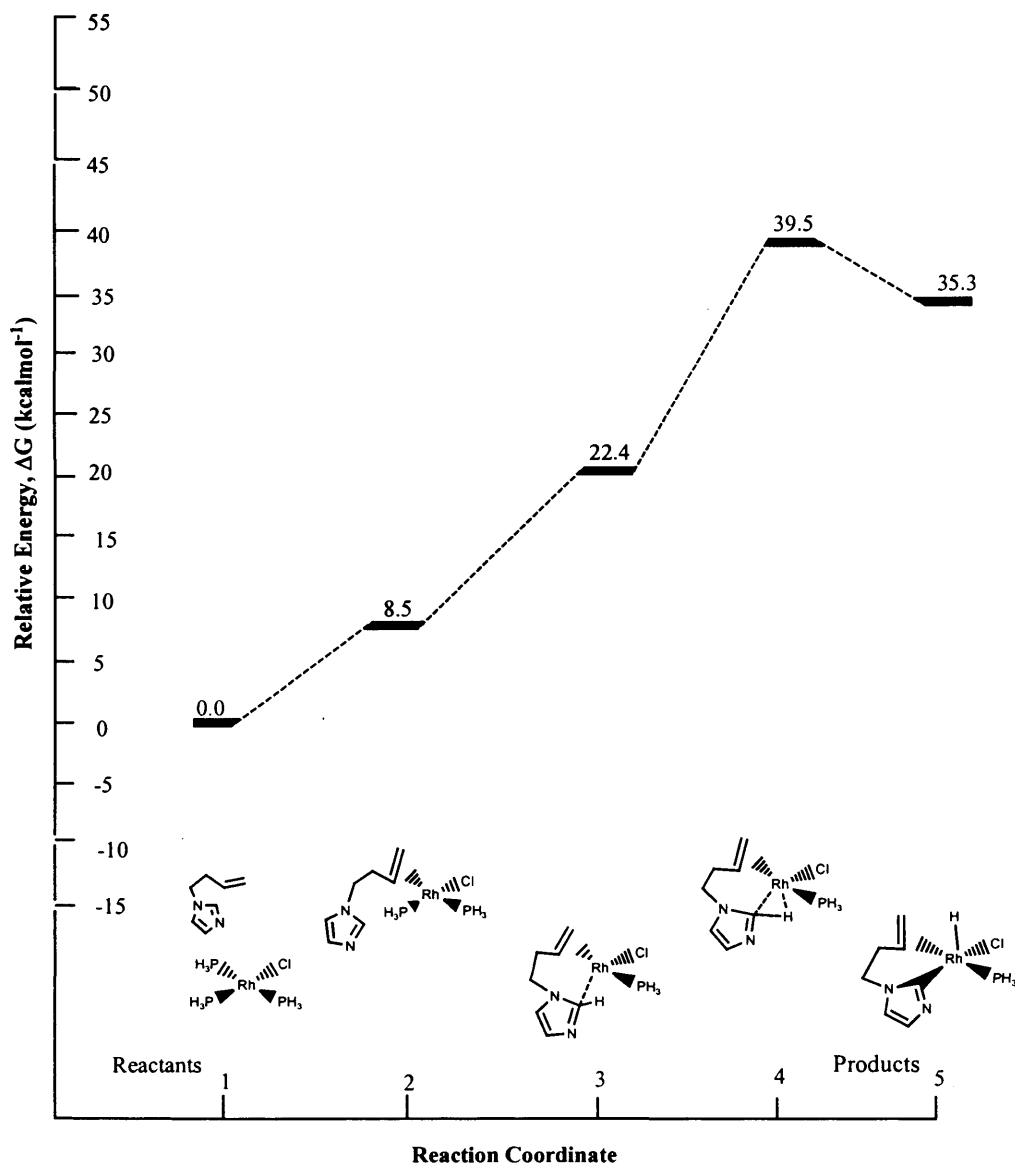


Figure 6-6 Oxidative addition step for rhodium C-C coupling catalysis

After the initial alkene complex has formed, dissociation of another phosphine to allow interaction between the imidazole and the metal centre is energetically reasonable, with a further 13.9 kcal mol⁻¹ required to allow the double dissociation. From this point, the oxidative addition transition structure requires an extra 17.1 kcal mol⁻¹ to overcome; a total of 39.5 kcal mol⁻¹ from the separated starting materials. This relatively high barrier is thought to be due in part to the dissociation required for reaction, and further to the strength of the C-H bond in the unactivated imidazole.

Further hindering the reaction is the stability of the oxidative addition product. The resulting aryl ligand is moderately weak and as such, the hydride product of the reaction is relatively unstable, lying $35.3 \text{ kcal mol}^{-1}$ higher in energy than the reactants.

With all these factors taken into consideration, the initial oxidative addition reaction is not a favourable one and results in a high-energy intermediate.

6.3.1.1.2 Formation of the carbene complex

The cycle proposed by Bergman uses the carbene complex resting state as the zero point energy of the reaction, with formation of the carbene occurring after C-H activation of the imidazole starting material as studied in the previous section². From the initial oxidative addition reaction, it is assumed the hydride ligand could migrate to the imidazole nitrogen, thus forming the carbene complex used as the starting point in Bergman's studies and as indicated in experimental conditions.

Formation of the carbene complex from the hydride appears to be a relatively straightforward process (Figure 6-7).

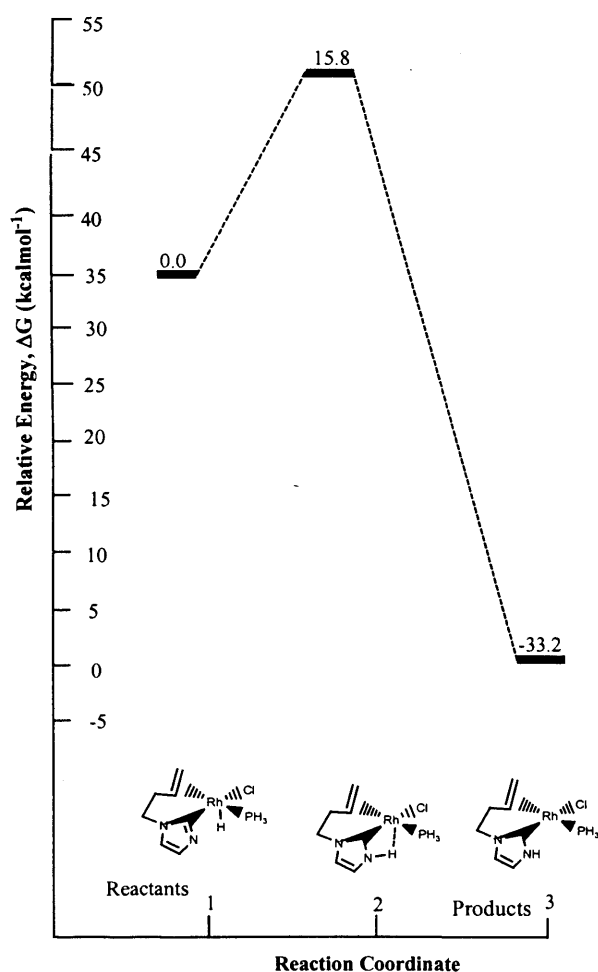


Figure 6-7 Formation of the rhodium carbene complex (kcal mol^{-1})

The geometry of the transition structure indicates that hydride migration to permit formation of the carbene complex requires the hydride to be relatively distant to both the metal and the imidazole nitrogen (Figure 6-8). Further, the rhodium switches from a formal Rh(III) state to Rh(I) in this step with the individual barrier $15.8 \text{ kcal mol}^{-1}$. Once formed however, the carbene complex proves to be highly stable and is $33.2 \text{ kcal mol}^{-1}$ lower in energy than the alkene hydride complex.

In addition, reversal of hydride migration from the carbene complex to the corresponding hydride complex is highly unlikely, requiring $49.0 \text{ kcal mol}^{-1}$ for activation and resulting in a much less stable intermediate.

6.3.1.1.3 *The overall Bergman cycle*

Combining the alkene coordination and oxidative addition steps with the cycle presented previously by Bergman² results in an interesting overall mechanism (Figure 6-9).

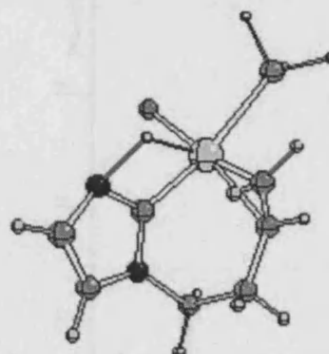


Figure 6-8 Transition structure for hydride migration to form the carbene complex

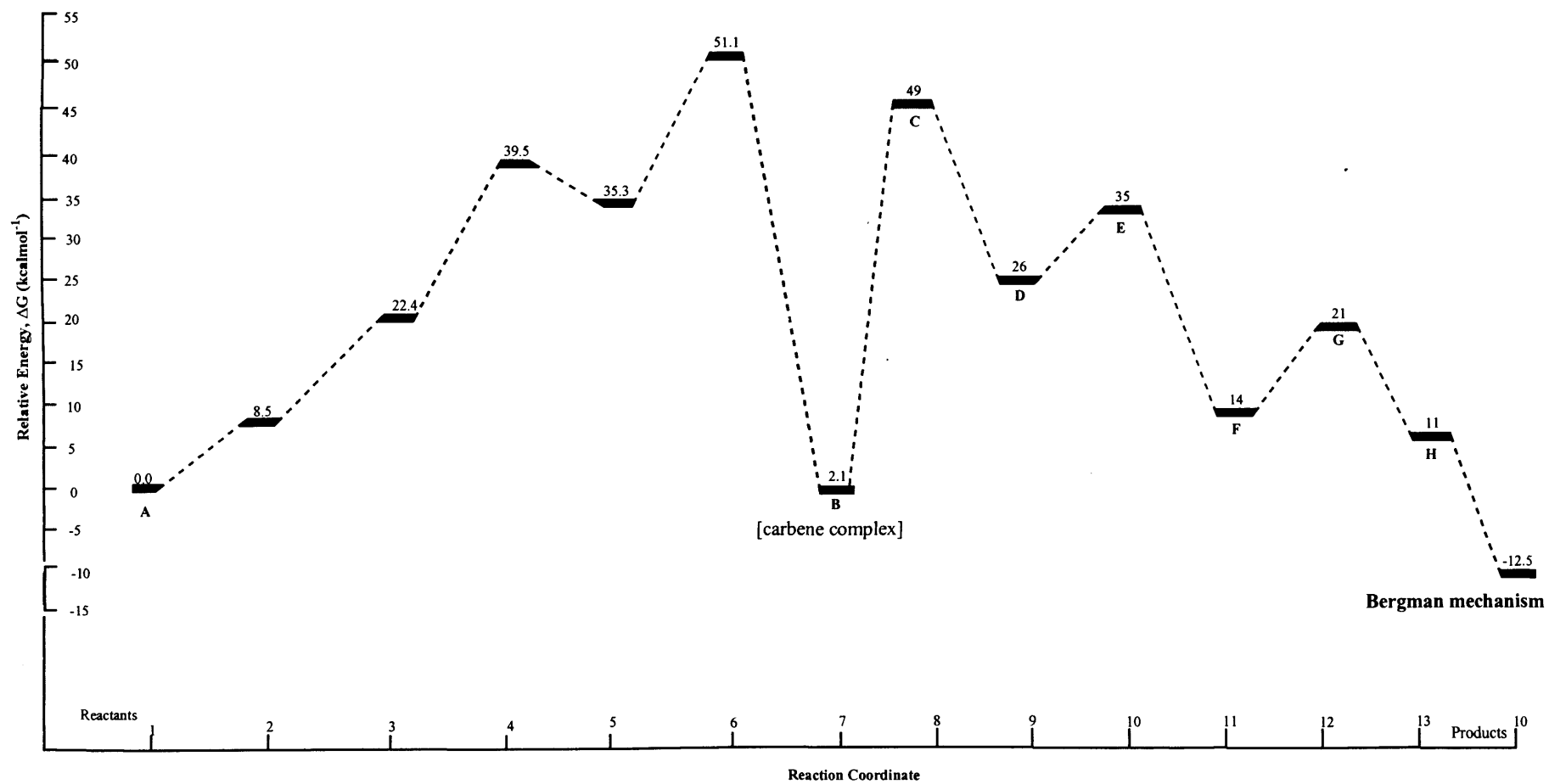


Figure 6-9 Overall Bergman mechanism including alkene coordination and oxidative addition

As indicated previously, the initial oxidative addition step is endothermic with a reasonable barrier to reaction and high-energy hydride product. Continuing with the catalytic cycle, hydride migration from the oxidative addition product to form the carbene complex may not appear restrictive as an individual step, however when viewed in sequence it adds a further barrier to the preliminary steps of the reaction, increasing the overall barrier from the separated reactants to the carbene complex to a high $51.1 \text{ kcal mol}^{-1}$ and without the presence of low energy intermediates.

Despite the challenge of the initial steps of the reaction, formation of the carbene complex results in a remarkably low-energy intermediate. At only $2.1 \text{ kcal mol}^{-1}$ higher in energy than the starting materials, this complex is over 20 kcal mol^{-1} more stable than any other of the central intermediates and it is unsurprising Bergman was able to isolate this complex in experimental conditions.

Interestingly, continuation of the cycle from the carbene intermediate requires only fractionally less energy than the reversal of the hydride migration and reductive elimination of the starting materials, with activation energies standing at $46.9 \text{ kcal mol}^{-1}$ and $49.0 \text{ kcal mol}^{-1}$ respectively. These high barriers on either side of the stable carbene complex are consistent with the isolation of the resting state of the cycle and regardless of whether for the forward or reverse reaction, it is expected reaction would proceed smoothly towards the separated products, with no remaining barrier in either direction exceeding 9 kcal mol^{-1} .

6.3.1.2 The Cavell/McGuinness mechanism

As discussed, the experimental work performed by Bergman included successful coupling of a range of azole species to alkenes in both inter- and intramolecular reactions to produce 2-addition products. In the previous chapter, we showed a similar reaction using azolium salts and a nickel catalyst followed a route of oxidative addition, alkene coordination and insertion into the metal hydride, followed by reductive elimination of the final product.

As rhodium is well known for supporting oxidative addition and reductive elimination cycles in catalysis, it seems plausible the same cycle could be followed for this reaction. In this case, the initial steps of the reaction, notably the alkene coordination and oxidative addition, would be identical to those described in the previous section for the Bergman reaction. From this point, the hydride migration studied by Bergman would be replaced by the direct insertion of the alkene into the Rh-C bond of the aryl ligand, followed by direct reductive elimination of the product.

To allow a direct comparison to the mechanism proposed by Bergman, we originally studied the cycle for the creation of the branched 5-membered ring product with a Rh(PH₃)Cl base. Described below are the results of the calculation for each of the individual steps, followed by a comparison of these results to those discovered by Bergman.

6.3.1.2.1 Alkene insertion

Once the rhodium hydride has formed from the alkene coordination via oxidative addition (Section 6.3.1.1.1), the insertion of the alkene into the metal hydride bond is relatively facile (Figure 6-4 **5** → **7**). As the geometry optimisation of the oxidative addition product indicated the alkene ligand is most stable perpendicular to the rhodium plane, only a small movement of the hydride ligand towards the alkene itself is required to reach the insertion transition structure (**6**). As the new carbon hydride bond forms, the other alkene carbon draws closer to the metal centre as a new alkyl to metal σ bond forms.

Due in part to the relatively small change in geometry required and close proximity of the alkene and hydride ligands, the barrier for the insertion reaction is very small at only 2.9 kcal mol⁻¹ (Figure 6-10).

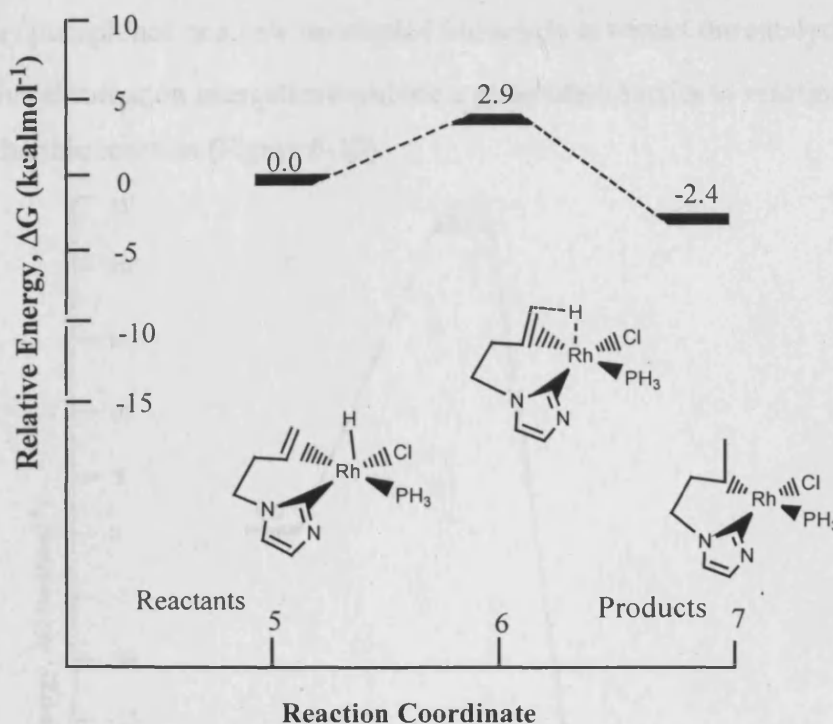


Figure 6-10 Alkene insertion step for rhodium C-C coupling catalysis

Despite this low barrier to insertion, the resultant alkyl complex is only 2.4 kcal mol⁻¹ more stable than the hydride alkene complex, and with a low barrier to reaction, the reverse β -hydride elimination reaction may occur as rapidly as the formation of the alkyl complex. As such, this step may be seen as a facile yet easily reversible step in the overall reaction.

6.3.1.2.2 Reductive elimination

The reductive elimination of the final product occurs when the imidazole and alkyl ligands produced by the alkene insertion draw closer to one another (Figure 6-4 7→ 9), with a twist of the imidazole allowing interaction with the orbitals of the alkyl ligand.

Due to the open nature and bonding ability of the divalent imidazole nitrogen, the product of the reductive elimination shows a strong nitrogen to metal bond as the product rotates and the nitrogen becomes available as a donor ligand (Figure 6-11). This interaction aids in stabilising the coordinatively unsaturated metal centre created by the coupling of the two organic ligands and must be broken by displacement of the resultant

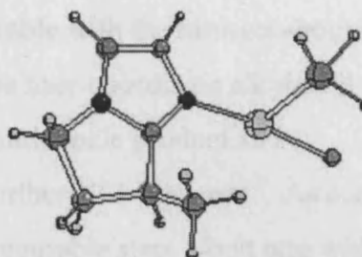


Figure 6-11 Reductive elimination nitrogen-rhodium interaction (9)

imidazole by phosphines or a new uncoupled imidazole to restart the catalytic cycle. The reductive elimination energetics combine a reasonable barrier to reaction with a highly exothermic reaction (Figure 6-12).

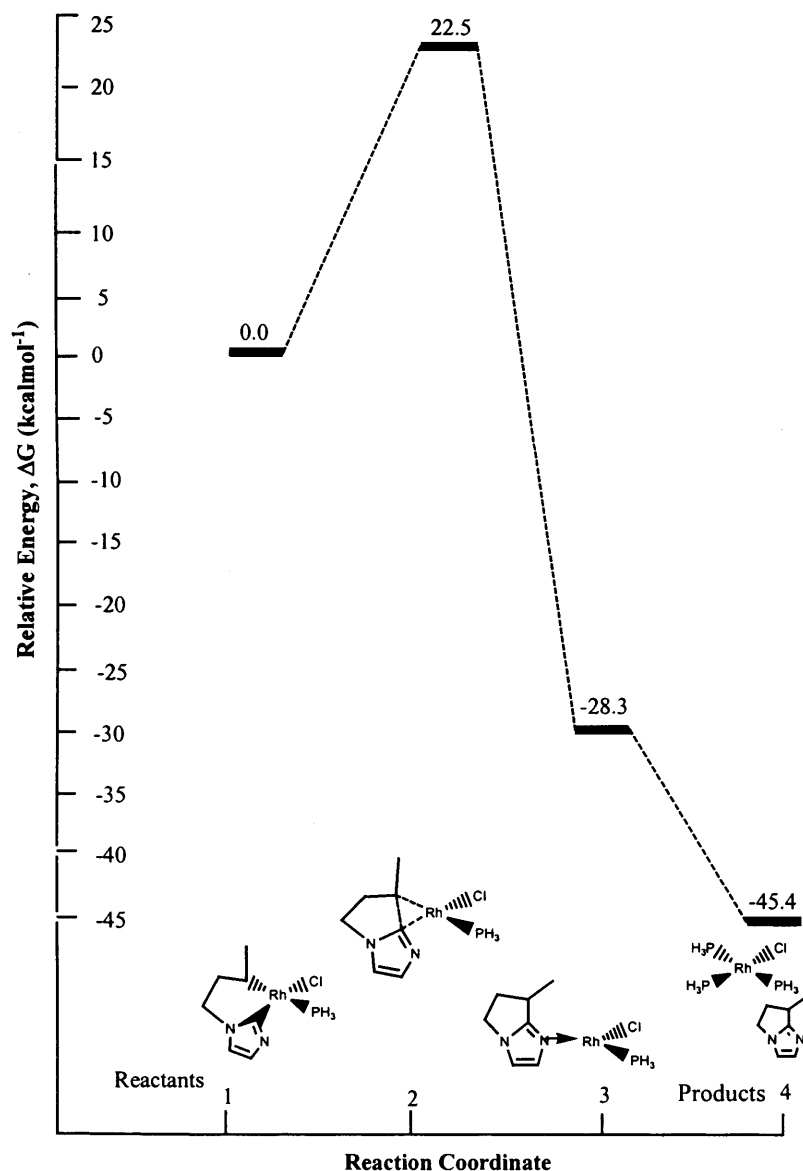


Figure 6-12 Reductive elimination step for rhodium C-C coupling catalysis

Standing at $22.5 \text{ kcal mol}^{-1}$, the barrier to reductive elimination is not insignificant. Once overcome however, the energy benefits are considerable with the nitrogen-bound imidazole product $28.3 \text{ kcal mol}^{-1}$ lower in energy than the four-coordinate alkyl/acyl complex, and the further separation of the loosely bound imidazole product and regeneration of the starting rhodium complex gaining a further $17.1 \text{ kcal mol}^{-1}$. As such, the reductive elimination itself is a thermodynamically favourable step, albeit one with a reasonable individual barrier to reaction.

6.3.1.2.3 *Overall cycle*

The overall results employing the Cavell/McGuinness mechanism exhibit a challenging catalytic cycle. As can be seen from the combined energy results, the overall route presents some high barriers to reaction with the majority of important intermediates relatively high in energy (Figure 6-13).

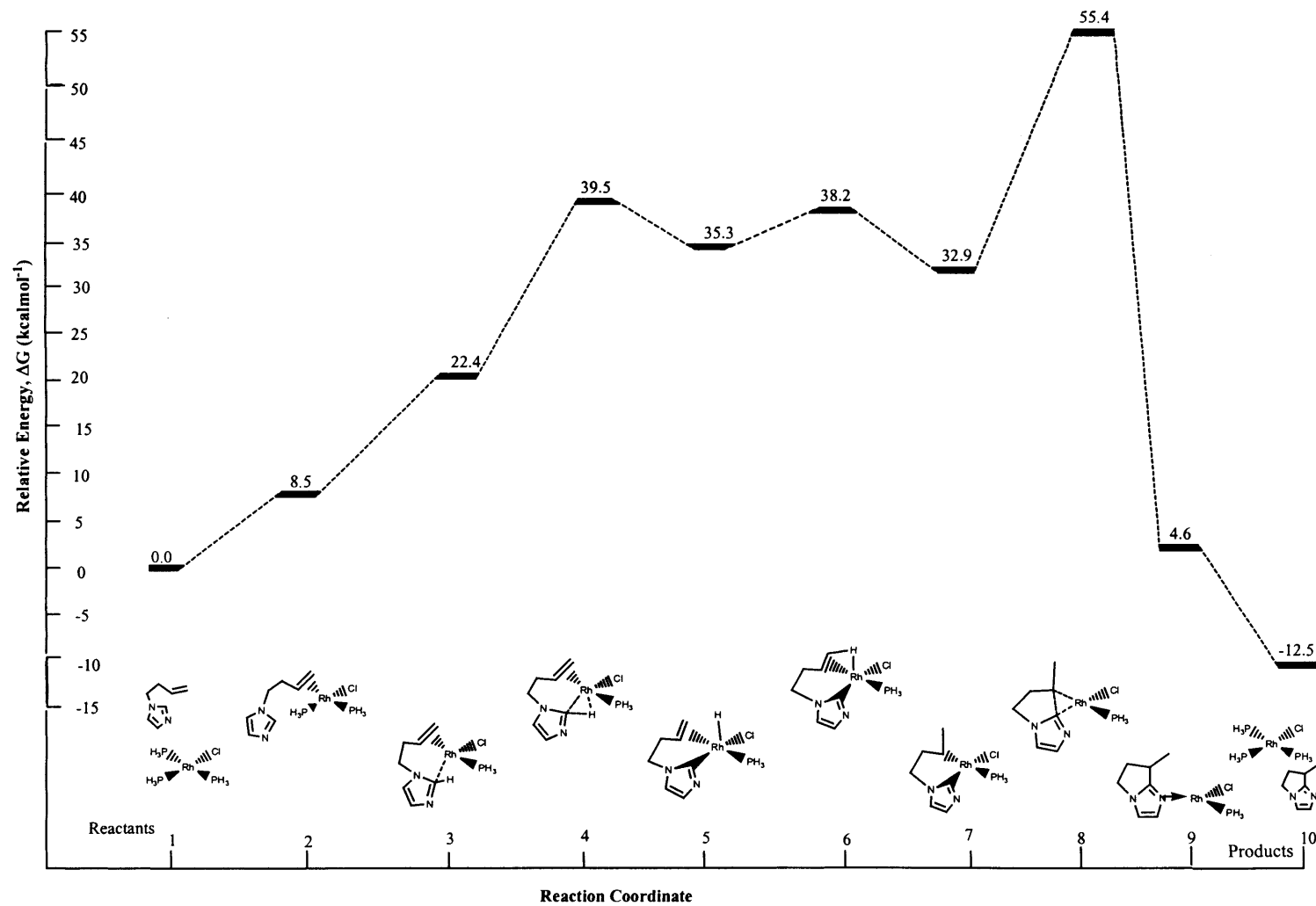


Figure 6-13 Energies for the Cavell/McGuinness catalytic cycle

The initial oxidative addition is unfavourable, with a large activation energy and a four coordinate hydride product $35.3 \text{ kcal mol}^{-1}$ less stable than the separated starting materials. While the insertion of the chelated alkene into the metal hydride appears relatively straightforward as an isolated step, the starting hydride and resultant alkyl complexes are still distinctly unstable with respect to the starting materials at 35.3 and $32.9 \text{ kcal mol}^{-1}$ respectively. Further, the high-energy alkyl product of the insertion reaction becomes the starting complex for the reductive elimination, which in itself has an individual barrier of $22.5 \text{ kcal mol}^{-1}$. While independently this is not a significant barrier, combined with the relative instability of the intermediates that lead up to the reductive elimination, the overall barrier to the cycle is found to be a restrictive $55.4 \text{ kcal mol}^{-1}$.

Despite the overall reaction being quite favourable with the C-C coupled product $12.5 \text{ kcal mol}^{-1}$ lower in energy than the separated reactant, it appears unlikely that the Cavell/McGuinness mechanism studied here would be the favoured route of reaction. The high barriers required for reaction are not countered by any energy gains from lower energy intermediates or catalyst resting states, with all but the final step easily reversible. As such, if this mechanism is competitive in experimental conditions, other factors not yet considered must have significant influence in the cycle. Consequently, recoordination and dissociation of phosphines, which may significantly affect the stability and characteristics of important intermediates, is examined in the next section.

6.3.1.2.4 *Floating phosphines*

In the initial study of the Cavell/McGuinness mechanism above, the rhodium centre studied contained only the ligands present in the Bergman mechanism to provide a direct comparison to his results. However, one of the most significant differences in the Cavell/McGuinness mechanism and that proposed by Bergman is the oxidation state of the metal centre. Bergman's mechanism proceeds from the rhodium(I) carbene intermediate, and continues with the formal +1 charge on the metal for the majority of the catalytic cycle. As such, the intermediates are generally square-planar with only a single phosphine attached to the metal at any one time. Conversely, the Cavell/McGuinness mechanism involves three negatively charged ligands and it is likely that the octahedral rhodium(III) is the favoured geometry when relatively small ligands are in use.

As experimental conditions generally have an excess of phosphine in the reaction systems and products or intermediates with potentially coordinatively unsaturated complexes did not seem favourable, we decided to study the Cavell/McGuinness mechanism allowing the phosphines to dissociate and reattach for stability at any point. Most structures along the pathway displayed improved stability with coordination of an extra phosphine (Figure 6-14).

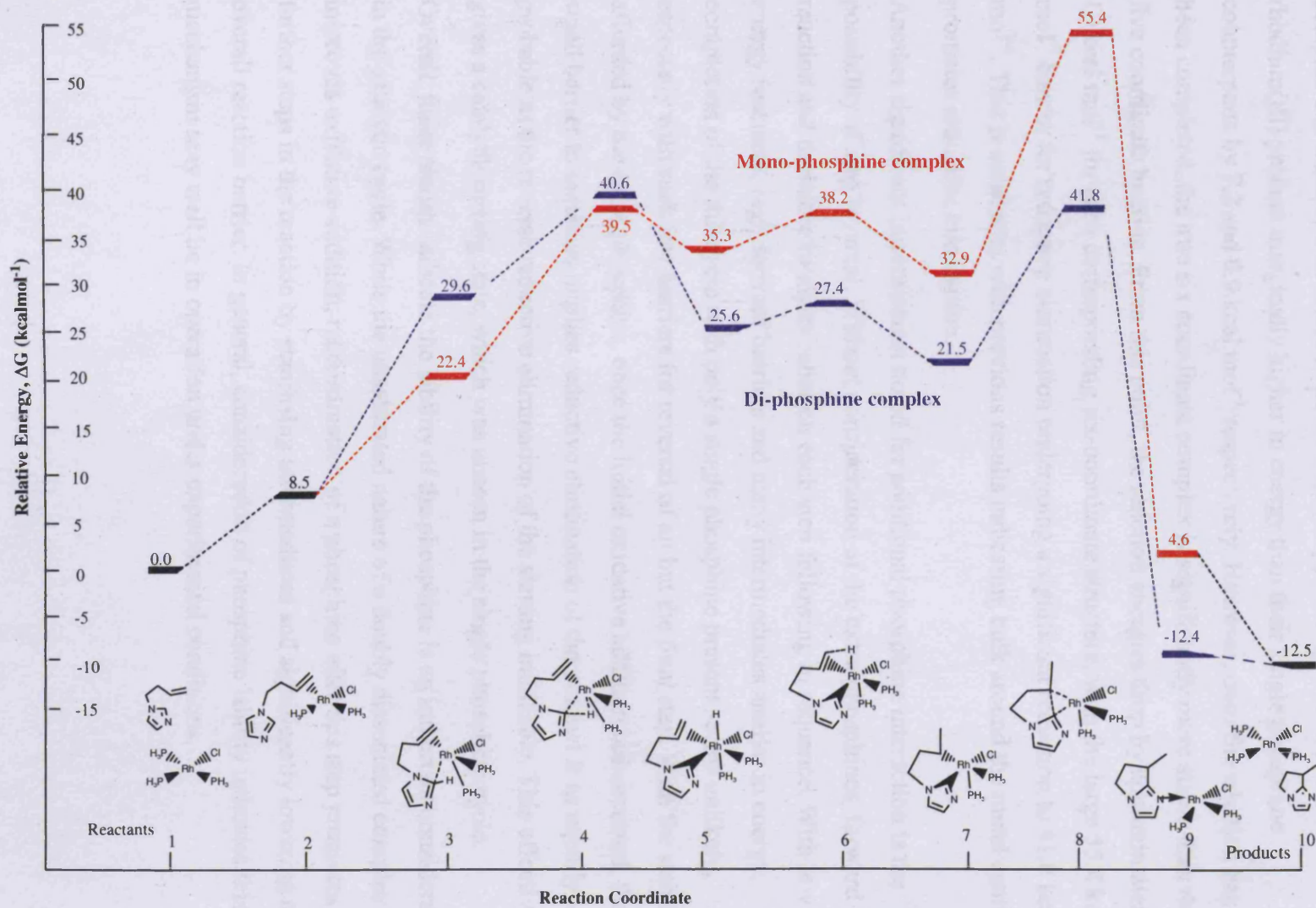


Figure 6-14 Energies for the Cavell/McGuinness catalytic cycle with extra phosphines

The oxidative addition reaction proves the only exception to the rule, with the precursor complex and transition structure from the rhodium(I) starting material to the rhodium(III) product marginally higher in energy than their single phosphine counterparts by 7.2 and 0.9 kcal mol⁻¹ respectively. However, once the addition has been completed, the true six coordinate complex is significantly more stable than the five coordinate hydride. From this point, the reaction energies drop by approximately 10 kcal mol⁻¹ for each corresponding six-coordinate structure, with the large 55.4 kcal mol⁻¹ barrier for reductive elimination undergoing a significant reduction to 41.8 kcal mol⁻¹. This is consistent with previous results indicating bulk around the metal centre promotes reductive elimination.

Another significant improvement noted for additional phosphine interaction is the possibility of step reversal. Without consideration of the extra phosphines, forward reaction and therefore catalysis relies on each step following in sequence. With low energy reactants, high forward barriers and many intermediates similar in energy, completion of the full cycle with only a single phosphine present seems unlikely, especially with such low barriers for reversal of all but the final step. With the stability afforded by the extra phosphine, once the initial oxidative addition has occurred, the small barrier to insertion implies reductive elimination of the product is as equally probable as the reverse reductive elimination of the starting imidazole. This effectively gives a catalytic resting state, which was unseen in the single phosphine cycle.

Overall, these results indicate the lability of the phosphine is an important consideration in the catalytic cycle. While the unsaturated nature of a doubly dissociated complex improves oxidative addition, recoordination of a phosphine after this step promotes all further steps in the reaction by stabilising intermediates and significantly lowering the overall reaction barrier. In general, consideration of phosphine lability indicates this mechanism may well be in operation under experimental conditions.

6.3.1.3 Comparison of the Bergman and Cavell/McGuinness mechanisms

A direct comparison of the energies for the Cavell/McGuinness and Bergman mechanisms reveals some interesting insights into catalytic cycles (Figure 6-15).

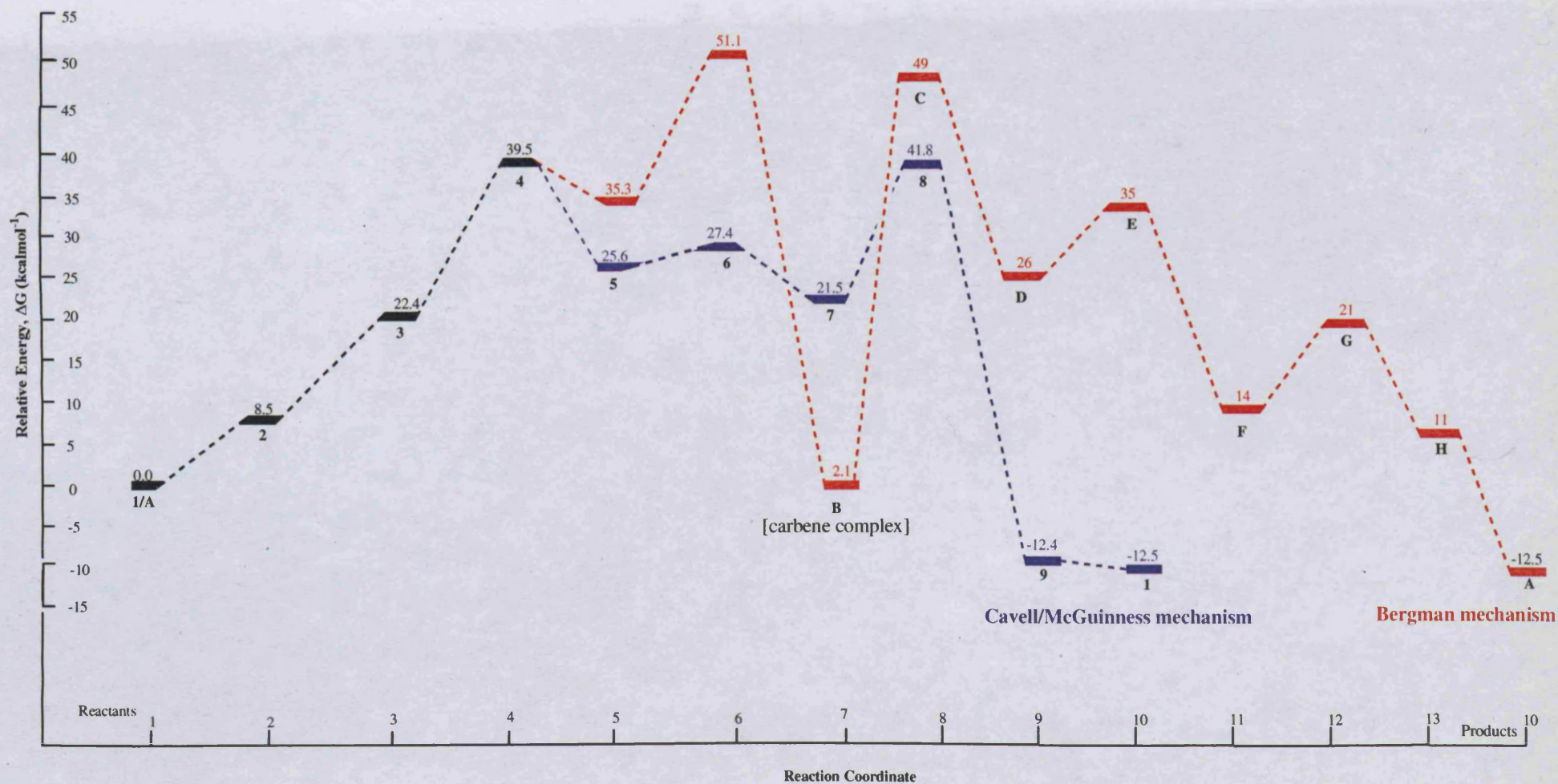


Figure 6-15 Energy comparison of the Cavell/McGuinness and Bergman mechanisms

At first glance, it seems likely the Cavell/McGuinness mechanism would be the preferred mechanism after the initial C-H activation with the majority of intermediates directly following oxidative addition lower in energy, fewer steps, and most importantly, only one large barrier for reductive elimination of the final product. Conversely, the Bergman mechanism contains two large barriers to reaction, and several more steps for reaction completion.

While these observations suggest the Cavell/McGuinness mechanism could be active for this reaction, the experimental evidence confirming the presence of the carbene complex by NMR observations during catalysis and the actual isolation of this complex indicate an alternate mechanism may be in operation at certain temperatures. With the exception of the reactants and final products, this complex is by far the most stable intermediate over both routes and as such, the energy gain from reaching this complex may be the driving force for the overall reaction.

Another important observation is the barriers on either side of the carbene complex. With these barriers within $2.1 \text{ kcal mol}^{-1}$ of each other, continuation of the cycle in either direction would be feasible, implying both mechanisms may be operating in tandem, as indicated below in Figure 6-16.

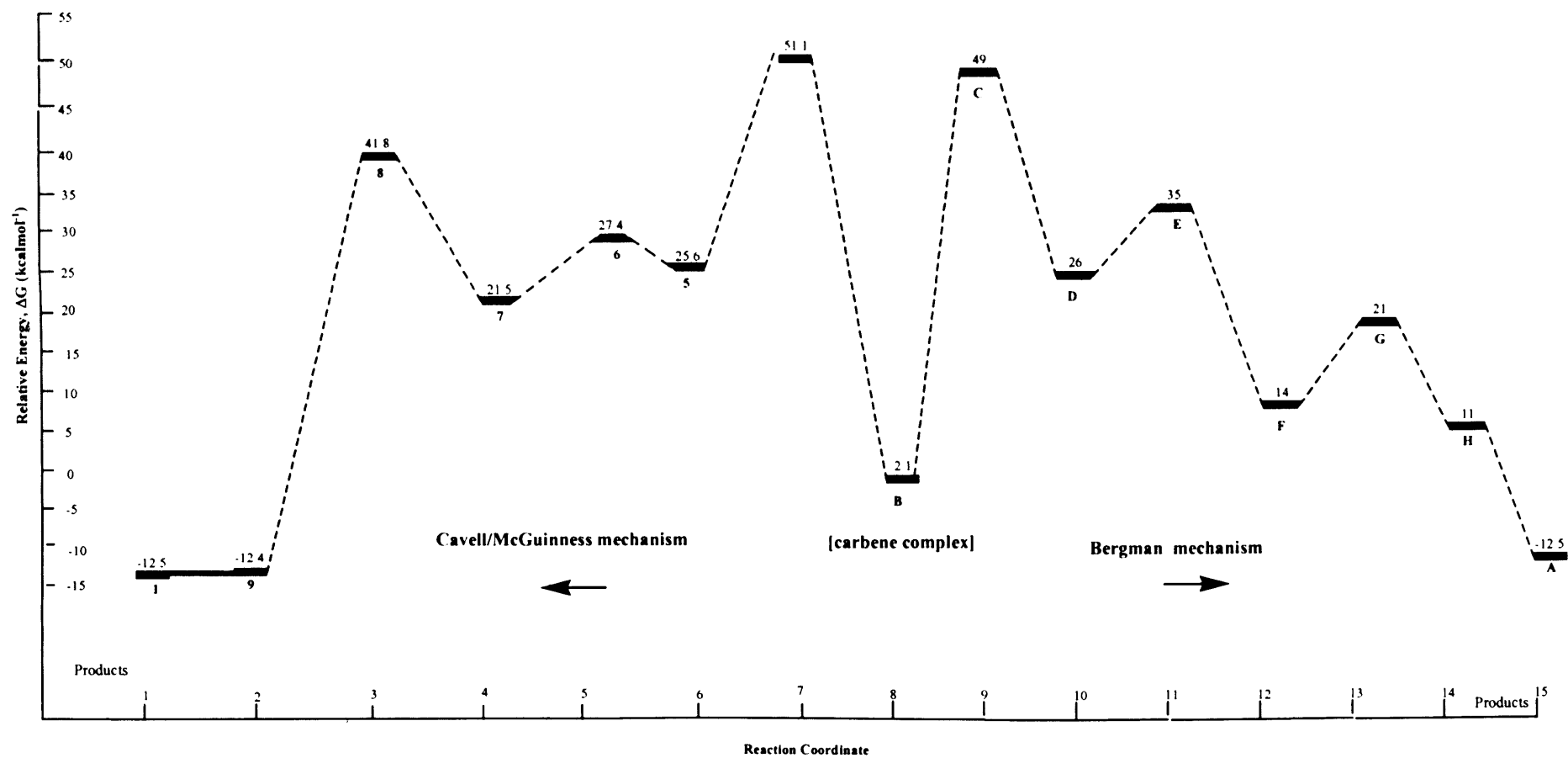


Figure 6-16 Cavell/McGuinness and Bergman mechanisms starting from the carbene complex

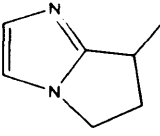
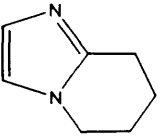
	
0.0 kcal mol ⁻¹	-4.9 kcal mol ⁻¹

Figure 6-19 Energies for the five- and six-membered products

It is envisaged that the different products would be the result of different interactions between the reactant and the metal centre. In the system studied herein, we considered two possible interactions that could affect the outcome of the reaction. Firstly, the direction of the coordinated alkene with respect to the other ligands, in particular the hydride ligand, could result in different intermediates and final products. Secondly, steric bulk from the geminal methyls may directly affect the interaction of the ligands leading to alternative intermediates and consequently, a different product. These possibilities are examined in more detail below.

6.3.2.1 Alkene binding direction

When the alkene is located on the end of the alkyl chain, as may occur for both reactants in Figure 6-17 and Figure 6-18, different binding methods to the metal may result in different products depending on the orientation of the alkene with respect to other reacting ligands (Figure 6-20).

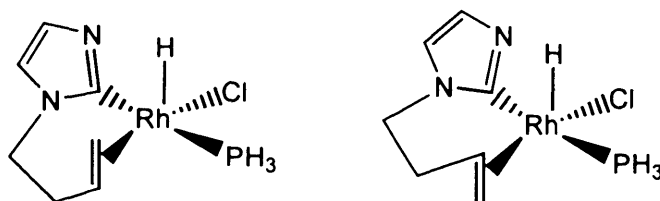


Figure 6-20 Different alkene binding methods

Further, as indicated in Bergman's initial paper on these coupling reactions¹, the *N*-homoallyl benzimidazole undergoes isomerisation in solution, which could also lead to alternative alkene binding and subsequent product formation (Figure 6-21).

6.3.2 Imidazole catalysis - alternative products

The mechanism studied theoretically by Bergman² concentrated on a branched five-membered heterocycle attached to the original imidazole ring as the reaction product. Experimentally, this product had been found where the *N*-homoallyl benzimidazole substrate was combined with Wilkinson's catalyst¹ (Figure 6-17).

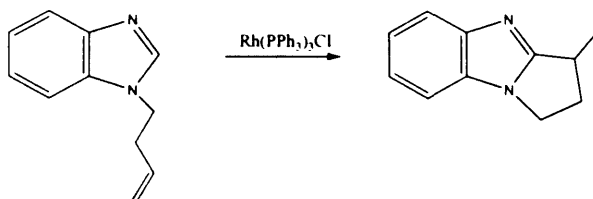


Figure 6-17 Conversion of *N*-homoallyl benzimidazole

However, when a similar alkene substrate was used with geminal methyl groups on the alkene arm, a non-branched six membered product was formed in preference² (Figure 6-18).

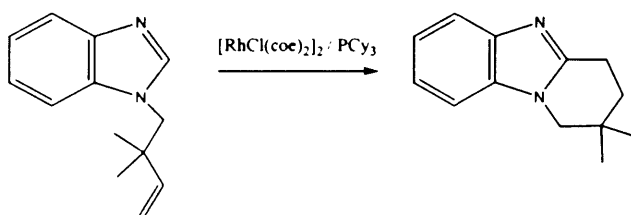


Figure 6-18 Conversion of *N*-homoallyl benzimidazole with geminal methyl groups

The isolation of a single, pure product in high yields in these reactions and not a mixture of isomers implies that a single mechanism is in operation. However, if the mechanism proposed by Bergman is adhered to in experimental conditions, then the substrates described in Figure 6-17 and Figure 6-18 should produce the same five-membered heterocycles, albeit with extra methyl groups in the resulting ring for the reactant in Figure 6-18.

A direct comparison of the two isomers for the products (excluding geminal methyl groups) indicates the six-membered product is thermodynamically favoured (Figure 6-19). What, then, are the distinguishing experimental factors that make the five-membered ring the preferred product for the straight alkene chain in Figure 6-17?

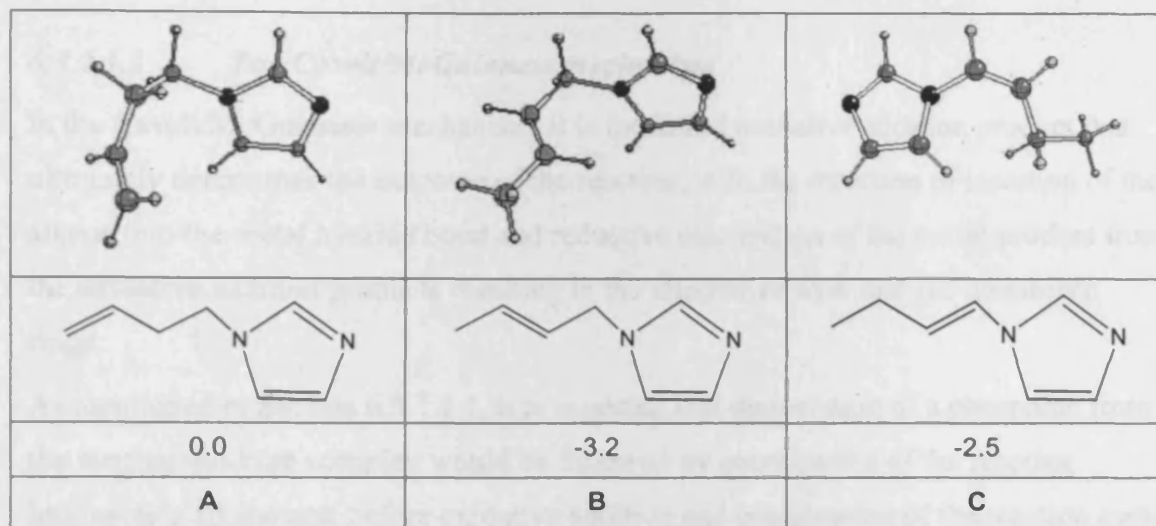


Figure 6-21 *N*-homoallyl benzimidazole isomers (kcal mol⁻¹)

Theoretical calculations and experimental results indicate the favoured isomer is in fact isomer **B** (Figure 6-21), however, the difference in energy between the three isomers is minimal, indicating all three would be available to react with the rhodium catalyst.

Preliminary investigations indicated isomer **C** is not able to coordinate to rhodium in a manner consistent for the catalysis required. With the alkene located so close to the C2 of the imidazole, steric strain disallows simultaneous coordination of the alkene and the imidazole ligand. As such, this isomer is not considered further in this study.

In general, while the two mechanisms discussed in previous sections will be affected in different ways, both can be influenced by the alternative alkene coordination described above. The affect of this coordination on the outcome of the reaction for both mechanisms is described in more detail below.

6.3.2.1.1 *The Cavell/McGuinness mechanism*

In the Cavell/McGuinness mechanism, it is the initial oxidative addition product that ultimately determines the outcome of the reaction, with the direction of insertion of the alkene into the metal hydride bond and reductive elimination of the cyclic product from the oxidative addition products resulting in the alternative five- and six-membered rings.

As mentioned in Section 6.3.1.1.1, it is expected that dissociation of a phosphine from the starting rhodium complex would be followed by coordination of the reacting imidazole's alkene arm before oxidative addition and continuation of the reaction cycle. This initial step may result in three different oxidative addition products capable of creating the five- and six-membered ring products. The first of these (Figure 6-22 A) is created from the 2,3 isomer and leads to formation of the five-membered product. The remaining two arise from the 1,2 isomer (Figure 6-22 B and C) and lead to the five- and six-membered products respectively.

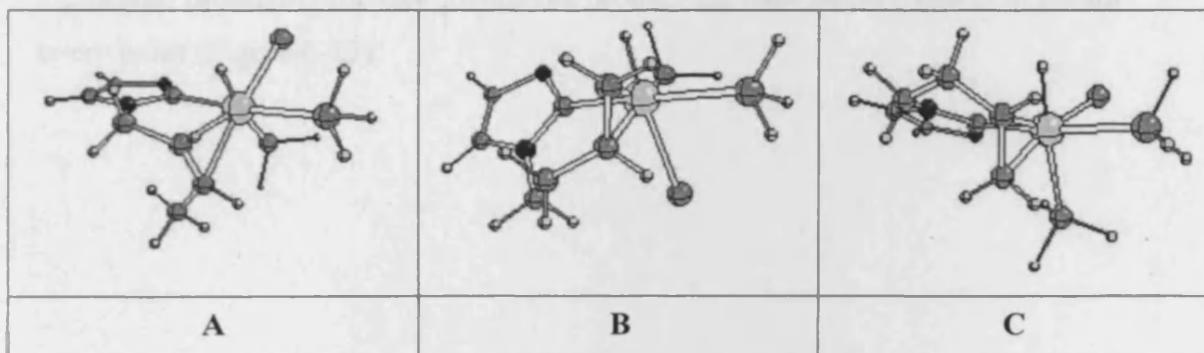


Figure 6-22 Oxidative addition product isomers

While the initial free alkene benefits from extra stability afforded by the secondary alkene, the effect on the overall catalytic cycle geometries is unfavourable. The extra bulk around the alkene provides protection for the free alkene, however, coordination of the alkene to the metal centre becomes more problematic as the direction of the end-chain methyl becomes significant. Further, shortening of the chain between the imidazole and alkene ligands requires a further twisting of the azole ligand with respect to the rhodium plane. Without chelation, the plane of the azole ring tends to lie perpendicular to the metal plane containing the bulkier ligands. When chelation is enforced, as found with the alkene located in the 2,3 position, the distance between the azole and alkene is restricted, in turn forcing a slightly distorted square plane and

increasing the dihedral twist of the azole ligand itself; a situation much more strained than the more free 1,2 alkene coordination.

For the 1,2 alkene isomer, the first notable difference between the two possible reactions is the lack of oxidative addition precursor complex for the reaction leading to the six-membered product (Figure 6-22 C). The initial C2-metal interaction found for the five-membered analogue simply does not occur for the six-membered alternative due to the steric strain introduced into the interaction caused by direction of alkene. This strain is also evident in the geometries of the oxidative addition product (Figure 6-22), with the strain introduced by alkene coordination in the complex leading to the six-membered product displaying a more planar carbene ring compared to the ligand plane than the five-membered analogue with dihedral angles of 141.2° and 135.8° respectively.

Further, the energies for all three corresponding cycles reflect the strain introduced for the 6-membered ring cycle and the 2,3 isomer for the 5-membered ring cycle, with the 1,2 isomer producing the five-membered product the most stable pathway at almost every point (Figure 6-23).

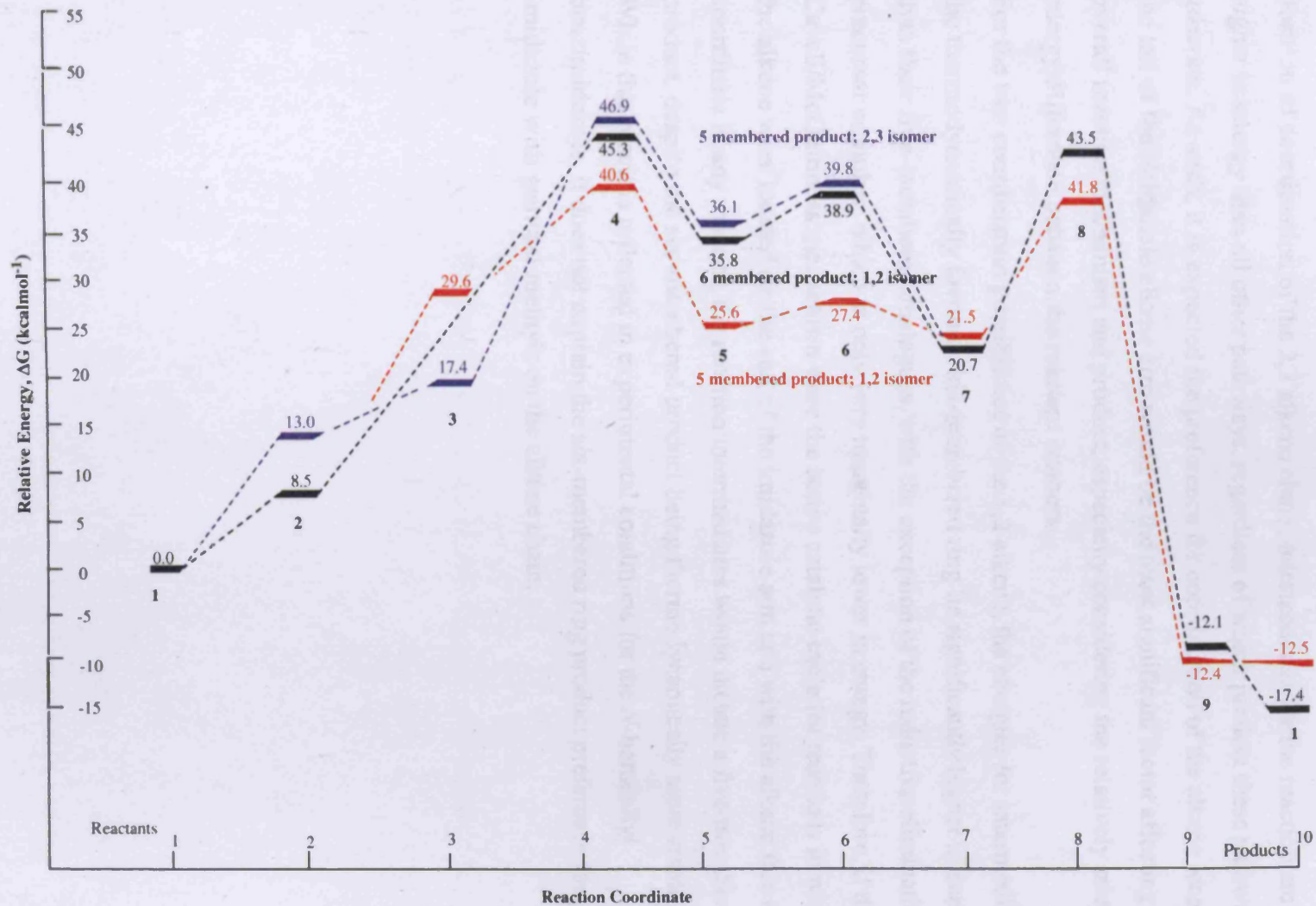


Figure 6-23 Energies for the Cavell/McGuinness mechanism for five- versus six-membered products

In general, the alkene isomerisation available for the straight chain *N*-butene-imidazole does not appear to have any benefit for the formation of the five-membered ring product. Due to the extra steric strain introduced into the rhodium complexes by the position of coordination of the 2,3 alkene chain, intermediates for the reaction are higher in energy than all other pathways, regardless of which product these pathways generate. As such, it is expected the preference for coordination of the alkene located on the tail of the imidazole alkene arm would be the most significant factor affecting the overall reaction mechanism and product, especially considering the relatively small energy difference between the reactant isomers.

For the two coordination possibilities of the 1,2 alkene, the energies for intermediates of the thermodynamically favoured six-membered ring lie significantly higher in energy than their five-membered analogues, with the exception of the reductive elimination precursor complex, which is only very marginally lower in energy. Therefore, if the Cavell/McGuinness mechanism were the active catalytic cycle for reactions in which the alkene were located on the end of the imidazole arm and with the alkene free to coordinate in any manner, the reaction intermediates would dictate a five-membered product, despite the six-membered product being thermodynamically more stable.

While this result is reflected in experimental conditions for the *N*-homoallyl benzimidazole, it does not explain the six-membered ring product preference for the imidazole with geminal methyls on the alkene chain.

6.3.2.1.2 *The Bergman mechanism*

In the case of the Bergman mechanism, it is the direction of interaction of the carbene and alkene ligands in the carbene complex that would create alternative products (Figure 6-24). Figure 6-24 **A** is formed from the 2,3 alkene isomer, with carbene insertion from this structure forming the five membered ring product. Figure 6-24 **B** and **C** are formed from the 1,2 alkene isomer with carbene insertion resulting in the five and six membered products respectively.

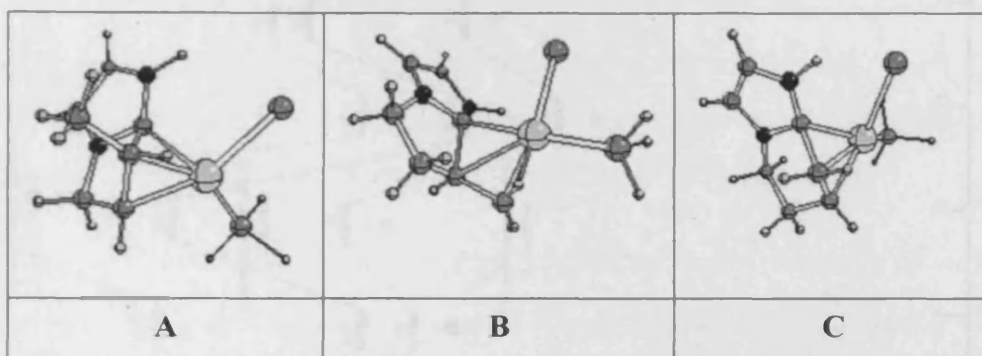


Figure 6-24 Azole insertion transition state geometries

As was found for the Cavell/McGuinness mechanism, the potential isomerisation of the alkene results in no benefits for the Bergman reaction. Due to the shortened distance between the coordinated alkene and the azole C2, all intermediates for the reaction are very strained with both the alkene and azole ring consequently tilted in most structures past their preferred 90° dihedral angle.

Once again, the trend for favouring of the 1,2 isomer mechanism is repeated for the Bergman mechanism (Figure 6-25).

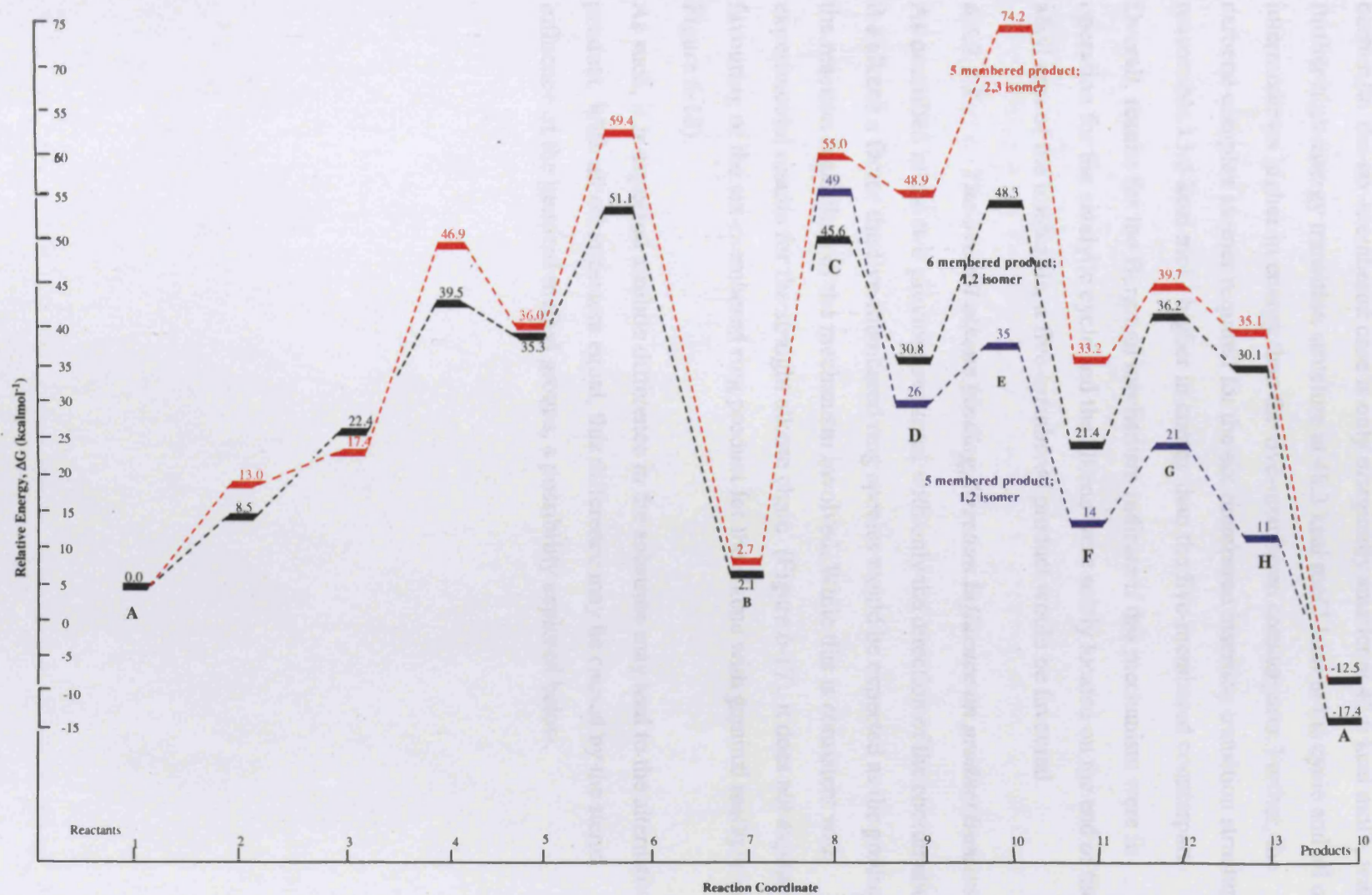


Figure 6-25 Energies for the Bergman mechanism for five-versus six-membered products

As can be seen in Figure 6-25, the transition structure to the carbene insertion into the metal-alkene for the five-membered case (Figure 6-25; C) lies a high 49 kcal mol^{-1} above the reactants and 47 kcal mol^{-1} above the carbene complex itself. However the barrier for the six-membered case is only marginally smaller at $45.6 \text{ kcal mol}^{-1}$, with a further high-energy transition structure at $48.3 \text{ kcal mol}^{-1}$ later in the cycle and all other intermediates higher in energy than the five-membered counterparts. Further, the carbene complex isomer required for the six-membered insertion transition structure is a reasonable $15.6 \text{ kcal mol}^{-1}$ higher in energy than the five-membered counterpart.

Overall, results for the Bergman mechanism indicate if this mechanism were in operation for the catalytic cycle and the alkene were solely located on the end of the alkyl arm of the imidazole, a five-membered product would be favoured.

6.3.2.1.3 *The overall alkene binding direction influence on product isomers*

As described in the two previous sections, with only the direction of the coordination of the alkene a factor the five-membered ring species would be expected as the product of the reaction regardless of the mechanism involved. While this is consistent with experimental results for the straight alkene chain¹ (Figure 6-17), it does not explain the favouring of the six-membered ring product for the alkene with geminal methyls (refer Figure 6-18).

As such, it is expected a subtle difference in the substrate may lead to the alternative product. With all other factors equal, this difference may be caused by the steric influence of the geminal methyl groups, a possibility explored below.

6.3.2.2 The influence of substrate geminal methyls

With the inclusion of extra methyl groups around the reacting centre, it is expected formation of the C-C coupled product could require more twisted and sterically crowded intermediates than those expected for the straight alkene chain. This proximity of the methyl groups to the metal centre in some important intermediates could determine which of the two likely products is favoured. The effect of these extra methyl groups on both mechanisms is detailed below.

6.3.2.2.1 *The Cavell/McGuinness mechanism*

Inclusion of the geminal methyls resulted in very little difference for the Cavell/McGuinness mechanism. All geometries were almost identical, with the extra methyl groups located away from the reacting centre. As such, the geometries for the overall reaction for both five- and six-membered ring products remained relatively unchanged (Figure 6-26).

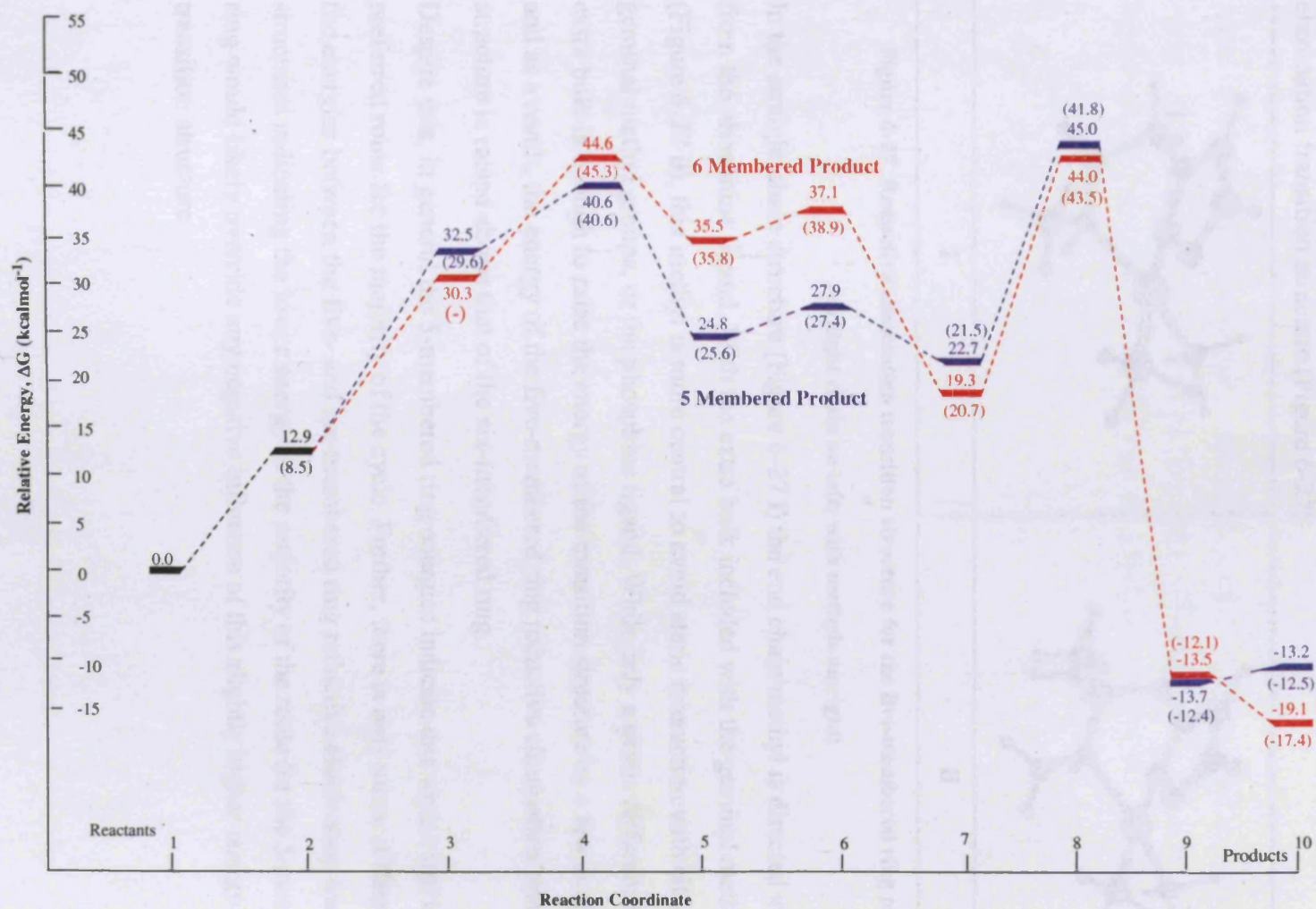


Figure 6-26 Energies for the influence of geminal methyls on the five- and six-membered products – straight chain energies in brackets (Cavell/McGuinness mechanism)

In general, the intermediates are within 1 kcal mol^{-1} of their methyl free counterparts for both product pathways. The only real exception is the five-membered reductive elimination transition structure (Figure 6-27).

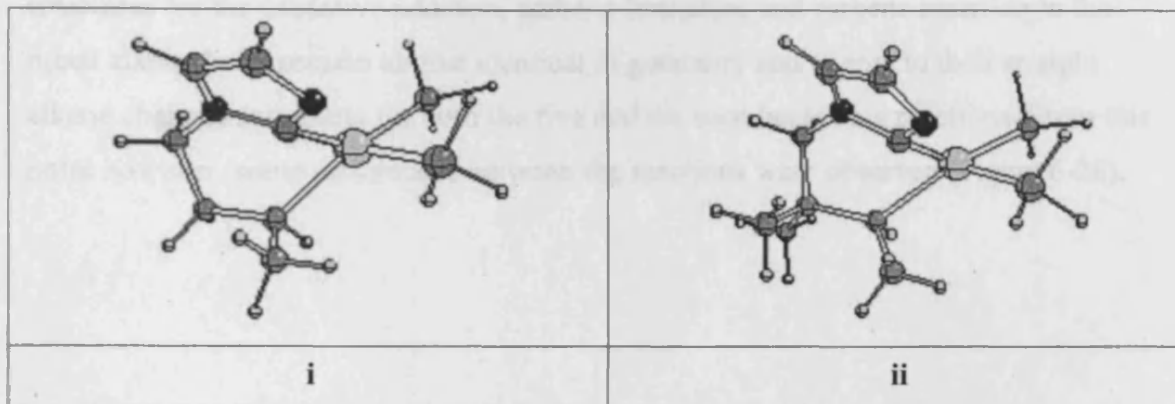


Figure 6-27 Reductive elimination transition structure for the five-membered ring product (straight chain on left; with methyls on right)

In the straight chain structure (Figure 6-27 **i**) the end chain methyl is directed away from the phosphine ligand. With the extra bulk included with the geminal methyls (Figure 6-27 **ii**), this methyl is more central to avoid steric interaction with either the geminal methyl groups, or the phosphine ligand. While only a subtle difference, this extra bulk is enough to raise the energy of the transition structure by a few kcal mol^{-1} and as a result, the energy of the five-membered ring reductive elimination transition structure is raised above that of the six-membered ring.

Despite this, in general the 5-membered ring energies indicate this would still be the preferred route for the majority of the cycle. Further, there is only minor difference in the energies between the five- and six-membered ring reductive elimination transition structures indicating the lower energy of the majority of the route for the 5-membered ring would likely override any negative influence of this slightly higher energy transition structure.

6.3.2.2 *The Bergman mechanism*

As found for the Cavell/McGuinness mechanism, the initial steps of the Bergman reaction remain unaffected by the extra bulk of the methyls on the alkene chain. All structures for the oxidative addition, carbene formation and carbene insertion in the metal alkene bond remain almost identical in geometry and energy to their straight alkene chain counterparts for both the five and six membered ring reactions. From this point however, some differences between the reactions were observed (Figure 6-28).

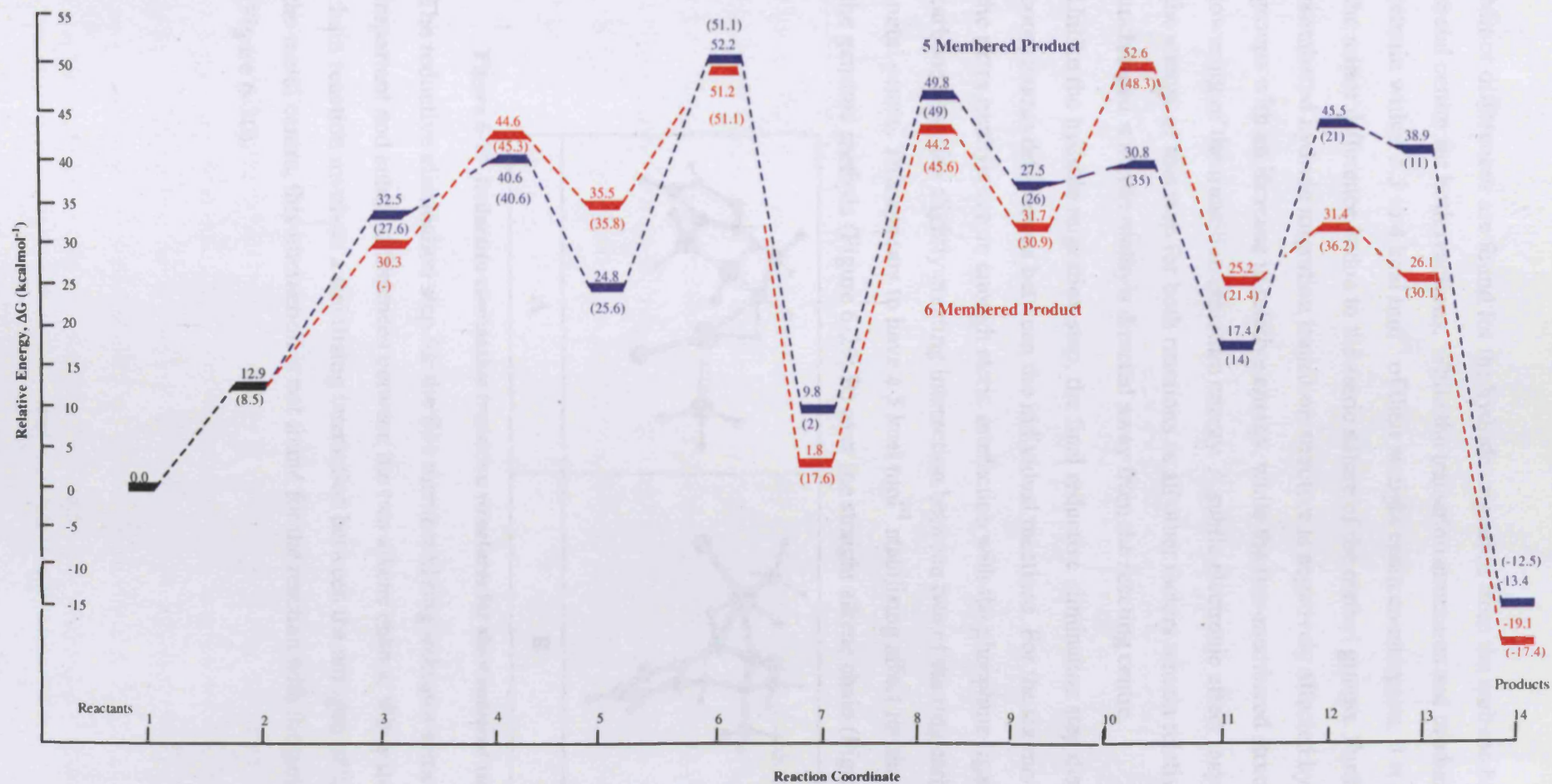


Figure 6-28 Energies for the influence of geminal methyls on the five- and six-membered products – straight chain energies in brackets

(Bergman's mechanism)

Minor differences are found for the hydride migration from the carbene back to the metal centre for both reactions. While the transition structures and products for this step remain within 3.5 to 4 kcal mol⁻¹ of their straight chain counterparts, it is not expected the minor difference is due to the steric nature of the methyl groups. Further, the six-membered hydride migration transition structure is negatively affected by the methyl groups with an increase in relative energy, while the five-membered structure displays a lowering of the transition structure energy. A subtle electronic effect may be altering the energy of this step for both reactions as all other factors remain relatively unchanged with the methyls directed away from the reacting centre.

Unlike the hydride migration step, the final reductive elimination step displays more conspicuous differences between the individual reactions. For the six membered ring, the extra methyls create enough steric interaction with the phosphine ligand, that the carbene ring tilts slightly creating interaction between two of the ring carbons and the metal centre. This appears to have a 5 kcal mol⁻¹ stabilising affect for the reaction with the geminal methyls (Figure 6-29; **B**) over the straight alkene chain (Figure 6-29; **A**).

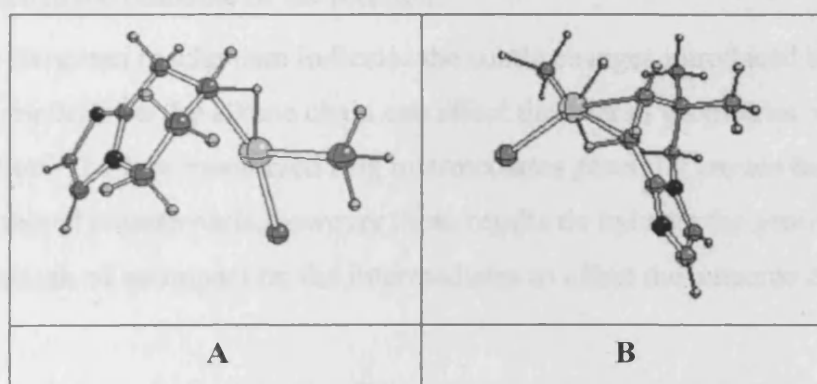


Figure 6-29 Reductive elimination transition structures for six-membered ring products

The reductive elimination step for the five membered ring indicates some very important and subtle differences between the two alkene chains. While the straight chain reaction involves a stabilising interaction between the nitrogen of the azole and the metal centre, this interaction is not found for the reaction with the geminal methyls (Figure 6-30).

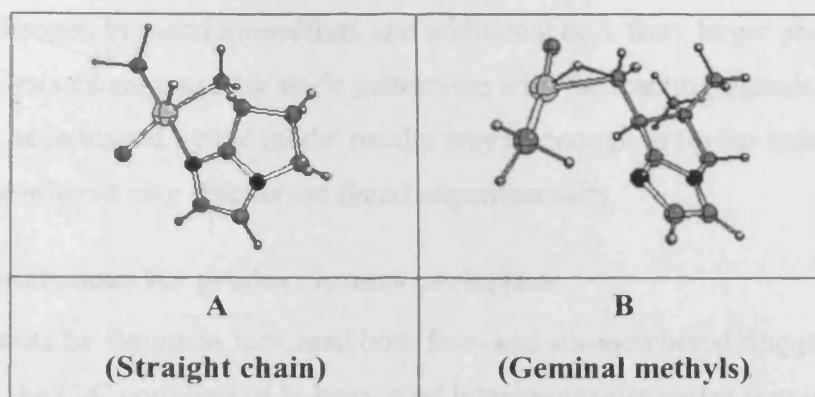


Figure 6-30 Reductive elimination transition structures for five-membered ring products

The stabilisation afforded by this interaction has a significant impact on the energetics of the final reaction step, with the imidazole interaction for the straight chain resulting in a $24.5 \text{ kcal mol}^{-1}$ lower energy transition structure for the five-membered ring.

Further, without this imidazole interaction in either the five or six membered case, the six membered reductive elimination has an almost 10 kcal mol^{-1} lower barrier than the five membered case. While other steps remain higher in energy for the six-membered ring, this observation indicates subtle differences in electronic and steric effects can greatly influence the outcome of the reaction.

Overall, the Bergman mechanism indicates the subtle changes introduced by including the geminal methyls on the alkene chain can affect the overall geometries and energies for the reaction. The five membered ring intermediates generally remain below those of the six-membered counterparts, however these results do indicate the geminal methyls may have enough of an impact on the intermediates to affect the outcome of the reaction.

6.3.2.2.3 Geminal methyl influence on product isomers

In general, the five-membered ring intermediates with inclusion of the geminal methyls on the alkene chain remain below those of the six-membered counterparts regardless of the reaction mechanism employed. However, results for the Bergman mechanism have some interesting implications. In the model system studied for this reaction the five-membered ring product is still generally favoured over the six-membered product, although this observation does not hold true for every step in the reaction with the geminal methyls displaying discernible influence on the reactivity of the metal complexes. In experimental conditions, the small influences indicated here would be exacerbated with coordinating solvents stabilising intermediates as indicated for the

imidazole nitrogen to metal interaction, and additional bulk from larger phosphines used in catalysis causing greater steric interaction with the reacting ligands. These two interactions as indicated by the model results may be enough to tip the balance in favour of the six-membered ring reaction as found experimentally.

6.3.2.3 Conclusions for product isomer preference

Pervious results by Bergman indicated both five- and six-membered ring products were possible for the C-C coupling of N-homoallyl benzimidazoles under certain experimental conditions. The theoretical study of the model system for both the Bergman and Cavell/McGuinness mechanisms give some indication of what factors may affect the outcome of the C-C coupling reaction.

Firstly, even though alkene isomerisation may be possible for a straight chain alkene, the chelation between the alkene and azole ligands restricts the coordination of these ligands to the metal centre, creating a strained environment for many of the important intermediates for either mechanism when the alkene is located closer to the body of the azole. When combined with the small energy difference between the isomers, it is expected the alkene located on the free end of the alkyl chain would be the reacting isomer in experimental conditions.

Secondly, when the alkene is located on the end of the alkene chain with no other restrictions on the reacting centres, intermediates for the five-membered product are lower in energy than their six-membered counterparts. Consequently, it is expected the five-membered product would be formed in preference regardless of mechanism and despite the thermodynamic favouring of the six-membered product; a fact reflected in experimental conditions¹.

Finally, subtle steric or electronic differences from inclusion of extra methyl groups on the alkene chain may steer the product preference towards six-membered ring as indicated experimentally². While generally the extra methyls had very little influence on reaction geometries or energies, subtle changes in particular for the reductive elimination step of the Bergman mechanism did indicate the additional bulk could affect the overall reaction, even on a model system. As such, it is expected this is the major cause for the preference of the six-membered ring over the five-membered ring as found for the straight chain alkene.

6.3.3 Acid catalysed coupling

After successfully catalysing the cyclisation of various alkene heterocycles, Bergman made the further observation that the rate and yield of catalysis could be improved by addition of a weak acid catalyst. One explanation for this improvement could be the protonation (or general activation) of the imidazole nitrogen, leading in turn to a more reactive imidazole 2-H and easing the initial oxidative addition reaction. Further, activation of the imidazole nitrogen throughout the catalytic cycle creates more stable carbene or carbene-like complexes as intermediates along the pathway.

This section examines how dramatically this activation affects both mechanisms and the reaction outcomes for the five-membered ring product.

6.3.3.1 Acid catalysed Cavell/McGuinness mechanism

Aside from introducing a carbene ligand, acid catalysis does not dramatically alter the proposed mechanism for the C-C coupling reaction as shown in Figure 6-31.

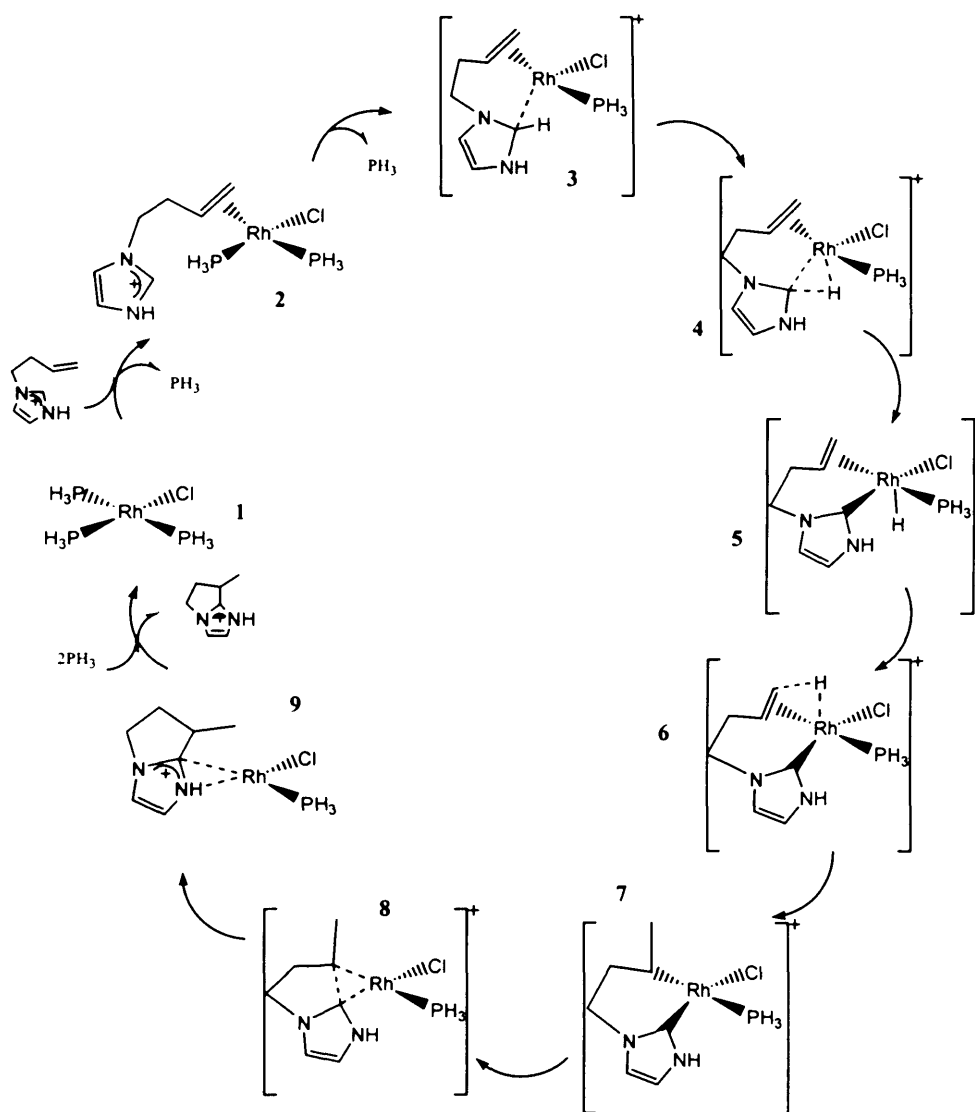


Figure 6-31 Acid catalysed Cavell/McGuinness cycle

Overall, the geometries of the reaction intermediates change very little from the unactivated cycle. The oxidative addition transition structure indicates the highest energy structure is found much earlier in the activation, with more distance between the interacting azole and the metal and a shorter unactivated C2-H distance. Aside from this, most intermediates displayed very similar geometries with the C2-Rh distance of the azole slightly closer but within 0.06\AA of the corresponding carbene distances. Similarly, the Rh-H distances were consistently closer for the azole complexes, but generally less than 0.08\AA shorter than the carbene counterparts.

Despite having little effect on the reaction geometries, *N*-activation by an acid catalyst does dramatically impact the energies for catalysis, with the barriers and the energies of the reaction intermediates to the C-C coupling reaction significantly reduced for the Cavell/McGuinness mechanism (Figure 6-32).

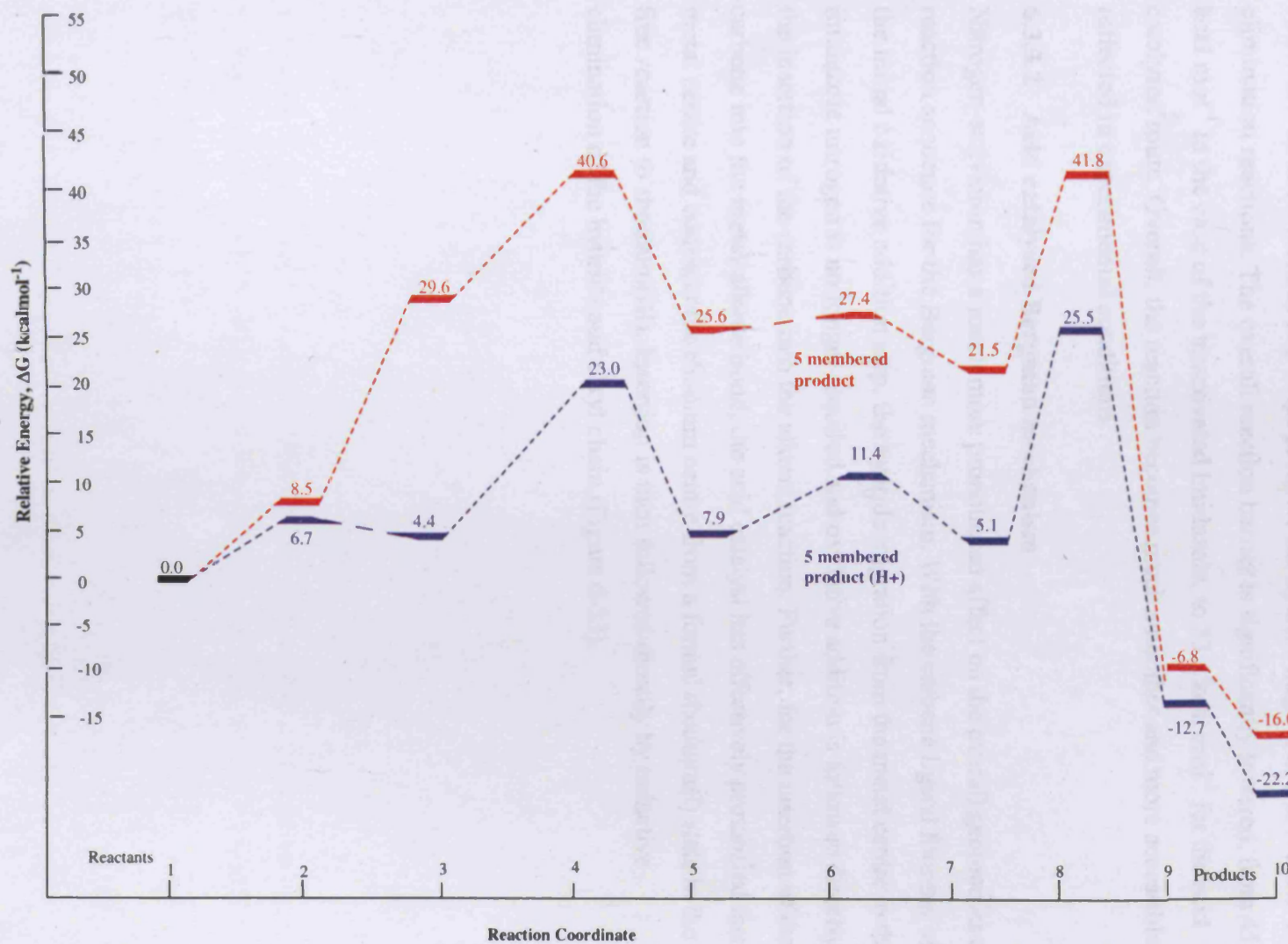


Figure 6-32 Energies for the acid catalysed Cavell/McGuinness route

The barrier to oxidative addition is lowered due to the higher acidity of the reacting azolium, while the strength and electron-donating capacity of the carbene ligand stabilises all intermediates and helps promote the hydride migration and reductive elimination reactions. The overall reaction barrier is significantly lowered, from 45.3 kcal mol⁻¹ in the case of the unactivated imidazole, to 33.1 kcal mol⁻¹ for the acid catalysed route. Overall, the reaction becomes much smoother and more accessible as reflected in experimental conditions.

6.3.3.2 Acid catalysed Bergman mechanism

Nitrogen-activation has a much more pronounced affect on the overall geometries and reaction sequence for the Bergman mechanism. With the carbene ligand forming after the initial oxidative addition step, the hydride migration from the metal centre to the imidazole nitrogen is no longer required and oxidative addition is followed directly by the insertion of the carbene into the alkene reaction. Further, for the insertion of the carbene into the metal-alkene bond, the acid catalyst has effectively protonated the metal centre and converts the rhodium centre from a formal rhodium(I) state in the acid-free reaction to rhodium(III). Insertion is then followed directly by reductive elimination of the hydride and alkyl chain (Figure 6-33).

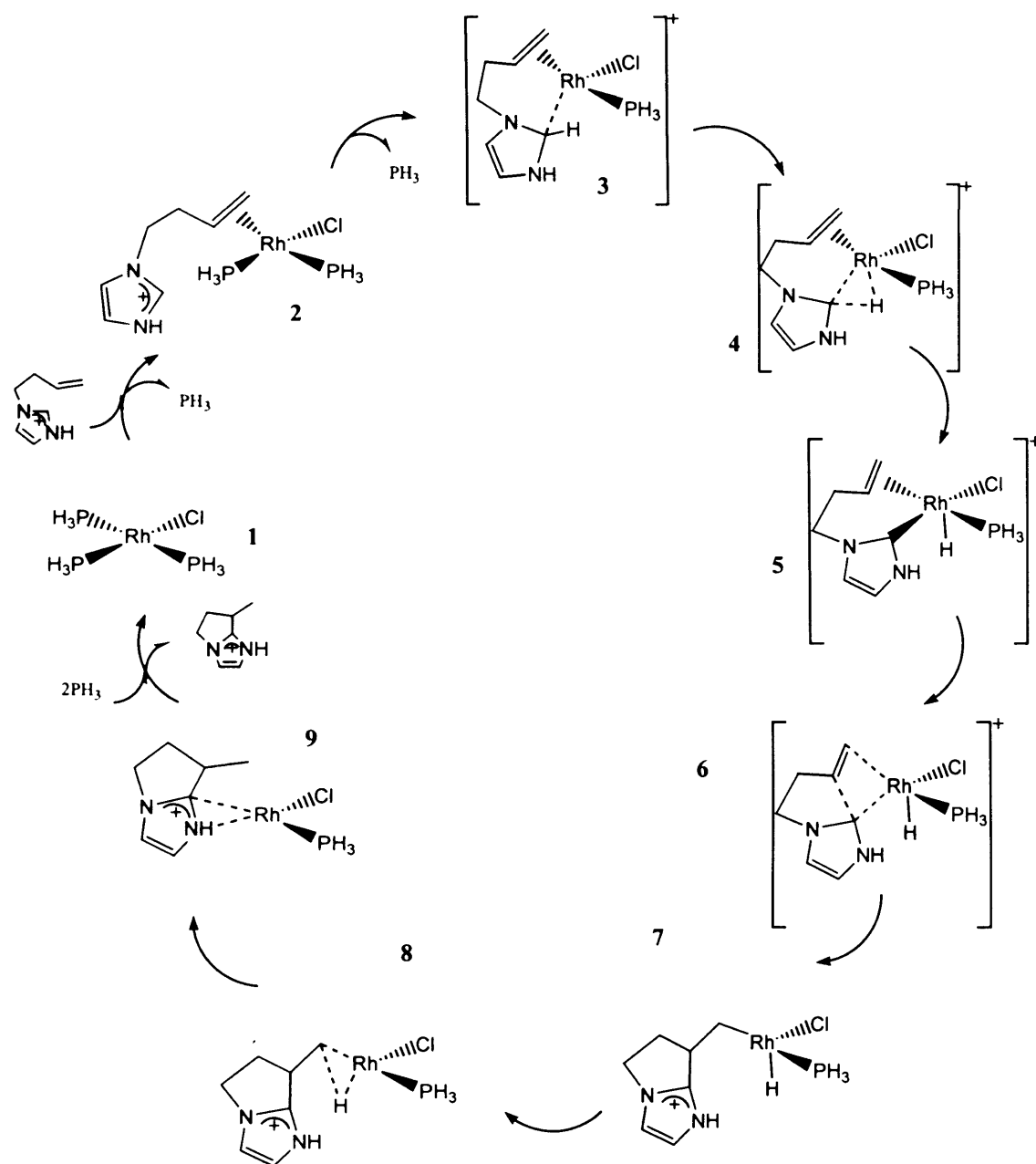


Figure 6-33 Acid catalysed Bergman cycle

While the *N*-activation did have an effect on the energies for the mechanism proposed by Bergman, the benefits were not as dramatic as was seen for the Cavell/McGuinness mechanism (Figure 6-34).

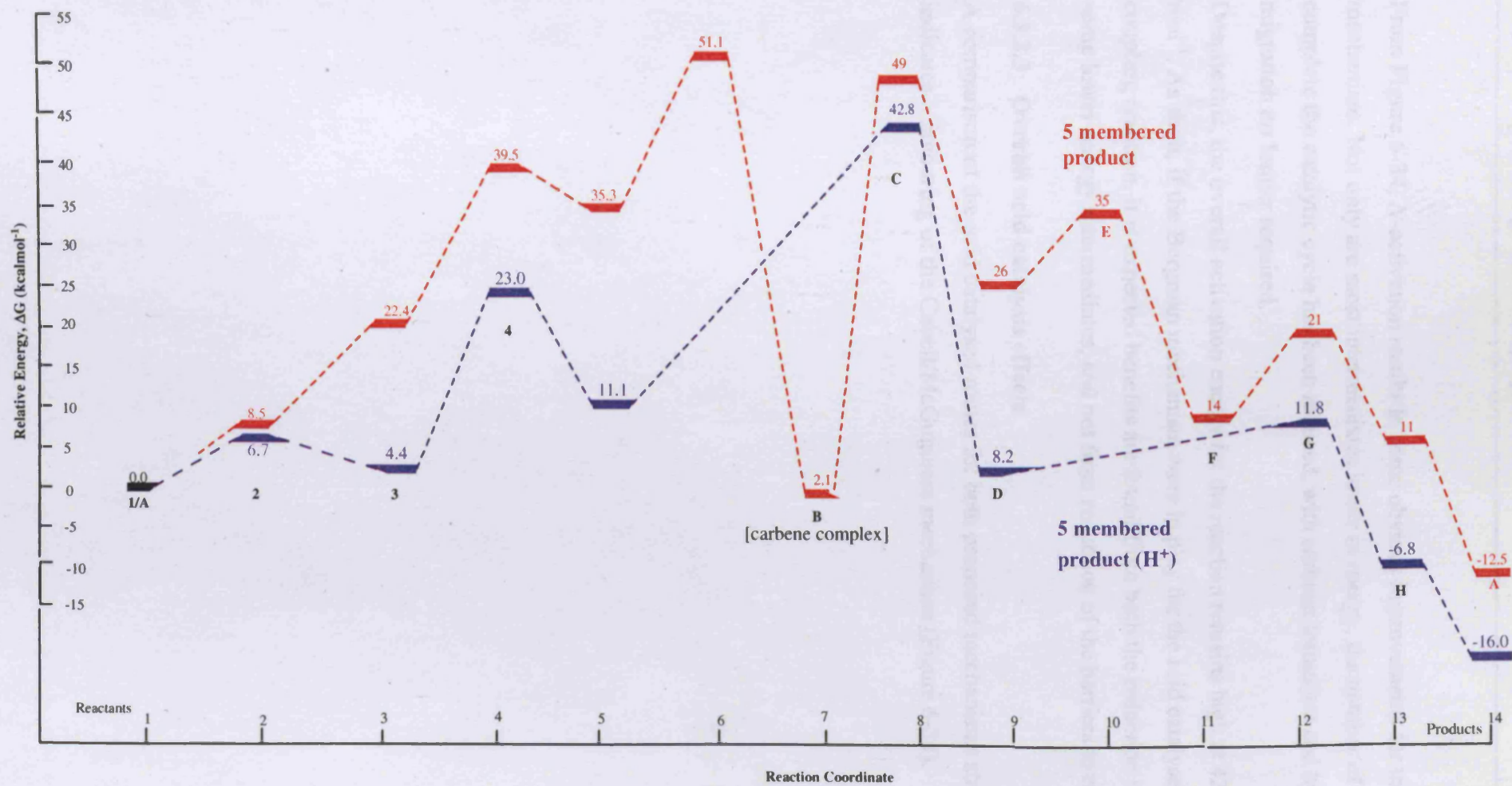


Figure 6-34 Energies for the acid catalysed Bergman route

From Figure 6-34, *N*-activation results in some obvious improvements for the Bergman mechanism. Not only are most intermediates lower in energy, the number of steps to complete the catalytic cycle has been reduced, with carbene formation and hydride migration no longer required.

Despite this, the overall activation energy for the reaction remains high at 42.8 kcal mol⁻¹. As such, if the Bergman mechanism were in play for the acid catalysed C-C coupling reaction, it is expected benefits are found from both the reduction in steps and some lower energy intermediates, and not from reduction of the barriers to reaction.

6.3.3.3 Overall acid catalysis effects

A comparison of the acid catalysed routes for both proposed mechanisms strongly indicates a favouring of the Cavell/McGuinness mechanism (Figure 6-35).

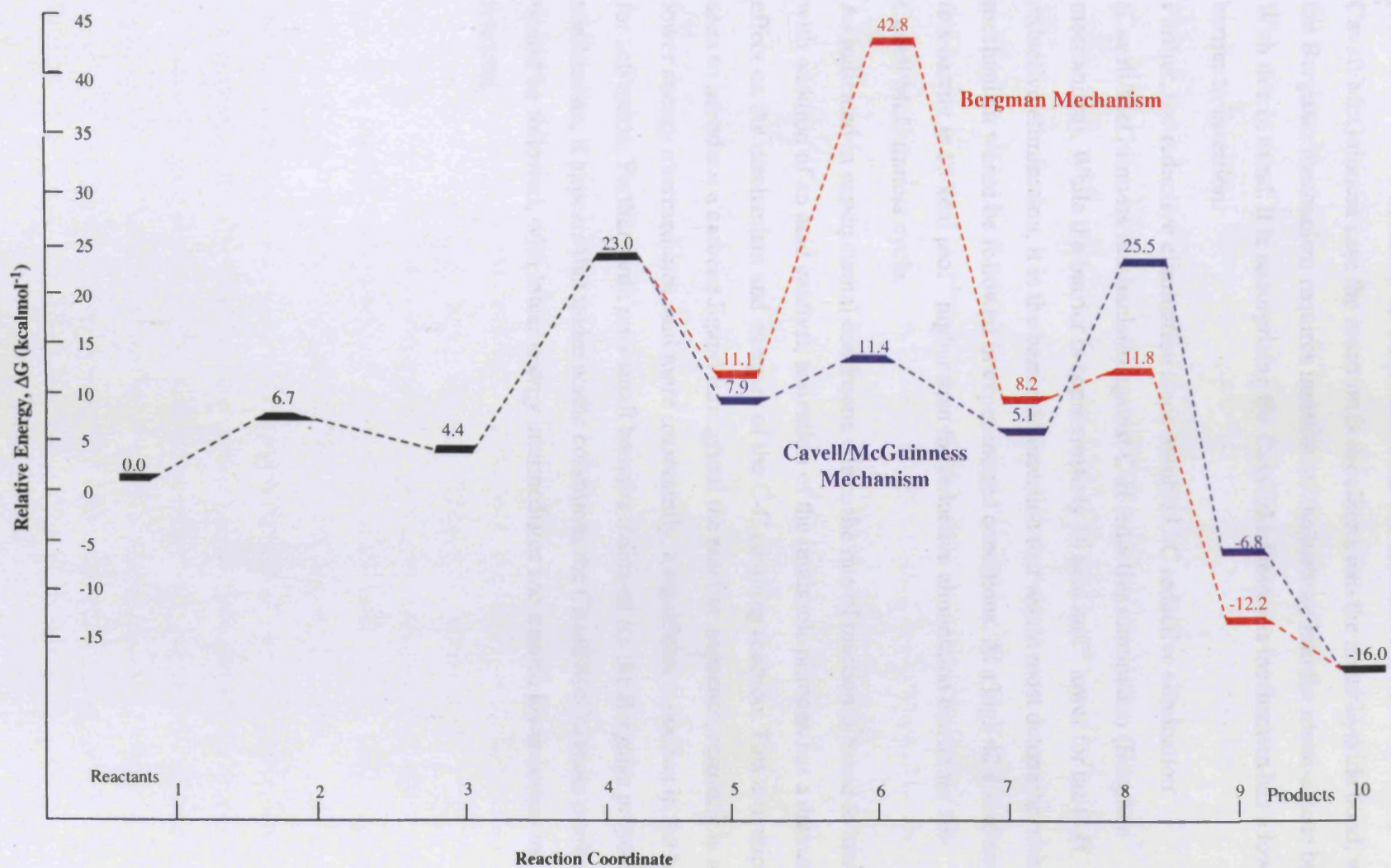


Figure 6-35 Comparison of acid catalysed energies for both proposed routes

Interestingly, with the inclusion of an acid catalyst, the difference between the Cavell/McGuinness and Bergman mechanisms becomes one of timing. Both follow a path of oxidative addition, insertion and reductive elimination; however in the Cavell/McGuinness case the insertion is the alkene into the metal-hydride bond, while the Bergman mechanism requires insertion of the carbene into the metal-alkene bond. With this in mind, it is unsurprising the Cavell/McGuinness mechanism has a lower barrier to insertion.

Further, the reductive elimination steps involve C-C reductive elimination (Cavell/McGuinness mechanism) against C-H reductive elimination (Bergman mechanism). While the barrier is approximately 14 kcal mol^{-1} lower for the C-H reductive elimination, it is the barrier to insertion that would most determine which mechanism would be followed in experimental conditions. At a high $42.8 \text{ kcal mol}^{-1}$, this barrier is 15 kcal mol^{-1} higher than the reductive elimination barrier for the Cavell/McGuinness cycle.

As indicated in experimental conditions where the rate of reaction is found to increase with addition of an acid catalyst, activation of the imidazole nitrogen has a dramatic effect on the mechanism and energies of the C-C coupling reaction. This activation is seen to introduce a carbene ligand throughout the reaction sequence, resulting in many lower energy intermediates, and more importantly, a significant reduction in the barriers for activation. Further, with only small benefits indicated for the Bergman proposed mechanism, it appears that under acidic conditions the Cavell/McGuinness mechanism would be followed, with lower energy intermediates and a much lower barrier to reaction.

6.4 Conclusions

After Bergman's group reported the intramolecular coupling of a range of alkenes to heterocycles to create 2-functionalised imidazoles under mild conditions, they proposed an unusual mechanism involving a carbene complex, followed by cycloaddition and reductive elimination. Experimental results supported their mechanism with the isolation of a stable carbene complex, thought to be an important intermediate. Similarity of their reaction with the nickel catalysed C-C coupling reactions examined in the previous chapter prompted a comparison of their mechanism to one involving oxidative addition, alkene insertion and reductive elimination (Cavell/McGuinness mechanism).

While both five and six membered products can be formed in certain experimental conditions, the five-membered product is favoured with a straight alkene chain, while the six-membered product was synthesised with geminal methyls incorporated into the alkene chain. Results indicate that despite being slightly less thermodynamically favourable, the six-membered product has lower activation barriers for both the Bergman and Cavell/McGuinness mechanisms. Further results indicated reactant isomerisation and alternative alkene coordination to the metal centre do not have enough influence to alter this preference for the six-coordinate product.

Overall, it is not clear whether the Bergman or Cavell/McGuinness route would be preferred under experimental conditions. While initial formation of the carbene complex in Bergman's route appears restrictive with an activation barrier of over 50 kcal mol⁻¹, reductive elimination of the C-C coupled azole in the Cavell/McGuinness mechanism has a similar barrier of around 42 kcal mol⁻¹. Overall, the Cavell/McGuinness mechanism appears to have a smoother path with many intermediates relatively close in energy; experimental isolation and NMR observation indicate the carbene complex is indeed involved in the catalytic cycle.

Despite the lack of clarity in isolating a mechanism for the azole C-C coupling reaction, it appears the Cavell/McGuinness mechanism would be followed with inclusion of an acid catalyst in the reaction mixture. Experimental results indicate inclusion of either a Lewis or Brønsted acid increases the rate of reaction significantly. Through activation of the imidazole nitrogen, it is expected the acid creates an azolium salt. The resultant

salt significantly favours the Cavell/McGuinness route, with little benefit found for the Bergman reaction.

6.5 References

- 1 K. L. Tan, R. G. Bergman and J. A. Ellman, *J. Am. Chem. Soc.*, 2001, **123**, 2685.
- 2 K. L. Tan, R. G. Bergman and J. A. Ellman, *J. Am. Chem. Soc.*, 2002, **124**, 3202.
- 3 K. L. Tan, R. G. Bergman and J. A. Ellman, *J. Am. Chem. Soc.*, 2002, **124**, 13964.
- 4 K. L. Tan, A. Vasudevan, R. G. Bergman, J. A. Ellman and A. J. Souers, *Org. Lett.*, 2003, **5**, 2131.
- 5 K. L. Tan, S. Park, J. A. Ellman and R. G. Bergman, *J. Org. Chem.*, 2004, **69**, 7329.
- 6 N. D. Clement, K. J. Cavell, C. Jones and C. J. Elsvier, *Angew. Chem. Int. Ed.*, 2004, **43**, 1277.
- 7 N. D. Clement and K. J. Cavell, *Angew. Chem. Int. Ed.*, 2004, **43**, 3845.
- 8 D. Bacciu, K. J. Cavell, I. A. Fallis and L. Ooi, *Angew. Chem. Int. Ed.*, 2005, **44**, 2.
- 9 R. H. Hertwig and W. Koch, *Chem. Phys. Lett.*, 1997, **268**, 345.
- 10 P. J. Stephens, J. F. Devlin, C. F. Chabalowski and M. J. Frisch, *J. Phys. Chem.*, 1994, **98**, 11623.
- 11 A. D. Becke, *J. Chem. Phys.*, 1993, **98**, 5648.
- 12 P. J. Hay and W. R. Wadt, *J. Chem. Phys.*, 1985, **82**, 299.
- 13 T. H. Dunning and P. J. Hay, 'Modern Theoretical Chemistry', Plenum, 1976.
- 14 B. F. Yates, *J. Mol. Struct. (THEOCHEM)*, 2000, **506**, 223.
- 15 M. J. Frisch, J. A. Pople and J. S. Binkley, *J. Chem. Phys.*, 1984, **80**, 3265.
- 16 A. D. McLean and G. S. Chandler, *J. Chem. Phys.*, 1980, **72**, 5639.
- 17 R. Krishnan, J. S. Binkley, R. Seeger and J. A. Pople, *J. Chem. Phys.*, 1980, **72**, 650.
- 18 M. J. Frisch, G. W. Trucks, H. B. Schlegel, G. E. Scuseria, M. A. Robb, J. R. Cheeseman, J. A. Montgomery Jr., T. Vreven, K. N. Kudin, J. C. Burant, J. M. Millam, S. S. Iyengar, J. Tomasi, V. Barone, B. Mennucci, M. Cossi, G.

Scalmani, N. Rega, G. A. Petersson, H. Nakatsuji, M. Hada, M. Ehara, K. Toyota, R. Fukuda, J. Hasegawa, M. Ishida, T. Nakajima, Y. Honda, O. Kitao, H. Nakai, M. Klene, X. Li, J. E. Knox, H. P. Hratchian, J. B. Cross, C. Adamo, J. Jaramillo, R. Gomperts, R. E. Stratmann, O. Yazyev, A. J. Austin, R. Cammi, C. Pomelli, J. W. Ochterski, P. Y. Ayala, K. Morokuma, G. A. Voth, P. Salvador, J. J. Dannenberg, V. G. Zakrzewski, S. Dapprich, A. D. Daniels, M. C. Strain, O. Farkas, D. K. Malick, A. D. Rabuck, K. Raghavachari, J. B. Foresman, J. V. Ortiz, Q. Cui, A. G. Baboul, S. Clifford, J. Cioslowski, B. B. Stefanov, G. Liu, A. Liashenko, P. Piskorz, I. Komaromi, R. L. Martin, D. J. Fox, T. Keith, M. A. Al-Laham, C. Y. Peng, A. Nanayakkara, M. Challacombe, P. M. W. Gill, B. Johnson, W. Chen, M. W. Wong, C. Gonzalez and J. A. Pople, Gaussian 03 (Revision C.02), Wallingford CT, 2004.

- 19 D. S. McGuinness, K. J. Cavell, B. F. Yates, B. W. Skelton and A. H. White, *J. Am. Chem. Soc.*, 2001, **123**, 8317.
- 20 D. S. McGuinness, K. J. Cavell and B. F. Yates, *Chem. Commun.*, 2001, **4**, 355.

